Interference Management in Impulse-Radio Ultra-Wide Band Networks

THÈSE N^{O} 4119 (2008)

PRÉSENTÉE LE 11 JUILLET 2008

À LA FACULTE INFORMATIQUE ET COMMUNICATIONS

LABORATOIRE POUR LES COMMUNICATIONS INFORMATIQUES ET LEURS APPLICATIONS 2

PROGRAMME DOCTORAL EN INFORMATIQUE, COMMUNICATIONS ET INFORMATION

ÉCOLE POLYTECHNIQUE FÉDÉRALE DE LAUSANNE

POUR L'OBTENTION DU GRADE DE DOCTEUR ÈS SCIENCES

PAR

Ruben MERZ

ingénieur en systèmes de communication diplômé EPF
de nationalité suisse et originaire de Domat/Ems (GR)

acceptée sur proposition du jury:

Prof. A. Martinoli, président du jury
Prof. J.-Y. Le Boudec, directeur de thèse
Prof. R. Knopp, rapporteur
Prof. A. Molisch, rapporteur
Dr J. Zory, rapporteur

ÉCOLE POLYTECHNIQUE
FÉDÉRALE DE LAUSANNE

Suisse
2008

Abstract

We consider networks of impulse-radio ultra-wide band (IR-UWB) devices. We are interested in the architecture, design, and performance evaluation of these networks in a low data-rate, self-organized, and multi-hop setting.

IR-UWB is a potential physical layer for sensor networks and emerging pervasive wireless networks. These networks are likely to have no particular infrastructure, might have nodes embedded in everyday life objects and have a size ranging from a few dozen nodes to large-scale networks composed of hundreds of nodes. Their average data-rate is low, on the order of a few megabits per second. IR-UWB physical layers are attractive for these networks because they potentially combine low-power consumption, robustness to multipath fading and to interference, and location/ranging capability.

The features of an IR-UWB physical layer greatly differ from the features of the narrow-band physical layers used in existing wireless networks. First, the bandwidth of an IR-UWB physical layer is at least 500 MHz, which is easily two orders of magnitude larger than the bandwidth used by a typical narrow-band physical layer. Second, this large bandwidth implies stringent radio spectrum regulations because UWB systems might occupy a portion of the spectrum that is already in use. Consequently, UWB systems exhibit extremely low power spectral densities. Finally IR-UWB physical layers offer multi-channel capabilities for multiple and concurrent access to the physical layer. Hence, the architecture and design of IR-UWB networks are likely to differ significantly from narrow-band wireless networks. For the network to operate efficiently, it must be designed and implemented to take into account the features of IR-UWB and to take advantage of them. In this thesis, we focus on both the medium access control (MAC) layer and the physical layer. Our main objectives are to understand and determine (1) the architecture and design principles of IR-UWB networks, and (2) how to implement them in practical schemes.

In the first part of this thesis, we explore the design space of IR-UWB networks and analyze the fundamental design choices. We show that interference from concurrent transmissions

should not be prevented as in protocols that use mutual exclusion (for instance, IEEE 802.11). Instead, interference must be managed with rate adaptation, and an interference mitigation scheme should be used at the physical layer. Power control is useless. Based on these findings, we develop a practical PHY-aware MAC protocol that takes into account the specific nature of IR-UWB and that is able to adapt its rate to interference. We evaluate the performance obtained with this design: It clearly outperforms traditional designs that, instead, use mutual exclusion or power control. One crucial aspect of IR-UWB networks is packet detection and timing acquisition. In this context, a network design choice is whether to use a common or private acquisition preamble for timing acquisition. Therefore, we evaluate how this network design issue affects the network throughput. Our analysis shows that a private acquisition preamble yields a tremendous increase in throughput, compared with a common acquisition preamble. In addition, simulations on multi-hop topologies with TCP flows demonstrate that a network using private acquisition preambles has a stable throughput. On the contrary, using a common acquisition preamble exhibits an effect similar to exposed terminal issues in 802.11 networks: the throughput is severely degraded and flow starvation might occur.

In the second part of this thesis, we are interested in IEEE 802.15.4a, a standard for low data-rate, low complexity networks that employs an IR-UWB physical layer. Due to its low complexity, energy detection is appealing for the implementation of practical receivers. But it is less robust to multi-user interference (MUI) than a coherent receiver. Hence, we evaluate the performance of an IEEE 802.15.4a physical layer with an energy detection receiver to find out whether a satisfactory performance is still obtained. Our results show that MUI severely degrades the performance in this case. The energy detection receiver significantly diminishes one of the most appealing benefits of UWB, specifically its robustness to MUI and thus the possibility of allowing for parallel transmissions. This performance analysis leads to the development of an IR-UWB receiver architecture, based on energy detection, that is robust to MUI and adapted to the peculiarities of IEEE 802.15.4a. This architecture greatly improves the performance and entails only a moderate increase in complexity.

Finally, we present the architecture of an IR-UWB physical layer implementation in ns-2, a well-known network simulator. This architecture is generic and allows for the simulation of several multiple-access physical layers. In addition, it comprises a model of packet detection and timing acquisition. Network simulators also need to have efficient algorithms to accurately compute bit or packet error rates. Hence, we present a fast algorithm to compute the bit error rate of an IR-UWB physical layer in a network setting with MUI. It is based on a novel combination of large deviation theory and importance sampling.

Keywords

Ultra-wide band, UWB, impulse-radio, medium-access control, cross-layer design, multi-user interference, impulsive interference, interference mitigation, energy detection, IEEE 802.15.4a, ns-2, large deviation, importance sampling.

Résumé

Le travail de cette thèse a pour but d'étudier les réseaux sans-fils basés sur une radio impulsive à bandes ultra-larges (ULB). Notre intérêt se porte sur l'architecture, la conception, ainsi que l'évaluation de performance des ces réseaux pour des applications bas-débits, nécessitant un comportement auto-organisés et des relais multiples.

Les radios impulsives ULB sont intéressantes pour les réseaux de capteurs et les réseaux sans-fils omniprésents. De tels réseaux ne nécessitent pas forcement une infrastucture fixe et sont souvent intégrés aux objets de la vie courante. Leur besoin en débit est faible, de l'ordre du mégabit par seconde, et leur taille peut varier, allant d'une douzaine à plusieurs centaines de noeuds pour les réseaux les plus vastes. L'attrait pour l'utilisation de radios impulsives ULB pour ces réseaux provient du fait qu'elles combinent à la fois une faible consommation, une bonne résistance aux phénomènes multi-trajet et à l'interférence, ainsi qu'une aptitude pour la localisation.

Les caractéristiques d'une radio impulsive ULB sont très différentes d'une radio traditionnelle à bandes étroites largement utilisées dans les réseaux sans fils existants. Tout d'abord, la bande passante est au minimum 500 MHz, ce qui représente environ dix à cent fois la largeur de la bande passante utilisée par les radios traditionnelles. Avec une telle bande passante, un système ULB risque d'empiéter sur des parties du spectre radio réservées à d'autres systèmes. Pour pallier à ce problème, les systèmes ULB ont une densité spectrale de puissance très faible. Enfin, les radio impulsives ULB offrent d'excellentes possibilités pour l'accès multiple au canal. De ce fait, l'architecture et la conception de réseaux basés sur une radio impulsive ULB diffèrent probablement largement des réseaux sans-fils à bandes étroites. Dans cette thèse, nous nous concentrons à la fois sur l'accès au médium et sur la couche physique. Notre objectif principal est de comprendre et déterminer (1) l'architecture et les principes régissant la conception de réseaux basés sur une radio impulsive ULB, et (2) comment implémenter cette architecture et ces principes en pratique.

Dans la première partie de ce manuscrit, nous montrons pour les réseaux basés sur une ra-

dio impulsive ULB que, contrairement aux réseaux à bande étroite, l'interférence créée par les autres émetteurs ne doit pas être gérée par un protocole d'exclusion, mais par une adaptation du débit et l'utilisation d'un mécanisme d'atténuation de l'interférence au niveau de la couche physique. Les transmissions en parallèles par plusieurs émetteurs sont autorisées. Le contrôle de puissance d'émission n'est de plus pas nécessaire. Nous avons développé un protocole d'accès au médium basé sur ces principes et avons évalué sa performance qui s'avère être largement supérieure à celle obtenue avec des protocoles plus classiques qui utilisent le contrôle de puissance ou l'exclusion. Un aspect très important pour les réseaux basés sur une radio impulsive ULB est la synchronisation nécessaire pour la réception de chaque paquet. Cette synchronisation utilise un préambule au début de chaque paquet. Ce préambule peut être unique pour tout le réseau, ou alors, unique pour chaque récepteur du réseau. Nous avons évalué l'impact sur le débit du réseau de ces deux possibilités. Notre analyse montre que le débit obtenu avec un préambule unique par récepteur est très supérieur à celui obtenu avec un préambule unique pour tout le réseau. De plus, des simulations avec TCP sur un réseau à relais multiples montre qu'un débit stable est obtenu avec un préambule unique par récepteur, ce qui n'est pas le cas du débit obtenu avec un préambule unique pour tout le réseau.

Dans la seconde partie du manuscrit, nous nous intéressons à un récent standard, IEEE 802.15.4a, pour les réseaux à bas-débit et faible complexité utilisant une radio impulsive ULB. Étant donné l'importance d'une faible complexité, les récepteurs basés sur le principe de détection d'énergie sont séduisants. Malheureusement, ils sont très sensibles à l'interférence multi-utilisateur. Dans un premier temps, nous avons donc évalué la performance d'un récepteur à détection d'énergie classique pour le standard IEEE 802.15.4a en présence d'interférence multi-utilisateur. La performance est sévèrement diminuée par la présence d'interférence multi-utilisateur. Partant de ce constat, nous avons développé un récepteur pour radios impulsives ULB, toujours basé sur la détection d'énergie, mais qui premièrement, est robuste et résistant à l'interférence multi-utilisateur, et qui deuxièmement, est adapté à la modulation spécifique de la couche physique du standard 802.15.4a. Avec ce récepteur, dont la complexité reste raisonnable, nous obtenons un gain de performance considérable.

Enfin, nous présentons l'architecture d'une implémentation d'une radio impulsive ULB pour le simulateur de réseaux ns-2. Cette architecture est suffisamment générale pour pouvoir simuler d'autres couches physiques à accès multiple et inclut un modèle pour la synchronisation. Les simulateurs de réseaux ont également besoin d'algorithmes à la fois efficaces et précis pour calculer les taux d'erreurs des paquets ou des bits. C'est pourquoi nous présentons également un algorithme rapide pour calculer le taux d'erreur des bits d'une radio impulsive ULB,

dans un environnement réseau, avec de l'interférence multi-utilisateur. Cet algorithme est basé sur une nouvelle combinaison d'éléments de la théorie des grands écarts et d'échantillonage par importance.

Mots clés

Ultra-large bande, ULB, radio impulsive, contrôle d'accès au médium, design multi-couche, interférence multi-utilisateur, interférence impulsive, atténuation de l'interférence, détecteur d'énergie, IEEE 802.15.4a, ns-2, grands écarts, échantillonnage par importance.

Acknowledgments

I want to thank first my advisor, Professor Jean-Yves Le Boudec, for bringing me to this exciting research topic, and guiding me during my PhD. I'm deeply grateful to him for his availability and help, not only in research, but in all other aspects of the PhD. It was a fantastic experience to work with him and be able to learn so many things.

I want to thank Professors Raymond Knopp and Andreas Molisch, as well as Dr. Julien Zory, for accepting to review this thesis and for the interest they demonstrate with respect to my work. I also want to thank Professor Alcherio Martinoli for accepting to preside over the jury.

I am indebted to Božidar Radunović, Jörg Widmer, Sonja Buchegger, and Olivier Dousse who were helpful, supportive, and friendly colleagues especially when most needed at the beginning of a PhD. I did not have many, but Mathilde Durvy was the best office mate I could ever hope for. I warmly thank my "wall-mate" Manuel Flury. I've spent two great years working with him and the second part of this thesis would probably not exist without him. All my colleagues from LCA are greatly acknowledged for creating a friendly and lively working environment. I'm also very thankful to the staff of the lab, Angela Devenoge, Danielle Alvarez, Holly Cogliati, Patricia Hjelt, Jean-Pierre Dupertuis, Marc-André Lüthi, and Philippe Chammartin for making everything work so smoothly.

Hardware development has still many secrets, but I want to thank James-Colli Vignarelli, Jérôme Vernez and Catherine Dehollain to make it a bit less obscure.

A special thank for my former flat-mate Basile, to Flavio and Martin. Everyone should have friends like them. My gratitude goes to Bertrand Théraulaz for everything I learned from him.

Finally, I want to thank my family, especially my parents for their unconditional love and for giving me the chance to choose my path; my sister Sarah, as well as Capucine, Perrine, Françoise and Michel for their support.

Last but not least, I would like to thank my wife, Amandine, for her love, patience, and persistence. "Mai tumse pyar karta hoo".

Contents

Chapter 1

Introduction

1.1 Motivations

The Internet of Things [1, 2], pervasive and sensor networks are deploying an increasing number of wireless networks, with nodes possibly embedded in everyday life objects. These networks might range from a few dozen nodes, to large-scale networks composed of hundreds of nodes. In addition, they might have dense topologies with a potentially high level of interference between nodes. Their average data-rate requirement is low, around a few megabits per second. Energy consumption is also a concern, as nodes might operate with batteries or energy harvesting techniques.

There are several challenges facing the designers and implementers of these networks. One challenge is robustness to interference and poor radio propagation. With the increasing deployment of wireless networks, uncontrolled interference becomes problematic. Uncontrolled interference typically occurs due to several independent networks functioning in close vicinity to each other. Furthermore, these networks might be operated in hostile environments with poor radio propagation properties, for instance heavy multipath in indoor environments. Another challenge is low power consumption and low radiated power. For environmental and health concerns, as well as coexistence with other wireless technologies, it is important that the level of radiated power per node be kept very low. From a network design point of view, these challenges are cross-layer. They concern not only the choice and design of an appropriate physical layer, but also the design of the upper layers.

For the physical layer, impulse-radio ultra-wide band (IR-UWB) appears to have the potential to overcome these challenges. The large bandwidth of UWB radios, typically on the order

of the gigahertz, allows for the resolution of multipath components. This property, combined with the use of a proper radio receiver, offers a great resistance to multipath fading that usually plagues narrow-band radios. The wide bandwidth also provides robustness to interference. The large number of degrees of freedom can be shared by several communications. In practice, time-hopping can provide multiple-access to an IR-UWB physical layer. In a low data-rate setting, it allows *a priori* for many asynchronous and concurrent transmissions with few interferences between simultaneous transmissions. Another advantage of IR-UWB radios is high precision ranging, with a potential for centimeter accuracy in indoor environments.

Because of their very wide bandwidth that would overlap with the bandwidth of existing systems, there are stringent radio spectrum regulations already in effect in several countries. Consequently, UWB systems are also characterized by extremely low power spectral densities.

Hence, an IR-UWB physical layer might provide both robust communication and ranging capabilities for dense and low data-rate wireless network scenarios. In fact, an IR-UWB physical layer has been chosen for the IEEE 802.15.4a amendment to IEEE 802.15.4, a standard that targets low data-rate wireless networks with extensive battery life and very low complexity. A UWB physical layer is also attractive in high data-rate settings: the wide bandwidth is then not shared among several transmissions, but used by only one to pack as many bits as possible. For instance, Wireless USB utilizes a UWB physical layer.

The properties of UWB physical layers are very different than those of narrow-band physical layers. As such, the design rules and the architecture of a network composed of IR-UWB nodes are likely to be fundamentally different than those for narrow-band wireless networks. In this thesis, we are interested in the design and architecture of the medium access control (MAC) and physical layers for IR-UWB networks.

Two of the main tasks of the MAC layer are to manage interference and multiple-access to the physical layer. Existing wireless MAC protocols for narrow-band or code division multiple-access (CDMA) physical layers mostly employ mutual exclusion schemes, or power control, or a combination of both. Carrier sense multiple-access with collision avoidance (CSMA/CA) [3] or time division multiple-access (TDMA) are examples of classic mutual exclusion schemes. They are used because of the assumption that simultaneous transmissions result in transmission errors. With mutual exclusion, interference is simply prevented. In contrast, thanks to the robustness of IR-UWB physical layers, it might well be that an exclusion scheme is not necessary. Then, allowing and intelligently managing interference might actually provide a better utilization of the resources and prove to be more efficient. For instance, power control is a well-known way to manage interference. But there are also less commonly exploited dimensions for

interference management. In particular, rate adaptation where the rate is adapted to the level of interference.

Asking *how* to manage interference for IR-UWB networks is actually the starting point of this thesis. Our first objective is to find out what are the design principles of the MAC and physical layer for interference management in IR-UWB networks. Our second objective is to develop practical protocols and algorithms built on these principles.

1.2 Dissertation Outline

We begin with the system model and assumptions in Chapter 2, which contains the necessary material on IR-UWB networks and physical layers for the understanding of subsequent chapters. In Chapter 3, we discuss related work. Then, the thesis is divided into three parts: in Part I we discuss physical layer (PHY-)aware MAC protocols for IR-UWB networks, in Part II we are interested in robust receivers for IEEE 802.15.4a networks, and in Part III we are concerned with the simulation of IR-UWB networks. Finally, in Chapter 12 we conclude the thesis and offer perspectives on the results. In the following, we describe the content of each part.

1.2.1 Physical Layer Aware MAC Protocols for IR-UWB Networks

In a PHY-aware MAC design, the MAC has access to some or all of the physical layer parameters. In this first part, we are interested in the design, implementation, modeling, and performance evaluation of PHY-aware MAC protocols for IR-UWB networks.

We begin with Chapter 4, where we study the optimal design of PHY-aware MAC for low data-rate IR-UWB networks. Because the choices made for rate efficient designs are not necessarily optimal when considering energy efficiency, there is a need to understand the design trade-offs between the two objectives of rate efficiency and energy efficiency. To this end, we first identify *what* functions a MAC design has to achieve: (1) interference management, (2) access to a destination and (3) sleep cycle management. Second, we analyze *how* these functions can be implemented, and we provide a list of the many possible building blocks that have been proposed in the literature. Third, we use this classification to analyze fundamental design choices. To obtain meaningful results on energy efficiency, we propose a method for evaluating energy consumption already in the design phase of IR-UWB systems. With the results of our analysis, we derive a set of guidelines for the design of IR-UWB networks. In particular, if an interference mitigation scheme at the physical layer is used, mutual exclusion is

not necessary. Interference from concurrent transmissions should not be prevented, but should be managed with rate adaptation. Furthermore, power control should not be performed.

In Chapter 5, we build on the findings of Chapter 4 to present a practical PHY-aware MAC protocol. Our MAC does not use power control or mutual exclusion but rate adaptation. The packet transmissions use the time-hopping sequence of their intended destination. This creates contention domains that are private to each destination. Hence, as rate adaptation is local to a sender/receiver pair, our MAC is completely uncoordinated except for arbitrating senders that want to talk with a common destination. Our MAC does not rely on carrier-sensing and does not require a global control channel. It also provides support for multi-hop communications. To avoid complex interference estimation, rate adaptation is performed with a simple but efficient scheme based on whether a packet was properly decoded or not. We evaluate the performance obtained with this design and it clearly outperforms the performance of traditional designs that instead use mutual exclusion or power control.

One crucial aspect of IR-UWB networks is packet detection and timing acquisition. This is the first step for correct packet reception: Before recovering the payload of the packet, the destination must detect that the packet is on the medium and determine when exactly the payload begins. Packet detection and timing acquisition rely on the presence of an acquisition preamble at the beginning of each packet. How this preamble is chosen is a network design issue and it may have quite an impact on the network performance. A simple design choice of the network is to use a common acquisition preamble for the whole network. A second design choice is to use an acquisition preamble that is private to each destination.

Consequently, in Chapter 6, we evaluate how using a common or private acquisition preamble for timing acquisition affects the network throughput. The throughput with a private acquisition preamble is likely to be much higher, albeit at the cost of learning the private acquisition preamble of a destination. We develop an analytical model for the throughput of an IR-UWB network and use it to show that a private acquisition preamble yields a tremendous increase in throughput compared to a common acquisition preamble. The throughput difference grows with the number of concurrent transmitters and interferers and this result is confirmed by simulations. Furthermore, simulations on multi-hop topologies with TCP flows demonstrate that a network using private acquisition preambles has a stable throughput. On the contrary, using a common acquisition preamble exhibits the presence of a compounding effect similar to the exposed terminal issue in IEEE 802.11 networks: the throughput is severely degraded and complete flow starvation may occur.

Finally, Chapter 7 is a short excursion to the very concrete world of IR-UWB hardware. We

present an overview of an IR-UWB testbed with one receiver and multiple transmitters in order to create a realistic interference environment. This testbed allows researchers to test, study, and design algorithms in realistic conditions. It also provides an invaluable feedback for the modeling and understanding of the physical layer. One original and extremely challenging goal was also to implement the MAC protocol of Chapter 5. It proved more difficult than expected and instead, we successfully implemented on the testbed an algorithm for packet detection and timing acquisition with concurrent transmissions from other transmitters. This demonstrates that concurrent transmissions in IR-UWB networks are feasible.

1.2.2 Robust Receivers for IEEE 802.15.4a Networks

In the second part of this thesis, we discuss the design and performance of receivers using energy detection for IEEE 802.15.4a networks.

The IEEE 802.15.4 standard targets low data-rate wireless networks with extensive battery life and very low complexity. As such, the use of energy detection for the implementation of practical receivers is appealing: energy detection receivers are known to have lower complexity than coherent Rake receivers, and to be robust with respect to timing impairments. However, they are more sensitive to multi-user interference (MUI).

Hence, in Chapter 8, we first evaluate the performance of an IEEE 802.15.4a physical layer with a classic energy detection receiver. The goal is to find out whether an acceptable performance is obtained with an energy detection receiver. A complete packet-based system is considered: we take into account packet detection and timing acquisition, the estimation of a power delay profile of the channel, and the recovery of the encoded payload. Such a full and detailed IR-UWB receiver is extremely complex to simulate and not easily integrated in a network simulator. Hence we do not simulate several receivers in order to obtain a full IEEE 802.15.4a network. Instead, we develop a methodology to obtain performance results that are meaningful in a network setting, where we only simulate a single receiver with several transmitters. The results show that an energy detection receiver is suitable in the case a single user is transmitting. However, MUI severely degrades the performance, even at low traffic rate. Using an IEEE 802.15.4a compliant energy detection receiver significantly diminishes one of the most appealing benefits of UWB, specifically its robustness to MUI and thus the possibility of allowing for parallel transmissions.

The poor performance obtained in the previous chapter is our motive for Chapter 9. We develop an IR-UWB receiver architecture, based on energy detection, that is robust to MUI and

adapted to the peculiarities of IEEE 802.15.4a. The two key elements of the robustness to MUI of this architecture are (1) an interference mitigation scheme based on thresholding, and (2) a robust algorithm for the estimation of the power delay profile of a received burst of pulses. This architecture greatly improves the performance and entails only a moderate increase in complexity, compared to a classic energy detection receiver. This architecture also shows the feasibility of a practical, and low-complexity interference mitigation scheme for IR-UWB.

1.2.3 Simulation of IR-UWB networks

In this last part, we are interested in the simulation of IR-UWB networks. In Chapter 10, we present the architecture of an IR-UWB physical layer implementation in ns-2, a packet-based network simulator. In particular, a packet detection and timing acquisition model is implemented. Furthermore, for each packet, a packet error rate (PER) can be computed as a function of the received power, interference from concurrent transmissions, and thermal noise. Our implementation for IR-UWB takes into account transmissions with different time-hopping sequences (THS). The underlying modulation is binary phase-shift keying (BPSK), followed by a variable rate channel code. This architecture is quite generic and allows for the simulation of several multiple-access physical layers where an accurate model of interference is of high importance, e.g., IR-UWB or direct-sequence CDMA.

Lastly, in Chapter 11, we propose a fast and efficient method to compute the bit error rate (BER) of an IR-UWB physical layer in a multipath environment with multi-user interference. This is a conditional BER given the realizations of the channels from source or interferers to destination and their delay differences. Our motive is the simulation of large-scale or dense IR-UWB networks. The conditional BER might be used in a packet-level simulator with a block fading channel assumption to sample packet transmission error events. Because of the timescale difference between physical layer events and network events, a pulse-level simulation of the BER in a multipath channel environment has an extremely high complexity. Indeed, whereas physical layer events take place on a sub-nanosecond timescale, higher layer events such as packet reception and forwarding occur on a timescale of milliseconds. This sheer number of events makes it infeasible to directly derive the BER from a pulse-level simulation of the physical layer. Hence, fast and accurate methods to compute the BER are necessary. Our solution is based on a novel combination of large deviation and importance sampling.

1.3 Contributions

The main contribution of this thesis is a practical architecture for interference management in a multi-hop and low data-rate IR-UWB networks. This architecture fully takes into account the advantages and the specifics of IR-UWB physical layers. In the chapters of this thesis, the performance of this architecture is thoroughly evaluated and issues at both the physical layer and the link layer are treated.

The detailed list of contributions is as follows:

- We derive the optimal rate efficient design principles for low data-rate IR-UWB networks: With an interference mitigation scheme at the physical layer, interference should not be prevented. It should be managed with a rate adaptation scheme. Power control is not necessary and sources can send whenever they a have a packet ready to transmit.
- The previous result is optimal in terms of rate efficiency. In terms of energy efficiency, this is not optimal. But we obtain evidence that it is close to the optimal.
- We propose a PHY-aware MAC protocol for IR-UWB networks that is based on the above rate efficient design principles. Notably, this protocol exhibits a stable throughput in multi-hop topologies with both TCP and UDP.
- We develop an analytical model to compute the saturation throughput of homogeneous and symmetric IR-UWB networks taking into account packet detection and timing acquisition. We obtain the equivalent of the classical Bianchi's formula for an IR-UWB network with packet detection and timing acquisition.
- We show the benefits and importance of using private acquisition preambles for IR-UWB networks: Using a common acquisition preamble leads to gross unfairness and huge performance anomalies.
- We implement and demonstrate on a hardware testbed a packet detection and timing acquisition mechanism with concurrent transmissions. This demonstrates the feasibility of concurrent transmissions in IR-UWB networks.
- For the performance evaluation of IEEE 802.15.4a with energy detection receivers, we cannot implement a full network due to the prohibitive complexity. Hence, we develop a methodology to obtain performance results that are meaningful in a network setting, where we only simulate a single receiver with several transmitters.

- We develop an IR-UWB receiver architecture, based on energy detection, that is robust to MUI and adapted to the peculiarities of the signaling of IEEE 802.15.4a. This architecture shows the feasibility of a practical, and low-complexity receiver with an interference mitigation scheme for IR-UWB networks.

- We develop an architecture of an IR-UWB physical layer implementation in ns-2, a packet-based network simulator. Our implementation comprises a packet detection and timing acquisition model and takes into account transmissions using different time-hopping sequences. This architecture is generic and allows for the simulation of multiple-access physical layers.

- We consider the computation of the bit error rate (BER) of an IR-UWB physical layer in a network setting. We take into account multipath propagation and multi-user interference. Based on a novel combination of large deviation and importance sampling, we develop a fast and efficient algorithm that computes the conditional BER given the multipath channels and delay differences between the transmitters and the receiver.

Chapter 2

IR-UWB Networks: System Model and Assumptions

In this chapter, we describe the system model and assumptions used throughout this thesis. We begin with the model of the network and the associated hypotheses. Then we move on to the model and assumptions of the IR-UWB physical layer. We provide the necessary information to understand the subsequent chapters. In particular, in addition to background materials and related work on impulse-radio, we also discuss the IEEE 802.15.4a IR-UWB physical layer. Indeed, in Parts I and III a traditional IR-UWB physical layer is used, but Part II uses the IEEE 802.15.4a physical layer.

2.1 Network Model and Assumptions

We generally consider multi-hop ad hoc networks with no infrastructure, and no central coordinators or clustered structure. Members of the network are interchangeably called *stations*, *nodes*, or *devices*. There is no global synchronization in the network, e.g. the nodes do not share a common clock. The network is packet-based and the first step towards the correct reception of a packet is packet detection and timing acquisition (see Section 2.2).

We focus on low data-rate systems, where the raw bit-rate offered by the physical layer is on the order of 1 Mbit/s (except for Chapter 5 where the bit-rate is higher, around 18 Mbit/s).

2.1.1 Network Assumptions

Here is a list of important assumptions on the network:

- The underlying physical layer is an IR-UWB physical layer with time-hopping (see Section 2.2 below). All nodes have the same physical layer.
- Nodes can either send, receive, or listen. They can transmit to, or receive from one node at a time. In particular, a node can achieve timing acquisition with only one source at at time.
- Nodes can listen, however, to IR-UWB signals transmitted with different time-hopping sequences at the same time.
- Carrier-sensing is not feasible. Due to the low emitted power of an IR-UWB signal, the intermittent nature of the signal, and the possible absence of an actual carrier, it appears hardly feasible to do carrier-sensing or clear channel assessment (CCA) without an actual decoding of the signal.

2.2 Physical Layer Model and Assumptions

IR-UWB physical layers make use of extremely short duration pulses that yield ultra-wide bandwidth signals (a pulse duration of 2 ns yields a bandwidth of roughly 500 MHz). The pulses are sent infrequently, with a typical duty cycle of 1% for low data-rate systems.

Due to their very wide bandwidth that typically overlaps with the bandwidth of existing systems, UWB systems are also characterized by extremely low power spectral densities. There are stringent radio spectrum regulations already in effect in the USA [4], in the European Union [5], in Switzerland [6], as well as Japan and Singapore. For example, in the European Union, the maximum mean e.i.r.p. spectral density is of -70.0 dBm/MHz from 3.8 to 6 GHz (-41.3 dBm/MHz from 4.2 to 4.8 GHz before 2011) and of -41.3 dBm/MHz from 6 to 8.5 GHz [1]. In contrast, the maximum e.i.r.p. indoor for IEEE 802.11 devices in Switzerland is equal to 100 mW. With a bandwidth per channel of 22 MHz, this corresponds to roughly 6.6 dBm/MHz.

2.2.1 IR-UWB with Time-Hopping

The classic IR-UWB physical layer model [7, 8, 9] is illustrated in Figure 2.1 and explained in the following. Time is divided into frames of duration T_f and there is one pulse of duration T_p transmitted per frame.

[1] The maximum mean e.i.r.p. spectral density is the highest signal strength measured in any direction at any frequency within the defined frequency range. The mean e.i.r.p. spectral density is measured with a 1 MHz resolution bandwidth, an RMS detector and an averaging time of 1 ms or less.

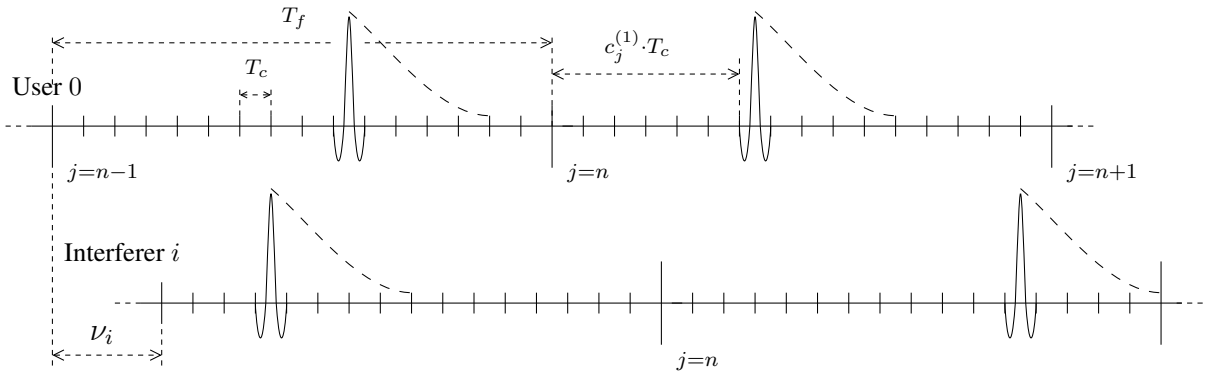

Figure 2.1: Impulse-radio UWB physical layer with time-hopping: $c_j^{(i)}$ denotes the time-hopping sequence of user i and ν_i is the delay between interferer i and the user of interest (user 0). The dashed curve following each pulse represents the multipath propagation channel. The time-hopping positions for user 0 are 9 and 6 and for user i are 3 and 12.

As the pulses are sent infrequently, several transmitters can share the medium concurrently. However, the transmission time of each pulse has to be randomized to avoid catastrophic collisions [7]. Hence, a frame is further subdivided into N_c non-overlapping *chips* of duration T_c, where T_c is generally larger than T_p and $N_c \cdot T_c = T_f$. For each frame, these chips define the possible locations for the transmission of a pulse. Due to the multipath propagation channel and to avoid inter-symbol interference (ISI), a guard time of duration T_g can reduce the number of available positions to $N_c - N_g$ where $N_g \cdot T_c = T_g$. A so-called time-hopping sequence (THS) of integers in $[0, N_c - N_g - 1]$ indicates which position to choose in each frame for the transmission of a pulse. In addition, by varying the duration between the transmission of subsequent pulses, the THS reduces or even avoids peaks in the power spectral density of the transmitted signal [10, 11].

In order to transmit information with an IR-UWB physical layer, several digital modulations can be employed[2]: in particular, pulse position modulation (PPM) and pulse amplitude modulation (PAM) [12]. With binary PPM (BPPM), a 1 is distinguished from a 0 by a slight delay of the pulse (typically, a few nanoseconds). Furthermore, pulse position modulation can easily be used with an M-ary alphabet with a given delay with respect to a reference position for each symbol of the alphabet [13]. With pulse amplitude modulation, a 1 is distinguished from a 0 by varying the amplitude of the pulse. For example, a positive and negative fixed amplitude can be use to differentiate between two symbols, which is equivalent to binary phase-shift keying (BPSK). Another possibility is on-off keying (OOK) where two symbols are transmitted

[2] [9] discusses analog modulation for IR-UWB

with the presence or absence of a pulse. A combination of PPM and PAM is also possible. More formally, a typical IR-UWB signal with BPPM can be modeled as

$$s(t) = \sum_i p(t - iT_f - c_i T_c - d_i T_m) \tag{2.1}$$

where $p(t)$ is a unit energy pulse, c_i is an element of the THS, $d_i \in \{0, 1\}$ is the information-bearing bit, and T_m is the position offset. This is a baseband model, that does not take into account a possible up-conversion. For BPSK, the transmitted signal can be modeled as

$$s(t) = \sum_i d_i \cdot p(t - iT_f - c_i T_c) \tag{2.2}$$

where now $d_i \in \{-1, 1\}$.

One distinctive characteristic of UWB systems is their multipath resolvability. In indoor environments, multipath occurs due to reflection, refraction and scattering of radio waves by surrounding structures. The transmitted signal reaches the receiver by more than one path [14]. In a narrow-band system, the components of the signal arriving from indirect paths and the direct path combine to produce a distorted version of the transmitted signal. In a UWB system, a direct consequence of the short duration of the pulse is that multiple paths may be separately identified [15, 16, 17]. In this case, the received signal comprises several delayed, distorted and attenuated pulses that each correspond to a particular path. A real-valued, continuous-time, baseband model for the channel impulse response is [18, 14]

$$\sum_{l=0}^{L-1} \alpha_l \delta\left(t - \tau_l - \nu\right) \tag{2.3}$$

where δ is a Dirac delta function, α_l is the attenuation coefficient and τ_l is the delay induced by the lth propagation path, L is the maximum number of paths, and ν is the propagation time between the source of the signal and the destination. This is a relatively simple model that ignores frequency and path dependent effects on the shape of the transmitted pulse $p(t)$ [17]. Also, this model is time-invariant as α_l and τ_l do not depend on t. Typically, this assumption corresponds to a packet based network where the channel impulse response is considered to be fixed for the duration of a packet transmission. A channel impulse response is then sampled from a given distribution for each packet to be transmitted.

There exists a large body of work regarding the characterization of propagation environ-

ments and of distributions for channel impulse responses [18, 14], and in particular for UWB channels [17, 19, 20, 21, 22, 23, 24, 25, 26, 27].

Taking the convolution of the transmitted BPSK signal (2.2) with the channel impulse response in (2.3), we obtain

$$r(t) = \sum_i d_i \sum_{l=0}^{L-1} \alpha_l p(t - iT_f - c_i T_c - \tau_l - \nu) \tag{2.4}$$

where $p(t)$ can represent the received pulse after being filtered by the transmission and reception antennas, as well as any other RF component, for instance a bandpass filter. To ease the notation and concentrate on the features or the receiver, we temporary ignore in equation (2.4) the contribution of thermal noise and interference.

2.2.2 From Rake Receivers to Energy Detection Receivers

To fully take advantage of the received signal in (2.4), the optimal single user receiver is a coherent Rake receiver [28] that performs maximum ratio combining (MRC) [29]. Because it is required in several chapters of this thesis, we describe the functioning of a Rake receiver for an IR-UWB signal with BPSK modulation. In such a receiver, the channel impulse response has been previously estimated to obtain the estimates $\hat{\alpha}_l$ and $\hat{\tau}_l$ for $l = 0, 1, \ldots, L-1$ of the quantities α_l and τ_l in equation (2.3). Furthermore, a timing acquisition algorithm has obtained an estimate $\hat{\nu}$ of the propagation time ν. We also assume that $p(t)$ is the received pulse. Note that the number of paths L is also a quantity that could be estimated. The received signal in equation (2.4) is first matched filtered with $p(-t)$:

$$y(t) = \int_{-\infty}^{\infty} r(\tau) p(-t + \tau) d\tau \tag{2.5}$$

With an appropriate change of variable and a few manipulations, (2.5) can be rewritten as

$$y(t) = \sum_i d_i \sum_{l=0}^{L-1} \alpha_l \Theta\left(t - iT_f - c_i T_c - \tau_l - \nu\right) \tag{2.6}$$

where $\Theta(t)$ is the auto-correlation of $p(t)$. Then, for each frame i, the output of the matched filter is sampled at

$$t_l = iT_f + c_i T_c + \hat{\tau}_l + \hat{\nu} \tag{2.7}$$

for $l = 0, 1, \ldots, L-1$, yielding L samples $y_0[i], y_1[i], \ldots, y_{L-1}[i]$. Finally, the MRC operation consists of computing a weighted sum. The output of the MRC is

$$\begin{aligned} Y[i] &= \sum_{l=0}^{L-1} \hat{\alpha}_l \cdot y_l[i] \\ &= d_i \sum_{l=0}^{L-1} \hat{\alpha}_l \sum_{l=0}^{L-1} \alpha_l \, \Theta\left(\hat{\tau}_l - \tau_l + \hat{\nu} - \nu\right). \end{aligned} \tag{2.8}$$

Hence, whether or not we gather all the transmitted energy depends on the bandwidth of $p(t)$ through the width of the support of $\Theta(t)$, on the channel characteristics through τ_l, and on the accuracy of our estimates of α_l, τ_l, and ν.

Instead of MRC, different sub-optimal combining schemes can be applied [30, 31], which yield close to optimal performances with a reduced complexity. MRC is optimal when the noise statistic is Gaussian. If the noise statistic is not Gaussian, it can be beneficial to combine and weight the samples according to a minimum mean-square error criterion (MMSE) [32].

However, most of the complexity associated with a Rake receiver comes from high sampling frequency requirements in order to (1) properly estimate the characteristics of the propagation channel between the source and the destination, in particular τ_l [33], and (2) ensures a fine synchronization with the transmitted signal because the performance of the Rake receiver for IR-UWB systems is significantly reduced by timing impairments [34, 35].

A possibly less complex option is to use an energy detection receiver [36]. An energy detection receiver might only need to estimate the power delay profile of the propagation channel [37] or the duration of the channel impulse response [38]. It can generally operate at a lower sampling frequency and is robust against timing impairments [39]. Unfortunately, it is also less robust to interference than a coherent Rake receiver. And it cannot take advantage of the full diversity offered by the ultra-wide band channel. The signal at the output of a very simple energy detection receiver is

$$y(t) = \int_t^{t+T} \left[r(u)\right]^2 du \tag{2.9}$$

where T is the integration time or integration window of the energy detection receiver.

From an energy detection receiver to a Rake receiver, there is a whole "space" of receiver, that use an increasing amount of information about the channel impulse response [40]. There exist other types of receivers, for instance differential detectors [41] or receivers based on a transmitted reference architecture [42, 30, 43, 44, 45]. These are not considered in this thesis.

2.2.3 IR-UWB as a Multi-Channel Physical Layer

The IR-UWB physical layer with time-hopping allows several users to share the medium concurrently. This multiple-access capability of IR-UWB physical layers stems from time-hopping. Unlike narrow-band systems, the collision of packets from different transmitters do not fully destroy the underlying radio signals. In fact, if several users transmit concurrently with distinctive THSs, only occasional signal collisions will occur between the concurrent signals because the pulses from the different users are not transmitted at the same time.

Additionally, interference mitigation schemes at the physical layer (see Section 2.2.4) can take advantage of the structure of impulse-radio signals to further reduce the effect of interference from concurrent transmitters [46, 47, 48], especially in near-far cases.

From a networking point of view, the IR-UWB physical layer can be seen as a multi-channel physical layer by considering each THS as a particular channel.

In the case where we have U signals transmitted at the same time, we can revisit the calculation of the output of the Rake receiver to add the contribution of the $U-1$ other signals. We still ignore the contribution of thermal noise. We add a superscript (u) to each quantity that is user specific and let the user with index 0 be the user of interest. The received signal of equation (2.4) becomes

$$r(t) = \sum_{u=0}^{U-1} \sum_{i} d_i^{(u)} \sum_{l=0}^{L^{(u)}-1} \alpha_l^{(u)} p(t - iT_f - c_i^{(u)} T_c - \tau_l^{(u)} - \nu^{(u)}). \tag{2.10}$$

The output of the filter in equation (2.6) becomes

$$y(t) = \sum_{u=0}^{U-1} \sum_{i} d_i^{(u)} \sum_{l=0}^{L^{(u)}-1} \alpha_l^{(u)} \Theta \left(t - iT_f - c_i^{(u)} T_c - \tau_l^{(u)} - \nu^{(u)} \right). \tag{2.11}$$

After sampling at $t_l = iT_f + c_i^{(0)} T_c + \hat{\tau}_l^{(0)} + \hat{\nu}^{(0)}$, the output of the MRC operation of equation (2.8) becomes

$$\begin{aligned} Y[i] &= \sum_{l=0}^{L-1} \hat{\alpha}_l \cdot y_l[i] \\ &= Y_0[i] + \sum_{u=1}^{U-1} Y_u[i] \end{aligned} \tag{2.12}$$

where

$$Y_0[i] \;=\; d_i^{(0)} \sum_{l=0}^{L^{(0)}-1} \hat{\alpha}_l^{(0)} \sum_{l=0}^{L^{(0)}-1} \alpha_l^{(0)}\, \Theta\left(\hat{\tau}_l^{(0)} - \tau_l^{(0)} + \hat{\nu}^{(0)} - \nu^{(0)}\right) \tag{2.13}$$

is the contribution from the user of interest and

$$\begin{aligned} Y_u[i] \;=\; & d_i^{(u)} \sum_{l=0}^{L^{(0)}-1} \hat{\alpha}_l^{(0)} \sum_{l=0}^{L^{(u)}-1} \alpha_l^{(u)}\, \Theta\left(\left(c_i^{(0)} - c_i^{(u)}\right) T_c + \hat{\tau}_l^{(0)} - \tau_l^{(u)} + \hat{\nu}^{(0)} - \nu^{(u)}\right) \\ & + d_{i-1}^{(u)} \sum_{l=0}^{L^{(0)}-1} \hat{\alpha}_l^{(0)} \sum_{l=0}^{L^{(u)}-1} \alpha_l^{(u)}\, \Theta\left(T_f + \left(c_i^{(0)} - c_{i-1}^{(u)}\right) T_c + \hat{\tau}_l^{(0)} - \tau_l^{(u)} + \hat{\nu}^{(0)} - \nu^{(u)}\right). \end{aligned} \tag{2.14}$$

is the contribution from the uth user. The reason behind the occurrence of both the ith and $(i-1)$th symbol from the uth user in $Y_u[i]$ depends on the particular value of the delay $\hat{\tau}_l^{(0)} - \tau_l^{(u)}$ between the user of interest and the uth user.

IR-UWB physical layers with time-hopping can also be interpreted as a code-division multiple access (CDMA) system with unbalanced spreading codes [49].

2.2.4 Interference in IR-UWB Networks

IR-UWB systems are subject to impulsive, non-Gaussian interference created by the system itself, or by other, similar systems (see [50, 51, 52, 53, 54] and a detailed discussion in Section 3.3.1). Further, UWB systems have to coexist with existing narrow-band technologies such as 802.11 [55]. Managing interference to and from such coexisting narrow-band technologies has been extensively studied (see for instance [56, 57, 58, 59]) and is not discussed in this thesis.

In this thesis, we consider the impulsive interference created by similar UWB systems. The main source of impulsive interference in IR-UWB systems are pulse collisions between concurrently transmitting sources. Pulse collisions occur even though nodes generally use different THSs. This is due to the fact that THSs in IR-UWB are usually not orthogonal and therefore do not completely prevent collisions. Furthermore, even if they were perfectly orthogonal, a tight synchronization between all the nodes would be needed to prevent interference caused by misaligned THSs.

Furthermore, the multipath propagation channel worsens the situation. The larger the delay spread of the channel, the more a pulse is spread in time. This increases the probability of

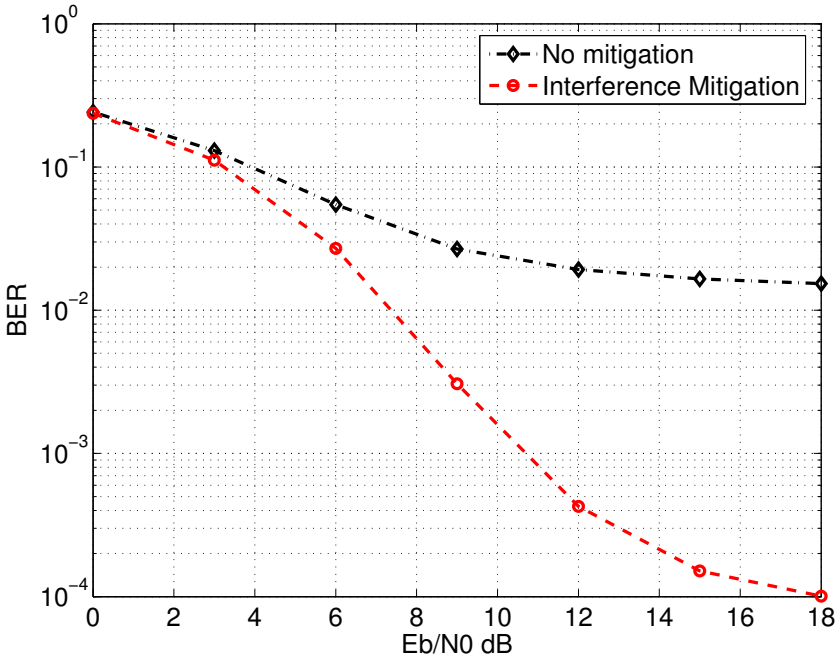

Figure 2.2: This example comes from [47]. In uncoordinated IR-UWB networks, especially in strong near-far scenario some form of interference mitigation at the physical layer is beneficial. We show the bit error rate (BER) versus signal-to-noise ratio at the receiver for a system with and without interference mitigation. The scenario is a very strong near-far case. Packets are generated according to a Poisson process at half the peak data rate. The channel model simulated is the 802.15.4a indoor NLOS model. Further, there are four interferers with power levels of 10dB, 13dB, 16dB and 20dB higher with respect to the user of interest. There is a simple repetition code with rate $1/4$. IR-UWB systems are generally very robust to interference, but near-far cases can still cause strong degradations as it can clearly be seen. The mitigation scheme used here is one using interference modeling (described in [47]).

signal collisions. As IR-UWB systems are likely to be used in environments exhibiting severe multipath (indoor, factories, etc.), this is a serious issue. Another factor that increases the probability of pulse collisions is the number of users trying to transmit simultaneously. Even in systems with a generally low duty-cycle, it can happen that many users access the channel at the same time. For instance, a sensor network detecting a fire outbreak. In this case, a specific event triggers simultaneous transmissions from a large number of nodes.

Still, the IR-UWB physical layer remains relatively robust to interference stemming from concurrent transmissions. But, one additional important factor concerning interference is the near-far effect: to quote Robert Scholtz "the near-far effect is only a factor when a strong pulse and a weak pulse happen to collide" [7]. Interferers close to the receiver can have a much higher signal strength compared to the user of interest. To ensure that small portions of these high power signals do not predominate the received signal an interference mitigation scheme can prove beneficial to prevent a huge performance loss. In Figure 2.2, we can clearly observe the detrimental effect of interference in a near-far scenario if no specific measure is taken.

The near-far problem is of course not specific to UWB systems. It is well known in CDMA systems. There, it is solved by power control. But even with power control, near-far signals can be created by transmitters running in other networks that are completely uncontrolled. One example might be several IEEE 802.15.4a piconets that run in close vicinity to each other.

2.2.5 Packet Detection and Timing Acquisition

As the network is packet-based and there is no global synchronization, the first step towards the correct reception of a packet is packet detection and timing acquisition. For a particular destination, it consists of detecting the packets that are intended for itself and find the time reference of the source. Only then can the destination recover the payload by demodulating the received signal. Notice that even if their exists a global synchronization in a network, packet *detection* may still be necessary.

Packet detection and timing acquisition is performed on a per packet basis and typically relies on the presence of a so-called acquisition preamble at the beginning of each packet. This acquisition preamble can be generated using a THS, amplitude modulation, or a combination of both. The exact functioning of a packet detection and timing acquisition algorithm is out of the scope of this thesis. The interested reader can consult [60, 61, 62, 12]. For articles specific to IR-UWB, the reader can consult [63] and the references therein.

2.2.6 IEEE 802.15.4a Physical Layer

The IEEE 802.15.4a amendment [64] specifies an IR-UWB physical layer for the IEEE 802.15.4 standard [65, 66] that can operate over several bands of 500 MHz (or 1.5 GHz) from approximately 3 GHz to 10 GHz.

As in the classic IR-UWB physical layer described previously, the IEEE 802.15.4a amendment uses time-hopping to smooth the spectrum of the signal and to mitigate the possible impact of multi-user interference. The modulation is a combination of BPPM and BPSK preceded with a concatenated Reed-Solomon/convolutional code. The Reed-Solomon (RS) code is a $(55, 63)$ code (rate 0.87) and the inner convolutional code has rate $1/2$. The exact details of both the RS code and the convolutional code can be found in [64]. The IEEE 802.15.4a amendment does not specify a particular receiver. Hence, if a coherent receiver is used, both the convolutional code and the RS code are used with the combination of BPPM and BPSK. However, with a non-coherent receiver, only BPPM is used with the RS code without convolutional encoding. As in this thesis we address energy detection receivers for IEEE 802.15.4a in Part II, we consider BPPM and RS coding only.

An IEEE 802.15.4a packet consists of a preamble followed by a data part. The main difference with respect to the classic IR-UWB physical layer lies in the signal format of the data part. Instead of sending a single pulse per frame, a short, continuous burst of pulses with pseudo-random polarity is sent. For a payload of L_p bits, the transmitted signal is made of L_p frames of duration T_f. A frame is further divided into N_c chips of T_c seconds. In each frame, a single burst of L_b pulses is transmitted. A burst of pulses is the concatenation of L_b pulses, whose amplitudes are modulated by a binary scrambling sequence. A pulse has duration T_p. The location of the burst inside the ith frame depends on the ith data bit d_i and on the time-hopping sequence: it is a sequence $\left[c_o, c_1, \ldots, c_{L_p-1}\right]$ of integers chosen in $\{0, 1, \ldots, N_{hop} - 1\}$ where $N_{hop} = \frac{T_f}{4L_bT_c}$. Note that half of the duration of the frame is not used to make sure that there is a sufficient guard time to avoid inter-symbol interference (ISI). The burst inside the lth frame is then time-shifted by $c_iL_bT_c + d_iT_f/2$ with respect to the beginning of the frame. The binary scrambling sequences and the time-hopping sequences are generated by a linear feedback shift register (LFSR, the reader shall refer to the amendment for the specification). Note that the LFSR is initialized to the same state for the transmission of each packet. Hence, all transmitters have the same scrambling sequence and time-hopping sequence. The transmitted signal of

an IEEE 802.15.4a data part can be modeled as

$$s(t) = \sum_{i=0}^{L_p-1} \sum_{j=0}^{L_b-1} b_{i,j} \cdot p\left(t - iT_f - c_i L_b T_c - d_i T_f/2 - jT_c\right). \tag{2.15}$$

where $b_{i,j} \in \pm 1$ is the pseudo-random polarity of the j-th pulse of the i-th symbol specified by the scrambling sequence. The received signal for the data part, after filtering with a bandpass filter of bandwidth B, is then given by

$$r(t) = \sum_{i=0}^{L_p-1} \sum_{j=0}^{L_b-1} b_{i,j} \cdot h(t - iT_f - c_i L_b T_c - d_i T_f/2 - jT_c) + n(t) \tag{2.16}$$

where $h(t)$ is the unknown channel response (including the convolution of the transmitted waveform with the impulse response of the channel and the bandpass filter), $n(t)$ accounts for thermal noise and MUI. It is assumed that the duration of $h(t)$ is shorter than $T_f/4$ to prevent ISI. Both c_i and $b_{i,j}$ are known to the receiver.

The preamble preceding the payload is constructed from a ternary preamble code: this preamble is a sequence of 31 elements in the set $\{-1, 0, 1\}$. Several preamble codes with perfect autocorrelation properties are available [64]. The preamble is constructed by first repeating the preamble code N_{sync} times, and then by up-sampling by a factor L_{up}[3]. A start frame delimiter (SFD) is added to the preamble. The SFD is constructed similarly to the preamble with N_{sfd} instead of N_{sync} (see [64] for the details). The resulting sequence is then amplitude modulated to produce the preamble. The main differences with respect to the data signal are that (1) no time-hopping is used and (2) single pulses are transmitted instead of bursts of pulses. Note that for each frequency band, the IEEE 802.15.4a amendment foresees the use of two different preamble codes. The transmitted signal $s^{pre}(t)$ of an IEEE 802.15.4a preamble can be modeled as

$$s^{pre}(t) = \sum_i c_i^{pre} p\left(t - iL_{up}T_c\right) \tag{2.17}$$

where c_i^{pre} is the preamble code. The corresponding received signal is

$$r^{pre}(t) = \sum_i c_i^{pre} \cdot h(t - iL_{up}T_c) + n(t). \tag{2.18}$$

[3]The up-sampling operation adds $L_{up} - 1$ zeroes between each elements.

2.2.7 Rate-Compatible Punctured Convolutional Codes

The IR-UWB physical layer can naturally provide some form of redundancy as a symbol can be transmitted over several pulses using a simple repetition code [7]. Similar to spread-spectrum systems, this repetition code provides a processing gain.

In several chapters, we use a more sophisticated rate-compatible punctured convolutional (RCPC) code [67] to replace or supplement the repetition code. A RCPC code is a variable rate channel code. It allows for data to be encoded and decoded at different rates with a single pair of an encoder and a decoder. This is possible thanks to puncturing: from a low rate codeword, bits are removed to obtain a higher rate codeword. Generally, from a parent code of rate $\frac{1}{n}$ we obtain a family of $(n-1)p$ different codes with rates

$$R = \frac{p}{np}, \frac{p}{np-1}, \ldots, \frac{p}{p+1}. \tag{2.19}$$

where p is the puncturing period [67]. Furthermore, with the rate compatibility feature, the bits of a codeword are always a subset of the bits of a lower rate codeword. Hence, RCPC code can provide incremental redundancy: Whenever a given codeword cannot be decoded, it is only necessary to send the additional bits to obtain a lower rate codeword and not the complete lower rate codeword.

In this thesis, we use the RCPC code from [68]. The available code rates are

$$R_n = \left\{ \frac{8}{9}, \frac{8}{10}, \frac{8}{11}, \ldots, \frac{8}{32}, \frac{1}{5}, \frac{1}{6}, \ldots, \frac{1}{10} \right\}, \quad n = 0, \ldots, 30, \tag{2.20}$$

where the codes of rate $\frac{1}{5}$ to $\frac{1}{10}$ are obtained by an additional nesting procedure where an additional generator polynomial is used. With this code, we obtain a fairly large set of available rates. They will be used for rate adaptation algorithms in Part I.

2.2.8 Physical Layer Assumptions

Thereafter, we shortly summarize the assumptions on the physical layer models used throughout this thesis.

We assume that the physical layer has a single transceiver, with single-user receivers. No multi-user receivers performing joint decoding of several transmitters are assumed. Such receivers have an extremely high complexity and require a receiver to be synchronized with all the signals to be decoded. We believe these requirements are currently not compatible with the

objective of low-complexity.

Parts I and III: Classic IR-UWB

In Parts I and III, we use a classic IR-UWB physical layer:

- BPSK modulation or BPPM.
- Time-hopping sequences chosen from a uniform distribution.
- Acquisition preambles constructed from the same time-hopping sequence than the data part.

Part II: IEEE 802.15.4a IR-UWB

In Part II, we use the IEEE 802.15.4a physical layer. We follow the mandatory set of parameters with an architecture of the receiver based on energy detection:

- BPPM only
- The time-hopping sequence depends on the preamble code used by the transmitter.
- Acquisition preambles constructed from the preamble code.

Channel Model

For every packet transmission, the channel impulse response is assumed constant. We generally sample channel impulse responses according to the distribution specified by an IEEE 802.15.4a channel model in [22].

In Chapters 4 and 5, for complexity issues during the simulations, we use a simpler, five-tap, multipath channel. The channel coefficients are then sampled according to the model in [21]. A Rake receiver is used with this channel model.

Interference Mitigation in Chapters 4 and 5

In conjunction with the five-tap multipath channels, an interference mitigation scheme can be combined with the Rake receiver. It is used for the physical layer simulations in Chapters 4 and 5.

This is a simple scheme, inspired by [46]. It uses thresholding on the absolute value of the output of the MRC operation (see equations (2.8) and (2.12)). The threshold is set to

$$|\hat{y}^{mrc}[i]| + k\,|\hat{n}[i]| \tag{2.21}$$

where $|\hat{y}^{mrc}[i]|$ and $|\hat{n}[i]|$ are the absolute values of the estimates of the signal of interest at the output of the MRC and of noise, respectively. The factor k allows for adjusting the sensibility of the thresholding operation. In Chapters 4 and 5, k is typically found by extensive simulations. Samples whose absolute value is larger than the threshold are replaced by an erasure symbol. It is then left to the channel decoder to recover the erased symbols.

As we pointed out, this a very simple scheme and there more sophisticated schemes. But the goal of this scheme, in conjunction with the Rake receiver and the five-tap channel, is to have a physical layer model that captures the essential features of the IR-UWB physical layer.

Nonetheless, there is a detailed discussion of interference mitigation schemes for IR-UWB in Section 3.3.3. And we present a practical and low-complexity interference mitigation scheme, applicable to IEEE 802.15.4a radios, in Chapter 9.

Chapter 3

Related Work

In this chapter, we discuss the existing work on IR-UWB networks. We first complete and expand the related work on IR-UWB physical layers from Chapter 2. Then, we discuss several topics related to IR-UWB networks: the characterization of interference, the optimal organization, MAC protocols, and interference mitigation.

There are several overview articles that exist on IR-UWB physical layers. In [69, 70] regulatory issues and application scenarios are discussed. [55] provides a review of UWB multiple-access and modulation schemes along with associated receivers. [32] is a tutorial on UWB communications: It overviews channel modeling, timing acquisition, and the design of transmitters and receivers for UWB radios. [71, 72] address hardware and system issues, in particular on sensor networks in [72]. Finally [73] discuss ranging and localization in IR-UWB networks.

An important aspect of UWB is regulation with respect to spectral emissions. The references [4] and [5] are the official documents, for the USA and the European Union respectively.

3.1 The IR-UWB Physical Layer

The IR-UWB physical layer is a spread-spectrum physical layer. A tutorial on spread-spectrum technology can be found in [62] and an historic overview in [74]. Interestingly, there are mentions of time-hopping and of using narrow pulses for a spread-spectrum physical layer in articles dating back to the sixties, for instance in [75].

The IR-UWB physical layer is described in [7, 8, 9]. These papers describe the traditional IR-UWB physical layer, with its frame format and time-hopping combined with BPPM. They

also give initial estimates of the performance of the IR-UWB physical layer with a Gaussian approximation on the statistics of the multi-user interference, and with a simple AWGN channel without multipath. Interestingly, [7] points out the potential advantage of time-hopping over code-division multiple access (CDMA) systems in case of near-far situations: for time-hopping systems, the near-far effect is only a factor when a strong pulse and a weak pulse happen to collide. The analysis in [9] is extended to M-ary PPM in [76]. The work in [77] also addresses M-ary PPM. From an information theoretic point of view, it was shown in [78] that the optimal wideband signaling scheme consists of sending infrequent short pulses.

An interesting comment is made in [79], where the author states that the combination of very narrow pulses and large number of multipath components require that the design of the receiver be fundamentally different than the design of receivers for narrow-band radios.

The robustness of an IR-UWB physical layer with a multipath propagation channel is assessed initially in [80, 15] and further studied in [13]. In addition, as already explained in Section 2.2.1, one distinctive characteristic of UWB systems is multipath resolvability [16, 17]. As such, the characterization of the properties of UWB multipath channels has attracted a very large interest. The properties of interest are the path loss, the delay spread, the distribution of the path amplitudes and delays, the correlation properties of these quantities, all in various propagation environment, with various bandwidths and center frequencies. The following is a list of relevant references: [17, 19, 20, 21, 22, 23, 24, 25, 26, 27]. Of particular interest are [22, 24], which describe the channel model for the IEEE 802.15.4a amendment used throughout this thesis. For references on channel modeling not specific to UWB, the reader can consult [18] and [14] and the references therein. Such channel models are useful for accurate simulations that require realistic models with the effects of path loss, multipath propagation, noise, and interference [81]. One example is for the design of IR-UWB Rake receivers, to understand whether or not the receiver needs to consider all the multipath to obtain a satisfactory performance.

The fine time resolution that allows for multipath resolvability is also advantageous for ranging [82, 73]. In fact, before being used for communications, impulse-radio was considered for radar applications [83]. The IR-UWB physical layer appears to be an excellent candidate for indoor ranging and localization applications [84], for distributed localization [85], and for joint distributed localization and communication applications [86, 87]. Ranging and localization are not topics that we address in this thesis. The reader can consult [73] for a UWB specific article on ranging and [88, 89, 90] for more general references. Another topic that we do not address is the detailed functioning of signal acquisition for packet detection and timing acquisition. The

interested reader can begin with [63] and the references therein, as well as [60, 61, 62, 12] for more tutorial explanations.

An IR-UWB physical layer has been considered for two standardization efforts. For the IEEE 802.15.3a amendment to the IEEE 802.15.3 standard [91, 92], the interest for an UWB physical layer was the very high rate obtained thanks to the large bandwidth. The document [93] describes one submission for an IR-UWB physical layer for the IEEE 802.15.3a amendment. For the IEEE 802.15.4a amendment [64] to the IEEE 802.15.4 standard [66, 65], an IR-UWB physical layer has actually been chosen. Compared to the existing narrow-band physical layer of the IEEE 802.15.4 standard, it should offer a better robustness against interference and multipath propagation channels, a higher data-rate, and the possibility of performing ranging between devices. The physical layer of the IEEE 802.15.4a amendment can operate over several bands of 500 MHz (or 1.5 GHz) from approximately 3 GHz to 10 GHz.

3.2 Rake Receivers and Energy Detection Receivers for IR-UWB

We already discussed the Rake receiver in Section 2.2.2, in particular sub-optimal combining schemes [30, 31, 94], the high sampling frequency required in order to properly estimate the channel characteristics [33], and its sensitivity to mistiming impairments [34, 35]. Indeed, due to the wide bandwidth, the coherent processing of IR-UWB signals is generally very sensible to timing jitters [34]. The performance of an IR-UWB Rake receiver in a multipath channel environment is addressed in [95, 13, 96]. As Part II concentrates on the design and performance evaluation of receivers based on energy detection, we will now discuss related work on energy detection receivers for IR-UWB.

The main advantage of an energy detection receiver is that it allows for exploiting the ranging capabilities and multipath resistance of IR-UWB with a relative low complexity. Both [97] and [39] considered a complete system with packet detection and timing acquisition followed by demodulation and exposed the excellent trade-off between complexity and performance of an energy detection receiver for IR-UWB. Energy-detection receivers are of interest for sensor networks applications, or IEEE 802.15.4 low data-rate networks, where energy consumption is of primary importance and devices should be inexpensive. Compared to Rake receivers, an energy detection receiver might only need to estimate the channel power delay profile [98, 37] and not the full channel statistics. The energy detection receiver can generally operate at a

lower sampling frequency and is robust against timing impairments [39, 99]. Unfortunately, it is less robust to interference than a coherent receiver [100]. Indeed, it cannot take advantage of the full diversity offered by the ultra-wide band channel, contrary to a Rake receiver [101, 102].

An energy detection receiver is to be used when no or partial knowledge of the propagation channel is available to the receiver. The work in [103] considers M-ary PPM and addresses the case where no information about the channel is available: The receiver simply collects the energies in the possible signal positions and compares them in order to produce the estimate of the transmitted symbol.

If some information about the propagation channel is available, many papers recognize that it is necessary to adapt the duration of the integration window of the energy detection receiver to the characteristics of the received signal (this duration is T in equation (2.9)). In fact, there is a trade-off to be found between the amount of signal integrated and the amount of noise collected [104]. There are several proposals of energy detection receivers where the integration time is adapted [38, 105, 106, 104, 107, 108]. There are also more sophisticated approaches [109, 98, 110, 37, 40], where the authors take advantage of partial channel state information in general for designing the receiver (and not only adapting the integration time), for instance, by using a weighting function. The work in [98, 37] clearly exhibits the optimality of an energy detection receiver with a weighting function when the interference consists only of additive white Gaussian noise (AWGN). For timing acquisition, [111] studies the use of a non-coherent Rake receiver: How many paths should be combined depending on the channel characteristics; how should they be combined; and what is the effect on the probability of false acquisition and missed detection. However, [111] does not suggest an algorithm to estimate the number of paths to select for a particular channel. In fact, to be really efficient, this receiver has to be adapted to the particular propagation channel of the received signal. Examples of hardware structures to implement an energy detection receiver can be found in [99, 112].

Even though energy detection receivers are extremely vulnerable to MUI, none of the work presented in the previous paragraph considers MUI. Furthermore, in the context of Part II, the related work also does not consider the transmission of bursts of pulses as used in the IEEE 802.15.4a amendment. As shown in Chapter 8, the performance degradation, if MUI is not taken into account, can be huge in the case a traditional energy detection receiver is used.

3.3 IR-UWB Networks

3.3.1 Characterization of Interference in IR-UWB Networks

We explained previously that IR-UWB with time-hopping is a spread-spectrum physical layer. Similarly to CDMA systems, IR-UWB can be used for multiple-access to the physical layer. However, the multiple-access interference (MAI) or multi-user interference (MUI) in IR-UWB systems exhibits very specific properties.

In particular, principally due to time-hopping, the statistics of the MUI can generally not be approximated with a Gaussian distribution [113]. Rather, the density of the MUI exhibits an impulsive shape and heavy tail characteristics [50, 51, 52, 53, 54, 114, 115]. In [113, 51], the BER obtained with a Gaussian approximation is not identical to results obtained with simulations. In [50, 53, 114], with the assumption of an AWGN channel, the distribution of the MUI obtained at the output of a matched filter exhibits an impulsive shape with a heavy tail. The same observation was made in [116], albeit with the assumption of a multipath channel. Using the same assumptions as [50] (simple AWGN channel), [53] shows that the distribution of the MUI is close to that of a Middleton Class A model [117, 118]. [52] identifies scenarios where the Gaussian approximation is invalid, for instance, when the average duration between the transmission of pulses is large or in the presence of heterogeneous received power levels. Finally, [54] studies why the MUI can not be approximated by a Gaussian approximation.

The modeling of the statistics of the MUI is important for several reasons: for example, when computing the BER with MUI in a network simulator, or for the performance evaluation of the physical layer. In fact, a statistical model of the MUI can be used for analytical computations or to speed-up Monte-Carlo simulations of the physical layer. Another example is the design of IR-UWB receivers robust to MUI, or the implementation of interference mitigation mechanisms at the physical layer or link layer. Such mechanisms become necessary with the increasing deployment of wireless networks, because interference management protocols can not prevent interference from uncontrolled activities in neighboring networks. Furthermore, as explained in [119] and further discussed in this thesis (see Chapter 4), there are cases where an exclusion protocol is not optimal and the implementation of an interference mitigation scheme at the physical layer is beneficial and necessary.

3.3.2 Computing Bit Error Rates in IR-UWB Networks

The efficient computation of the BER is one of the topics of Part III. Earlier work on the computation of the BER of an IR-UWB link with a single-user receiver and MUI [9, 76] uses a Gaussian approximation for the MUI. However, as the Gaussian approximation is not appropriate (see Section 2.2.4), subsequent work on the computation of the BER assumes non-Gaussian models for the MUI.

This work can be mainly divided into three areas. First, in [120, 50], the interference stemming from a single interferer at the output of the matched filter is modeled as a mixture of a Dirac function and uniform random variable. Assuming perfect power control, a combinatorial convolution formula is developed to compute the BER. Such an approach quickly suffers from combinatorial explosion when the number of interferers increases. Second, in [121, 122, 51] a characteristic function approach is taken. To obtain the BER, it requires numerical integrations for the inverse transform, which may not permit a fast implementation. Finally, a different approach is to use a statistical model for the MUI and to use it in the computations. Such an approach is very convenient for working analytically, but suffers from the difficulty of easily and accurately identifying the parameters of the distribution used to model the MUI with the characteristics of the physical layer. In [123], the interference is modeled as a Poisson distributed train of impulses. In [124] a generalized Gaussian approximation is used and in [116] a Gaussian mixture model is employed. In [125], the authors combine a combinatorial approach with a linear approximation of the cumulative distribution function of the MUI.

Note that except for the recent work [116] that takes into account the multipath propagation channel, most of the existing work makes the assumptions of an AWGN channel and the use of a coherent receiver.

3.3.3 Interference Mitigation

Interference mitigation is discussed in Chapter 4 and is one of the central topics of Part II. In the following paragraphs, we discuss interference mitigation techniques that can be implemented at the physical layer. Of course, one of the simplest way to mitigate interference is to prevent it, for example by coordinating access to the physical layer. But, as we already explained, this cannot prevent MUI due to uncontrolled activities in neighboring networks (e.g., several IEEE 802.15.4a piconets running in parallel). Interference must be taken into account already in the design of the physical layer.

Early work on the design of optimal receivers for the detection of signals in non-Gaussian

interference [126, 127] suggests applying a non-linear function on the received signal prior to demodulation. This suggestion stems from the approximation of the optimal receiver with an impulsive interference model, as the optimal receiver is too complicated for a realistic implementation. In [128], the author uses very simple thresholding operations as possible non-linearities. It is also shown in [128] that a Middleton Class A density can be approximated by a mixture of Gaussian distributions or a mixture of a Gaussian distribution with another heavy-tail distribution. There are several papers that study different thresholding operations or other non-linearities for receivers with non-Gaussian, impulsive interference: see for instance [129, 130, 131, 132, 133]. In particular, [133] shows the benefit of a hard-limiting correlator for a DS-CDMA receiver with impulsive noise.

In [134, 135] and [46], the use of a thresholding operation was rediscovered for IR-UWB to effectively mitigate MUI. In [46] the benefits of a thresholding structure on the achievable rate in IR-UWB networks are shown. In [135, 136] a thresholding structure is used for an IR-UWB channel with MUI and a AWGN channel. Surprisingly, the connection between non-Gaussian noise and the MUI for IR-UWB physical layer is only made in [53]. It is also interesting to note that an interference mitigation scheme such as [136] can be seen as an adaptive, single-user version of the multi-user "blinking receiver" in [137] in that it requires only the knowledge of the THS of the user of interest. Additional examples of receivers using such structures can be found in [138, 139, 140, 141, 115]. Other examples that do not use an impulse-radio physical layer but a DS-CDMA one, with an extremely simple channel model, are [142, 143]. All the related work reviewed so far used interference mitigation for demodulation. But interference mitigation schemes can be used for timing acquisition [63] or for time-of-arrival estimation. In this case, another recent idea is to use non-linear filters on the received signal as in [144] and [145].

Another possibility to design a receiver robust to MUI is first to derive the optimum receiver for a given non-Gaussian interference distribution and then to fit the non-Gaussian distribution to the measured distribution of the MUI [146, 47, 147, 48, 148]. For instance, in [47], the optimal receiver for an IR-UWB physical layer with a multipath channel and noise following a Gaussian mixture distribution is derived. Then, this receiver is used in a packet based schemes. At the beginning of each packet, a preamble is used to fit the Gaussian mixture distribution to the MUI and interference.

In order for schemes based on thresholding to be effective in practice, the threshold must be continuously adapted. In particular, with respect to the signal-to-noise ratio of the signal of interest. This adaptation is actually far from being trivial and no solution to this particular

problem is mentioned in the related work. In addition, schemes based on interference modeling are usually quite resource intensive. Also, except for [46] no prior work has considered the use of a thresholding mechanism with an energy detection receiver. All the related work considers coherent receiver structures.

We do not address interference mitigation techniques for narrow-band interference in this thesis. The interested reader can begin with [56, 57, 58, 59] and the references therein. There are also techniques integrated with the link layer to mitigate interference. We discuss them later in this chapter. Finally, it is important to understand that the interference mitigation schemes discussed in this section are not multi-user receivers. They are single user receivers that are obtained by assuming a noise statistic that is not Gaussian. For a detailed discussion on multi-user reception for IR-UWB, the reader can consult [149] and the references therein.

3.3.4 Optimal Organization of IR-UWB Networks

The work in [119] and in [150] addresses the optimal design of IR-UWB networks. There are several important findings in [119]. First, in a multi-hop IR-UWB network, unlike in wideband networks, the optimal MAC protocol does not depend on the choice of the routing. Hence, a traditional layered network architecture is applicable and the MAC protocol can be designed regardless of the choice of the routing protocol. Furthermore, for static networks, minimum energy routing is optimal, both from an energy and rate performance viewpoint. A second finding is about the optimal design of the MAC: while receiving a node should maintain an exclusion region around itself; nodes inside the exclusion region should remain silent during the reception, whereas nodes outside of this region can transmit in parallel. The size of the exclusion region depends only on the power constraints of the source of the transmission, and not on the length of the link or the positions of other nodes. Additionally, the receiver and its corresponding sender should adapt the rate of the transmission according to the amount of noise and interference at the receiver. Finally, when a node is transmitting, it should do so with maximum power. These findings give directions for the implementation of routing and MAC protocols. A routing protocol should be based on a distributed shortest path algorithm considering inverse links attenuations as the costs of links. To this end, any standard ad hoc network routing protocol (AODV, DSR) could be used to calculate the shortest path to the destination.

The optimal MAC protocol in an IR-UWB network should be a combination of rate adaptation and mutual exclusion. The size of the exclusion region should be adapted to the parameters

of the network. For low-rate, low-power IR-UWB networks, it might be that the size of the exclusion region is small enough that no exclusion protocol is necessary. Actually, in [150], the authors show that with a receiver able to mitigate interference at the physical layer, a non-coordinated MAC exhibits better performance than more complex coordinated solutions. An exclusion protocol, or power control, is not the optimal strategies in this setting. This result further suggests that most of the complexity should be invested in a receiver design (to mitigate MUI, as in [47]) instead of intricate MAC or signaling protocols. The work in [119, 150] is the foundation of Part I. There are other articles treating essentially the same topic with similar conclusions [151, 152, 153]. An earlier article [154] also demonstrated that nodes should transmit at maximum power. For articles discussing routing in IR-UWB networks with more details, the reader can consult [155, 156, 157]. Another interesting article that focuses on routing and energy efficiency is [158].

Another source of inspiration for the work in this thesis is [159]. In this article, sources have information to send to a central base station over a wireless channel. They do so at full power, as soon as they have something to transmit, but adapt the channel code in order to allow the central destination to properly decode in the presence of interfering sources. A striking feature of the model in [159] is that the optimal scheme does not require any power control.

3.3.5 MAC Protocols for IR-UWB Networks

There is a large body of work on practical MAC protocols for IR-UWB networks [160, 154, 161, 162, 163, 164, 165, 166, 167, 168, 169, 170]. All the MAC protocols use the IR-UWB physical layer with time-hopping of [7].

In [154], a joint power and rate link assignment problem is solved. Based on the solution to the optimal optimization problem, a suboptimal distributed algorithm is proposed: it is a distributed control admission function based on mutual exclusion. For each potential transmission, the potential interference that would be caused on existing transmission is evaluated. To do so, a source broadcasts an RTS-like control packet before sending data. Every neighbor that receives this control packet responds to the source, adding information that allows the source to evaluate if the data transmission is admissible or not. The approach is similar to [160]. In [161] an invitation based scheme is proposed. A node that is ready to receive broadcasts an invitation for other nodes to compete for access to it on a broadcast channel. There is no power control or rate adaptation in [161]. In [154, 160, 161] a separate broadcast channel is used to transmit all control packets. The broadcast channel is implemented with a specific THS known

to all nodes in the network. More recently, the work in [162, 163, 167] assumes that a specific hardware, based on a frequency-domain detection method, provides a way to detect activity on the medium for an IR-UWB physical layer. A CSMA [3] based MAC protocol is then proposed with a busy tone approach [171] to alleviate the hidden terminal problem inherent in CSMA. There is no power control or rate control used and the authors failed to recognize that multiple channels are available with an IR-UWB physical layer. The complexity, feasibility, and power consumption of the frequency-domain detection method is not evaluated. $(\text{UWB})^2$ is the MAC protocol described in [164]. As in [154], a pseudo-random THS is chosen dynamically for each packet transmission with a prior exchange of control packets on a broadcast channel. Whenever a device wants to talk to a particular destination, it starts an RTS/CTS exchange on a common channel. If the destination is not busy, it answers on the common channel and includes the particular dedicated THS in the CTS packet. The subsequent data transmission uses the particular time-hopping sequence proposed in the CTS packet. There is no power control or rate adaptation. The MAC protocol presented in [166] is called U-MAC. This protocol also uses dynamically chosen THSs for each packet transmission. Similar to [154], U-MAC tries to optimally set both the rate and the transmission power for each packet transmission. In [168], a MAC protocol based on mutual exclusion is proposed for a single-hop network. Except for [164], most of these protocols fail to recognize the radically different nature of the IR-UWB physical layer. They do not fully take advantage of the multiple channels available and of the robustness to interference of the physical layer. Furthermore, if they use multiple channels thanks to different THSs, all the protocols still rely on a common control channel. This creates a central point of contention in all these protocols. Also, several of them need mutual exclusion because they are designed for high-rate applications.

The MAC protocols in [169] and [170] explore the additional use of multiple UWB frequency bands. For instance, instead of transmitting an IR-UWB signal over a frequency band of 5 GHz, 10 bands of 500 MHz could be used. And it appears in [170] that a multiple band approach may offer a better throughput than a single band approach.

The IEEE 802.15 Task Group 3a reviewed proposals for an alternate UWB physical layer for the IEEE 802.15.3 MAC [92]. The MAC is not distributed but based on the concept of piconets, where a piconet coordinator grants access to members of the piconet on a TDMA basis.

There is a survey of MAC protocols for IR-UWB networks in [165] with additional references therein. In [172], a MAC using CSMA with a rate adaptation scheme is used on top of a direct-sequence UWB physical layer. But the rate adaptation scheme is only used to to track

the state of the channel and adapt the signal to noise ratio at the receiver (basically, the distance to the source and the destination). Rate adaptation is not used to adapt to MUI, which is managed by mutual exclusion or treated as collisions. The concept of rate adaptation has also been proposed for 802.11 networks [173, 174] for the same purpose. In contrast, in Chapters 4 and 5, we use rate adaptation as a mechanism to support multiple-access. Another interesting MAC protocol is CA-CDMA [175]. It is a power control protocol and originally implemented on a traditional DS-CDMA physical layer. A new transmission can proceed if it does not destroy any ongoing transmission in its vicinity. Power control is necessary, because of the asynchronism between the transmissions from different devices. Even if orthogonal sequences are used for the CDMA physical layer, transmissions still interfere with each other and are subject to near-far effects. The power control algorithm is similar to the one in [154]. Information about neighbors is obtained by exchanging control packets on a separate control channel and by overhearing.

The IR-UWB physical layer is actually a multi-channel physical layer and there are already several papers discussing MAC protocols for multi-channel narrow-band physical layers. The reader can start with [176] and the references therein.

3.3.6 Modeling of IR-UWB Networks

The approach we use in Chapter 4 for deriving an analytical model of an IR-UWB network makes a mean-field assumption and requires solving a fixed-point equation. This is similar to previous work in [177, 178, 179, 180]. Indeed, a mean-field assumption (or decoupling assumption) is done in [179, 180]. And [177, 178] rely on a similar independence hypothesis. However, our work is different in that it takes into account the IR-UWB physical layer with very different properties than the narrow-band physical layer assumed in the previous work. Moreover, we explicitly address packet detection and timing acquisition and study its effect on the network. To the best of our knowledge, packet detection and timing acquisition is ignored in the previous work on networking.

3.3.7 Simulation of IR-UWB Networks

To the best of our knowledge, except the work presented in Chapter 10, there is currently no other model of an IR-UWB physical layer available for ns-2 [181] or an other network simulator. Networks simulators (see the excellent list of references in [182]) such as ns-2, GloMoSim/Qualnet, Jist/SWANS, OMNET++, OPNET, yans [182] or GTNetS[183] allow for

the use and implementation of an error model at the physical layer. However, none of them appears to implement characteristic properties of the IR-UWB physical layer such as multiple channels, or to finely model an explicit packet detection and timing synchronization phase. But they allow the use of error models at the physical layer.

In particular, there are several extensions and modifications of ns-2[1]. In the case of 802.11, [173, 184] both implemented an error model based on signal to noise ratio computation but did not take the cumulative interference into account. Also in the case of 802.11, [185] implements an error model based on a signal to noise ratio calculation with a cumulative interference model. An interesting and more recent approach is [186] where the cumulative interference is taken into account: They do not use an error model, but rather declare a successful reception if the SINR is higher than a given threshold. Compared to our work in Chapter 10, the previous approaches are unfortunately specific to 802.11. Furthermore, there is no implementation of multiple channels or a precise model of the packet detection and timing synchronization state. A very promising work in the case of 802.11 is [187] (but not yet implemented in a network simulator); they propose a model to take into account transmissions on multiple overlapping frequency bands.

It is also worth noting the large body of work that addresses the impact of radio channel and propagation models on wireless network simulations. The reader can refer to [188, 189] and the references therein. Finally, [190] addresses the important issue of validation. Validation is currently very difficult in our case due to the lack of standard hardware. This situation should evolve with the successful completion of the IEEE 802.15.4a standard and the availability of IR-UWB transceivers.

[1] "Contributed Code" section of the ns-2 website available at
`http://nsnam.isi.edu/nsnam/index.php/Contributed_Code`, June 2008

Part I

Physical layer Aware MAC Protocols for IR-UWB Networks

Chapter 4

How to Design a PHY-Aware MAC for IR-UWB Networks: a Trade-offs Analysis

For the possible applications of low data-rate and low power IR-UWB networks, which we discussed in Chapter 1, there is a dual objective for the design of the network: the energy consumption should be minimized and the rate should be maximized. Usually, depending on the application, one of these objectives is more important than the other.

In order to satisfy these objectives, there exist numerous implementation possibilities offered by the medium access control (MAC) layer and the physical layer; a very large design space is available. Furthermore, if one option meets the rate objective it will not necessary minimize the energy consumption. A trade-off exists between these two objectives. The aim of this chapter is to understand the design and the implementation trade-offs for IR-UWB networks.

In traditional designs, there is a clear frontier between the MAC layer and the physical layer. The MAC layer manages interference with an exclusion protocol. It ensures that only one, single transmission occurs in a given interference domain. As a node can only receive a single transmission at a time, the MAC layer also arbitrates access to a given destination between concurrent sources. The MAC layer decides which nodes are allowed to transmit and when their transmissions are scheduled. In addition, the MAC should permit nodes to sleep when no data communication is necessary. The physical layer is responsible for packet detection and timing acquisition, modulation, and channel coding. It controls the rate and power level of the transmission. The physical layer is responsible for the actual transmission of information bits between the nodes that should communicate. In general, there is no interaction between the two layers and the MAC layer has no control over the power or rate used by the physical layer.

In a physical layer aware MAC design (or simply PHY-aware MAC), the MAC layer has access to some or all of the physical layer parameters. For example, as we will see in Section 4.1.1, interference does not need to be completely prevented, but it needs to be managed. The rate or the transmitted power at the physical layer can be dynamically adapted to the level of interference by the MAC layer. A PHY-aware MAC design is not a full cross-layer design. In a full cross-layer design, the physical layer might have access to information at the MAC or upper layers. This is not the case in a PHY-aware design. The motive to consider PHY-aware designs is to reduce the design space and the potential complexity.

An important design decision for a PHY-aware MAC is whether to allow interference by permitting concurrent and interfering transmissions or to enforce mutual exclusion. There are other important design decisions: Whether to allow random access or to impose some form of temporal structure within which transmissions have to occur; deciding whether to use power control; and how to coordinate nodes such that many of them can sleep. These choices have implications on both the physical layer and the MAC layer. As we will demonstrate in the first part of this thesis, a PHY-aware MAC protocol can significantly improve the performances.

This chapter is organized as follows: in Section 4.1, we explore the design space of PHY-aware MAC protocols; we discuss *what* functions a PHY-aware MAC design must provide (Section 4.1.1), *how* to implement them (Section 4.1.2) and how they are implemented in existing UWB designs (Section 4.1.3). Even though we focus on UWB in Section 4.1.3, the rest of Section 4.1 is not specific to UWB. In Section 4.2 we analyze the performance implications of fundamental design choices. We propose a method for evaluating energy consumption in the design phase of IR-UWB systems (Section 4.2.1) and derive a set of guidelines that can be used by system architects to orientate fundamental choices early in the design process (Section 4.2.3). We conclude this chapter in Section 4.3.

4.1 The Design Space of PHY-Aware MAC Protocols

4.1.1 What Functions Should a PHY-Aware MAC Provide ?

A PHY-aware MAC layer globally *manages* the interference and medium access on a shared communication channel. There are two complementary goals: to maximize the overall lifetime of the network, and to maximize the rate offered to each node, and possibly remaining fair. Hence, a PHY-aware MAC must provide the following set of functions:

- *Interference management*: A source can *control* the interference it creates by controlling

the transmission power or the time when a packet is transmitted, or it can *adapt* to the existing interference, by reducing its rate to permit reliable reception at the destination.

- *Access to a destination*: We assume that a node can either send or receive from one source. Thus, an exclusion protocol is necessary to enforce that only one source communicates with the destination. This *private* exclusion protocol only involves the potential sources and the destination.

- *Sleeping management*: It is of crucial importance in a low-power context. There exists an important trade-off between long sleep cycles, that permits for efficient energy savings, and short cycles that facilitate communication and improve responsiveness.

4.1.2 How Can the Functions of a PHY-Aware MAC be Implemented ?

In this section we review, according to published designs, how the functions above can be implemented. We give a list of nine building blocks, each of them contributing to one or several functions. The mapping between building blocks and functions is given in Table 4.1.

Rate Adaptation

Often, the transmission rate is adapted as a function of the channel condition (essentially the attenuation) between the source and the destination. However, the rate can also be adapted as a function of the interference created by other devices in the network.

Rate control with IR-UWB can be done by controlling the modulation order, the duration T_f of the frame, or the channel code rate used at the physical layer. The rate is often adapted based on feedback from the destination. This feedback is based on statistics gathered at the receiver either in a predictive or in a reactive manner. For the former, a source inserts *pilot symbols* in a packet and the channel is measured at the receiver based on the received pilot symbols. For the latter, the receiver typically looks at local statistics such as the likelihood ratios at the output of the receiver.

Interestingly, rate control involves no nodes other than the source-destination pair.

Transmitted Power Control

The transmission power can be adjusted to keep the signal-to-interference-and-noise ratio (SINR) at the destination above a given threshold for reliable decoding. It is also used to minimize the amount of interference created on the neighbors.

Contrary to rate control, power control requires interaction with other devices in the network. If a source increases its transmission power, it will create more interference on concurrent receivers. Hence, a source needs to know not only the minimum power required by its destination to ensure proper signal detection and decoding but also the maximum interference that ongoing transmissions in the vicinity of the transmitter can tolerate.

Mutual Exclusion

A mutual exclusion protocol prevents nodes from transmitting at the same time. Most traditional protocols use mutual exclusion to manage interference, but, as we will see in Section 4.2.3, mutual exclusion is not always necessary in IR-UWB networks. It is often implemented by control packet signaling (for example with an RTS/CTS handshake as in IEEE 802.11 [191]). The number of nodes affected depends on the transmission power of the control packets.

Multiple Channels at the Physical Layer

In a multi-channel protocol, the transmission medium is separated into several orthogonal or quasi-orthogonal transmission channels. There is no interference between transmission occurring on orthogonal channels, whereas there might be some interference occurring between transmissions on quasi-orthogonal channels. Because simultaneous transmissions can occur with multiple channels, there is a clear advantage in terms of rate increase. Still, a potential disadvantage (e.g., for broadcast) is that it becomes impossible to overhear transmissions from other active nodes on other channels. Quasi-orthogonal channels are inherent with an IR-UWB physical layer thanks to time-hopping. Note that for the channels created with time-hopping sequences to be perfectly orthogonal, a very accurate synchronization is required among transmitters and the sequences need to be non-overlapping and aligned in time. Other possibilities are to separate the bandwidth into non-overlapping sub-bands.

Quasi-orthogonal and orthogonal channels inherently solve the traditional hidden-node terminal problem present in single-channel protocols. Still, a physical layer with quasi-orthogonal channels might suffer from near-far scenarios.

Multi-User Reception

With a single-user receiver, all signals apart from the one coming from the user are treated as noise. With a multiple-user receiver, signals coming from several users can be successfully

received in a joint manner [192]. For example, a near-far interferer would be jointly received instead of being treated as interference. This annihilates near-far effects and makes multi-user reception potentially attractive. However, it generally requires the receiver to be accurately synchronized with all the sources that it wishes to decode and furthermore, the knowledge of all the transmitted signal characteristics. In addition, the complexity of a multi-user reception scheme is generally excessively high. Nevertheless, thanks to the particular structure of IR-UWB signal, there exists several sub-optimal techniques that are still worth considering, such as the interference mitigation techniques described in Sections 3.3.3 and 4.1.3.

Random versus Scheduled Access

Random access schemes are straightforward to implement in their simplest form, for instance Aloha [193, 194]. However, with a high utilization, their throughput becomes extremely low. As such, random access protocols are often improved with some of the following components:

- Carrier-sensing [3] avoids sending a packet on the channel if the channel is already busy. With IR-UWB physical layers, carrier-sensing is not well defined because there is not necessarily a carrier. One possibility for emulating carrier-sensing with IR-UWB is to actively decode. This is especially complex in a network with multiple time-hopping sequences, because a node has to sense for all possible time-hopping sequences.

- A back-off procedure with timer management is used to resolve collisions.

- A hand-shake procedure [195, 196] where nodes exchange control packets before each transmission is used to reserve medium access for data transmission. Because these packets are much shorter than data packets, the performance penalty in case of a collision is generally low in single-hop scenarios. However, they can drastically affect the performance in multi-hop scenarios (see [197] in the case of 802.11 networks). Such a hand-shake procedure can be private between a source and its destination or can involve more nodes.

Random access is typically used in ad hoc networks because it requires none or very few coordination among nodes.

An alternative is *scheduled access*. A schedule decides when and which nodes are allowed to send. It can allow only a single node to transmit (TDMA), or it can allow for multiple transmissions if they do not interfere significantly. Although this approach is more efficient

from a medium access point of view, it is very difficult to implement in large, self-organized networks where nodes do not all "hear" each other.

Time-slotted Structure

Slotted transmissions can reduce interference (as in slotted Aloha [198, 199]) or improve power saving because a node can sleep during unused slots. It also facilitates timing acquisition: with slots, the nodes are coarsely time synchronized.

Sleeping Mechanism: Slotted versus Unslotted temporal Structure

Letting nodes sleep is the most effective way to conserve energy in a wireless network and to maximize the lifetime. However, this requires a mechanism that allows nodes to be contacted, even though they might sleep from time to time.

There are two types of sleeping protocols. The first one is time slotted and uses a periodic beacon. This beacon provides a coarse-level synchronization and denotes the start of a so-called *super-frame*. Generally, a super-frame has two parts: a reservation window, during which potential senders announce transmission requests, and a data transmission window, during which the actual packet transmissions take place. Receivers can then sleep for most of the second part, except for the periods when announced transmissions occur.

The second approach is unslotted: each receiver wakes up according to its own listening schedule. A transmitter that wants to communicate with a given receiver first needs to learn the listening schedule of this receiver. This is the approach implemented in S-MAC [200]. Another similar approach is to let all nodes have the same sleeping schedule (but maybe delayed in time). Then, a transmitter does not need to learn the schedule. It simply has to send a long preamble, as long as the maximum sleeping time. The destination, sure to wake up at some time in between, will receive the preamble and answer to the transmitter. This is the approach implemented in B-MAC [201].

Centralized Architecture

A design choice for all the above possibilities is to have either a fully-decentralized or a more centralized, master-slave architecture where the network consists of one or several sub-networks, each controlled by a coordinator. A coordinator can be a base-station or an arbitrary node elected by a network. We do not discuss coordinator election in this thesis.

		Aloha	802.11	CA-CDMA	Bluetooth	802.15.4
Rate adaptation			I			
Power control				I		
Mutual exclusion			I,A	I,A	I,A	I,A
Multi-channel				I	I	
Multi-user detection						
Access	Random	A	A	A		A
	Scheduled				A	A
Time slots			S		A,S	A,S
Sleeping	Slotted		S			
	Unslotted					
Centralized architecture					S	S

		MBOA	Power and rate controlled [154]	UWB[2]	DCC-MAC
Rate adaptation			I		I
Power control			I		
Mutual exclusion		I,A	I,A		
Multi-channel			I	I	I
Multi-user detection					I
Access	Random	A	A	A	A
	Scheduled	A			
Time slots		A,S			
Sleeping	Slotted	S			
	Unslotted				
Centralized architecture					

Table 4.1: Each row is a building block of a PHY-aware MAC described in Section 4.1.2. The table shows which function a building block contributes to in existing designs proposed in the literature: I stands for interference management, A for access to a destination and S for sleeping management.

4.1.3 Which Building Blocks are Used by Existing Designs ?

We now use the building blocks presented in the previous section to analyze several designs that have been proposed for UWB. For each of the three functions described in Section 4.1.1, we analyze which building blocks are used for each function. We summarize the results of this section in Table 4.1. As many of the concepts of UWB designs are borrowed from narrow-band designs, we also add Aloha [193, 194], the IEEE 802.11 protocol [191], Bluetooth [202], IEEE 802.15.4 (Zigbee) [66] and a CDMA design [175] to Table 4.1 for comparison purposes.

This section is not meant to be a precise description of each of the selected protocols. We only describe which building blocks are used and how they are used for each function. For more

information on the IR-UWB protocols, the reader can refer to the related work in Chapter 3. We begin with the IR-UWB protocols, and then describe the other designs. The joint power and rate controlled design for a IR-UWB physical layer in [154] was already presented in Chapter 3: Interference is managed by a mixture of mutual exclusion, power and rate adaptation, and by taking advantage of the quasi-orthogonal channels provided by time-hopping sequences. If after a distributed handshake procedure on a control channel, there exists no satisfying power and rate assignment, no data communication occurs (exclusion). The number of nodes affected by mutual exclusion is variable. In fact, for every receiver there exists an interference margin, which indicates by how much the interference can increase without destroying ongoing transmissions. The smaller the interference margin, the larger the number of nodes prevented from sending. The variable rate permits an adaptation to the interference at the receiver. The variable power allows for the reduction of the interference created by a transmitter. Access to a destination is enforced by the same RTS/CTS type of handshake that is used for finding the power and rate assignment.

With UWB^2 [164], also presented in Chapter 3, interference is managed by pseudo-orthogonal channels and access to a destination is managed by a handshake procedure.

DCC-MAC is the design presented later in Chapter 5. It uses rate adaptation but no power control. It takes advantage of the infrequent nature of collisions at the physical layer with an interference mitigation scheme. The interference mitigation scheme declares erasures on symbols that could not be properly received. The loss of information due to the erasures is recovered by an error-correcting code. At the cost of a small rate reduction, this greatly alleviates the effect of one or several near-far interferers. Note that interference mitigation does not necessitate any synchronization between the transmitters. It probably marginally increases the power consumption.

As we demonstrate later, with interference mitigation, mutual exclusion becomes unnecessary. With DCC-MAC, interference is managed by rate adaptation, pseudo-orthogonal channels through time-hopping sequences and a suboptimal multi-user type of receiver. DCC-MAC avoids the need for a control channel. As such, the problem of access to a destination is managed by a subtle control of timers and careful use of time-hopping sequences.

We do not discuss sleeping management for the three previous protocols because they do not address it. We now turn to the other designs.

The Aloha protocol is the simplest design where interference (and access to the same destination) are not managed at all. The 802.11 protocol [191] is based on CSMA/CA with an optional RTS/CTS mechanism. In the first version of the protocol the MAC had practically no

interaction with the physical layer; the physical layer provided two rates and the only task of the MAC was to arbitrate access to the channel. Subsequent versions of the standard saw an increase in the number of different rates offered by the physical layer. Coupled with an automatic repeat request (ARQ) mechanism, it allows the MAC to dynamically control the transmission rate and to adapt to the channel condition between the source and the destination. Furthermore, the 802.11h standard [202], an evolution of the 802.11a standard, performs transmission power control in order to reduce the interference created. In addition, it permits dynamical switching from a given channel to another for a better spectrum utilization. Nevertheless, interference management and access to a destination are enforced essentially by mutual exclusion. Indeed, only one node can use the channel at a time. To enable sleeping in the infrastructure mode, the access point broadcasts beacons that permit devices to easily and regularly switch to *doze* mode. In ad hoc mode configuration, each device broadcasts its own beacon. It is then up to a source to listen to the beacon of a desired destination.

Multiple channel designs based on 802.11, such as [203], take advantage of the several channels available for 802.11 networks to operate in. Indeed, 802.11b provides at least three orthogonal channels where parallel transmission can occur. Hence, in the case of [203] interference is managed by orthogonal channels and exclusion. There is still obviously a need for exclusion as two nodes might still want to use the same channel for a transmission. Access to a destination is enforced thanks to a modified RTS/CTS procedure taking place on a dedicated control channel. To avoid wasting an entire channel for control signaling, the authors use a slotted procedure. On a regular interval, all nodes switch to the control channel to arbitrate access. Once this is done, the control channel too can be used as a data channel.

Bluetooth (or IEEE 802.15.1) [202] is based on a piconet paradigm where any communication occurs in a master-slave fashion. The physical layer of Bluetooth is based on frequency-hopping spread-spectrum and every piconet uses one out of 79 available hopping patterns. It is a slotted protocol. There is no rate or power adaptation. Interference is managed by mutual exclusion and multiple channels thanks to the frequency-hopping sequences; indeed, only one node can transmit in any hopping slot. This implies that all devices belonging to a given piconet must be synchronized with the piconet coordinator. Access to a given destination is centrally managed by the piconet controller. For sleeping management, the centralized and slotted structure permits nodes to easily sleep and wake up when necessary.

The IEEE 802.15.4 (Zigbee) protocol [66], although based on a narrow-band physical layer, is also of interest since the IEEE 802.15.4a Task Group has standardized an alternative IR-UWB physical layer. The IEEE 802.15.4 MAC is a single-channel protocol based on CSMA/CA (with

an optional RTS/CTS mechanism). Its main operating mode is the so-called beacon-enabled mode where the network is organized as a slotted *piconet*. A piconet coordinator periodically broadcasts beacons. Access inside a given slot uses exclusion and is arbitrated through CSMA/CA. Hence, interference is managed entirely by mutual exclusion, thanks to the slotting procedure. Access to a destination is ensured by the optional RTS/CTS procedure or relies on collision detection and a backoff mechanism. For sleeping management, the centralized and slotted structure permits nodes to easily sleep and wake up when necessary. There is also a distributed operating mode where communication occurs on a point-to-point basis using CSMA/CA.

The CA-CDMA MAC using distributed power control for a CDMA physical layer [175] is already discussed in Chapter 3. Interference is managed by a combination of mutual exclusion, power control and pseudo-orthogonal channels. Any attempt to communicate starts with a handshake between the source and its potential destination on a separate control channel. If no admissible power is found, no data transmission occurs. Devices take advantage of a CTS-like packet on the control channel to insert their power margin. This information can then be overheard on the control channel by other nodes. The handshake procedure is also used for access to a destination. Sleeping is not addressed.

The MBOA protocol [204, 205] shares similarities with IEEE 802.15.4. It emerged from the inconclusive effort of the IEEE 802.15.3a Task Group that worked on an alternative UWB physical layer for IEEE 802.15.3. There is only a beacon based mode, with slotted access in between beacon transmissions. The UWB physical layer adopted by MBOA is not based on impulse-radio but on a multi-band OFDM radio.

4.2 Performance Analysis of the Different Design Choices

In this section we use the classification developed in the previous sections to evaluate several important design choices for low-power, low data-rate IR-UWB networks. Our results are obtained either by review of the literature, or by ad-hoc analysis and simulations. We derive six facts that can be used as guidelines. But first, we define the energy consumption model and the performance metrics used in the analysis.

4.2.1 Energy Consumption Model

Our goal is to define an energy model that can be applied early in the design process, before an actual hardware is developed. This is a serious challenge, but we can take advantage of the nature of IR-UWB to derive a generic model, flexible enough to account for a large set of options.

With IR-UWB, time is divided into frames of N_c short duration chips, we one pulse transmitted per frame. We use this to define a *chip-level* model of energy consumption. During a chip, the physical layer can either transmit a pulse, receive a pulse, perform timing acquisition, be in an active-off state, or sleep. The active-off state occurs due to time-hopping: When a node is between two pulse transmissions or receptions, energy is consumed only to keep the circuit powered up, but no energy is used for transmitting or receiving pulses.

Hence, we model the energy consumption by considering the energy *per chip* for each state. An energy consumption model is defined by the vector

$$\vec{q} = [q_{tx}\ q_{rx}\ q_{ao}] \tag{4.1}$$

where q_{tx} is the cost for transmitting a pulse, q_{rx} receiving a pulse and q_{ao} for being in the active-off state. As the same transceiver elements are used for timing acquisition and reception, the acquisition energy consumption is also equal to q_{rx}. The cost while sleeping is negligible compared to transmission or reception.

Due to the lack of hardware implementation of UWB transceivers, it is currently impossible to give precise figures for $\vec{q}$. However, only relative values are relevant to our performance evaluation. It is thus possible to limit our analysis to a small set of scenarios. The numerical values of $\vec{q}$ are shown for each scenario on the top of Table 4.2.

We now show on an example how our energy model is used. The energy consumption E_{packet} to receive a packet of 127 bytes (including a synchronization preamble of 20 bytes) using binary modulation (one pulse carries one bit) is

$$E_{packet} = 8 \cdot \left(\underbrace{20 \cdot N_c \cdot q_{rx}}_{\text{Energy for the preamble acquisition}} + \underbrace{107 \cdot q_{rx}}_{\text{Energy when a pulse is present}} + \underbrace{107 \cdot (N_c - 1) \cdot q_{ao}}_{\text{Energy in the active-off state}} \right) \tag{4.2}$$

where the factor eight appears because we consider bytes. With this model, the energy consumed for each received or transmitted packet can be easily computed. The lifetime of a node is then the time necessary to consume all the energy contained in the battery of the node.

4.2.2 Performance Metrics and Simulation Parameters

We use two metrics to be consistent with the goal of maximizing network lifetime while keeping rates as high as reasonably possible. The metrics are the sum of logs of node lifetimes and the sum of logs of average link rates. The reason we use log utility metrics is to take fairness into account. Log utility metrics are known to achieve a good trade-off between efficiency and fairness [206].

The remaining assumptions about the physical layer parameters and the topology for the simulations are given in Table 4.2. Note that the physical layer supports several transmission rates by using the rate compatible punctured convolutional (RCPC) codes of [68] presented in Section 2.2.7. The rates range from 100 kbit/s to 1 Mbit/s. For the simulations involving a physical layer model, we assume the five-tap multipath channel with a Rake receiver as described in Section 2.2.8. The interference mitigation scheme is used if necessary, with $k = 2.8$. This value was found by extensive simulations.

The lengths of the packets are computed assuming the smallest data-rate. For the simulations, all nodes have an identical physical layer and the same initial battery power.

4.2.3 Conclusion From the Performance Analysis: Guidelines for the Optimal Design

We conduct our performance analysis by analyzing existing literature and by performing extensive simulations when needed. All the simulation code can be found online at [207]. The performance analysis results lead to the following six facts about the optimal design for low data-rate, low-power IR-UWB networks.

Fact 1: Rate control is needed.

If the rate (from modulation and coding) is fixed to some predefined value, this value has to be small enough to be feasible for all channel conditions. This in turn imposes the same small rates on good channel conditions. If transmission rates are low, packet transmissions last longer, and more energy is consumed to keep circuits running. This is highly inefficient from a rate or lifetime viewpoint [119, 208]. Furthermore, if transmissions last longer, they generate more interference. This interference further decreases the performance of links that are already operating. Therefore, we can easily conclude that rate control is needed. In addition, most of the recent designs, including the ones considered previously in Section 4.1.3, allow a form of rate adaptation through variable modulation and coding.

Energy consumption models $\vec{q} = [q_{tx}\ q_{rx}\ q_{ao}]$	1	$\vec{q} = [1\ 1\ 1]$	Baseline model
	2	$\vec{q} = [1\ 5\ 1]$	Higher cost for reception
	3	$\vec{q} = [1\ 1\ 0.5]$	Lower cost for active-off
	4	$\vec{q} = [1\ 5\ 0.5]$	Higher cost for reception, lower cost for active-off

Physical layer parameters	Frame length $N_c = 1000$ chips Chip duration $T_c = 1$ ns Rates (convolutional code with puncturing): $R = \left\{1, \frac{8}{9}, \frac{8}{10}, \ldots, \frac{8}{32}, \frac{1}{5}, \frac{1}{6}, \ldots, \frac{1}{10}\right\}$ Mbit/s Energy per pulse $E_p = 0.2818$ mW 802.15.4a channel model

Sleeping protocols parameters	$T_b = 50\mu$s, $T_{fa} = 10\mu$s
	$T_{RTS} = T_{CTS} = T_{ACK} = 800\mu$s The size of control packets is 20 bytes
	$T_{DATA} = 10200\mu$s The size of data packet is 127 bytes

Topology for the simulations	Nodes position randomly distributed on a 20×20 meters square Links are chosen randomly

Table 4.2: Energy consumption model, physical layer parameters and assumptions for the performance analysis

Fact 2: Transmitted power control is not needed.

Different power adaptation strategies for low-power UWB networks have been discussed in [119] and [208]. One of them is $0/P_{max}$: whenever a node transmits data, it is with the maximum allowed transmission power P_{max}. It is shown in [208] that any feasible rate allocation and energy consumption (hence lifetime) can be achieved with this simple power adaptation strategy. Hence power adaptation is not needed. A similar conclusion was also obtained in [154].

Intuitively, because the SINR with impulse-radio UWB is convex in interference, increasing the transmission power of a source has more effect on the received signal at the destination than on interference on other nodes. As such, it is beneficial for a node to transmit with maximum power. This ensures a high data-rate and data transmissions terminate quickly to let other nodes

transmit. In contrast, using a lower transmission power prolongs the transmission duration which is detrimental to reducing power consumption. With a short transmission time, we use the circuits for a shorter period of time and thus increase the lifetime of a node.

Fact 3: A suboptimal and simple form of multi-user detection is beneficial.

Optimal multi-user detection is an efficient way to manage multiple access. However it remains impractical in our setting: we consider low-complexity devices and multi-user detection requires synchronization among transmitters as well as the knowledge of their channel characteristics.

Nonetheless, there are clear benefits for IR-UWB when using sub-optimal solutions such as interference mitigation as demonstrated in [46, 136, 63, 47, 48] (see Section 3.3.3) and in Chapters 5 and 9. In Chapter 5, at the cost of a small data-rate reduction, an interference mitigation scheme greatly alleviates the effect of one or several near-far interferers.

Fact 4: Mutual exclusion is not needed when interference mitigation is applied.

In case of near-far scenarios (even with a very low data-rate), it might seem desirable to enforce some form of mutual exclusion. However, if interference mitigation is applied, a large part of the interference is eliminated. We simulate the impact of mutual exclusion on rate and lifetime when interference mitigation is present.

Our starting point is the result from [119] discussed in Section 3.3.4. Here is the setting of the simulations. We assume each active receiver has a mutual exclusion region of radius γ around it; during reception, no node inside the exclusion region is allowed to transmit. For each value of γ between zero and 30 meters, we find all the subsets of nodes and rate of these nodes that maximize the rate metric and satisfy the exclusion region constraints. Nodes send with maximum power. We use the baseline energy model (model 1). It turns out that the results are similar with the other energy models. A detailed explanation of how the simulations are performed is given in Appendix A.1.

The average rate achieved for different γ is depicted in Figure 4.1. It can be observed that it is optimal to let all nodes transmit concurrently at all times (the maximum is reached for $\gamma = 0$). Without interference mitigation, the optimal exclusion region size is approximately two meters. Thanks to interference mitigation, no mutual exclusion is required. The rate reduction due to interference mitigation is traded for an increased spatial reuse due to the absence of mutual exclusion

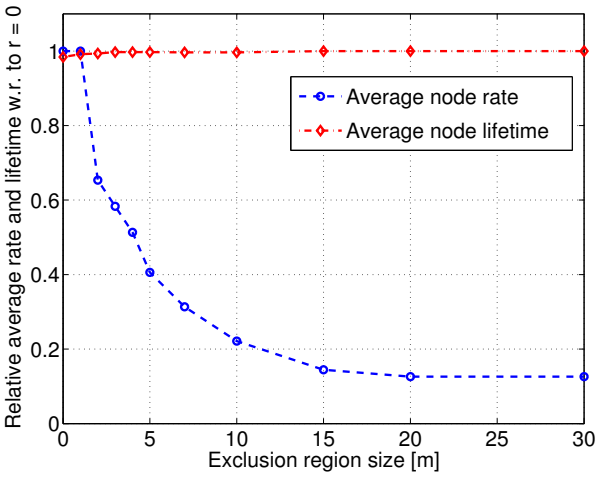

Figure 4.1: Average node rate (dashed blue curved) and average node lifetime (red dot dashed curve) relative to the values at $\gamma = 0$ versus the size of the exclusion region γ. We use the baseline energy model (model 1), the results are similar with the other energy models. No exclusion region is required from a rate point of view. The presence of an exclusion region has negligible impact on the lifetime.

In the case of the lifetime metric, we also evaluate the optimal γ using numerical simulations. The results are depicted in Figure 4.1. With large γ, the lifetime of the node is only slightly increased. When rate constraints are low, each node transmits only during a small fraction of time. This in turn reduces the energy consumed to keep the circuits running. Hence the total interference created is small and the energy consumed is minimized. Furthermore, interference mitigation handles most of the interference, and there is no need to implement an exclusion protocol.

It is also important to remember that with an exclusion mechanism comes the cost of a practical protocol. The overhead of this protocol and its cost is actually not taken into account by the simulations, which reinforce our conclusion.

Fact 5: A slotted sleeping scheme is better than unslotted if occasional bursts of data must be supported.

We consider a slotted and an unslotted sleeping protocol (Section 4.1.2) as depicted in Figure 4.2. We analyze which protocol is more efficient with respect to the average lifetime of a node.

For the slotted protocol, a so-called super-frame is defined. A super-frame begins with a beacon sent by a coordinator. It is followed by a reservation window. If a node wants to

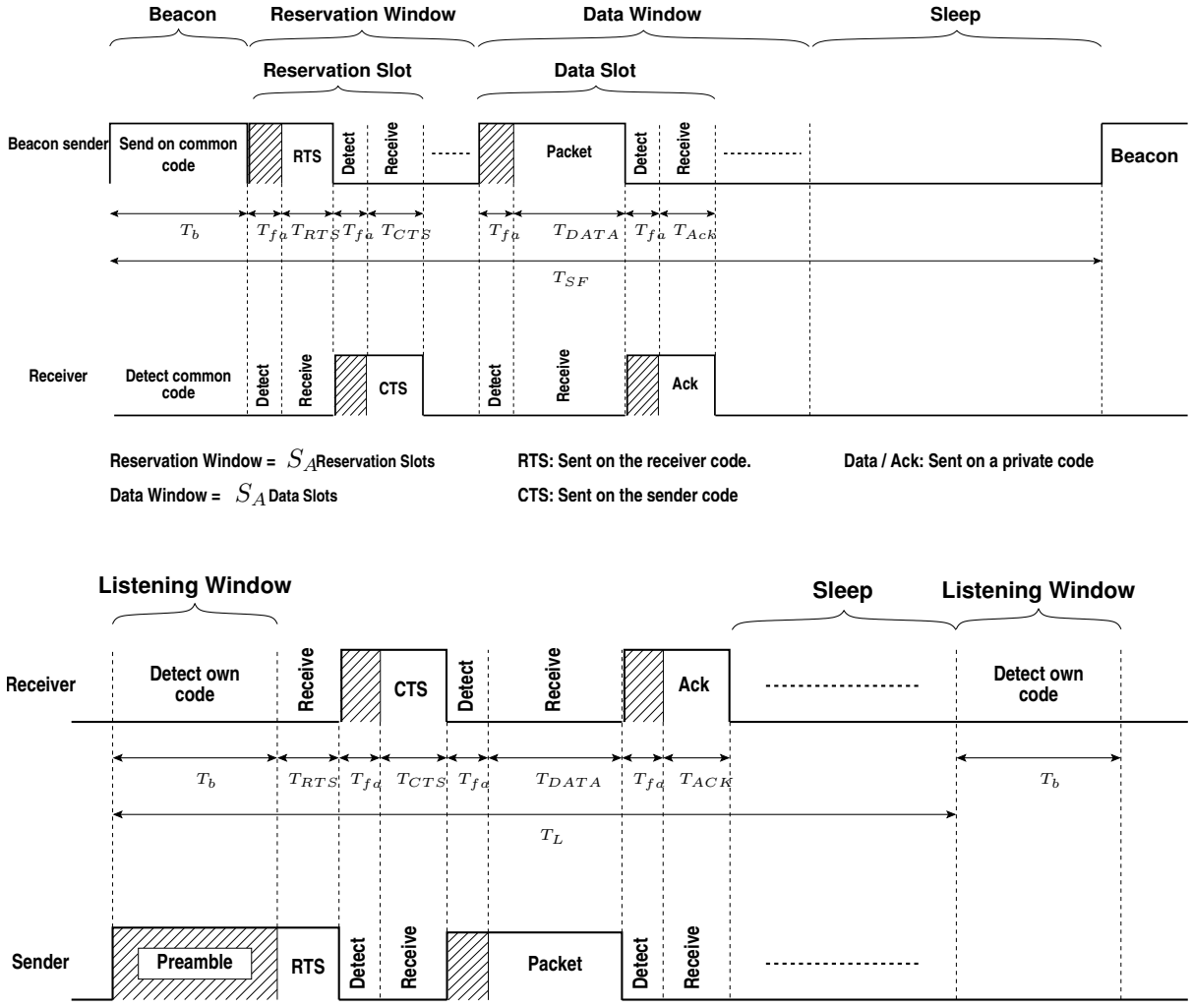

Figure 4.2: The *slotted sleeping protocol* is depicted on the top. We consider a transmitter and a receiver and assume in this example, that a transmitter is also a coordinator). The protocol defines a so-called super-frame. A super-frame begins with a beacon sent by a coordinator. It is followed by a reservation window. If a transmitter wants to transmit, it sends a RTS in a reservation slot using the THS of the receiver. As such, concurrent reservations for different receivers are possible. The receiver replies with a CTS if it accepts the reservation. If a reservation is successful, the actual data transmission occurs in the corresponding data slot, and is followed by an acknowledgement packet (ACK). In the beginning of a super-frame, nodes need a long beacon of duration T_b to achieve a coarse level synchronization. Afterward, there is only a short preamble of duration T_f before every packet. In the *unslotted sleeping protocol* (bottom), every node has a regular interval of duration T_L, called listening schedule. Reservations are done during the listening window at the beginning of the interval, and if successful, are followed by a packet transmission. Since a pause between two reservation periods can be long, we need a long preamble at the beginning. One packet at most can be received during T_L.

transmit a packet, it sends first a RTS in a reservation slot using the THS of the receiver. As such, concurrent reservations for different receivers are possible. The receiver replies with a CTS if it accepts the reservation. If a reservation is successful, the actual data transmission occurs in the corresponding data slot, and is followed by an acknowledgement packet (ACK). In the beginning of a super-frame, nodes need a long beacon of duration T_b to achieve a coarse level synchronization. Afterward, there is only a short preamble of duration T_f before every packet.

For the unslotted protocol, every node has a regular interval of duration T_L, called a listening schedule. Reservations with RTS/CTS are done during the listening window at the beginning of the interval, and if successful, are followed by a packet transmission. They are used to arbitrate access between concurrent sources for the same destination. Since a pause between two reservation periods can be long, we need a long preamble at the beginning. One packet at most can be received during T_L.

We compute the lifetime assuming that most of the time the node is subject to a load λ_0. However, the network is designed to occasionally sustain a traffic load $\lambda_{max} > \lambda_0$ per receiver during burst intervals.

Let us define by Γ the network utilization. In the slotted case, a receiver can receive $\Gamma \frac{S_A}{T_{SF}}$ packets per second where S_A is the number of reservation slots in the reservation window and T_{SF} is the super-frame length. In the unslotted case it can receive $\Gamma \frac{1}{T_L}$ where T_L is the time interval between two listening windows. One packet at most can be received during T_L. Since a network with utilization close to 100% is unstable, we take $\Gamma = 0.7$ to guarantee stability. Note that if two requests to the same destination overlap, one is very likely to be accepted due to time-hopping and the signal acquisition procedure [63]. Therefore, we assume that the total submitted traffic is close to λ_0 per receiver.

For two extreme values of S_A equal to 5 and 20, and the four energy models, we compare the lifetimes achieved with the slotted and unslotted protocols. The parameters T_{SF} and T_L are chosen to sustain the bursty maximum load λ_{max}. The lifetime is then computed assuming a load $\lambda_0 = 10$ kbit/s. The ratios of the lifetime in the slotted over the unslotted case are plotted on Figure 4.3(a). With slotted sleeping protocols, the lifetime is 15% to 50% longer. If the lifetime is around one year, it can be significantly increased by two to six months. If the slotted structure comes at a low cost, or for free (as in a master-slave system like Bluetooth), its use is optimal. If this is not the case, we need to compare the implementation overheads to compare the two protocols. The main overhead of a slotted protocol is distributing the beacon and managing the cases when communicating nodes hear several different super-frames. The

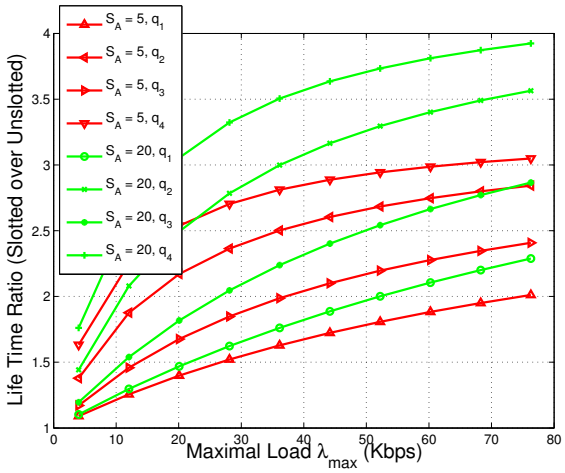

(a) Ratio of the average node lifetime in the slotted case over the unslotted case with respect to the maximal load λ_{max} (q_i stands for energy model i). In all cases, the slotted protocol outperforms the unslotted one by 15% to 30%.

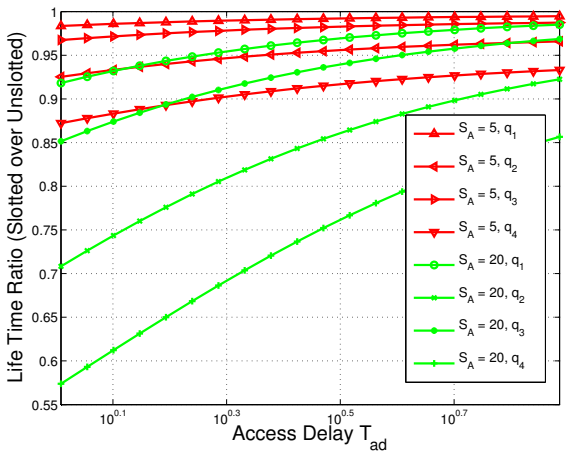

(b) Ratio of the average node lifetime in the slotted case over the unslotted case with respect to the access delay T_{ad} (q_i stands for energy model i). In this case, the unslotted protocol outperforms the slotted one.

Figure 4.3: Lifetime comparison for slotted and unslotted sleeping protocols under various traffic constraints. We compare the performance for S_A equal to 5 and 20 and all energy models (Table 4.2), q_i stands for energy model i. In all cases $\lambda_0 = 10$ kbit/s.

main overhead of an unslotted protocol is the time necessary when a node learns the schedules of its neighbors, either due to a topology change or due to a clock drift.

Fact 6: An unslotted sleeping scheme is better than slotted if occasional maximum latency must be supported.

We consider a variant of the previous section. We still assume that most of the time, the network is subject to an average traffic load λ_0. However, it has to occasionally support a small number of unpredicted, but very urgent messages instead of a bursty high load.

When a node generates a packet, it cannot send it immediately. For the slotted protocol a node has to wait at most T_{SF} to send a packet. For the unslotted one, the worst case delay is T_L. In both cases, we assume that the worst case is limited by application constraints to the access delay T_{ad}. We then compare the energy savings for the two approaches as a function of T_{ad} for the different energy models.

The ratios of the lifetime in the slotted case over the unslotted case are plotted in Figure 4.3(b). The conclusions are the opposite of the previous section: the unslotted protocol always performs better or equal to the slotted protocol. Indeed, the unslotted protocol has only

one listening window per time T_{ad}, whereas the slotted one has S_A reservation slots and every node has to listen for an RTS during these S_A slots.

Again, as in deciding whether mutual exclusion is necessary or not, there are protocol overhead costs that are not modeled in this short analysis of sleeping protocols. The main overhead of a slotted protocol is in electing a coordinator. Each node has to hear at least one super-frame, hence it has to be in transmission reach of at least one coordinator (otherwise, it can become coordinator itself). Also, coordination requires energy. The role of coordinator has to be delegated equally to all nodes, in order to provide equal energy consumption [209]. Finally, an additional management is needed for nodes that hear more than one super-frame, or in cases when a source and a corresponding destination hear different super-frames. The main overhead and cost of the unslotted protocol is to learn the sleeping schedule. Whenever a neighborhood of a node changes, for example due to mobility, it needs to learn again the listening schedules of its peers. Also, if a node does not transmit to a destination for a long time, it may need to learn its schedule again due to clock drift.

4.3 Discussion and Conclusion

In this chapter, we have first explored the design space of PHY-aware MAC protocols. We describe their functions and the various ways they can be implemented. This is directly useful for protocol designers to understand and exploit the large range of possibilities they have for designing PHY-aware MAC protocols for UWB or other physical layers.

In the second part of this chapter, our performance analysis leads us to formulate six guidelines for the design of low data-rate, low-power IR-UWB networks. We also introduce an energy consumption model for impulse-radio systems. The guidelines clearly call for an uncoordinated and decentralized protocol using rate adaptation but no power control, and with an interference mitigation scheme at the physical layer. The MAC should primarily manage access by adapting rate to interference, without attempting to exclude competing sources by a mutual exclusion protocol. These results are valid from a rate maximization point of view. They appear to be close to optimal for minimizing the energy consumption. But more work is required in this case.

It also interesting to compare the results in this chapter with those in [119] (see Section 3.3.4). In [119], the conclusions are also to not use power control and to adapt the rate of a link to the interference at the receiver. However, [119] shows that there is an exclusion region around nodes receiving a packet. Other nodes in this exclusion region are not allowed

to transmit. The results in this chapter demonstrate that in a low data-rate setting, and with an interference mitigation scheme at the physical layer, the size of this exclusion region is negligible.

The next chapter will actually present DCC-MAC, a practical protocol that is built on these findings. It also contains additional simulation results, with strong near-far scenarios, that confirm the findings of the present chapter. A practical and low-complexity IR-UWB receiver with interference mitigation capabilities is presented in Chapter 9.

Of course, a complete design targeting energy efficiency should also consider energy efficient routing. A first step in this direction is [158]. We did not discuss whether all nodes should use the same THS or not. And we also did not discuss issues related with packet detection and timing acquisition. These issues are actually treated separately in Chapter 6.

Chapter 5

DCC-MAC: a PHY-Aware MAC Layer for IR-UWB Ad Hoc Networks

In the previous chapter, we obtained guidelines on the optimal design for IR-UWB networks. The guidelines clearly call for an uncoordinated and decentralized protocol using rate adaptation and no power control, but with an interference mitigation scheme at the physical layer. We also compared our findings with the results in [119] and they agree: In a low data-rate setting and with an interference mitigation scheme at the physical layer, it turns out that the size of the exclusion region becomes negligible. We use these findings as a foundation for a practical PHY-aware MAC protocol.

We begin this chapter with simulations to further verify that an exclusion mechanism is useless with an interference mitigation scheme at the physical layer. But we consider a topology with severe near-far cases instead of the random topologies of the previous chapter. It is not *a priori* manifest that the size of the exclusion region is negligible in this case. In fact, even with interference mitigation, the activity of one near-far user can have a severe effect on the rate achievable by other users. The results of these additional simulations validate the findings of the previous chapter. They confirm that the MAC should still manage interference by adapting the rate to interference, even in near-far cases. It yields a better throughput than attempting to exclude competing sources by a mutual exclusion protocol.

However, this does not mean that a protocol is not necessary at the link layer. First, a rate adaptation protocol is required. We present our dynamic channel coding (DCC) protocol to continuously adapt the rate to variable channel conditions and interference (Section 5.2.1). To avoid the problem of signal to interference and noise ratio (SINR) measurements, the optimum

rate of the code is determined after packet reception and piggybacked in the acknowledgment to the sender. Furthermore, there actually remains some exclusion to implement because we assume that a node can be engaged exclusively in either the reception or the transmission of a single packet. This is enforced by the "private MAC" (Section 5.2.2) that resolves contention for the same destination. The private MAC utilizes the THS of the destination for the transmission of packets. The THS of a node is generated by using the MAC address of the node as seed for a pseudo-random number generator. This has two consequences: the THS is identical for every packet to the same destination; and learning the THS of a node is equivalent to learning its MAC address. Finally, there is the challenge of absence of carrier-sensing. We solve it by an elaborate signaling protocol that alternates between direct access to a receiver and an invitation-based scheme. We do not use any separate channel for control signaling to avoid any global contention possibilities. Our protocol is fully implemented in ns-2 along with a model of the physical layer (see Chapter 10). Simulation results show a significant increase in throughput compared to traditional protocol design.

5.1 Taming the Exclusion Region With Interference Mitigation

In this section, we demonstrate that the size γ of the exclusion region around a destination is negligible in a low data-rate setting with an interference mitigation scheme at the physical layer. Even in near-far scenarios, rate adaptation remains more efficient that an exclusion protocol.

5.1.1 Performance Metric and Simulation Parameters

Our performance metric in this section is the bit error rate (BER). The physical layer model in this chapter has slightly different parameters that in other chapters. We assume that $T_c = 0.2$ ns and that the support T_p of the pulse $p(t)$ is equal to T_c. This results in roughly 5 GHz of bandwidth. Furthermore the normalized energy per pulse $E_p/T_c = 0.28$ mW [93]. Hence, with $N_c = 280$, we obtain an average radiated power of 1 μW. In addition, the maximum rate of our physical layer is $\frac{1}{N_c \cdot T_c} \simeq 18$ Mbit/s. Given the large bandwidth of 5 GHz, we still consider 18 Mbit/s as a relatively low data-rate.

As in Chapter 4, we assume the five-tap multipath channel with a Rake receiver as described in Section 2.2.8. The interference mitigation scheme is used if necessary, with $k = 2.8$. This value was found by extensive simulations.

5.1.2 Computing the Size of the Exclusion Region

In networks with arbitrary topology, all destinations $D_1, \ldots, D_n$ have a different exclusion region size γ_k, $k = 1, 2, \ldots, n$. In such scenarios, computing γ_k is known to be a hard problem [119]. We therefore resort to the symmetric topology of Figure 5.1 where $\gamma = \gamma_1 = \ldots = \gamma_n$. The links $\{S_1, D_1\}, \ldots, \{S_n, D_n\}$ are placed in an alternate way on a cylinder of length $\mathcal{L}_c$. This is a strong near-far scenario.

The distance between two parallel links is d. If $\gamma < d$, then it is optimal to let all nodes transmit at the same time. The achievable rate on a link in this case is $R_{all}(d)$. If $\gamma > d$, then it is optimal to have only the nodes on one side of the cylinder to transmit at the same time (half of the sources). In this case, the achievable rate on a link is $R_{excl}(d)$. In the limit case, when $\gamma = d$, we have $R_{all}(d) = R_{excl}(d)$ [119]. We use this property to determine the size of the exclusion region. For a given number of destination n and $\mathcal{L}_c$ we compute $R_{all}(d)$ and $R_{excl}(d)$ for various values of d and determine where $R_{all}(d) = R_{excl}(d)$.

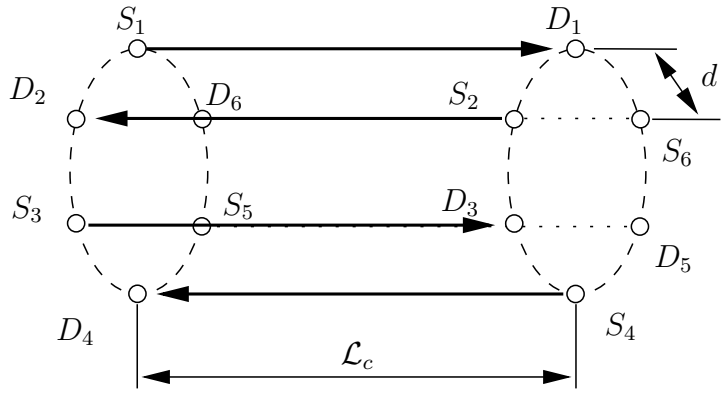

Figure 5.1: Multiple near-far interferers scenario: nodes are symmetrically distributed on the edges of a cylinder. Corresponding peers are located on adjacent disks. This is a strong near-far scenario. There are $n = 6$ links in total and every second link is inverted such that each destination is close to an interfering source. The distance between a source and a destination is the length of the cylinder $\mathcal{L}_c$, and the distance between a destination and the adjacent interfering source is d.

To determine the best $\mathcal{R}_{all}(d)$ and $\mathcal{R}_{excl}(d)$ that S_1 can achieve in the presence of interferers S_j, $j = 2, \ldots, n$, we first set a BER threshold μ^*. A typical value for μ^* in a wireless environment is 10^{-5} [12]. We then determine the maximum possible rate R_i, $i = 1, 2, \ldots, N$ that drives the BER below μ^*. Modeling the multi-user interference (MUI) in equation (2.12) as Gaussian would permit an analytical expression to be used [9] for γ in an uncoded IR-UWB

physical layer. However, in our settings, this assumption does not hold for IR-UWB [51]. Since we further use convolutional channel codes and a multipath channel, we turn to simulations to derive γ (we use Matlab). We furthermore consider two types of channel decoding policy, hard-decision and soft-decision. With a hard-decision policy, only the sign of the demodulator output is passed to the channel decoder, whereas the sign and the amplitude are passed in the case of soft-decision decoding. Usually, the soft-decision policy performs better than a hard-decision policy [12]. However, the underlying assumption in this case is that the total interference (MUI and noise) has a Gaussian density. This justifies our interest in analyzing the performance of a hard-decision policy.

The results are shown in Figure 5.2. We consider $n = \{4, 8, 16\}$ links and use link lengths of $\mathcal{L}_c = \{2, 6, 12, 18\}$ to obtain varying signal and interference intensities. When hard-decision is used, there is no exclusion region i.e., $\mathcal{R}_{all}(d) > \mathcal{R}_{excl}(d)$, $\forall d$. However, the performance is very poor for large values of d, when interferers are distant and the dominant interference is Gaussian noise. In the soft-decision case, an exclusion region of 1 to 4 meters is present depending on $\mathcal{L}_c$ and n. Although the probability of collision $P_{col}(n) = 1 - \left(1 - \frac{2T_c}{T_f}\right)^n$ with interfering pulses is low ($< 1\%$ for $n = 1$, 7.5% for $n = 10$, and ignoring the multipath propagation), they have an impact in the case of nearby interfering sources. A collision results in a received sample with a large value that propagates over the decoding of several subsequent samples. It significantly deteriorates the decoding process and causes several decoding errors. This does not happen with a hard-decision policy since only the sign of the output sample is used. However, soft-decision decoding clearly outperforms hard-decision decoding at large values of d.

Intuitively, the optimal decoding policy should be an adaptive combination of hard-decision when strong interferers are present and soft-decision otherwise. These observations are the reason to use an interference mitigation scheme based on thresholding. This reduces γ compared to a soft-decision scheme and still avoids the complexity of an exclusion scheme.

5.1.3 Replacing Exclusion by Interference Mitigation

We demonstrate how an interference mitigation (IFM) scheme at the physical layer reduces the effect of strong interferers and how it can replace an exclusion scheme. We use the IFM scheme presented in Section 2.2.8. This scheme cancels the samples resulting from a collision with pulses from a strong interferer. It replaces them by erasures to skip them in the decoding process.

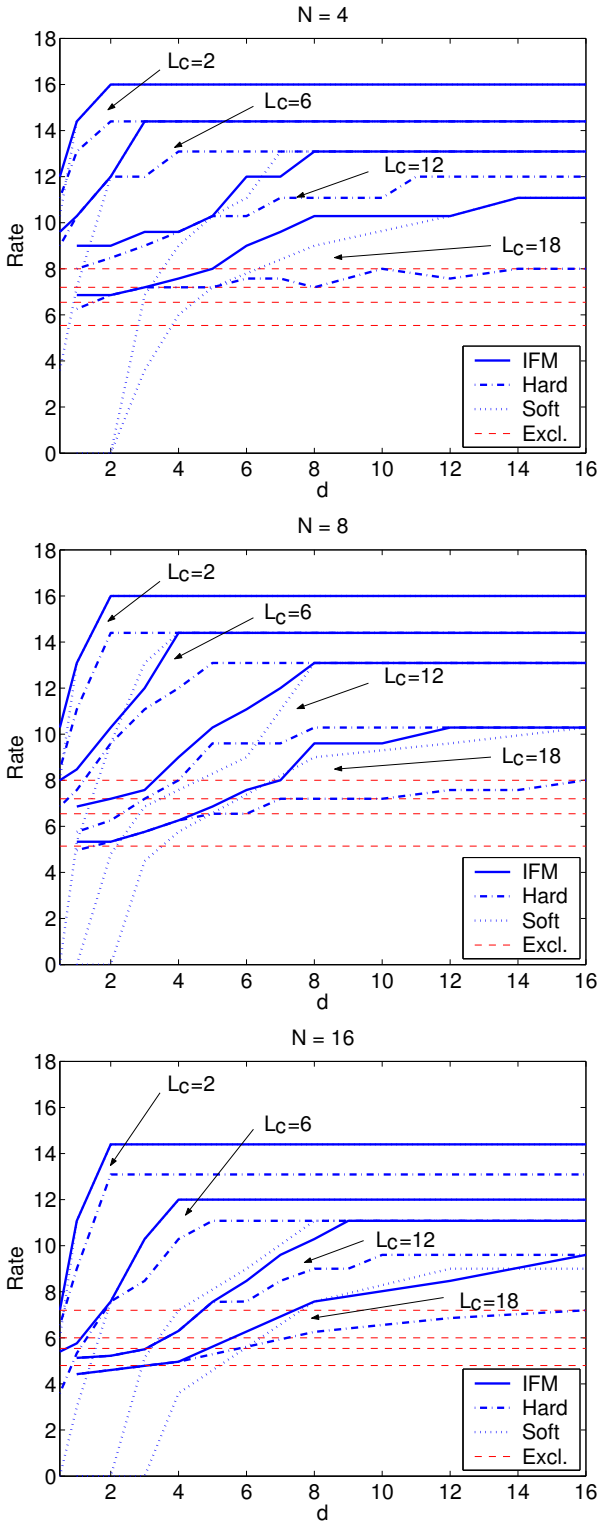

Figure 5.2: We show $R_{all}(d)$ (all sources send at the same time) as well as $R_{excl}(d)$ (one side of the cylinder sends at the same time) vs. interferer distance d. We determine $R_{all}(d)$ for interference mitigation decoding (IFM), soft-decision decoding (Soft), and hard-decision decoding (Hard). The intersection between $R_{all}(d)$ and $R_{excl}(d)$ gives γ, the size of the exclusion region.

Using the same simulation model and parameters as in the previous section, the rates achieved with IFM are depicted in Figure 5.2. With IFM, we take full advantage of the soft-decision policy for large values of d. For low values of d, interference mitigation considerably reduces the effect of collisions with pulses from strong interferers. With up to 8 links, there is no exclusion region. For 15 links, a small exclusion region is present for link distances of 12 and 18 meters. However, the rate difference between the exclusion case and the case when all sources send together is small. All in all, we find that the size of the exclusion region is negligible.

5.2 The DCC-MAC Protocol

5.2.1 Rate Adaptation: Dynamic Channel Coding with Incremental Redundancy

We propose a dynamic channel coding (DCC) procedure where the rate is constantly adapted to the level of interference experienced at a receiver. Ideally, DCC should always use the highest code rate that still allows for the decoding of the data packet. Thanks to the Viterbi decoding algorithm used with the RCPC codes, a destination that can decode can also determine the highest possible code rate. To ease the discussion of the DCC procedure, the set of available rates is denoted by

$$R_0 = 1 > R_1 > \ldots > R_N. \tag{5.1}$$

DCC works as follows[1].:

- A source S keeps a variable $\texttt{codeIndex}(D)$: it is the code index to be used for communication with D. Initially or after a sufficiently long idle period, S uses the lowest rate code with $\texttt{codeIndex}(D) = N$.
- When D sees that a packet is sent but cannot decode it, it sends a NACK back to S.
- As long as S receives NACKs, further packets with punctured bits (each time up to the size of the original packet) are sent, until the transmission succeeds or no more punctured bits are available. In the latter case, S may attempt a retransmission at a later time.
- As soon as D can decode, it computes the smallest index j such that rate R_j would have allowed to successfully decode. D returns index $j + 2$ in the ACK to S.

[1]Note that in contrast to the data part of a packet, the MAC header is encoded with rate R_N so that a receiver can determine that it received a packet even if it is not able to decode the data. Also control packets always use rate R_N.

- When a source with $\texttt{codeIndex}(D) = i$ in the cache receives an ACK with index $j+2$, if $j + 2 < i$ then $\texttt{codeIndex}(D) = i - 1$, else $\texttt{codeIndex}(D) = j + 2$.

- If S receives neither an ACK nor a NACK, it is likely that D is not listening (see Section 5.2.2). In this case, S will abort the transmission (without sending incremental redundancy) but may retry at a later time.

Figure 5.3(a) gives an example of the rate adaptation procedure. Because it is hard to measure the SINR in UWB, we determine the optimum code after packet reception. To do so, we take advantage of the Viterbi decoder: Decoding of a data packet encoded with rate R_i is performed by step-wise traversal of the trellis of the Viterbi decoder [12]. At each step, a trellis branch is chosen, where a branch corresponds to a specific decoded bit. The packet is then reproduced from the bits corresponding to the sequence of selected branches. Hence, as soon as the outcome of a decoding step for a higher rate code $R_j > R_i$ differs from that of the actual channel code, code R_j can be eliminated. Because of the rate compatibility feature of RCPC codes, this allows to also eliminate all codes with $R_k > R_j$. The highest rate code that remains is still powerful enough to decode the packet.

For good performance and a short transmission delay, sending redundant information should rarely be necessary. It is more important that the transmission succeeds directly without having to send additional punctured bits than using the highest possible code rate. Ideally, the more stable the channel conditions, the closer the code used for the next transmission should be to this highest rate code. In practice, we use a safety margin to reduce the probability of retransmission when channel conditions deteriorate. We find that the heuristic of using a channel code rate R_{j+2} if the highest possible code rate is R_j performs sufficiently well. The code R_{j+2} is indicated to the sender in the acknowledgment packet (ACK). The same calculations are performed for all subsequent data transmissions to maintain the same safety margin. If conditions improve and the safety margin is larger than two, the code index is reduced and if the safety margin is violated the code index is increased accordingly.

5.2.2 The Private MAC: Resolving Contention at a Destination

With the IR-UWB physical layer, many senders may communicate simultaneously within the same collision domain and a sender cannot know if the intended receiver is idle or busy other than by actively listening for packets to or from it. To design an efficient, low overhead MAC layer, a careful orchestration of the transmissions of the nodes is required. Our MAC layer is

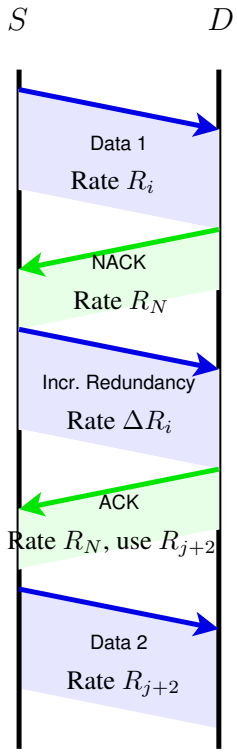

(a) Dynamic Channel Coding example: The first transmission attempt fails and additional data has to be transmitted so that the packet can be decoded. The rate to be used for subsequent packets is adjusted accordingly.

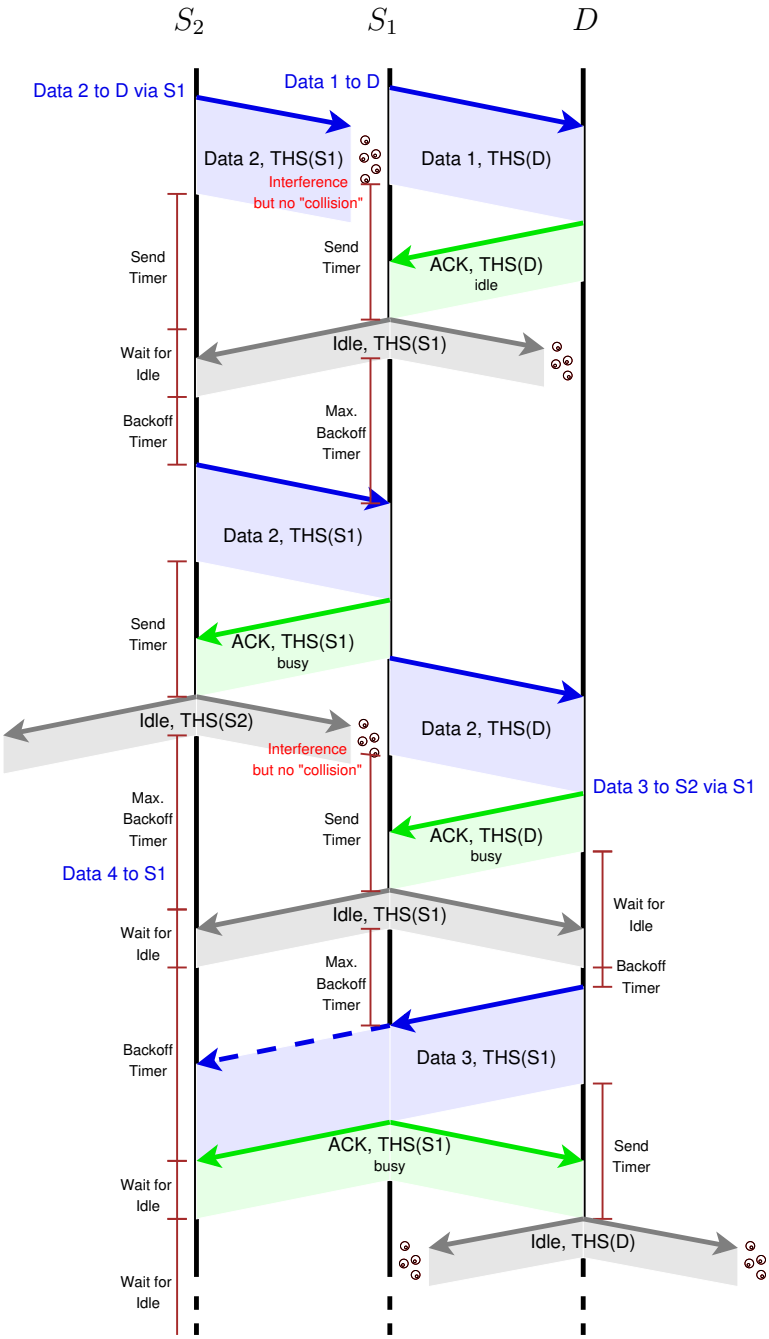

(b) Multi-hop scenario: Transmission from S_2 to D via S_1 fails since S_1 is already sending to D. S_2 retries after receiving an idle signal from S_1. After reception at S_1, the packet is immediately forwarded to D. D then sends data back to S_2 (again via S_1). The interplay of $wait\_for\_idle$ timer and backoff timer results in short idle times and forwarding delays and very few unnecessary transmissions to a destination that is busy.

Figure 5.3: Functioning of the MAC layer with dynamic channel coding (left) and multiple-access control (right)

based on a small amount of signaling between communicating nodes and careful selection of timeout values and THSs to listen on.

We use receiver-based THSs, which means that the data packets are transmitted using the THS of the receiver. A node listens to up to three THSs at the same time. It always listens on the broadcast THS, which is the same for all nodes, and on its own THS. When sending data to another node, it further listens on the THS of the destination. We denote by $THS(S)$ the THS of node S and by $THS(B)$ the broadcast THS.

Successful Transmission

A successful data transmission consists of the actual data packet, an ACK, and an idle signal. The code used for the data packet depends on previous channel conditions whereas ACK and idle are always coded with the lowest rate code.

Assume a node S_1 has data to transmit to an idle node D, as in the first transmission shown in Figure 5.3(b). S_1 will send the data packet using $THS(D)$ and will also start listening on $THS(D)$. As soon as D can decode, it sends back an ACK using its own $THS(D)$. The ACK carries an idle flag. It is set if the interface queue of D is empty (i.e., D was the final destination of the current packet and it neither has an own packet to transmit nor another packet to forward). While S_1 is waiting for the ACK from D, it disables listening on its own THS to avoid receiving a data packet and therefore missing the ACK. Upon reception of the ACK, S_1 transmits an idle signal on its own $THS(S_1)$, ceases to listen on $THS(D)$, and starts listening on its own THS again.

A node may do a backoff between zero and the maximum backoff time t_{max} before sending. To ensure that any node that wants to send to S_1 can do so after the idle signal, S_1 waits for a time interval of t_{max}. Only if no node sends a packet to S_1 during this time interval, S_1 is allowed to send the next packet. Otherwise, it first has to receive a data packet from another node as shown in the example in Figure 5.3(b). It can then send an ACK with the busy flag set to indicate that it will now send the next data packet. In the example, S_1 has to further forward the packet it received from S_2 and will do so immediately after the transmission of the ACK.

This scheme ensures that nodes alternately send and receive (unless there is nothing to send or to receive). It is vital for a fair sharing of resources (i.e., access to nodes). A probability of 50% for sending and receiving is near the optimal operating point for the relay simulations considered in [210]. We found that directly alternating between sending and receiving instead of doing it randomly improves forwarding performance with our MAC layer.

Failed Transmission

A node S_1 is only allowed to immediately send data to a destination D if none of the previous transmission attempts to D failed (or if S_1 and D did not communicate at all for a certain amount of time and D is idle). If D is busy, such a transmission attempt will fail, but will usually only cause a small amount of interference and will not disrupt the ongoing communication of D (as indicated by the bubbles in the graph). If D is already receiving data on $THS(D)$, a data packet from S_1 will be sent on the same THS. Due to the time asynchronism and the multipath propagation channel, a transmission on the same THS will create the same interference as a transmission on a random THS. Only in the case of two almost simultaneous transmissions, the interference might result in a packet loss. In any case, any further transmissions from S_1 to D are only possible after S_1 receives the corresponding idle signal. If, instead, D is sending to another node, the communication will take place on a different THS and S_1 will only cause some interference. A node may repeat a failed transmission a certain number of times (we use four in our simulations).

Deferred Transmission

In the example, node S_2 transmits to S_1 while S_1 itself is transmitting to D. Therefore, the transmission of S_2 will fail. After the transmission of the data packet, S_2 will start listening on $THS(S1)$ for the ACK. If it does not immediately receive an ACK (or NACK) after the time it takes to send the ACK and twice the maximum propagation delay (i.e., after the expiration of the `send` timer), it knows that the transmission failed. It will then set a `wait_for_idle` timer to the duration of a packet transmission with the lowest rate code, the transmission time of an ACK and twice the maximum propagation delay. When this timer expires, the data packet is resent.

If during this time S_2 receives an idle signal or an ACK with the idle flag set from S_1, as shown in the example, it will cancel the `wait_for_idle` timer and start the backoff timer. If the backoff timer was still paused from a previous transmission attempt, it will resume the backoff with the current value of the backoff timer. When the backoff timer expires, S_2 sends a data packet. If it sees a data packet for S_1 before the timer expires, it would pause the backoff timer and restart the `wait_for_idle` timer. If, instead, S_2 were to receive an ACK from S_1 with the busy flag set, it would know that S_1 will transmit a packet and would therefore start the idle timer anew and continue to listen for the next idle signal. S_1 has to issue an idle after its own packet transmission and when this idle signal is received, S_2 can resume with its backoff

timer.

This is shown in the example for the transmission of data packets 3 and 4. Both D and S_2 have a packet to transmit to S_1 and their backoff timers are running. The timer of D expires first. Assume that S_2 can decode the MAC header encoded at the lowest rate code (but will not necessarily be able to decode the data part of the packet). S_2 will pause its backoff timer and set the `wait_for_idle` timer. In the example, the timer is started anew after S_2 receives an ACK from S_1 with the busy flag set. In case S_2 cannot even decode the MAC header, it will send a packet after the expiration of the backoff timer but as mentioned before, this transmission will usually only create some interference.

In the special case where a node wants to send to the node it just received a packet from, as is the case with data packet 3 from D, the node *always* has to wait for the idle signal even if it would otherwise be allowed to send immediately. This is necessary to prevent that the data packet is sent at the same time as the idle signal and is therefore lost. It is further possible to piggyback data onto the ACK packets. For simplicity, this is not done in the example figure but it significantly improves performance when two-way communication is common (e.g., when TCP is used as transport protocol). After such an exchange, both nodes have to issue an idle signal or an ACK with the idle flag set to allow other nodes to contact them.

While a node is waiting for an idle signal, it will listen on the THS of the destination to receive the idle packet, as well as its own THS. In case a data packet is received, it will reply with an ACK and then resume waiting for the idle signal.

A node may resume sending without waiting for an idle signal (or an ACK with the idle flag set), when the idle timer expires and the following transmission succeeds (i.e., no idle signal is received for the maximum transmission time but the destination was in fact idle). Dynamically switching between immediate transmission and an invitation-based scheme allows to keep access delays low in a lightly loaded network and at the same time provides fair access to nodes as soon as there is contention. Futile packet transmissions to destinations that are busy are almost completely avoided.

5.3 Performance Evaluation

So far, we analyzed the basic properties of our protocol in very simple scenarios by means of Matlab simulations. The main goal of the simulations in this section is to investigate if our protocol works as expected under more realistic conditions. To this end, the well-known network simulator ns-2 [181] has been significantly extended by incorporating a model for a UWB

physical layer as well as new MAC layer protocols. The details of the ns-2 implementation are described in Chapter 10.

5.3.1 Performance Metric and Simulation Parameters

The performance metric is the average data throughput achieved by all nodes, taking into account the loss in bit rate due to channel coding and the overhead due to the transmission of control packets.

For comparison purpose, we simulate several MAC protocols. For all of them, the *same* UWB physical layer model is used. The parameters of the physical layer are the ones described in Section 5.1.1. Since we are interested in very low-power MAC protocols, we allocate the same maximum power limit for the exclusion-based MAC protocols as for the DCC-MAC protocol.

The following protocols are compared to our dynamic channel coding-based MAC protocol (DCC-MAC):

Power control The power control MAC is based on the CA/CDMA protocol [175]. We adjusted the protocol to work together with a UWB physical layer instead of CDMA for which it was originally designed. While our implementation abstracts from some protocol details, it captures the main aspect of adjusting the power instead of the channel code. We define a minimum signal-to-interference ratio that is necessary to achieve a given probability of error. The transmission power of the packet is then set so as to achieve the desired SINR plus a safety margin, which allows for a limited amount of future transmissions to overlap with the current transmission. If the required power level exceeds the maximum power limit at the sender or the interference margin of ongoing transmissions, the sender defers from transmitting and retries after a random backoff.

Mutual exclusion with random access (RA) All nodes use the same THS. Therefore, if a node is transmitting, all other nodes within communication range will receive the packet and cannot send (since a node cannot send and receive at the same time). All nodes but the destination discard the packet. If a node has a packet to transmit while another node is sending, it retries after a backoff.

Mutual exclusion with TDMA We do not actually implement this protocol in ns-2. Instead, we simulate the transmission of every link independently of others, and obtain the rate for each

one. We assume each link has the channel access for the equal fraction of the time, and from that we calculate the average data-rate per link. This corresponds to an ideal TDMA protocol where the schedule is obtained at no cost.

While the details differ, the principles on which the implemented power control MAC is based are the same as the ones of other power control protocols proposed for UWB, such as [154, 160]. Similarly, the MAC layer proposed for IEEE 802.15.3 [92] can be seen as a combination of TDMA and the exclusion-based random access MAC.

5.3.2 Simulation Results

We have obtained simulations results for several scenarios.

Random Topology Scenario

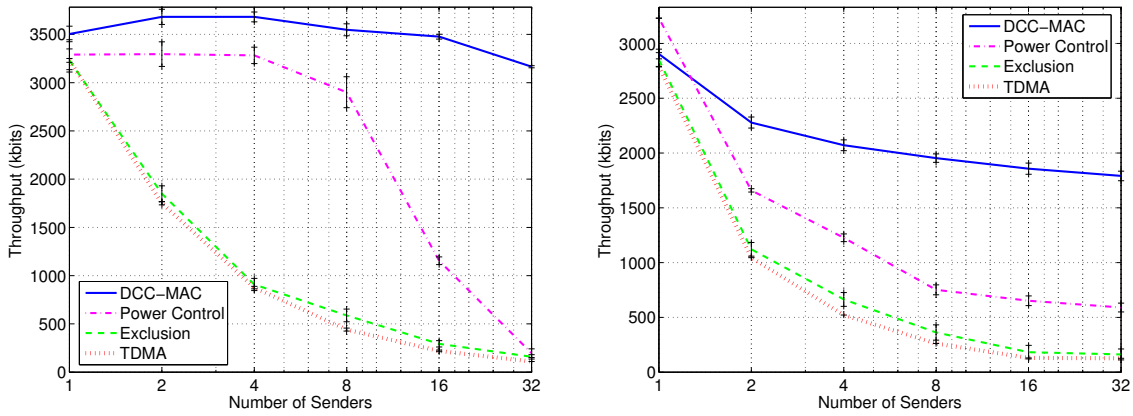

(a) Random topology scenario with nodes placed on 20×20 meters square.

(b) Near-far topology scenario with sender-receiver distance of 20 meters and receiver-interferer distance of one meter.

Figure 5.4: Average throughput per user vs. number of senders for the random and near-far topologies scenario with single-hop communication. The performance benefits of the DCC-MAC protocol are particularly apparent in scenarios with strong interference.

In this scenario, nodes are randomly placed on a square surface of 20×20 meters. Source-destination pairs are randomly chosen such that each node is either a source or a destination of exactly one link. The sender sends UDP packets at the highest possible rate to the receiver. The number of senders varies between one and 32.

For up to eight senders, power control performs almost as well as DCC-MAC since the adaptation of the transmission power allows the nodes to send concurrently for most of the

simulated topologies. However, for 16 or more senders, the performance of power control quickly drops to that of the exclusion based protocols, since the increased interference exceeds the allocated interference margins. For the exclusion-based protocols we see that the achieved throughput is inversely proportional to the number of senders. DCC-MAC only has a slight decrease in rate for larger numbers of senders due to the dynamic rate adaptation that becomes important when the number of nodes (and therefore interference) is high.

Generalized Near-far Topology Scenario

Since ns-2 does not allow for three-dimensional simulation topologies, the near-far topology we use for the simulations is an "unfolded" two-dimensional version of the one shown in Figure 5.1. Again we consider scenarios with one to 32 senders. The distance L between sender and receiver varies from one meter to 20 meters but for reasons of brevity we only show the worst case graph with $L = 20$ meters. The distance d from a receiver to the closest interferer is one meter.

The arrangement of the nodes in a near-far topology results in much stronger interference than in the random scenario. As can be seen from Figure 5.4(b), DCC-MAC clearly outperforms the other MAC solutions. There is a moderate drop in rate from 2900 kbit/s to 1800 kbit/s when we increase the number of senders from one to 32. For the other MAC protocols, the drop in rate with an increasing number of senders is much more pronounced. Again, power control comes closest to DCC-MAC performance since it allows for a limited amount of concurrent transmissions. However, the difference in performance is more obvious than in the random scenario. It achieves between 75% and 30% of the rate of DCC-MAC in a near-far setting. Both exclusion-based protocols, TDMA and random access, have very similar performance which is significantly worse than that of power control and DCC-MAC. The improvement in SINR and the resulting higher channel code rates cannot compensate for the loss in transmission time due to exclusion.

Multi-hop Scenario

Multi-hop forwarding in wireless networks has been extensively studied and was shown to be difficult for exclusion-based MAC protocols (see for example [197, 211]). As is usually done, we investigate the multi-hop performance of the different MAC protocols using a topology where nodes are equally spaced along a line. Source and destination are at either ends of the line of nodes; intermediate nodes forward packets between them. The distance between nodes

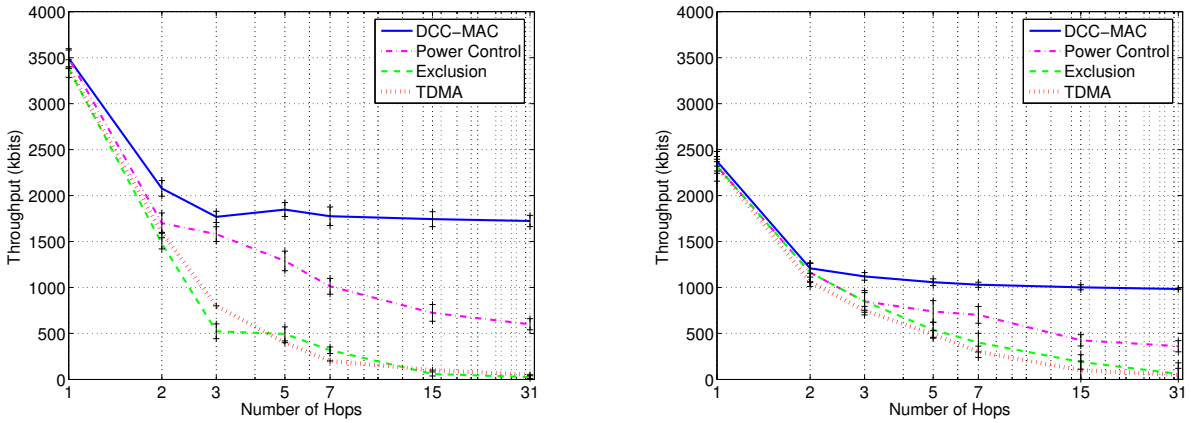

Figure 5.5: UDP (left) and TCP (right) throughput achieved in the multi-hop scenario. We show average throughput vs. number of hops. There is almost no drop in throughput for the DCC-MAC protocol as the number of hops increases.

is 20 meters.

The simulation results are shown in Figure 5.5. In general, TCP throughput is lower than UDP throughput since TCP data packets compete with acknowledgments traveling on the return path.[2] The most apparent drop in throughput occurs when the number of hops increases from one to two. The intermediate node in a two hop topology can either send or receive which necessarily halves the throughput for all of the protocols. A striking feature is that DCC-MAC is able to maintain this rate when the number of hops increases beyond two. For UDP, there is a small drop in throughput from two hops to three hops and from there on the rate remains constant. The decrease with TCP is also on the order of a few percent. This excellent performance of DCC-MAC is mainly due to the good interplay of timers and signals which results in close to optimal schedules (no piggybacking of data is used.) For power control, there are a number of schedules that allow concurrent transmissions over at least a few of the hops; throughput is therefore in between that of DCC-MAC and the exclusion-based protocols.

5.4 Discussion and Conclusion

We have presented a practical PHY-aware MAC for IR-UWB ad hoc networks. Our design radically differs from existing ones. We implement a rate adaptation algorithm that does not require interference estimation. We address contention at destinations with the private MAC, and we overcome the absence of carrier-sensing with an elaborate signaling protocol. Our

[2]For TCP we use the TCP Sack implementation of ns-2 version 2.27 with default parameters.

scheme works very well for low data-rate IR-UWB, i.e., when N_c is large. Our initial results indicate that even for medium values of N_c (around 100) the performance remains similar. For very low N_c, interference mitigation is not sufficient. Furthermore, inter-symbol interference creeps in. Exclusion mechanisms such as TDMA or CSMA/CA are then likely required.

It is interesting to observe that DCC-MAC is actually quite close to the mandatory MAC protocol in the IEEE 802.15.4a amendment [64] with the following notable exceptions: in IEEE 802.15.4a a common acquisition preamble is used, there is no rate adaptation and no idle packet.

For our design we assumed BPSK modulation. Other modulation schemes exist and it seems that our MAC protocol would apply with little change to such modulation schemes. We adapt the rate with a variable rate channel code. But we could also take advantage of using a variable M-ary PPM modulation scheme to increase the data-rate when the interference is low. But this also remains for further study.

Finally, we have developed a protocol guided by the idea of arranging the physical layer and the MAC protocol such that collisions may be replaced by rate reduction. This idea is optimal for our setting, but it could prove interesting in other settings as well. The optimal MAC protocol in narrow-band systems is likely to be a combination of rate adaptation and mutual exclusion. Mutual exclusion has severe performance problems, as witnessed by the intense research on improving the 802.11 MAC protocol for use in ad-hoc and mobile networks. In contrast, rate adaptation does not appear to have these problems, as it is a private affair between a source and a destination. Therefore it would be interesting to add this component to existing MAC layers.

Chapter 6

Performance Evaluation of IR-UWB Networks Using Common or Private Acquisition Preambles

The low data-rate IR-UWB networks that we consider are packet based and have no global synchronization. Hence, the first step towards correct packet reception is packet detection and timing acquisition: Before recovering the payload of the packet, the destination of the packet must detect the packet on the medium and determine when exactly the payload begins. Actually, even if there exists a global synchronization in the network, packet detection is still necessary. Packet detection and timing acquisition are performed on a per packet basis and both typically rely on the presence of an acquisition preamble at the beginning of each packet. How this preamble is chosen is a network design issue and, as we demonstrate in this chapter, has an impact on the performance of the network.

We compare two possible design choices in order to evaluate how the choice of the acquisition preamble affects the throughput for IR-UWB networks. First, as in the IEEE 802.15.4a amendment, a simple design choice of the network is to have an identical and common acquisition preamble for the entire network. Second, as for DCC-MAC or [164], another design choice is to have a *private* acquisition preamble per destination. For example, with DCC-MAC, a source generates the acquisition preamble of its intended destination using the THS of this destination. As we explained in Chapter 5, this THS is itself derived from the MAC address of the destination.

The throughput of a network using a private acquisition preamble is likely to be much higher

than the throughput of a network using a common acquisition preamble. Indeed, in a network with a common acquisition preamble, a packet might contend for timing acquisition with packets sent by any node in the entire network. In contrast, with a private acquisition preamble, the contention is reduced to packets transmitted to the same destination. Of course, a private acquisition preamble comes with the cost of learning the acquisition preamble of the destination. Hence the throughput increase must be large (maybe larger than 100%) in order to alleviate the associated cost[1]. In fact, with digital hardware implementations, the use of private acquisition preambles is essentially not more costly than a single common preamble [72]. In fact, a node does not need to listen to more than a few preambles as explained, in Section 5.2.2: Generally, a node needs to listen to its own preamble, the one from the destination and a preamble for the broadcast address.

For the performance evaluation, we use two different approaches. Our first approach is to derive an analytical model to compute the saturation throughput, thus establishing an equivalent for an IR-UWB network of the celebrated Bianchi's formula [177, 178] (equations (6.15) and (6.16)). In saturated conditions, a source always has a packet available to transmit, and queueing at the source is ignored. Even though IR-UWB networks are expected to be low-data rate networks, the performance in saturation conditions still matters. For instance, in case of sudden bursts of activity, it is important to ensure that the network is able to sustain the sudden load. The detection of a fire is a typical event that can produce a sudden burst of activity in a sensor network. Due to the inherent difficulty, the computation of the saturation throughput is solved for symmetric and homogeneous networks only, where all nodes are in range of each other. Our analytical model is built on a mean-field assumption and involves the resolution of a fixed-point equation (see Section 6.1). The mean-field assumption is equivalent to the decoupling approximation in [180].

Our second approach is to turn to ns-2 [181] simulations. First, they allow for the validation of the results obtained with our analytical model. Second, we can address more realistic scenarios with multi-hop topologies and TCP.

For both the analytical model and the ns-2 simulations, we assume that the underlying acquisition algorithm is the one in [63]. At the link layer, we assume that the DCC-MAC protocol (see Chapter 5) is used. The reason for choosing the acquisition algorithm in [63] is its robustness to multi-user interference (MUI). The packet detection and timing acquisition

[1]If TCP/IP is running, nodes have a unique identifier that must be known by neighboring nodes and the acquisition preamble can be easily generated from the unique identifier. Furthermore, IEEE 802.15.4 nodes have a unique EUI-64 identifier that could also be used to generate an acquisition preamble.

algorithm uses the knowledge of the THS that generated the acquisition preamble to distinguish this acquisition preamble from noise and concurrent transmissions using different acquisition preambles. In the case of concurrent transmissions with a common acquisition preamble, the algorithm in [63] allows for a successful timing acquisition with one of the concurrent signals.

For both the analytical model and the ns-2 implementation, packet detection and timing acquisition is not modeled at the level of detail of the physical layer. Due to the time-scale difference between events at the physical layer and events at the upper layers, the complexity is prohibitive. Rather, we use the probability of missed detection and the probability of false alarm at the physical layer derived in [63] as inputs to a model of packet detection and timing acquisition (see Section 6.1.2). Furthermore, in the analytical model, we consider noise and MUI only during packet detection and timing acquisition. We expect that interference in the data transmission part will have little effect on the result of our comparison, as we focus on the timing acquisition. This is a reasonable assumption in low data-rate conditions with an optimal Rake receiver at the physical layer where, with the addition of an error correcting code, the bit error rate can be negligible. In addition, in the case of unintentional packet acquisition (i.e. a packet not for the destination), we consider two options: with *early discard*, a destination drops the packet right after reading the header containing the hardware address; with *late discard*, the packet is fully received. Late discard is often necessary, because a packet may have to be fully received in order to decode a possible checksum at the end of the packet. Note that even in the case of private acquisition preambles, unintentional packet acquisition can occur due to noise and MUI [63].

Our contributions in this chapter are the following. First, we develop an analytical model to compute the saturation throughput of an IR-UWB network. One novelty of our model, compared with previous works, is that it explicitly takes into account packet detection and timing acquisition. Our model can be easily used with different MAC layers or different acquisition algorithms. Then, using the model, we show that a private acquisition preamble offers a large throughput gain compared to a common acquisition preamble. Moreover, the throughput difference grows with the number of concurrent transmitters and interferers. Finally, with ns-2 simulations on multi-hop topologies with TCP flows, we demonstrate that a network using private acquisition preambles exhibits a stable throughput. On the contrary, using a common acquisition preamble exhibits the presence of a compounding effect similar to the exposed terminal issue in IEEE 802.11 networks: the throughput is severely degraded and complete flow starvation may occur.

The remainder of this chapter is organized as follows. In Section 6.1, we develop the an-

alytical model to compute the saturation throughput of a symmetric and homogeneous UWB network. The performance evaluation follows in Section 6.2. We discuss the results and conclude the chapter in Section 6.3.

6.1 A Saturation Throughput Analysis of an IR-UWB Network with Packet Detection and Timing Acquisition

In this section, we compute the saturation throughput of an IR-UWB network. We assume that the underlying physical layer is a classic IR-UWB physical layer as in Section 2.2.8. No particular assumption need to be made on the propagation channel or the receiver. In the following we give the problem description and important modeling assumptions.

Saturation Throughput Analysis and Mean-field Assumption

We begin by defining a few symbols:

- $\lambda_0^{(i)}$ is the saturation throughput of a source i in packets per second.
- $\lambda^{(i)}$ is the rate of packet transmission *attempts* per second. Note that $\lambda^{(i)} \geq \lambda_0^{(i)}$, because $\lambda^{(i)}$ comprises successful packet transmissions and packet retransmissions.
- $p_{\text{acq}}^{(j)}$ is the average probability of proper packet detection and timing acquisition at a destination j.
- S and D are the total number of sources and destinations in the network respectively.

Generally, finding the exact saturation throughput of every source is a highly difficult problem to solve [180]. In fact, we have to model the interactions of each node with every other node. Therefore, in order to keep the analysis tractable we make the following two assumptions:

1. The network is symmetric, homogeneous, and single-hop. Every destination has the same number of sources.
2. We make a mean-field assumption [179] where we assume that all sources have an identical and independent behavior. Hence $\lambda_0^{(i)} = \lambda_0$ and $\lambda^{(i)} = \lambda$ for $i = 0, \ldots, S-1$, and $p_{\text{acq}}^{(j)} = p_{\text{acq}}$ for $j = 0, \ldots, D-1$. The mean-field assumption is also known as the decoupling approximation in [180].

The first assumption also implies that all stations use the same physical layer and the same MAC layer (in our case the DCC-MAC protocol). Second, we assume that in a saturated regime, the network model is ergodic. Indeed, there is no queueing and every source waits until a packet is successfully transmitted before attempting the transmission of a new packet. Therefore, there should not be any possible walk to infinity. Finally, we break our general problem, of finding the saturation throughput, into two subproblems.

1. Given a source and its intended destination, the saturation throughput λ_0 of the source depends on the probability of successful packet acquisition p_{acq} at the destination. Hence, our first subproblem is to compute λ_0 and λ given p_{acq} i.e. $[\lambda_0, \lambda] = f(p_{\text{acq}})$. We solve this problem in Section 6.1.1.

2. In the second subproblem we have a receiver with several sources with saturation throughput λ_0 and attempt rate λ. We want to compute p_{acq} i.e. $p_{\text{acq}} = g(\lambda_0, \lambda)$. We solve this problem in Section 6.1.2.

Hence, the saturation throughput is given by $f(x)$ where x is the solution of the fixed point equation

$$g(f(x)) - x = 0, \quad x \in [0, 1]. \tag{6.1}$$

We solve the fixed point equation numerically. Section 6.1.1 explains how to solve the first subproblem in order to compute the values of λ_0 and λ given p_{acq}.

6.1.1 Computing λ_0 and λ as a Function of p_{acq}: Modeling the DCC-MAC Protocol

Modeling DCC-MAC

The DCC-MAC protocol uses both a rate adaptation algorithm and a binary exponential backoff (see Chapter 5). In the modeling, we assume that DCC-MAC uses a fixed rate. Indeed, in a steady state all sources in the symmetric and homogeneous network have the same rate. Hence, the behavior of DCC-MAC depends solely on the binary exponential backoff and can be modeled by a discrete-time, homogeneous, Markov chain [180]. We will use this Markov chain to compute both λ_0 and λ given p_{acq}.

The Retransmission Markov Chain X_n

Let X_n be the retransmission state of a station (see Figure 6.1(a)) and R the maximum number of retransmissions before a packet is dropped. The Markov chain X_n has $R+2$ states (numbered

from 0 to $R+1$): a packet transmission attempt always initiates and finishes in state 0. A packet retransmission corresponds to a transition from state i to $i+1$. A successful packet transmission corresponds to a transition from any state $i=0,\ldots,R$ to the state 0. Finally, the packet is dropped if state $R+1$ is reached. The transition probabilities are the following:

$$\begin{aligned} &p_X\left(i,i+1\right)=1-p_{\text{acq}}=p_{\text{fail}}, && i=0,\ldots,R \\ &p_X\left(i,0\right)=p_{\text{acq}}, && i=0,\ldots,R \\ &p_X\left(R+1,0\right)=1 \end{aligned} \tag{6.2}$$

where $p_X\left(i,j\right)=\mathbb{P}\left(X_{n+1}=j|X_n=i\right)$. The stationary distribution of X_n is

$$\pi_X(i)=\frac{p_{\text{acq}}\left(1-p_{\text{acq}}\right)^i}{1-\left(1-p_{\text{acq}}\right)^{R+1}}, \quad i=0,1,\ldots,R+1 \tag{6.3}$$

where we used $\sum_{k=0}^{n}x^k=\frac{1-x^{n+1}}{1-x}$.

Using the Markov Chain X_n to Compute λ_0 and λ

Each packet transmission attempt corresponds to a trip on the chain X_n starting in state 0 and returning back to the state 0. The saturation throughput λ_0 can be computed by dividing the average number of successful packet transmissions per trip by the average duration of a trip. Similarly, the attempt rate λ can be computed by dividing the average number of packet transmission attempts per trip by the average duration of a trip.

For a trip from state 0 back to state 0, we define three random variables:

- N_{s} is the number of successful packet transmissions per trip: N_{s} is equal to 0 or 1.
- N_{a} is the number of packet transmission attempts per trip. N_{a} can take values in the range $[1,2,\ldots,R]$.
- T is the duration of a trip.

To figure out the average of N_{s} per trip, the key observation is that a successful packet transmission corresponds to a transition from any state $i=0,\ldots,R$ to state 0. Hence, in order to compute the average of N_{s} per trip, we need to compute the average number of transitions per trip from any state $0,1,\ldots,R$ to the state 0. Likewise, a packet transmission attempt corresponds to a transition from state i to $i+1$. Consequently, to compute the average of N_{a} per trip, we need to compute the average length of a trip on the chain X_n *before* a transition back

to state 0 (excluding the transition to state 0). Finally, to compute the average of T per trip, notice that each state transition on the chain X_n corresponds to a succession of events in the underlying MAC protocol with a given duration. For instance, a transition from state 0 to state 1 corresponds to the duration of a failed packet transmission. This duration comprises the duration of a packet transmission, the expiration of one or more timers, and the average backoff time in stage 1.

More formally, in addition to the transition probabilities, we define $m(i,j)$ to be the *cost* of a transition from state i to state j. Depending on whether we compute the average of N_s, N_a, or T per trip, we assign different values to $m(i,j)$. For instance, for N_s, we set $m(i,0) = 1$ for $i = 0, \ldots, R$ and 0 otherwise. Then, we compute the average cost of a trip from the state 0 back to the state 0 with the proper values for $m(i,j)$. The cost of a particular trip is simply the sum of the cost of each transition in this trip.

The following two definitions formalize the content of the previous paragraphs.

Definition 1 (Time of first return to state 0)**.** *Let us assume that $X_0 = 0$ (i.e. the state of the Markov chain X_n is 0 at time 0), then*

$$\tau_1 = \inf_n \{n \geq 1 \mid X_n = 0\} \tag{6.4}$$

is the time of first return to state 0.

Definition 2 (Expected cost of a trip from state 0 to 0)**.** *Using the previous definition, the expected cost of a trip from state 0 back to state 0 is*

$$\mathbb{E}\left(\sum_{n=1}^{\tau_1} m\left(X_{n-1}, X_n\right) \middle| X_0 = 0\right). \tag{6.5}$$

Therefore, the key to compute λ_0 and λ is

1. To properly assign costs $m(i,j)$ to the transitions (see Equations 6.6, 6.7, and 6.8 for N_s, N_a, and T respectively).

2. To compute (6.5) with the proper costs depending on whether we want to find the average of N_s, N_a, or T.

In the following subsections, we first define the costs for N_s, N_a, and T. Then, we explain how to compute (6.5) using Palm calculus [212, 213]. And we finally apply (6.5) to compute λ_0 and λ.

Definition of the Costs to Compute λ_0 and λ

For N_{s}, we must compute (6.5) with the the costs

$$m_{N_{\text{s}}}(i,0) = 1, \quad i = 0, \ldots, R \tag{6.6}$$

and 0 otherwise. For N_{a}, we use instead

$$m_{N_{\text{a}}}(i,i+1) = 1, \quad i = 0, \ldots, R \tag{6.7}$$

and 0 otherwise. Finally, for T, the costs are

$$\begin{aligned} &m_T(i,0) = t_{\text{acq}} + t_{\text{tx}}, && i = 0, \ldots, R \\ &m_T(i,i+1) = t_{\text{acq}} + t_{\text{fail}}(i), && i = 0, \ldots, R \\ &m_T(R+1,0) = t_{\text{drop}} \end{aligned} \tag{6.8}$$

and 0 otherwise. The quantity $t_{\text{acq}} + t_{\text{tx}}$ corresponds to the duration of a packet acquisition and timing synchronization followed by a successful data exchange, $t_{\text{acq}} + t_{\text{fail}}(i)$ is the duration incurred by a failed packet acquisition, and t_{drop} is the time taken when the backoff algorithm reaches the $(R+1)$-th state where the packet to be transmitted is dropped. As they are protocol specific, the details of t_{acq}, t_{tx}, $t_{\text{fail}}(i)$, and t_{drop} are given in Section 6.2. Still, note that $t_{\text{fail}}(i)$ depends on i, i.e. it depends on the particular retransmission state; typically, as the number of retransmissions increase, the size of the contention window for the backoff timer increases.

Computing the Expected Cost of a Trip Using Palm Calculus

We begin by recalling what a Palm probability and a Palm expectation are. This allows us to reformulate (6.5). Then, we state one of the central results of Palm calculus, which is the Palm inversion formula, and we use it to compute (6.5).

Definition 3 (Palm probability and Palm expectation)**.** *Given an integer valued point process T_n of rate Λ, the Palm probability $\mathbb{P}^0$ is the conditional probability given that $T_0 = 0$. Similarly, the Palm expectation $\mathbb{E}^0$ is the conditional expectation given that $T_0 = 0$.*

We can take advantage of Palm calculus to rewrite (6.5) as follows,

$$\mathbb{E}\left(\sum_{n=1}^{\tau_1} m\left(X_{n-1}, X_n\right) \Big| X_0 = 0\right) = \mathbb{E}^0\left(\sum_{n=1}^{\tau_1} m\left(X_{n-1}, X_n\right)\right). \tag{6.9}$$

Using the previous formula, we have

$$\lambda_0 = \frac{\mathbb{E}^0(N_\mathrm{s})}{\mathbb{E}^0(T)}, \quad \lambda = \frac{\mathbb{E}^0(N_\mathrm{a})}{\mathbb{E}^0(T)} \tag{6.10}$$

where

$$\mathbb{E}^0(\mathcal{X}) = \mathbb{E}^0\left(\sum_{n=1}^{\tau_1} m_{\mathcal{X}}\left(X_{n-1}, X_n\right)\right)$$

for $\mathcal{X} = N_\mathrm{s}, N_\mathrm{a}$ or T.

Now, to compute (6.9), we use the following result, available in [212] or [213] (see also in these references for a precise definition of joint stationarity):

Lemma 1 (Palm inversion formula)**.** *Let Y_n be a discrete-time random process and T_n an integer valued point process of rate Λ. If T_n, Y_n is jointly stationary, then*

$$\Lambda\mathbb{E}^0\left(\sum_{s=1}^{T_1} Y_s\right) = \mathbb{E}\left(Y_0\right)$$

Hence, in order to compute (6.9), we use the Palm inversion formula with $Y_n = m_{\mathcal{X}}\left(X_{n-1}, X_n\right)$ and $T_n = \tau_n$ (the times of visit to state 0), (6.9) becomes

$$\begin{aligned}\mathbb{E}^0\left(\sum_{n=1}^{T_1} m_{\mathcal{X}}\left(X_{n-1}, X_n\right)\right) &= \frac{\mathbb{E}\left(m_{\mathcal{X}}\left(X_{n-1}, X_n\right)\right)}{\Lambda} \\ &= \frac{\sum_i \pi_X(i) \sum_j p_X\left(i,j\right) m_{\mathcal{X}}\left(i,j\right)}{\pi_X(0)}\end{aligned} \tag{6.11}$$

for $i, j = 0, \ldots, R+2$.

Using the Expected Cost to Compute λ_0 and λ

Now, using (6.11) and the appropriate values of the costs (6.6), (6.7), and (6.8), we can compute $\mathbb{E}^0(N_\mathrm{s})$, $\mathbb{E}^0(N_\mathrm{a})$, and $\mathbb{E}^0(T)$. We have

$$\begin{aligned}\mathbb{E}^0(N_\mathrm{s}) &= \frac{1}{\pi_X(0)} \sum_{i=0}^{R} \pi_X(i) p_X\left(i,0\right) \\ &= p_\mathrm{acq} \frac{\sum_{i=0}^{R} \pi_X(i)}{\pi_X(0)},\end{aligned} \tag{6.12}$$

$$\begin{aligned}\mathbb{E}^0(N_{\text{a}}) &= \frac{1}{\pi_X(0)}\sum_{i=0}^{R}\pi_X(i)p_X\left(i,i+1\right)\\ &= p_{\text{fail}}\frac{\sum_{i=0}^{R}\pi_X(i)}{\pi_X(0)},\end{aligned} \tag{6.13}$$

and

$$\begin{aligned}\mathbb{E}^0(T) = \frac{1}{\pi_X(0)}\Bigg[&p_{\text{acq}}\left(t_{\text{acq}}+t_{\text{tx}}\right)\sum_{i=0}^{R}\pi_X(i)\\ &+p_{\text{fail}}\sum_{i=0}^{R}\left(t_{\text{acq}}+t_{\text{fail}}(i)\right)\pi_X(i)+t_{\text{drop}}\pi_X(R+1)\Bigg]\end{aligned} \tag{6.14}$$

Finally, we can use equations (6.12) to (6.14) to replace $\mathbb{E}^0(N_{\text{s}})$, $\mathbb{E}^0(N_{\text{a}})$, $\mathbb{E}^0(T)$ in (6.10), and

$$\sum_{i=o}^{R}\pi_X(i) = 1-\pi_X(R+1)$$

to obtain the following two equations:

$$\lambda_0 = \frac{p_{\text{acq}}\left(1-\pi_X(R+1)\right)}{p_{\text{acq}}\left(t_{\text{acq}}+t_{\text{tx}}\right)\left(1-\pi_X(R+1)\right)+p_{\text{fail}}\sum_{i=0}^{R}\left(t_{\text{acq}}+t_{\text{fail}}(i)\right)\pi_X(i)+t_{\text{drop}}\pi_X(R+1)} \tag{6.15}$$

$$\lambda = \frac{p_{\text{fail}}\left(1-\pi_X(R+1)\right)}{p_{\text{acq}}\left(t_{\text{acq}}+t_{\text{tx}}\right)\left(1-\pi_X(R+1)\right)+p_{\text{fail}}\sum_{i=0}^{R}\left(t_{\text{acq}}+t_{\text{fail}}(i)\right)\pi_X(i)+t_{\text{drop}}\pi_X(R+1)}. \tag{6.16}$$

Equations (6.15) and (6.16) are the equivalent of Bianchi's formula [177, 178] for an IR-UWB network. They are also fairly general results that allow us to calculate the saturation throughput of a station given p_{acq}. The details of the MAC protocol and of the backoff algorithm are abstracted in the values of $t_{\text{acq}}+t_{\text{tx}}$, $t_{\text{acq}}+t_{\text{fail}}(i)$, t_{drop}, and in the stationary distribution of the Markov chain X_n.

Now that we have equations (6.15) and (6.16) for calculating λ_0 and λ respectively, we can turn to the resolution of the second subproblem.

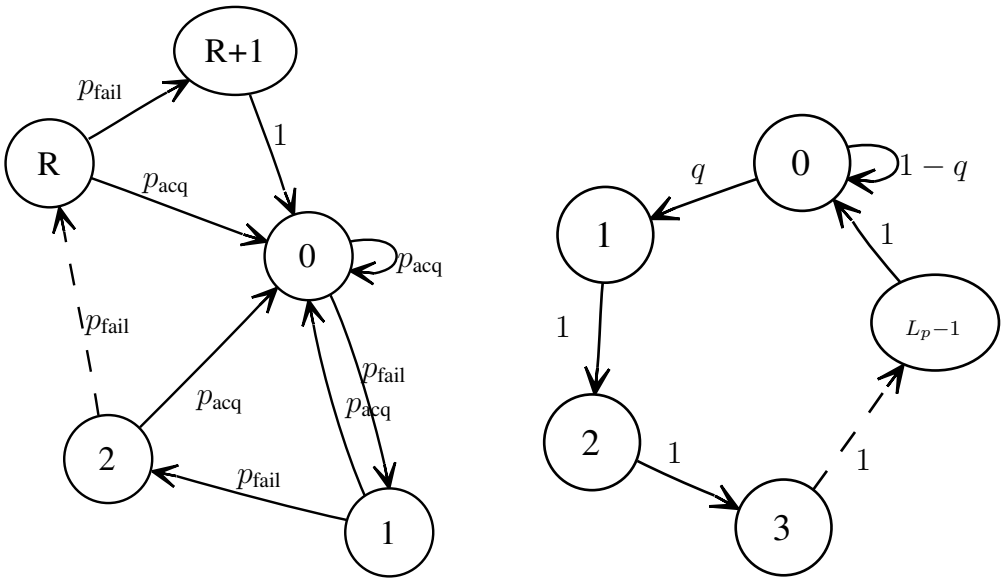

(a) X_n (b) Z_n

Figure 6.1: Retransmission Markov chain X_n (left) and transmission Markov chains Z_n (right) with their transition probabilities. For X_n, note that p_{fail} is simply $1 - p_{\text{acq}}$.

6.1.2 Computing p_{acq} as a Function of λ_0 and λ: Modeling Packet Detection and Timing Acquisition

Remember that p_{acq} is the average probability of proper packet detection and timing acquisition at *any destination*. We compute p_{acq} as a function of λ_0 and λ. We begin by defining a few symbols:

- S_{D} is the number of stations transmitting to the destination of interest. They use the same acquisition preamble than the destination of interest.
- S_{I} is the number of stations using the same acquisition preamble than the S_{D} ones but transmitting to another destination.
- I is the number of stations using a different acquisition preamble.

Modeling Packet Detection and Timing Acquisition at a Destination

A necessary condition for packet detection and timing acquisition to be achieved is that the destination not be busy. Following the model in Chapter 10, the behavior of the physical layer of a station is modeled with four states:

- IDLE: The physical layer listens to the medium. We assume that a station never sleeps and is always available.

- SYNC: The physical layer believes it has detected a packet on the wireless medium and attempts to synchronize with the beginning of this packet.

- RECV: The physical layer receives the packet. It assumes that the physical layer has correctly detected that there is a packet and is synchronized with its beginning.

- SEND: The physical layer transmits a packet.

A station is considered busy when it is in the RECV or SEND state. A transition from the IDLE state to the SYNC state occurs whenever a packet from any of the S_D or S_I sources reaches the destination. Then, for a period of time equal to the duration of the acquisition preamble of the packet that caused the transition, other packets from any of the $S_D + S_I - 1$ sources may reach the destination and compete for acquisition. This period of time is called the "vulnerable period". At the end of the vulnerable period there are two possibilities: (1) one of the competing packets is acquired by the destination or (2) due to missed detection, the whole procedure fails. In the first case, a transition to the RECV state occurs. In the second case, the destination returns to the IDLE state. The probability that a missed detection occurs depends on the level of interference and on how many concurrent transmissions start from any of the $S_D + S_I + I - 1$ other stations. In addition to increasing the level of interference, the packets from the I stations with another acquisition preamble may spur occasional false acquisitions. Such false acquisitions trigger transitions to the RECV state and keep the destination busy as if it were receiving a packet from a valid station. Remember that we consider multi-user interference only during packet detection and timing acquisition.

Accordingly, the probability of packet acquisition at the destination of interest can be modeled as

$$p_{\text{acq}} = (1 - P_{\text{busy}})\,\gamma \tag{6.17}$$

where P_{busy} is the probability that the destination is busy and γ is the conditional probability, given that the destination is not busy, that a packet from one of the $S_D + S_I$ sources is properly acquired without any missed detection. False acquisitions are taken into account in the probability P_{busy}. Although it is not explicitly written in (6.17), both P_{busy} and γ depend on λ_0 and λ.

We first proceed with γ, the probability P_{busy} is computed in the next section. We model γ as

$$\gamma = \sum_{k=0}^{S_{\text{D}}+S_{\text{I}}-1} P_k \sum_{i=0}^{I} P_i \left[\frac{1}{k+1} \left(1 - P_{\text{MD}}^{(k,i)} \right) \right] \tag{6.18}$$

where P_k is the probability that there are k concurrent transmissions from any of the S_D+S_I-1 *other* stations[2] (with the same acquisition preamble), and P_i is the probability that there are i concurrent transmissions from any of the I stations (with a different acquisition preamble). The probability of *missed detection* $P_{\text{MD}}^{(k,i)}$ depends on k and i. The probability $1 - P_{\text{MD}}^{(k,i)}$ that there is no missed detection is uniformly divided by $k+1$ as there is the packet to be acquired and the k competing packets from the S_D+S_I-1 other stations. Remember that we do not have an explicit model for $P_{\text{MD}}^{(k,i)}$. Rather, we use numerical values from extensive simulations obtained with the packet detection and timing acquisition algorithm in [63]. The probabilities P_k and P_i are modeled as

$$P_k = \left(\begin{array}{c} S_{\text{D}} + S_{\text{I}} - 1 \\ k \end{array} \right) \left(1 - Q(L_{acq})\right)^k Q(L_{acq})^{S_{\text{D}}+S_{\text{I}}-1-k} \tag{6.19}$$

and

$$P_i = \left(\begin{array}{c} I \\ i \end{array} \right) \left(1 - Q(L_{acq})\right)^i Q(L_{acq})^{I-i} \tag{6.20}$$

where $Q(L_{acq})$ is the probability that a station does not start a packet transmission during the "vulnerable period" of length L_{acq} chips (L_{acq} is equivalent to the length of the acquisition preamble in chips).

The set of equations (6.17) and (6.18) along with (6.21) to compute P_{busy} and (6.33) to compute $Q(L_{acq})$ is the main result of this part. It allows for the calculation of p_{acq} given λ_0 and λ. Notice that this set of equations is fairly general. The equations model a physical layer with multi-channel capability: in the case of IR-UWB physical layers, these channels are created by the different THSs (Section 2.2.3).

In the following, we describe first how to compute P_{busy} and second how to compute $Q(L_{acq})$.

A Model for P_{busy}

There are three cases for which a destination can be busy:

[2] with one transmission per source

- The destination is properly receiving a packet from any of the $S_D - 1$ other competing sources.
- The destination is kept busy by a packet from any of the S_I other sources with the same acquisition preamble but a different destination.
- The destination is kept busy by the false acquisition of a packet from the I sources with another acquisition preamble.

Remember that the packets from the S_I stations are acquired with probability p_{acq} (which takes into account the fact that the receiver could be busy). However, for the I stations with a different THS, only a fraction P_{FACQ} of their packets is falsely acquired (assuming the destination is not busy). Hence, we model P_{busy} as

$$P_{\text{busy}} = \lambda_0 \left(S_{\text{D}} - 1\right) t_{\text{D}} + \lambda \left(p_{\text{acq}} S_{\text{I}} + P_{\text{FACQ}} I\right) t_{\text{I}} \tag{6.21}$$

where t_{D} is the time that a packet acquired from any of the $S_{\text{D}} - 1$ sources keeps the destination busy and t_{I} is the equivalent of t_{D} for the packets from the S_{I} and I stations. Note that $t_{\text{I}} < t_{\text{D}}$ (see Section 6.2 for their numerical values).

The fraction P_{FACQ} is expressed as

$$P_{\text{FACQ}} = \frac{\lambda \left(1 - P_{\text{busy}}\right) \Theta}{\lambda_0 \left(S_{\text{D}} - 1\right) + \lambda p_{\text{acq}} S_{\text{I}} + \lambda \left(1 - P_{\text{busy}}\right) \Theta I} \tag{6.22}$$

where Θ is a parameter that depends on the underlying physical layer and on the particular packet detection and timing acquisition method used.

Computing $Q(L_{acq})$ with the Transmission Markov Chain Z_n

In this section, we explain how we obtain equation (6.33) to compute $Q(L_{acq})$, the probability that a station does not begin a packet transmission during the "vulnerable period" of length L_{acq} chips. This is the last quantity required to be able to calculate p_{acq} given λ_0 and λ.

In order to determine $Q(L_{acq})$, we model the behavior of a station transmitting a packet at the physical layer with a discrete-time, homogeneous Markov chain Z_n. We begin by defining the transition probabilities of Z_n, then we relate Z_n with X_n (see Section 6.1.1), and finally we use Z_n to obtain $Q(L_{acq})$.

Let L_p be the number of chips per packet. Because our model must take into account the fact that a source can only transmit *one* packet at a time, Z_n has L_p states; state 0 is the state

where the source waits for a new transmission to occur, the states 1 to $L_p - 1$ are the states where a packet transmission is happening (see Figure 6.1(b)).

Let q be the probability that a packet transmission starts. The transition probabilities of Z_n are

$$\begin{aligned} p_Z(0,0) &= 1-q \\ p_Z(0,1) &= q \\ p_Z(i,i+1) &= 1, \qquad i = 1,\ldots,L_p-1 \\ p_Z(L_p-1,0) &= 1. \end{aligned} \tag{6.23}$$

The stationary distribution of Z_n is

$$\pi_Z(0) = \frac{1}{1+q(L_p-1)} \tag{6.24}$$

$$\pi_Z(i) = \frac{q}{1+q(L_p-1)}, \quad i = 1,\ldots,L_p-1. \tag{6.25}$$

In order to properly relate X_n with Z_n, we need to relate λ with q. Let N_p be the number of packets transmitted during a time interval t. As $N_p = \lambda t$, we have $\pi_Z(1) = \frac{N_p}{t} = \lambda$. Therefore, using (6.25) for $i = 1$ we obtain

$$q = \frac{\lambda}{1-\lambda(L_p-1)}. \tag{6.26}$$

Now that we have defined the transmission Markov chain Z_n, we can use Z_n to compute $Q(L_{acq})$. Formally, we have

$$\begin{aligned} Q(L_{acq}) &= \mathbb{P}\left(\text{A source does not visit state 1 in } [0, L_{acq}-1]\right) \\ &= \mathbb{P}\left(Z_0 \neq 1, Z_1 \neq 1, \ldots, Z_{L_{acq}-1} \neq 1\right). \end{aligned}$$

In addition, we define

$$Q(L_{acq}|i) = \mathbb{P}\left(Z_0 \neq 1, Z_1 \neq 1, \ldots, Z_{L_{acq}-1} \neq 1 | X_0 = i\right).$$

Hence

$$Q(L_{acq}) = \sum_{i=0}^{L_p-1} Q(L_{acq}|i)\pi_Z(i). \tag{6.27}$$

We already know how to obtain $\pi_Z(i)$ thanks to (6.25), but $Q(L_{acq}|i)$ for $i = 0, 1, \ldots, L_p - 1$

are still remaining. We compute them in an iterative fashion. By definition

$$Q(0|i) = \begin{cases} 0 & \text{if } i = 1 \\ 1 & \text{otherwise} \end{cases} \tag{6.28}$$

and by construction

$$Q(L_{acq}|i) = \begin{cases} 0 & \text{if } i = 1 \\ \sum_{j \neq 1} p_Z(i,j) Q(L_{acq} - 1|j) & \text{otherwise} \end{cases}. \tag{6.29}$$

Now, let's define the vector

$$\vec{y}_{L_{acq}} = \left[Q(L_{acq}|0)\ 0\ Q(L_{acq}|2)\ \ldots\ Q(L_{acq}|L_p - 1) \right]^T, \tag{6.30}$$

so that we have

$$\vec{y}_{L_{acq}} = A \vec{y}_{L_{acq}-1} = A^{L_{acq}} \vec{y}_0 \tag{6.31}$$

where $\vec{y}_0 = [1\ 0\ 1\ \ldots\ 1]^T$ and A is equal to the transition matrix of the transmission Markov chain Z_n, except for the elements of the second row and second column, which are set to 0, i.e.

$$A(i,j) = \begin{cases} 0 & \text{if } i = 1 \text{ or } j = 1 \\ p_Z(i,j) & \text{otherwise} \end{cases}.$$

Thanks to the structure of A, it turns out that (6.31) becomes

$$\vec{y}_{L_{acq}} = \begin{bmatrix} (1-q)^{L_{acq}} \\ 0 \\ (1-q)^{\max(0, L_{acq} - (L_p - 3))} \\ \vdots \\ (1-q)^{\max(0, L_{acq} - 2)} \\ (1-q)^{\max(0, L_{acq} - 1)} \end{bmatrix}. \tag{6.32}$$

Finally, putting (6.27), (6.30), and (6.32) together, $Q(L_{acq})$ can be calculated with

$$Q(L_{acq}) = \frac{(1-q)^{L_{acq}} + q \sum_{i=1}^{L_p - 3} (1-q)^{\max(0, L_{acq} - i)}}{1 + q\,(L_p - 1)}. \tag{6.33}$$

6.1.3 Summary of our Method to Compute the Saturation Throughput

The saturation throughput λ_0 is obtained by solving (6.1) numerically. The first subproblem, i.e. computing $[\lambda_0, \lambda] = f(p_{\text{acq}})$, is solved by using Equations (6.15) and (6.16) in Section 6.1.1. For the second subproblem, computing $p_{\text{acq}} = g(\lambda_0, \lambda)$, it is solved by starting from (6.17) using (6.21) with (6.22) and (6.18) with (6.33) in Section 6.1.2.

Because equations (6.17), (6.21), and (6.22) all depend on p_{acq}, we must solve a quadratic system of equations in order to obtain P_{busy} and p_{acq}.

6.2 Performance Evaluation

In this section, we evaluate the performance of an IR-UWB network with packet detection and timing acquisition. In particular, we compare the performance of a network that uses a common acquisition preamble with the performance of a network that uses private acquisition preambles. First, we use the analytical model derived previously to obtain performance results for a symmetric and homogeneous IR-UWB network. In this case, our performance metric is the saturation throughput λ_0. Second, we turn to ns-2 [181] simulations to address more general scenarios with multi-hop topologies and TCP as the transport protocol.

6.2.1 Scenarios and Parameters of the Performance Evaluation

The MAC protocol that is used in the modeling is the DCC-MAC protocol described in Chapter 5. But, compared to the original specifications in Chapter 5, the parameters of DCC-MAC have been adapted for an IEEE 802.15.4a type of network. In particular, the maximum physical layer bit-rate is 1 Mbit/s. The maximum range is around 50 meters.

Parameters and Scenarios for the Analytical Model

The fixed point equation (6.1) is solved numerically. The code for the fixed point problem is implemented with Matlab; the source code is available online [207]. For t_{acq}, t_{tx}, $t_{\text{fail}}(i)$, $i = 1, \ldots, R$ and t_{drop} in the equations (6.8), we have the following values:

- The acquisition time t_{acq} corresponds to the length of the acquisition preamble. With the packet detection and timing acquisition algorithm in [63], the duration of the acquisition preamble is 64000 ns.

- The transmission time t_{tx} is the sum of the following durations: the DATA packet duration (minus the length of the acquisition preamble), the round-trip time, the ACK packet duration, the SIGIDLE packet duration (the SIGIDLE packet corresponds to the idle signal in Chapter 5), and the maximum backoff time.

- The elapsed time in case of a failed packet transmission $t_{\text{fail}}(i)$ for $i = 1, \ldots, R-1$ is the sum of the DATA packet duration, of the send timer, of the average duration of the idle timer (see Section 5.2.2), and of the average backoff time in backoff stage i. For $i = R$, $t_{\text{fail}}(i)$ is only the sum of the DATA packet duration and of the send timer. For the average duration of the idle timer, it is obtained by extensive simulations of the DCC-MAC protocol. Indeed, the idle timer is stopped when a SIGIDLE packet is received from the destination of interest. Hence, its distribution and average value can only be obtained by simulation.

- In case of a packet drop, t_{drop} is the maximum backoff timer length.

For t_{I} and t_{D} in (6.21), we have the following values:

- The value of t_{I} depends on whether we do an early discard or not. For early discard, it is equal to the duration of an ACK packet transmission (i.e. a preamble followed by header and no payload). For late discard, it is equal to the duration of a DATA packet.

- The value of t_{D} is equal to the duration of a DATA packet followed by the duration of an ACK packet.

The detailed numerical values are found in the source code of the implementation of DCC-MAC [207]. Values for $P_{\text{MD}}^{(k,i)}$ in (6.18) are derived by extensive simulations from [63]. Values for Θ in (6.22) correspond to the probability of false alarm of the packet detection and timing acquisition scheme in [63].

To obtain the throughput from λ_0, we simply multiply λ_0 with the size of the payload of a DATA packet; the throughput is

$$\lambda_0 P_{\text{packet}}$$

where P_{packet} is the payload of a packet in bits.

The scenario we analyze with our analytical model is a symmetric, homogeneous, and single-hop network. All destinations have the same number of identical sources, and the distance between the source and the destination is the same for all links.

Parameters and Scenarios for the ns-2 Simulations

The DCC-MAC protocol is implemented in ns-2, along with an IR-UWB physical layer model. The version of ns-2 used in this chapter is 2.29. All details on the IR-UWB physical layer implementation can be found in Chapter 10. In this paragraph, we give a short summary of how packet detection and timing acquisition is implemented in our ns-2 implementation. When a packet arrives at a destination, all further packets that arrive during the duration of the acquisition preamble are stored in a list. If a private acquisition preamble is used, we add to the list only the packets intended for the destination. In the case of a common acquisition preamble, we add all packets that arrive during the duration of the acquisition preamble to the list. At the end of the duration of the acquisition preamble, a packet in the list is chosen randomly (with a uniform distribution). This packet is further received by the physical layer with a probability $1 - P_{\text{MD}}^{(k,i)}$ where k is the number of packets in the list (with the same acquisition preamble than the destination) and i is the number of packets that have another acquisition preamble than the destination. Packets with a different acquisition preamble can create a false acquisition with a probability Θ (see (6.22)). For false acquisitions, we assume only late discard in the ns-2 simulations.

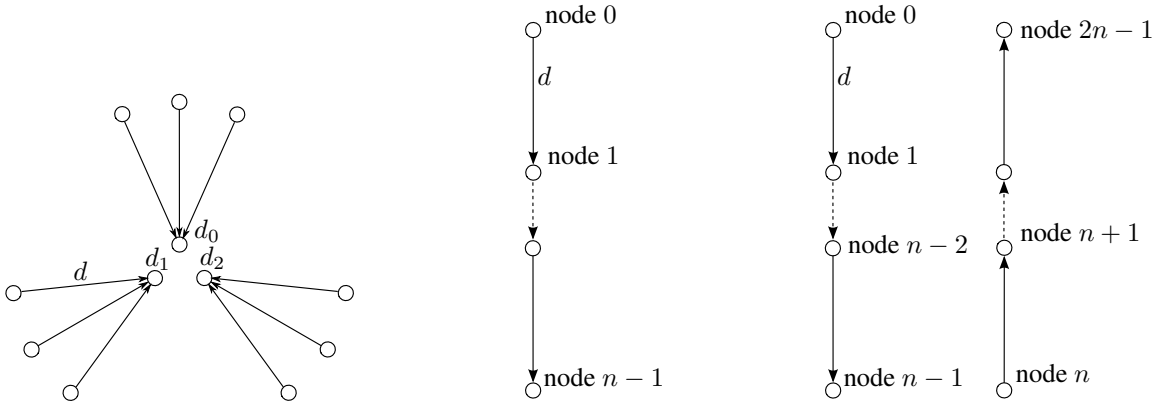

(a) Multiple piconets (b) Line topology (c) Parallel lines topology

Figure 6.2: Topologies used for the ns-2 simulations. The link distance is d.

For our performance evaluation with ns-2, we consider three different scenarios. Each scenario has a different topology and UDP or TCP as the transport protocol. The scenarios are the following:

- For the exposed piconets scenario, the topology consists of n piconets with 3 sources and 1 destination per piconet (see Figure 6.2(a)). All nodes are in range of each other

and all sources of a given piconet have the same destination inside the piconet. The distance between the sources and their destination is 10 meters. The distance between the respective destinations of the n piconets is 4 meters. The transport protocol is UDP.

- For the TCP line scenario, the topology consists of a line of equidistant nodes (Figure 6.2(b)). The distance between neighboring nodes is 10 or 20 meters. The sender and the destination are placed at each extremity of the line. The transport protocol is TCP.

- For the parallel TCP lines scenario, the topology consists of two parallel lines of equidistant nodes (Figure 6.2(c)). The distance between neighboring nodes on a line is 10 or 20 meters and the distance between the two lines is 20 meters. Each line has one source at one extremity and its associated destination at the other extremity. However, the two sources are not on the same extremity. The transport protocol is TCP

For all scenarios, traffic is generated by a CBR source with a rate high enough to make sure that the lower layers are in saturated traffic conditions. The size of the payload is 127 bytes ($P_{\text{packet}} = 127$). The topologies for the TCP line and the parallel TCP lines imply that multi-hop forwarding is used. Hence, for both scenarios, we configure static multi-hop routes thanks to the NOAH routing agent in ns-2. Finally, for all results obtained with ns-2 simulations in Section 6.2.3, DCC-MAC runs with the rate adaptation algorithm enabled. For every scenarios, several simulation runs are performed and each of them lasts 300 seconds. We always show the 95% confidence interval for the median.

6.2.2 Saturation Throughput of a Homogeneous IR-UWB Network

We first validate our analytical model. We compare the throughput obtained with our analytical model with ns-2 simulations with the exposed piconet scenario and UDP traffic. We set a distance of 10 meters between the sources and their destination. In Figure 6.3, we plot the aggregated (sum of all sources) saturation throughput obtained with the analytical model and the ns-2 simulations versus the number of sources n per destination. We consider 1 and 2 destinations. As it can be observed, in both cases there is a slight discrepancy when the number of transmitters n is small. This is expected as the mean-field assumption becomes valid for a large number of stations.

For the the saturation throughput of a homogeneous IR-UWB network, we look at three cases: 1, 2, and 9 destinations. For each case, there are n sources per destination. In Figure 6.4, we plot the aggregated saturation throughput versus n for a network with a common acquisition

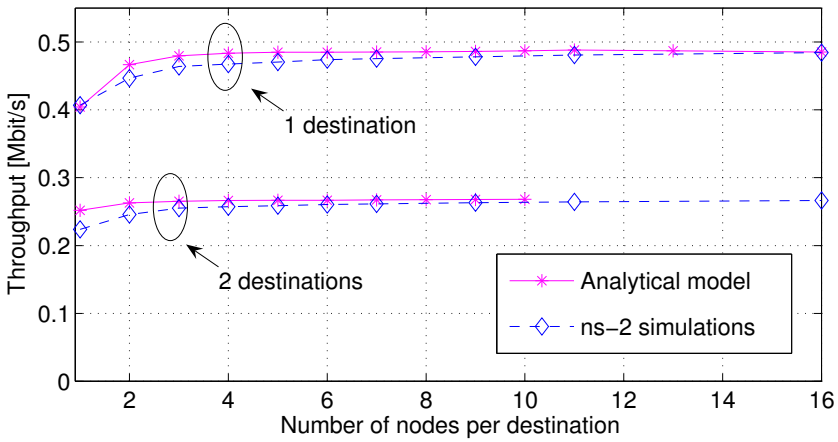

Figure 6.3: Validation of the results obtained with the analytical model. The aggregated saturation throughput is plotted (sum of the throughput of all sources) versus the number of sources per destination n. The plain curve is the analytical saturation throughput, the dashed curve is the ns-2 simulations. The upper pair of curves are for one destination with n transmitters. For the bottom pair of curves, there is a second destination with n concurrent transmitters using the same acquisition preamble.

preamble. The results with the private acquisition preamble are shown separately in Figure 6.5 because they almost overlap with the results with one destination. The throughput is notably increased when the packets that were unintentionally acquired are dropped as early as possible. On the contrary, the throughput is greatly reduced when all sources use the same acquisition preamble. In Figure 6.5, we also have 1, 2, and 9 destinations but for a network with private acquisition preambles. There is a small reduction of the aggregated throughput with 9 destinations compared to 1 destination. The results are all with late discard. With early discard, the results are not shown because they are not discernible from the aggregated throughput with 1 destination. The very small throughput difference comes from the robustness of the packet detection and timing acquisition algorithm in [63] and also, from the fact that we ignore interference on the payload part. All in all, these results clearly show the strong effect of packet detection and timing acquisition on the performance of an IR-UWB network if a common preamble is used.

6.2.3 NS-2 Simulations

We now turn to ns-2 simulations for an evaluation with more realistic scenarios. We begin with the exposed piconets scenario.

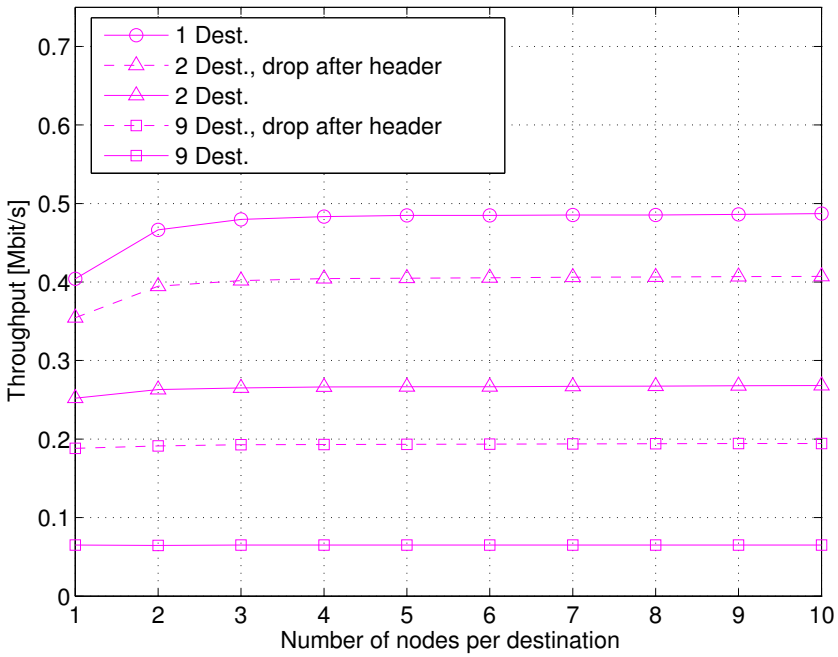

Figure 6.4: The aggregated throughput (sum of the throughput of all sources) is plotted versus the number of nodes per destination n. We have 1,2 and 9 destinations with a common acquisition preamble. The results with the private acquisition preamble are shown separately in Figure 6.5 since they almost overlap with the result with 1 destination. There is a large drop in throughput when all sources use the same acquisition preamble. Early discard significantly increases the throughput.

Exposed Piconets

Remember that for this scenario, the number of sources per destination is fixed to 3. We plot the aggregated saturation throughput per piconet versus the number of piconets (or equivalently the number of destinations). The throughput is strongly reduced when a common acquisition preamble is used. The difference between the throughput with a private acquisition preamble and a common acquisition preamble grows with the number of interferers. Furthermore the confidence intervals have a larger width in the case of a common acquisition preamble compared to private preambles. This indicates that there are very large throughput variations and instabilities with a common preamble.

TCP Line and Parallel TCP Lines Scenario

For the TCP line scenario, we plot the throughput of the source as a function of the number of nodes. For the parallel TCP lines, we show the result for the two sources separately. There are two cases, with a link distance of 10 or 20 meters.

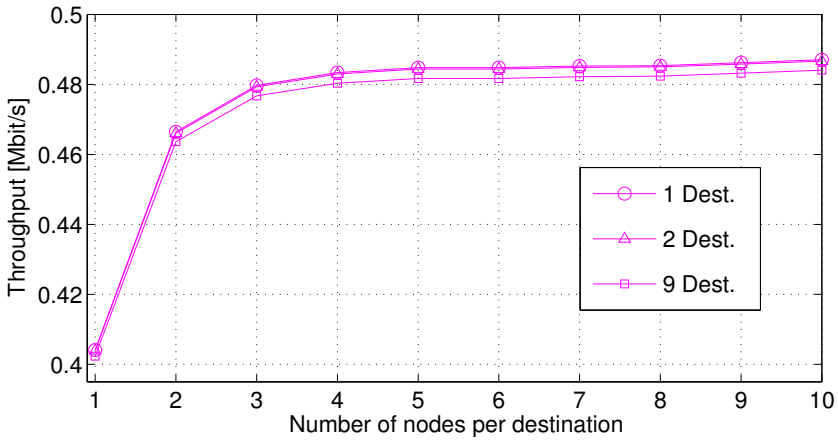

Figure 6.5: The aggregated throughput (sum of all throughputs) is plotted versus the number of nodes per destination n. We have 1,2 and 9 destinations with private acquisition preambles.

In the line TCP scenario (Figure 6.7), we first observe that a stable throughput is reached for more than 4 nodes with the use of private acquisition preambles. However, we observe a dramatic throughput reduction when all nodes use the same acquisition preamble. For more than 6 nodes, the throughput reaches zero for some simulation runs. And in the case of 12 nodes, the network does not function at all. In addition, as in the exposed piconet scenario, there is much more variability in the network behavior with a common preamble than using private acquisition preambles.

In Figure 6.8, even more severe effects are observed when using a common acquisition preamble in the case of the parallel TCP lines scenario. There are two plots, one for a link distance of 10 meters and one for a link distance of 20 meters. The distance between the two lines is always 20 meters. We always plot the throughput of both flows with flow 1 on the left and flow 2 on the right. For the case where a common acquisition preamble is used, we observe an almost complete collapse of the network when the number of nodes is larger than six (i.e. more than two hops). In addition, there is a great unfairness between the two TCP flows. The throughput variations are much larger with the smaller link distance of 10 meters. Note that we have 12 simulation runs per scenario. And to obtain smoother curves would require more simulations. On the contrary, the use of private acquisition preambles allow to obtain a much higher and more stable throughput.

The unfairness that we observe is very similar to what can happen in IEEE 802.11 networks in the exposed node case [214]. Also, the interference model for the payload used currently in the implementation of the IR-UWB physical layer is rather optimistic (see Chapter 10). It corresponds to the use of an optimal Rake receiver at the physical layer. Hence, the collapse of

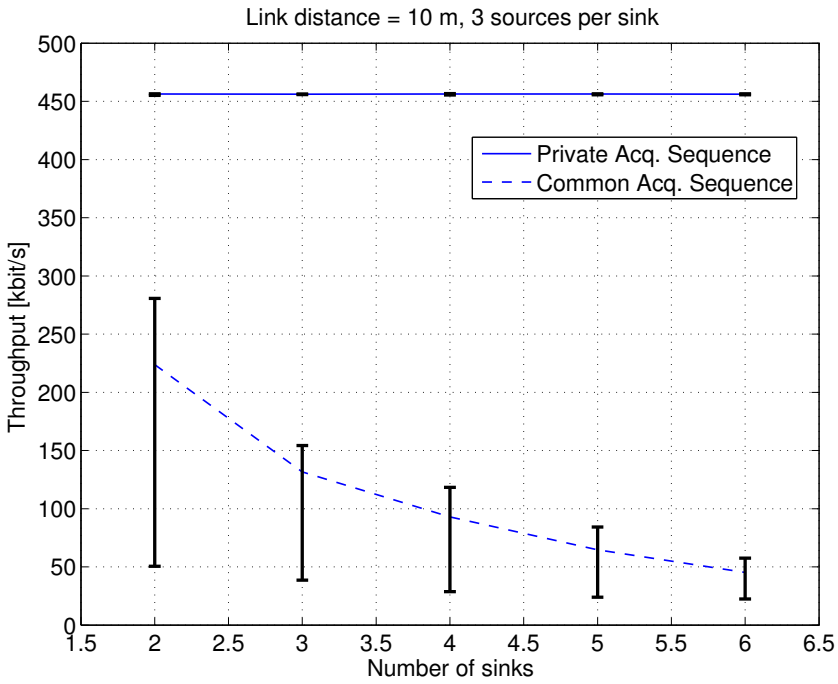

Figure 6.6: Exposed piconets scenario: aggregated saturation throughput per piconet versus number of piconets for the exposed piconets scenario (see Figure 6.2(a)). The difference between the throughput with a private acquisition preamble and a common acquisition preamble grows with the number of interferers. In addition, the network is much more unstable when all sources use the same acquisition preamble as indicated by the large confidence interval values.

the network results strictly from the fact that a common acquisition preamble is used for packet detection and timing acquisition.

6.3 Discussion and Conclusion

The approach we use for our analytical model with a fixed-point equation is similar to previous work in [177, 178, 179, 180]. Indeed, a mean-field assumption (or decoupling assumption) is done in [179, 180]. And [177, 178] rely on a similar independence hypothesis. However, our work is different in that it takes into account an IR-UWB physical layer that has different properties than the narrow-band physical layer assumed in the previous works. Moreover, we explicitly address packet detection and timing acquisition as they are an important factor in IR-UWB networks. To the best of our knowledge, packet detection and timing acquisition are ignored in the previous works on networking.

In this chapter, we have analyzed how using a private or common acquisition preamble

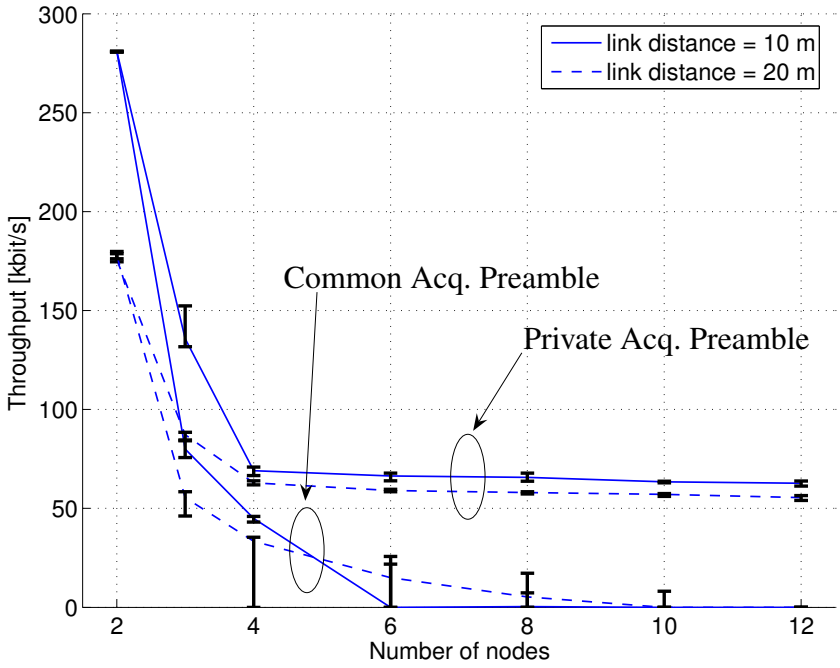

Figure 6.7: Line TCP scenario: throughput versus number of nodes. This scenario shows a dramatic compounding effect where the throughput in case of a common acquisition preamble drops to zero for more than 6 nodes. The network is also much more unstable when all sources use the same acquisition preamble.

affects the performance of IR-UWB networks. We develop an analytical model to compute the saturation throughput of an IR-UWB network. One novelty of our model is to explicitly take into account packet detection and timing acquisition. Our model can be easily used with different MAC layers or different acquisition algorithms. Using the model, we show that a private acquisition preamble offers a large throughput gain (larger than 100%) compared to a common acquisition preamble. Moreover, the throughput difference grows with the number of concurrent transmitters and interferers. Finally, with ns-2 simulations on multi-hop topologies with TCP flows, we demonstrate that a network using private acquisition preambles exhibits a stable throughput. On the contrary, using a common acquisition preamble exhibits the presence of a compounding effect similar to the exposed terminal issue in IEEE 802.11 networks: the throughput is severely degraded and complete flow starvation might occur. Further, the use of a common acquisition preamble results in very large performance fluctuations in some scenarios. Future work should explicitly take into account the cost of learning the acquisition preamble of a destination. Also, a proper modeling of the interference on the payload is necessary.

The results in this chapter also complete the results from Chapter 4 on the optimal design for

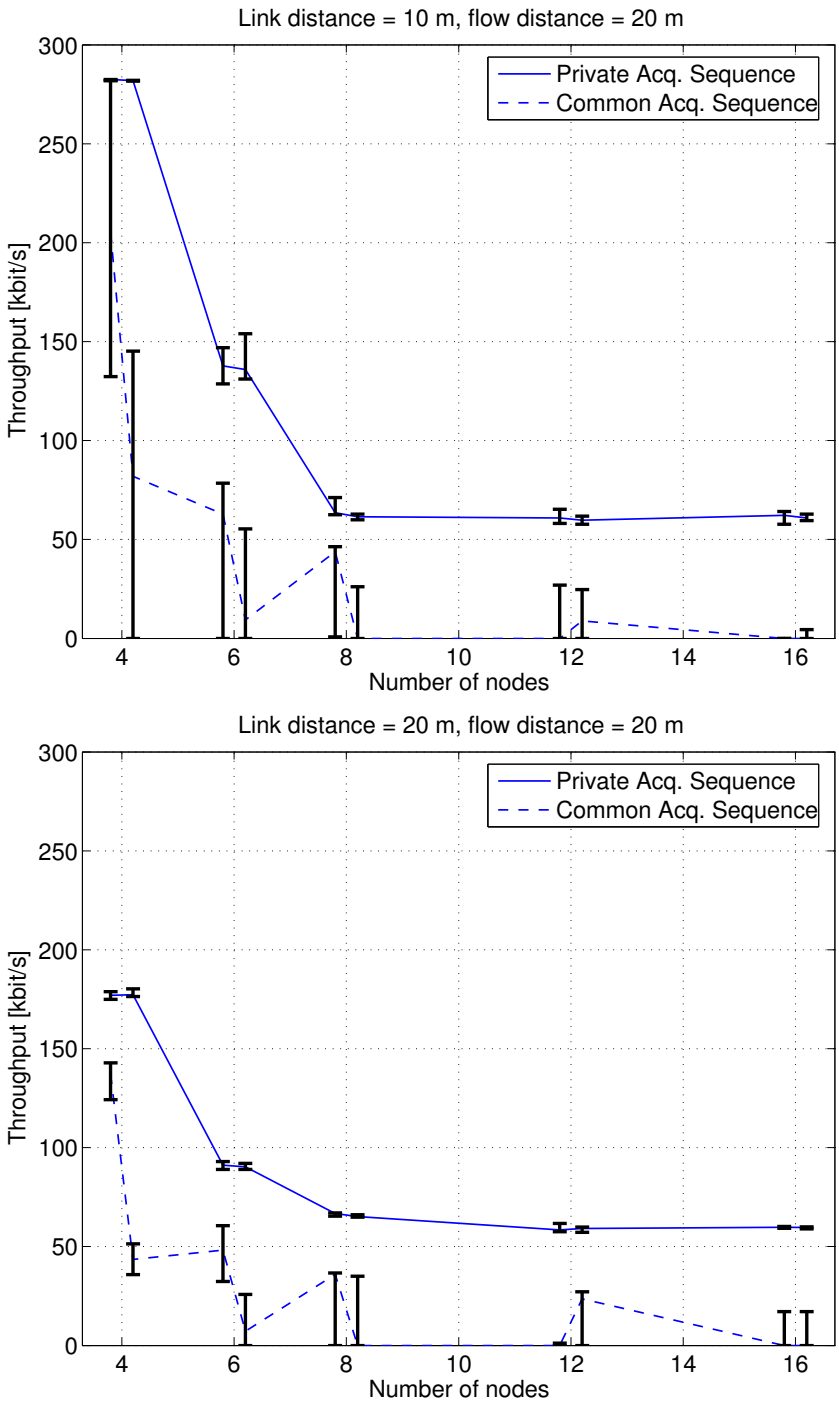

Figure 6.8: Parallel TCP lines scenario: throughput per flow versus number of nodes. For each set of nodes, flow 1 is on the left, flow 2 is on the right. On the top the link distance is 10 meter and 20 meters otherwise. This scenario shows a dramatic compounding effect where the network completely collapses in case of a common acquisition preamble for more than two hops. There is also a high unfairness between the two flows.

IR-UWB network. They clearly demonstrate that nodes in the network should take advantage of the multi-channel capabilities of the IR-UWB physical layer.

6.4 Acknowledgements

We would like to thank Saravanan Vijayakumaran for helpful discussions and his contribution early in the work presented in this chapter.

Chapter 7

An IR-UWB Software Radio Testbed with Multi-User Interference

Interference in wireless networks is a cross-layer issue: it can affect all layers of a network, from the physical layer to the transport layer. As such, it becomes crucial to take interference into account as early as possible when designing radio hardware and algorithms. In particular, a radio testbed is extremely valuable for testing algorithms and hardware implementations with the interference found in real-world conditions.

In this chapter, we present an overview of an IR-UWB software radio testbed with multi-user interference (MUI). Our initial motivation behind this testbed is twofold. First, to implement the DCC-MAC protocol. This is actually a very challenging objective that we have not reached yet. Our second motivation is to create an IR-UWB environment with MUI for fast prototyping.

An important design goal of this testbed is that it should be modular and flexible: for instance, it should be easy to exchange components in the RF chain. It should also give full access to the parameters of the physical layer (for example, the modulation format, or the duration of a frame). It should be easy to implement and test new algorithms at the receiver, either by programming an FPGA for real-time processing, or by capturing signal traces that can be used offline with an algorithm implemented in a high-level programming language. Lastly, the testbed should be useful for communities of researchers from different areas: hardware, communication technology, and networking.

Our testbed consists of several IR-UWB transmitters and one receiver. On the transmission side, an FPGA is connected to the IR-UWB transmitters. They have a center frequency of

4.05 GHz and a -10 dB bandwidth of 500 MHz. The parameters of the transmitted signals can be easily varied thanks to the FPGA. The direct-conversion RF chain of the receiver is built around a data acquisition board that performs sampling at 2 GS/s. The sampled signal is fed into the FPGA where it may be processed in real-time or transferred to a computer for offline processing. The architecture and more details on the various components are given in Section 7.1.

Because the focus of the testbed is to create an IR-UWB environment with MUI for fast prototyping, we have not yet engaged on low-power hardware development, or on system integration. These are long term objectives, also with interference robustness as the main focus. Therefore, most of the RF elements are either off-the-shelf components or are built with discrete components. We do not give all the details of the components of the testbed in this chapter. Rather, we concentrate on the many serious challenges associated with building IR-UWB transmitters and RF components with discrete elements at 4.05 GHz. We describe these challenges in Section 7.1.1.

Even though we have not implemented DCC-MAC, we successfully implement and verify in practice the robust packet detection and timing acquisition scheme from [63]. Thanks to the robustness to MUI of this scheme, we show in Section 7.2 how the receiver can synchronize with the signal from a particular transmitter while other transmitters are active. The algorithm in [63] does not require any complex multi-user detectors, but takes advantage of the wide bandwidth and intermittent nature of IR-UWB signal. This packet detection and timing acquisition scheme is an important building block for the implementation of MAC protocols for IR-UWB such as DCC-MAC or [164] where concurrent transmissions are allowed. This implementation shows that concurrent transmissions in IR-UWB networks are feasible.

7.1 Architecture of the Testbed

The testbed consists of several transmitters and one receiver. They are managed by a computer and are all built around analog and digital circuits (see Figure 7.1). The digital side is based on a FPGA board for generating the transmitted signal and an acquisition board with a fast analog to digital converter (ADC) for capturing and processing the received signal. The analog side consists of two parts: The first part comprises the transmitters with their antenna which generate UWB impulses. The second part is the receiver which amplifies, filters, and down-converts the received signal for the acquisition board. Almost every element of the receiver is built with evaluation boards, while the transmitter, the antennas [215] and the low noise amplifier (LNA)

are built with discrete components and on-the-shelf integrated circuits. All of the hand-made circuits are made with Duroid substrate because of the requirement for low resistive loss at high frequency. The circuits also need to be placed in a shielding box because circuits operating at such high frequency radiate strong undesired interference.

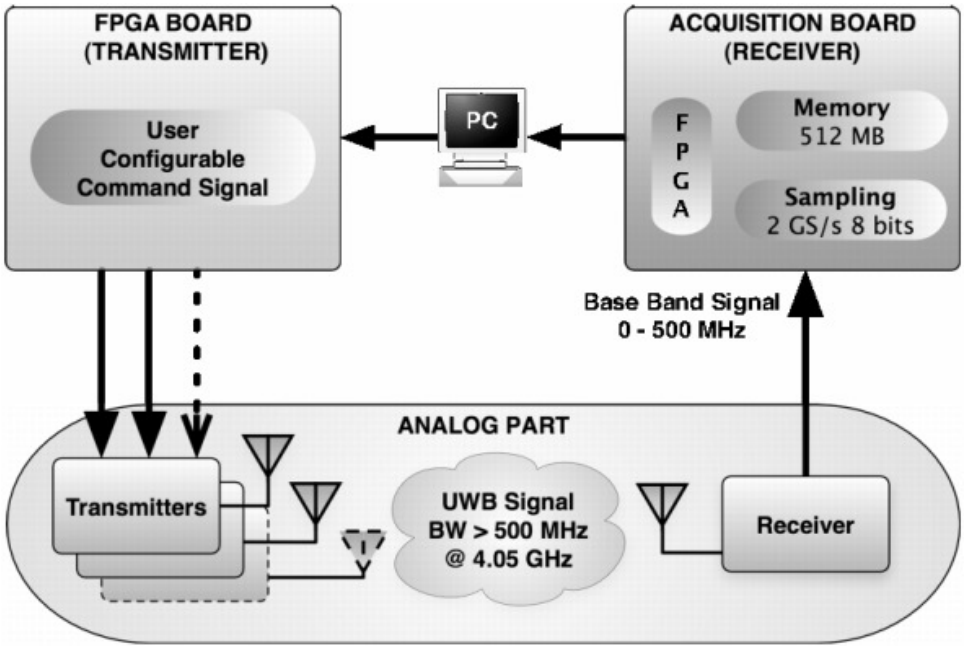

Figure 7.1: The FPGA board (transmitter) is programmed and configured by the computer in order to drive the transmitters with the desired signal characteristics. The receiver amplifies, filters and down-converts the received signal to the base band. The acquisition board (receiver) samples the base band signal and sends it to the computer for the final processing. The FPGA of the acquisition board is used for memory management and data conversion.

7.1.1 Implementation Challenges for a Testbed with Discrete Components

The focus of the transmitter part is to produce several IR-UWB signals with a bandwidth of at least 500 MHz. For this purpose, the FPGA creates user configurable command signals in order to drive the transmitters. The command signal is based on a time-hopping sequence (THS) and is implemented as shown in Figure 7.2. The main parameters are the number of independent command signals, the type of time-hopping code (none, deterministic, or random), the number of chip N_c, the number of frame N_f, the number of sequence N_s (repetition of the same time-hopping pattern), and the duration of the driving signal sent to the transmitters. This duration is a multiple of the chip duration T_c which depends on the clock frequency. The hardware architecture is implemented in VHDL and can be configured by the computer through

registers. This user configurable command signal may be used for generating a preamble signal as described in Section 7.2.

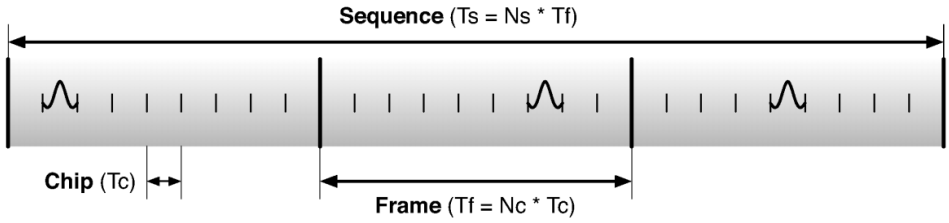

Figure 7.2: Definition of the user command signal parameters. We have the chip duration T_c, the number of chip per frame N_c and the length of sequence N_s are all configurable.

The maximal clock frequency of the FPGA is 166 MHz so the chip time is limited to a minimum of 6 ns. The only available mean to output the driving signals is through a Micro DB 15 pins connector. Unfortunately, this connector has poor high frequency characteristics. The output signals may also become worse depending on the output buffers configuration. In addition, the length of the cable has to be as small as possible to avoid signal distortion and coupling between channels. For all these reasons, a trade-off has to be found between output impedance, output voltage and signal degradation, so the LVDCI_25 (Low Voltage Digitally Controlled Impedance 2.5 V) standard was chosen among the signals available for its fixed impedance of $50\ \Omega$.

One challenge is to build an analog transmitter that creates the UWB impulse with digital commands from the FPGA independently from the driving signal degradation. This transmitter has a simple, reliable and cheap architecture shown in Figure 7.3. A sine wave oscillator running at 4.05 GHz is connected to the antenna through a mixer (indeed an analog multiplier) which behaves like a switch when driven by a square signal. This oscillator is designed using discrete components and transmission line filters. The oscillator circuit consists of an active circuit connected in positive feedback with a microstrip filter. The active circuit is designed using a SiGe NPN transistor. The transistor is biased in common emitter configuration at 5 mA. The input and output of the active circuit are matched to $50\ \Omega$ using lumped components. A single section of the hairpin filter is used in the feedback of the oscillator. The filter can be modeled as a parallel LC network, and the center frequency of the filter can be tuned after fabrication by adjusting the length of the microstrip lines. The insertion loss of the filter is -1.5 dB and the active circuit gain is around 6 dB at 4.05 GHz. A phasing line is added at one end of the filter to have a total phase shift of 360 degrees around the circuit. The output power of the oscillator is $+10$ dBm for a load impedance of $50\ \Omega$ and henceforth can be directly

connected to the input of the mixer. The main part of the transmitter is the square impulse generator. By using the command signal from the FPGA board, it creates a short impulse of 2 ns which drives the mixer. This impulse is obtained by splitting the command signal in two parallel delay lines and recombining them with an AND gate. Their respective delays do not need to be very short since it is the difference between the two delays that produces the impulse. This technique is useful for generating signals shorter than the propagation delay of the logic circuits themselves. However, care is required because some components values are experimentally adjusted depending on the driving signals coming from the FPGA board (considering their time and voltage).

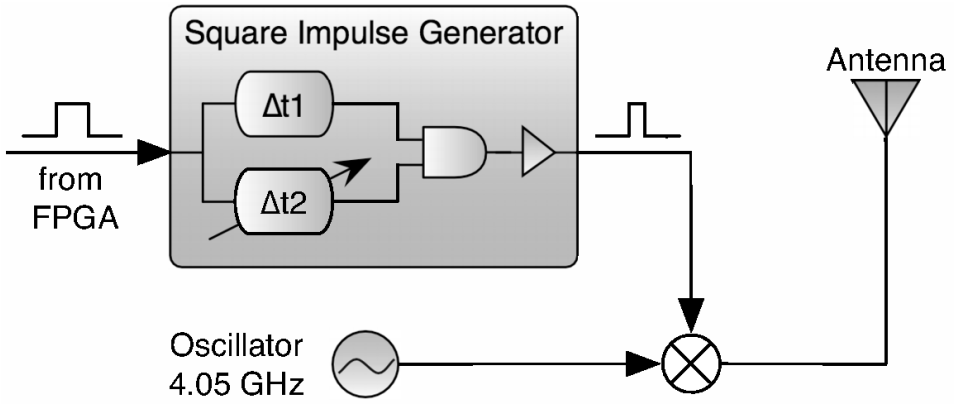

Figure 7.3: The transmitter works as follows: The square impulse generator creates a short impulse of 2 ns from the driving signal given by the FPGA board. The mixer, thanks to this impulse, switches on and off the sine wave which comes from the oscillator and thus produces the UWB signal.

The spectrum of the output signal is shown in Figure 7.4: it is a wideband spectrum centered around 4.05 GHz. This measurement is made at the output of the transmitter, so the filtering effect of the antenna does not appear here. It can be noticed that, due to a weak isolation between the output of the 4.05 GHz oscillator and the output of the mixer, there is a small peak at the center frequency.

The focus of the receiver part is to acquire signal traces in order to digitally process them. It is a classic direct-conversion circuit as shown in Figure 7.5. The signal received by the antenna is amplified by a LNA and a power amplifier, which is necessary to have enough power with only two amplifier stages (with more stages, the receiver becomes unstable). The signal is then band-pass filtered and down-converted with a mixer driven by a 4.05 GHz sine wave.

The acquisition board samples the received signal at 2 GS/s with a resolution of 8 bits and stores the samples in a 512 MB dynamic RAM. The access to the DRAM requires to

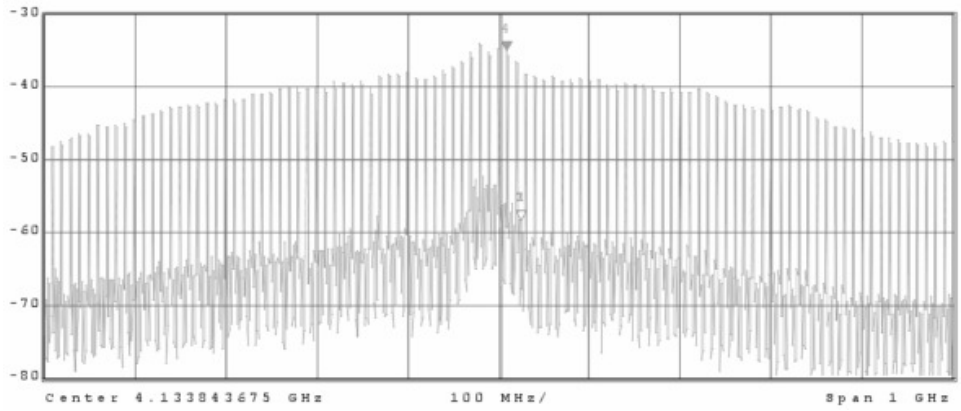

Figure 7.4: This is the output spectrum of the transmitter. It shows the wide bandwidth nature of the switched sine wave before the antenna. The center frequency of the spectrum analyzer is shifted a bit in order to better show the peak.

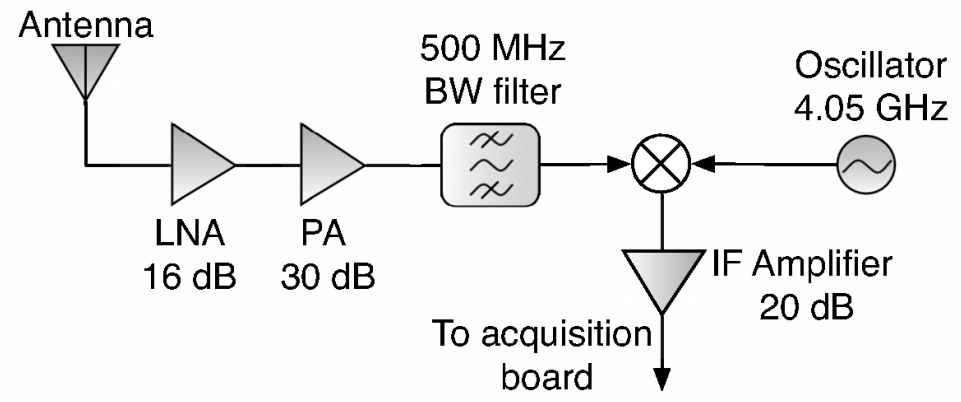

Figure 7.5: The receiver works as follows: the received signal is amplified and filtered before being down-converted by the mixer. The mixer has its local oscillator frequency at 4.05 GHz. The IF (base band) signal is amplified and then sent to the FPGA for sampling.

pre-process data at 2 GS/s inside the FPGA and to manage the complexity of the memory interface. Since the FPGA internal bus speed is different than the speed of the PCI link to the PC (2 GS/s versus 100 MB/s), the PC waits until the end of a capture before reading the DRAM. The acquisition board and the internal registers of the FPGA must be carefully configured by Matlab by doing configuration steps in a specific order; in addition, since the format of data inside the board is completely different from the format accepted by Matlab, a conversion algorithm is required. Several Matlab scripts needed to be translated in C in order to improve time performance.

7.2 Timing Acquisition with Concurrent Transmitters

In this section, we describe the results we obtained with the implementation of the packet detection and timing acquisition scheme in [63]. Contrary to traditional scheme, the algorithm in [63] is known to be robust to MUI. We have a scenario with three IR-UWB transmitters. The goal is to acquire the timing of the first transmitter while the two others are transmitting at the same time. Each transmitter has its own particular acquisition preamble, which consists of a sequence of impulses (see Figure 7.2) repeated several times. This allows the algorithm at the receiver to distinguish the three concurrent signals. On the receiver side, we use the timing acquisition algorithm in [63]. It performs a non-coherent timing acquisition since the phase information of the received signal is unknown. The timing acquisition algorithm is based on correlations between the received signal and a known impulse template. This template is based on the acquisition preamble of the transmitter of interest. Contrary to a traditional correlation between the template and the received signal, the algorithm in [63] adds an additional thresholding operation to every *sub*-correlation between an impulse and a portion of the received signal. This thresholding operation is the key to the robustness of the timing acquisition algorithm in [63] to overcome near-far situations. It avoids that large interference samples in the received signal propagates and pollute the full correlation.

The parameters of the underlying THS of the acquisition preamble is $N_c = 128$ chips and $N_f = 8$ frames. The algorithm is currently run offline and efficiency reason, the timing acquisition algorithm is implemented in C. Indeed, even a short capture of a few thousand nanoseconds easily results in a large dataset. Matlab is used to start and control the capture of the signal trace as well as to run the timing acquisition algorithm on the captured signal. The algorithm returns the index of the sample that corresponds to the beginning of the acquisition preamble. In Figure 7.6, several timing acquisitions are performed with one, two or three transmitters. The three transmitters are placed at equal distance of the receiver (around 30 cm). This a very high signal to noise (SNR) scenario. Lower SNR scenarios are possible, but require longer acquisition preamble that do not lead to easily visible results. The first transmitter sends a known acquisition preamble. The second transmitter sends an unknown random one, and the third transmitter sends an acquisition preamble based on a periodic THS.

Figure 7.6 shows three different cases, where one, two, or three transmitters are active. For each case, the same correct timing acquisition result is obtained, in spite of the one or two other interfering transmitters. For all cases, the timing acquisitions are successful with a pulse template well aligned on the impulses of the first transmitter. The timing acquisition algorithm

is indeed robust to the impulsive interference created by other transmitters. It is also robust to the small sinusoid perturbations created by the mismatch in carrier frequencies between the various transmitted signals.

Several parameters influence the results of the timing acquisition: the length of the acquisition preamble, the threshold applied for each sub-correlation, and finally the width of the square impulses in the template. For instance, in a lower SNR scenario, a longer preamble would be required. For an extremely strong near-far scenario a lower threshold in the algorithm in [63] is necessary.

7.3 Discussion and Conclusion

In this chapter, we have presented ongoing work on an IR-UWB software radio testbed with MUI. This testbed is built around an FPGA coupled with a fast data acquisition board for the receiver, and supports several independent IR-UWB transmitters. This chapter is an overview, where we have concentrated on describing the important implementation challenges that we faced. This testbed demonstrates that concurrent transmissions in IR-UWB networks are feasible, if a robust timing acquisition algorithm is used. The testbed was also used for ranging experiments [216]. The detailed list of electronic devices used in the testbed is given in Appendix A.2.

For future work, we plan to implement the validation part of the timing acquisition algorithm. To derive statistics, such as the probability of missed detection and the probability of false alarm, we also need to fully automate our measurement setup and the acquisition of signal traces. Finally, we will transmit full packets in order to add the demodulation of a data payload.

7.4 Acknowledgements

We would like to acknowledge James Colli-Vignarelli, Jérôme Vernez, Catherine Dehollain, Stephan Robert, Prakash Egambaram Thoppay, Gabriela Quintero Diaz de Leon, Anja Skrivervik, Jean-François Zürcher, as well as the ACI and ACORT team from EPFL-STI.

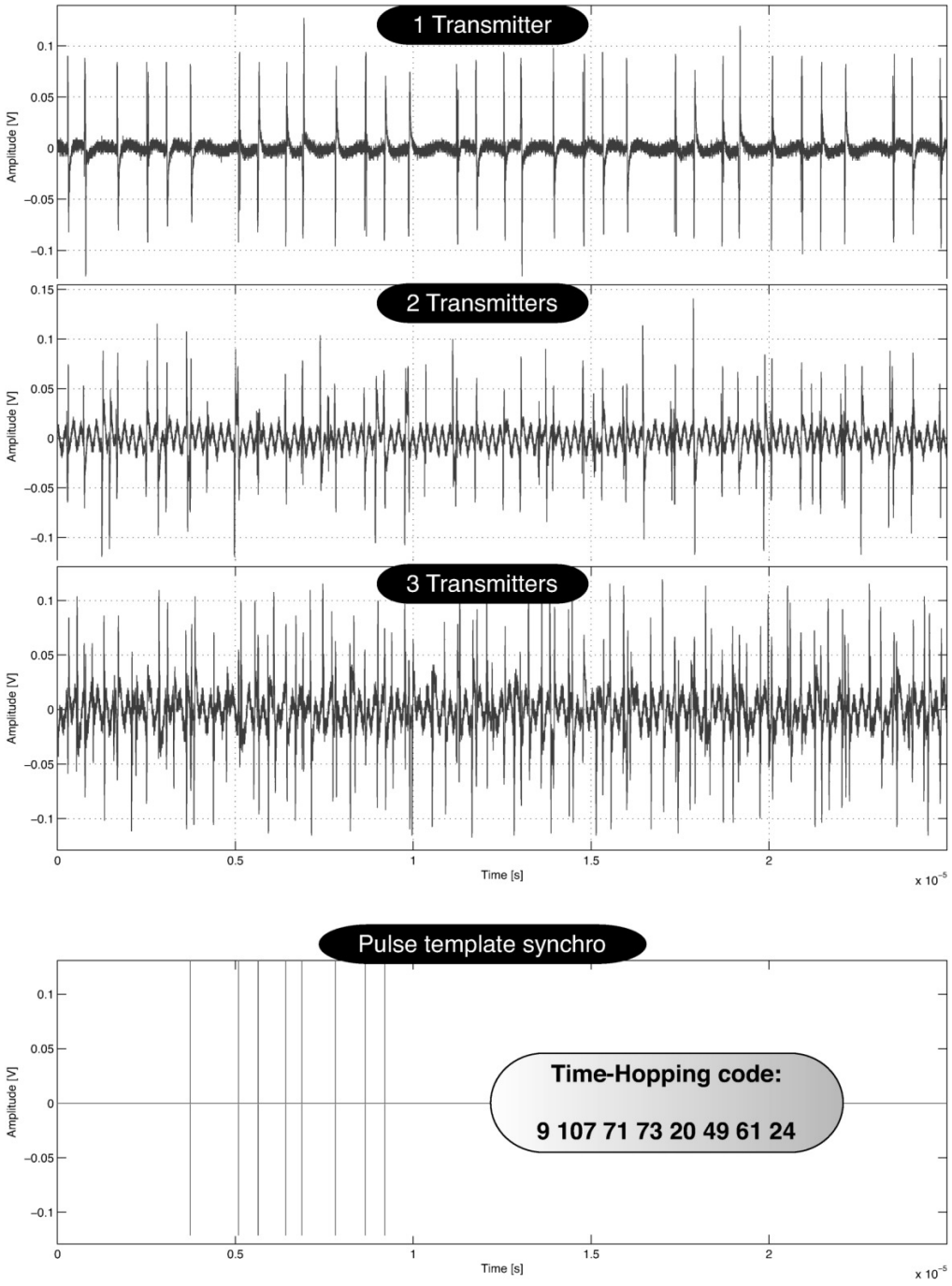

Figure 7.6: Timing acquisition with concurrent transmitters. The three transmitters are placed at equal distance of the receiver (around 30 cm). The first transmitter sends a known acquisition preamble. The second transmitter sends an unknown random acquisition preamble, and the third transmitter sends a preamble based on a periodic THS. The parameters of the underlying THS are $N_c = 128$ chips and $N_f = 8$ frames. There are three different cases, where one, two, or three transmitters are active. For each case, the same correct timing acquisition result is obtained, in spite of the one or two other interfering transmitters. The timing acquisition is successful with a pulse template well aligned on the impulses of the first transmitter in all cases.

Part II

Robust Receivers for IEEE 802.15.4a Networks

Chapter 8

Performance Evaluation of IEEE 802.15.4a with an Energy Detection Receiver and Multi-User Interference

The IEEE 802.15.4 standard targets low data-rate wireless networks with extensive battery life and very low complexity. Its physical layer is based on a narrow-band radio, operating in the unlicensed ISM band at 2.4 GHz. The IEEE 802.15.4a amendment [64] adds an IR-UWB physical layer to 802.15.4 that can operate over several bands of 500 MHz (or 1.5 GHz) from approximately 3 GHz to 10 GHz. Compared with the narrow-band physical layer, The IR-UWB physical layer offers higher data-rates and the possibility of performing ranging between devices. It should also offer a better robustness against interference and multipath propagation channels

The IEEE 802.15.4a physical layer allows for implementing either, a coherent receiver (for instance, a Rake receiver), or a non-coherent receiver (for instance, based on energy detection). We have discussed and compared the Rake receivers and the energy detection receivers in Sections 3.2 and 2.2.2. For the applications considered by the the IEEE 802.15.4 standard, a long lifetime and low complexity are the first objective. As such, an energy detection receiver appears to be the ideal solution. But, as we pointed out in Section 3.2, it is less robust to multi-user interference (MUI) than a coherent receiver.

MUI occurs due to concurrent packet transmissions and is hard to avoid in 802.15.4a networks: the mandatory medium access control (MAC) protocol in the IEEE 802.15.4a amendment is Aloha (without any form of clear channel assessment). In such a case, concurrent

transmissions inevitably occur. The choice of a simple Aloha protocol is justified by the potential robustness of UWB to interference and by the low data-rate requirements of the envisioned applications. But this low data-rate assumption is also subject to some restrictions: even a network with a low traffic rate can experience a sudden increase of traffic. In a sensor network used for fire detection, the detection of a fire would generate a large number of packets from several sources at the same time. Furthermore, MUI can occur from another, uncontrolled, 802.15.4a network running in parallel.

Hence, our objective in this chapter is to evaluate the performance of an IEEE 802.15.4a IR-UWB physical layer implementation with an energy detection receiver *and* MUI. We consider a complete system, with packet detection and timing acquisition, the estimation of channel characteristics, and the recovery of the encoded payload.

Our results show that the performance of an energy detection receiver is severely degraded by MUI. We find that an 802.15.4a compliant energy detection receiver only shows a very limited capture effect. If several transmissions are active concurrently, its performance is quite close to a case where all packets are lost. In a near-far scenario with one strong interferer we do not even have any capture effect at all.

Due to the complexity of the scenarios that we study, we do the performance evaluation through extensive simulations. The code used for our simulations is readily available [207].

The remainder of this chapter is organized as follows: In Section 8.1, we describe the receiver architecture that we consider. In Section 8.2, we first introduce the scenarios and parameters of the simulations. Then, we present the results of our performance evaluation. We conclude this chapter in Section 8.3.

8.1 A Simple Energy Detection Receiver for IR-UWB with Channel Mask Estimation

In this section, we describe the architecture and the mechanism of the receiver used in the performance evaluation. The IEEE 802.15.4a physical layer is described in Section 2.2.6. We recall here some important details:

- A preamble is added before the payload. This preamble is used for packet detection and timing acquisition, as well as the estimation of a channel mask used by the energy detection receiver.

- With respect to the data signal, there are two important differences in the structure of the preamble signal: (1) no time-hopping is used and (2) single pulses are transmitted instead of bursts of pulses.
- The preamble is generated using a preamble code: it is a ternary sequence of length 31.
- For each frequency band, the 802.15.4a standard foresees the use of two different preamble codes.

8.1.1 Architecture of the Energy Detection Receiver

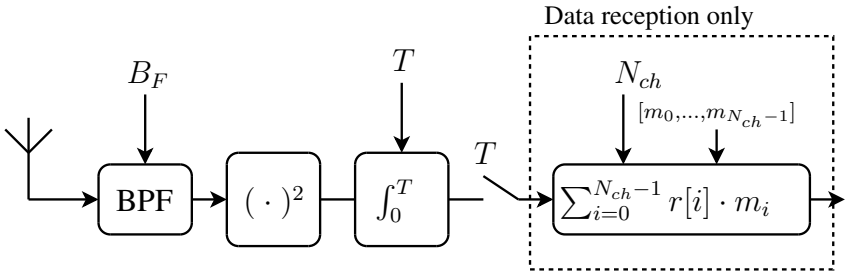

Figure 8.1: Architecture of the energy receiver. The antenna is followed by a bandpass filter of bandwidth B_F, a square device, and an integrator. The signal at the output of the integrator is sampled every T seconds. Finally, a scalar product is computed between a block of N_{ch} samples $r[0],\ldots,r[N_{ch}-1]$ and the channel mask $[m_0,\ldots,m_{N_{ch}-1}]$.

The architecture of the energy detection receiver is depicted in Figure 8.1; the antenna is followed by a bandpass filter of bandwidth B_F, a square device, and the integrator. The signal $r(t)$ at the output of the integrator is sampled every $T = \frac{1}{f_s}$ seconds to obtain the discrete time signal $r[i]$. Our receiver uses a *channel mask* to properly set the total integration time per symbol of the energy detection receiver. A channel mask is an estimation of the average power-delay profile of the received signal [98]. In our case, it is a binary vector of length N_ch. Hence, it also allows for ignoring output samples of the integrator in order to avoid integrating the received signal when it mostly consists of noise. The exact values of the parameters of the receiver are given in Table 8.1 in Section 8.2.1. There are three steps for packet detection and timing acquisition: (1) coarse timing acquisition, (2) fine timing acquisition, and (3) SFD detection. The coarse timing acquisition step is not strictly necessary. The acquisition procedure could be done entirely with the fine timing mechanism. But the initial coarse timing acquisition allows for reducing the memory requirement of the receiver. Following the fine timing acquisition, the estimation of the channel mask is performed. To ease the explanation of the

mechanism for coarse and fine timing acquisition, and channel mask estimation in the following sections, we already assume that the physical layer is operated with the mandatory data rate of 0.85 Mbit/s, with the low pulse-repetition frequency (LPRF) mode [64]. Furthermore, we set the sampling frequency f_s at the output of the receiver is 125 MHz (or a sample period T of 8 ns).

8.1.2 Coarse Timing Acquisition

During coarse timing acquisition, we try to locate the starting time of one of the N_{sync} repetitions of the preamble code. With $L_{up} = 64$, the timing accuracy of the coarse timing acquisition phase is $T_c L_{up} = 128$ ns. With an integration time of $T = 8$ ns, the length of a preamble code symbol corresponds to $T_c L_{up}/T = 16$ samples of the discrete time signal $r[i]$. Hence, we first create a correlation template by repeating each of the 31 elements of the preamble code 16 times. We repeat the obtained template G times to provide for some processing gain. We then correlate this template with the received signal $r[i]$, and down-sample the result by a factor 16. Finally, we group the output of the correlation by consecutive blocks of 31 elements $[\mathcal{R}_0[j], \ldots \mathcal{R}_{30}[j]]$ and look for the maximum element

$$R_{max}[j] = \max(\mathcal{R}_0[j], \ldots \mathcal{R}_{30}[j])$$

within each block.

If $R_{max}[j]$ lies above a certain threshold τ_{coarse}, we select its position within the jth block as a possible synchronization point. A verification process is then started on the subsequent V blocks of 31 elements. If for all the blocks $k = j+1, \ldots, j+V$, we find that $R_{max}[k] > \tau_{coarse}$ and that the position of $R_{max}[k]$ within the kth block is the same as $R_{max}[j]$, the coarse timing acquisition succeeds. We use $V = 5$ in the performance evaluation (see Table 8.1).

Assuming additive white Gaussian noise (AWGN) with known variance σ^2 (since it is generated by the circuitry of the receiver), the threshold τ_{coarse} can be analytically determined as a function of σ^2. According to [217], the distribution of the samples $r[i]$ at the output of the integrator if only AWGN is present can be approximated with a Chi-square random variable with $2B_F T$ degrees of freedom. We set τ_{coarse} such that the probability that a sequence consisting purely of noise exceeds τ_{coarse} is smaller than a certain threshold probability p_{thld}, i.e.

$$\tau_{coarse} = \sigma^2 F^{-1}_{\chi^2_K}(p_{thld}) \tag{8.1}$$

where $F_{\chi^2_N}(K)$ is the cumulative distribution function of the chi-square distribution with K degrees of freedom. In our case, K is the product of $2B_FT$ with G and with the number of non-zero preamble code symbols, which is 16.

8.1.3 Fine Timing Acquisition, Channel Mask Estimation, and SFD Detection

During fine timing acquisition, we improve the accuracy of the synchronization point to obtain a timing accuracy in the order of the integration time T. We look for the beginning of the signal in the vicinity of the coarse timing acquisition point. This is achieved by correlating the received signal $r[i]$ with a finer template and with a search-back procedure. The template for the fine timing acquisition is obtained by up-sampling the preamble code by a factor of 16 and repeating the obtained sequence G times.

Between fine timing acquisition and SFD detection, we estimate the channel mask. It is a sampled and binary quantized version of the power-delay profile of the channel represented as a binary vector

$$[m_0,\ m_1, \ldots,\ m_{N_{ch}-1}], \quad m_i \in \{0, 1\}, \quad \forall i.$$

The channel mask is used to reduce the amount of noise accumulated by the energy detection receiver. The estimation is done by averaging G_{chest} blocks of N_{ch} samples of the received signal. A threshold is then applied to quantize the N_{ch} values to zero or one. This threshold is computed in a similar manner as τ_{coarse} in the previous section. In the same averaging process, we also estimate the received signal level contained in the channel mask.

After the estimation of the channel mask, we begin to look for the SFD sequence. The mandatory 802.15.4a SFD is a sequence of eight modulated preamble codes scrambled by the so-called SFD code [64]. It is found with a correlation procedure taking into account the noise variance and the estimated received signal level. Note that when searching for the SFD, the channel mask is applied to the received signal.

Because it is not the primary interest of this chapter, we do not explain the timing acquisition algorithm up to the finest details. However, we do believe that it comes close to what would be used in a real-world implementation of a non-coherent, 802.15.4a compliant receiver. Also, the thresholds (τ_{coarse} and the one for the channel mask quantization) are computed assuming only AWGN and no MUI. Indeed, the receiver has no knowledge of when an interferer might be transmitting or of the statistics of the MUI.

8.1.4 Decoding of the Payload

Following the detection of the SFD, we can start decoding the data. For each frame, two scalar products

$$s_j = \sum_{i=0}^{N_{ch}-1} r_j[i] \cdot m_i, \quad j = 0, 1,$$

are computed where the values $r_0[0], \ldots, r_0[N_{ch}-1]$ correspond to where the bit 0 is expected and the values $r_1[0], \ldots, r_1[N_{ch}-1]$ to where the bit 1 is expected. A comparator $1_{\{s_0 > s_1\}}$ produces a binary output which is fed to the Reed-Solomon decoder.

8.2 Performance Evaluation

In this section, we evaluate the performance of our IEEE 802.15.4a compliant energy detection receiver in the presence of MUI.

8.2.1 Performance Metrics and Simulation Parameters

We use two different performance metrics; the bit error rate (BER) and the packet error rate (PER).

For the mandatory data rate of 0.85 Mbit/s, the 802.15.4a proposal defines two transmission modes for the data frame: the low pulse-repetition frequency (LPRF) mode and the high PRF (HPRF) mode. We consider the LPRF mode. The values of N_c, T_c, L_b, and N_{hop} for the LPRF mode are given in Table 8.2. A $(55, 63)$ Reed-Solomon (RS) code is used for error-correction [64]. We send 1014 bit per packet: with RS encoding, this corresponds to 1209 symbols. We assume the use of the mandatory frequency band 3, with a center frequency of 4.49 GHz. The two possible preamble codes are code 5 and 6 [64]. The sampling frequency f_s at the output of the receiver is 125 MHz (or a sample period T of 8 ns). This value corresponds to the length of a burst in the LPRF mode of the 802.15.4a proposal. The other parameters of the energy detection receiver are listed in Table 8.1.

T	f_s	B_F	G	V	N_{ch}	G_{chest}	p_{thld}
8 ns	125 MHz	1 GHz	4	5	16	8	0.9999

Table 8.1: Parameters of the energy detection receiver

At the time this work was performed, the 802.15.14a amendment was still in a draft state at version D6. In version D6, the LFSR is initialized to the same state for the transmission of

Mandatory data rate of 0.85 Mbit/s (LPRF mode)							
	N_c	T_c	L_b	N_{hop}	L_{up}	N_{sync}	N_{sfd}
LPRF	512	2 ns	4	32	64	64	8

Table 8.2: Parameters of the IEEE 802.15.4a physical layer

each packet. Hence, all transmitters have the same scrambling and time-hopping sequence.

We perform a packet-based simulation, and we simulate a full IEEE 802.15.4a system with coarse and fine timing acquisition, estimation of the channel mask, SFD detection, and RS decoding. We denote by N_u the number of users that are transmitting packets. For complexity reasons, we cannot simulate the full MAC protocol because this implies to simulate the reception and decoding of every single packet from *any* user at its respective destination, as well as the transmission and reception of the acknowledgment packets. Acknowledgment packets are necessary in order to correctly simulate the backoff algorithm.

Instead, we attempt to decode only the packets from the user of interest. We simulate several transmitters, but only the receiver for the user of interest. We ignore the transmission of acknowledgment packets back to the user of interest. To generate MUI, we consider that each user has a queue with a packet arrival rate λ_i, $i = 0, 1, \ldots, N_u - 1$. When a packet reaches the front of the queue, we draw a backoff time according to the IEEE 802.15.4a procedure with the backoff exponent set to its maximum value since we ignore acknowledgement packets. When the backoff expires, the packet is transmitted on the channel.

We simulate the whole physical layer with an accuracy of 100 ps (a *simulation* sampling frequency of 10 GHz). This appears to be a good trade-off between complexity and accuracy. We use the IEEE 802.15.4a channel model 1 [22]. The RMS delay is around 18 ns.

In our simulations, we define the signal to noise ratio (SNR) as

$$\mathrm{SNR} = \frac{E_p}{N_0} \tag{8.2}$$

where E_p is the received energy *per pulse* (after the convolution of the pulse with the impulse response of the channel), and $N_0/2$ is the variance of a zero mean, Gaussian noise process bandlimited to B_F. As the simulation sampling frequency is larger than $2B_F$, the Gaussian noise samples are correlated. We use the algorithm in [218] to generate the correlated noise samples.

8.2.2 How to Evaluate and Compare the Performance with MUI

For the simulations with MUI, we consider two different scenarios; in scenario A, all the devices use the same preamble code. In scenario B, the user of interest uses preamble code 5 and the other users use preamble code 6. In both cases, we consider $\lambda_0 = \lambda_1 = \lambda$ with either a high traffic case where $\lambda = 200$ packet/s, or a low traffic case where $\lambda = 10$ packet/s. The saturation throughput with our modeling is 226.4 packet/s. Hence, in the high traffic case the network is not yet saturated In terms of bitrate, $\lambda = 200$ packet/s ($\lambda = 10$ packet/s, respectively) corresponds to an effective data rate of 241.8 kbit/s (12.1 kbit/s). Also, because we are using the maximum backoff exponent, our results are independent of the arrival rate of the user of interest ($\lambda_0 = \lambda_1 = 200$ packet/s yields the same results as $\lambda_0 = 10$ packet/s, $\lambda_1 = 200$ packet/s).

In order to understand how robust energy detection is with respect to MUI, we compare the performance obtained by simulations with the performance when considering two very specific capture models. With the "Destructive Collisions" model, a packet is lost whenever there is more than one active transmission at the same time. If there is only one active transmission, single user performance is then assumed. This is the worst case performance. With the "Perfect Capture" model, all active users may compete during packet detection and timing acquisition. Only one of them succeeds (chosen uniformly at random) and this winning user experiences single user performance. This is the ideal performance, which one would obtain if transmissions would be perfectly orthogonal.

8.2.3 Performance Evaluation Results: Single-User Case

In Figure 8.2, we show the PER and BER obtained for a single user (with no MUI). For the BER, there is 1.5 dB difference with respect to the BER of binary pulse position modulation (BPPM) on AWGN channels (which is obtained as $Q\left(\sqrt{SNR}\right)$ assuming a matched filter). We also plot the percentage of missed packets by the timing acquisition procedure. With a multipath channel and no MUI, we can conclude that the receiver is well balanced between the timing acquisition procedure and the decoding of the data. Indeed, there are no missed packets above 12 dB and the BER is below 10^{-5} above 14 dB.

8.2.4 Performance Evaluation Results: Multiple Users Case

In Figure 8.3 we first show the PER obtained with two users with equal received powers, $\lambda = 10$ packet/s, in the case of scenario B (different preamble codes). Clearly there is an error-floor with MUI, even in this low traffic case. Further, we look at two more cases with unequal

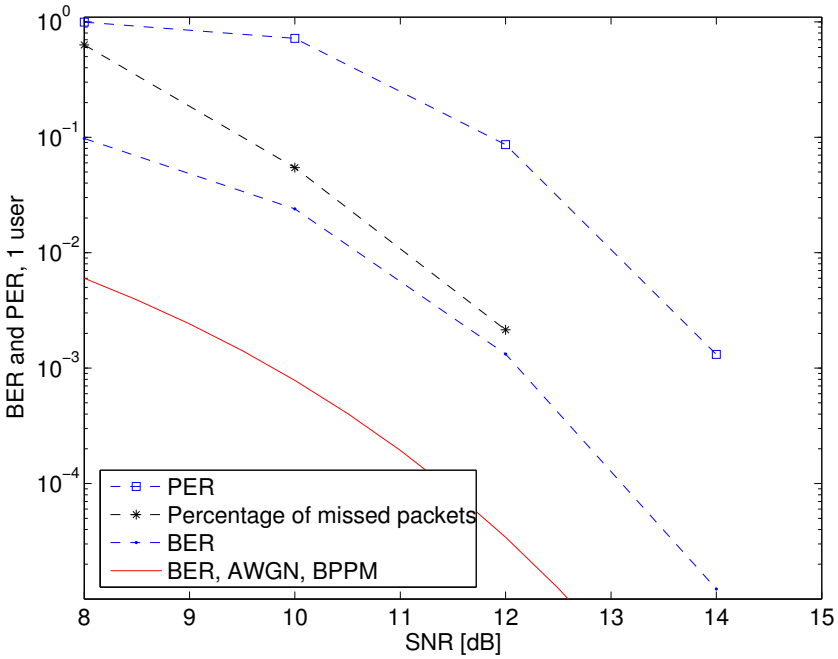

Figure 8.2: PER, BER, and percentage of packets missed by the timing acquisition for a single user, on a multipath channel, with no MUI. The plain curve represents the performance of BPPM on an AWGN channel.

received powers: first, a near-far case, where the received power of the second user is 10 dB higher; second, a case with four users, where the received powers of the three interferers are 3 dB lower than the received power of the user of interest. We also compare the previous results with those obtained with the "Destructive Collisions" and "Perfect Capture" models. We find that the energy detection receiver operates quite close to the worst case scenario of the "Destructive Collisions" model, and shows only limited capture effect. Its performance is even identical to the "Destructive Collisions" model in the presence of only one strong interferer.

It appears that using an energy detection receiver with an 802.15.4a physical layer annihilates one of the most appealing benefits of UWB, specifically its robustness to MUI and thus, the possibility of allowing for concurrent transmissions. The conclusions are identical for $\lambda = 200$ packet/s.

When analyzing packet errors, we observe that they occur for two reasons: (1) a packet is missed during the timing acquisition phase or (2) it is received with more errors than the Reed-Solomon code could correct. In the first case, we can further distinguish two cases:

(1a) We miss the packet because of a missed detection (MD): the receiver is trying to acquire a packet but is not able to acquire timing, or it acquires timing correctly but later misses

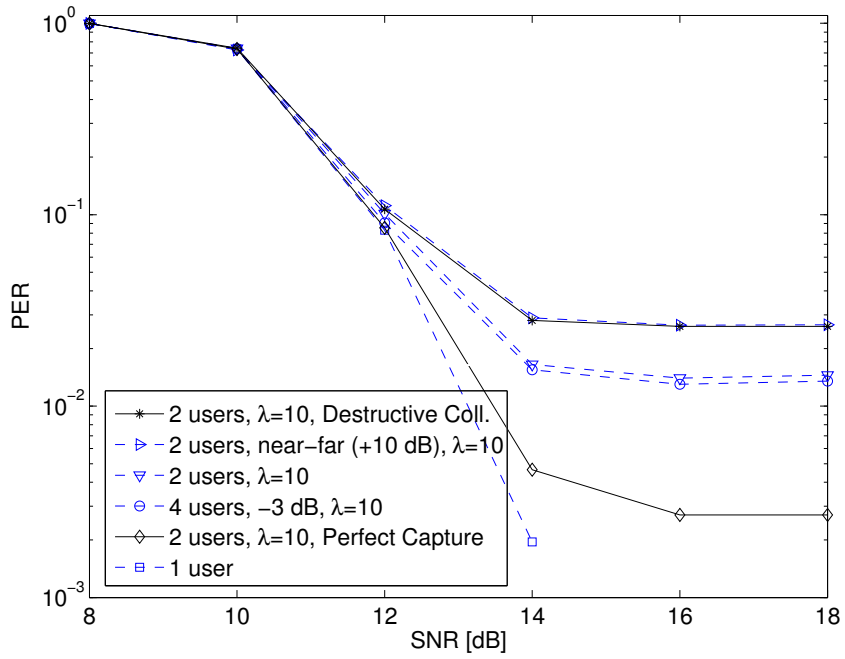

Figure 8.3: PER with MUI and different preamble codes (scenario B). Dashed lines from top to bottom: simulation results for two users in a low traffic case ($\lambda = 10$ packet/s), where the received power of the interferers is to $+10$ dB or 0 dB; four users where the received power of the interferers is -3 dB; no interference. Plain lines: "Destructive Collisions" and "Perfect Capture" models. The performance with MUI is close to the "Destructive Collisions" model.

the SFD.

(1b) We miss the packet because of a false alarm (FA): the receiver is not trying to acquire a packet because it wrongly assumes to be already successfully synchronized.

Now, if both the interferer and the user of interest use the same preamble code (scenario A), the receiver will miss lots of packets due to false alarms. Hence, we expect a much worse performance compared to the case where they use different codes (scenario B). A comparison of these two scenarios is shown in Figure 8.4 where it can be seen that the difference is surprisingly small. Looking at the percentage of packets missed during the timing acquisition phase (see Figure 8.5) confirms that the receiver misses more packets in scenario A than in scenario B.

We can further see in Table 8.3 that of the missed packets in scenario A, 98% are effectively missed because of a false alarm. However, if we consider the BER of the packets that are correctly acquired (see Figure 8.5), we notice that the acquired packets generally have more errors in scenario B than scenario A. We conclude that the packets additionally acquired by the

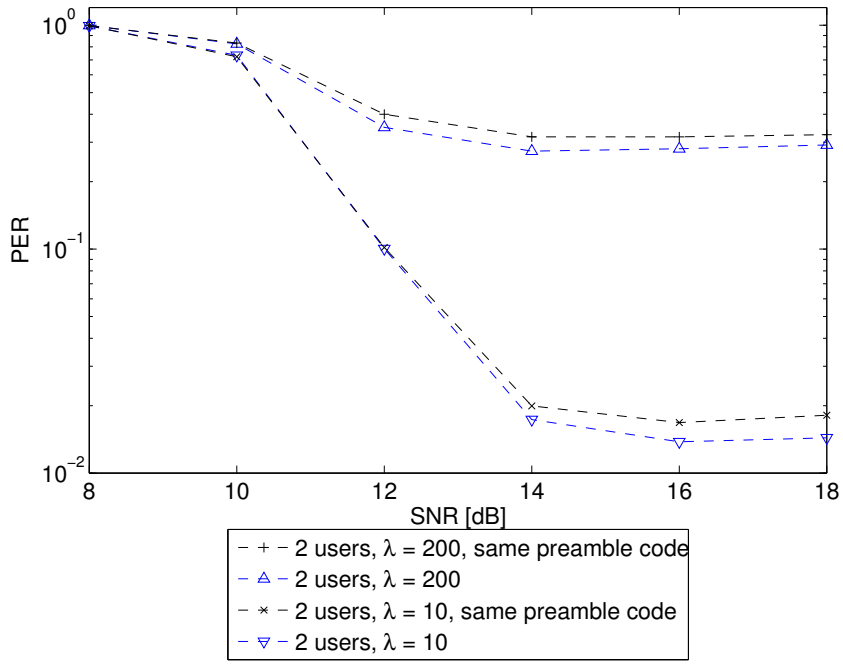

Figure 8.4: Comparison of the PER when two users use the same preamble code or different preamble codes. The two users have equal power at the receiver. We show a high ($\lambda = 200$ packet/s) and a low traffic case ($\lambda = 10$ packet/s). There is a negligible difference whether we use the same preamble code or a different preamble code.

receiver in scenario B are packets with lots of interference. Therefore, a lower rate of missed packets does not translate to a huge performance improvement in terms of PER.

Another observation that may come as a surprise is the fact that even in scenario B, more than 50% of the missed packets are missed because of a false alarm (see Table 8.3). In order to understand this phenomenon, let us classify false alarms into two categories:

(Category 1) The receiver acquires timing correctly but wrongly declares detection of the SFD. This can happen if noise or the signal of the interferer make the receiver exceed the SFD

	Same Code	Different Code
Percentage of missed packets	25.3%	15.7%
Out of which missed due to false alarm (FA)	98.0%	52.1%
Out of which FA due to wrong timing acquisition	99.0%	99.1%

Table 8.3: Percentage of missed packets and classification of the reason they were missed. Numbers shown are for packet arrival rate of $\lambda = 200$ packet/s and at an SNR of 18 dB.

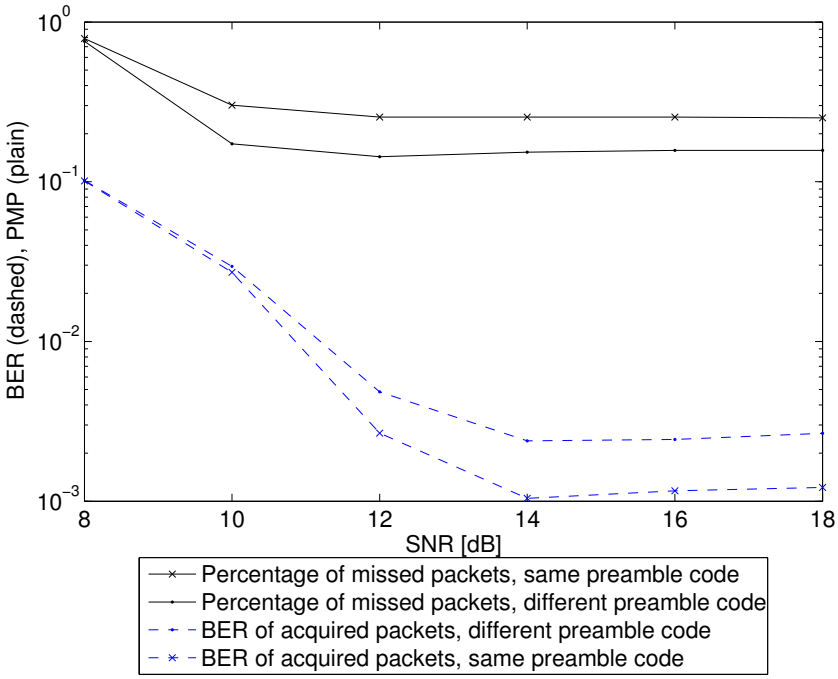

Figure 8.5: Percentage of missed packets (plain lines) and BER (dashed lines) when two users use the same or a different preamble code. We consider the high traffic case ($\lambda = 200$ packets). If different codes are being used, there are less packets missed. However, the packets additionally acquired, have generally more interference, which translates into a higher BER.

detection threshold even though the SFD of the user of interest is not present.

(Category 2) Noise and interference lead the receiver to acquire a wrong timing and then wrongly declare detection of an SFD.

Analyzing false alarms in scenario B, we observe that more than 90% of them fall into category 2. Hence, it seems that even if the receiver and the interferer use a different preamble code, the receiver still synchronizes with the interferer often. A reason for this behavior becomes apparent if we look at the correlation between preamble codes. In Figure 8.6(a), we first show the correlation of preamble code 5 (the correlation template) with a periodic repetition of itself (representing the sequence of the user of interest) and secondly with a periodic repetition of preamble code 6 (representing the sequence of an interferer)[1]. We observe that the first correlation has a peak only when there is a perfect alignment between the sequence and the template. On the other hand, there are 10 out of the 31 possible shifts that lead to a peak in the correlation of the interferer sequence and the template. Even though these peaks are lower

[1]Note that in the case of an energy detection receiver, the ternary preamble code sequence is transformed into a binary one because of the squaring operation.

Avg. number of ones in channel mask (perfect timing acquisition)						
Correct packets	1.00	2.17	3.30	4.28	5.09	5.97
Erroneous packets	1.61	2.39	3.15	4.52	5.58	6.08
SNR [dB]	8	10	12	14	16	18

Table 8.4: Average number of ones in channel mask (perfect timing acquisition, two users with $\lambda = 200$ packet/s)

when the sequence does not match the template, they might (depending on the signal level of the interferer and the noise) still exceed the detection threshold of the coarse timing acquisition phase and consequently lead to false alarms. To verify this assumption, we classify wrong timing acquisitions in our simulations according to the offset (in number of code symbols) with respect to the closest packet (in time) of an interferer. The result for $\lambda = 200$ packet/s at an SNR of 18 dB is shown in Figure 8.6(b); the offsets with the largest number of packets correspond exactly to the offsets producing peaks in the correlation.

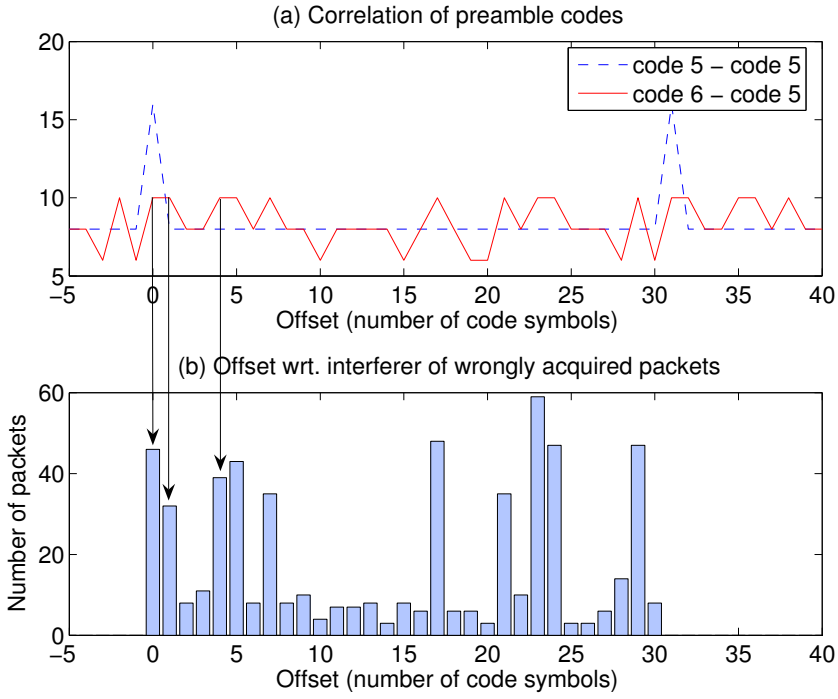

Figure 8.6: (a, top) Correlation of preamble code 5 with a periodic repetition of itself and with a periodic repetition of preamble code 6. (b, bottom) Classification of wrong timing acquisitions according to the offset with respect to the closest packet of an interferer. Correspondence of peaks in (a) and (b) suggests that wrong timing acquisitions are due to the correlation properties of the preamble codes.

In Figure 8.7, we compare the PER shown in Figure 8.3, with a PER obtained with a

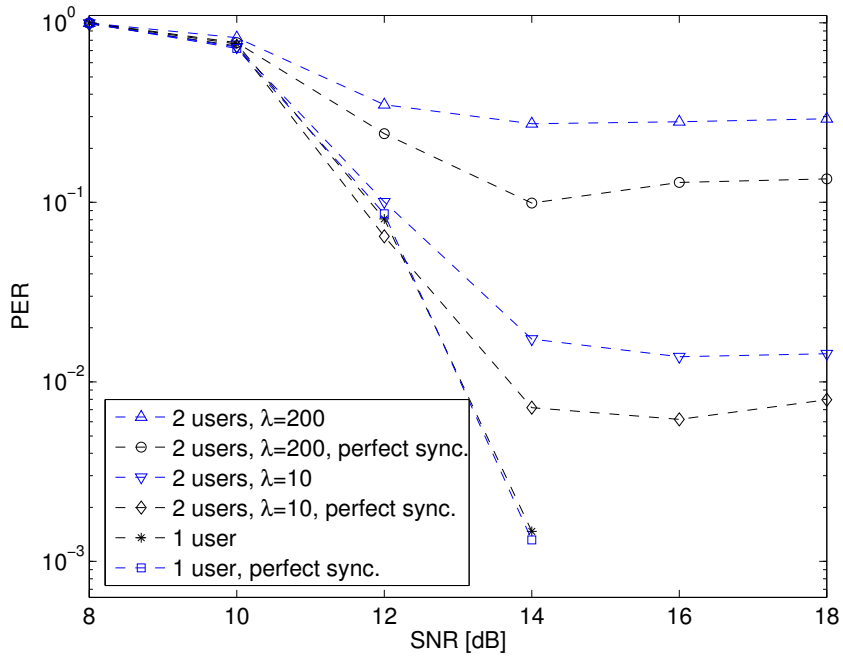

Figure 8.7: Comparison of the PER between our implementation of the timing acquisition and channel mask estimation algorithm and a perfect timing acquisition and channel mask estimation. The perfect channel mask estimation assumes no MUI.

perfect timing acquisition and channel mask estimation algorithm: an oracle returns the exact beginning of the packet of the user of interest. Hence, there are no false alarms or missed detections. Besides, the estimation of the channel mask assumes perfect timing acquisition and no MUI. Thus, Figure 8.7 allows for assessing whether the performance degradation is solely due to the timing acquisition phase or whether MUI also significantly affects the data decoding phase. Even in the case of perfect timing acquisition, there is a clear error floor. MUI during timing acquisition and MUI during data decoding are equally responsible for the performance degradation.

It can also be observed in Figure 8.7 that the error-floor of the BER shows an increasing trend after 14 dB. Table 8.4 shows that the average number of ones in the channel mask increases proportionally with the SNR. A large number of ones in the channel mask implies a higher likelihood of suffering from MUI as we integrate a larger amount of the received signal.

In Figure 8.8, we show the coded and uncoded BER. The uncoded BER is obtained by not using the RS code in the simulations. All the results in Figure 8.8 are obtained with perfect timing acquisition and channel mask estimation, and we look at the high and low traffic case. Clearly, the RS code appears to be more efficient against Gaussian noise that MUI.

The preamble and payload of an IEEE 802.15.4a packet have a different format. Hence,

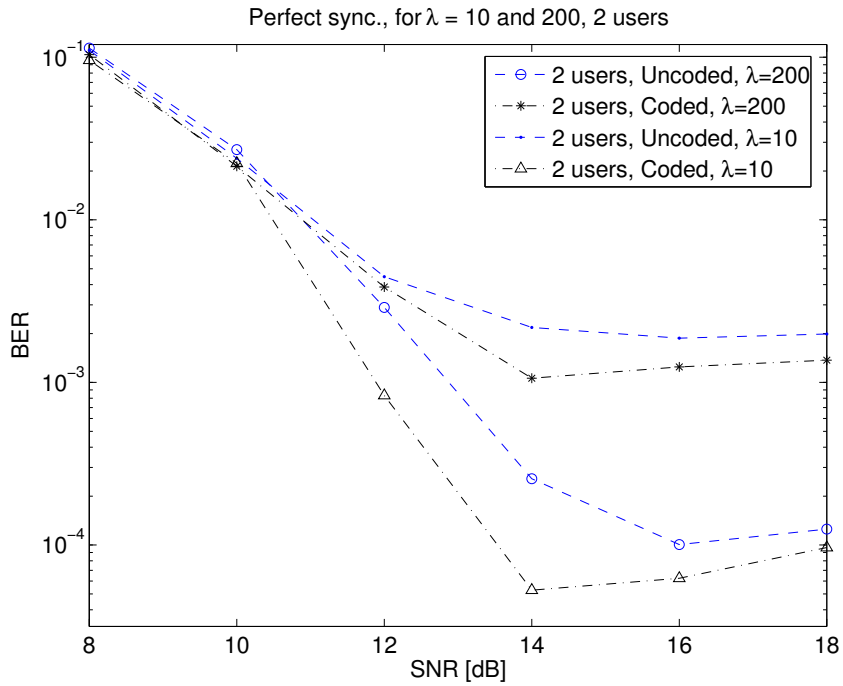

Figure 8.8: Comparison of the BER for two users in the case of coded and uncoded data transmissions with a perfect timing acquisition and channel mask estimation. There is the high and low traffic case. Clearly, the RS code appears to be more efficient against Gaussian noise that MUI.

it is interesting to assess whether packet errors are caused by an interfering preamble or an interfering payload. The following analysis is done with the interferer having an equal received power but using a different preamble code than the user of interest. The SNR is 18 dB and $\lambda = 200$ packet/s (PER shown in Figure 8.3). Our conclusions are similar for other cases presented in this chapter. Looking first at packets that are correctly acquired but incorrectly decoded, 91.3% of these packets have an overlap of more than 30% with an interfering payload. Moreover, 46.1% of these packets have no overlap at all with an interfering preamble. We conclude that errors in this case are mostly due to an interfering payload.

We then look at packets that are missed during the timing acquisition phase. Table 8.3, Figure 8.6, and the corresponding analysis already demonstrated that false alarms mostly happen because the receiver synchronizes with an interfering preamble. Missed detections occur if (1) the receiver is not able to acquire timing, or (2) it acquires timing but later misses the SFD. In our simulations, 92.6% of missed detections are of the second type, the remaining 7.4% are of the first type. For both types, an average of 80% of the preamble overlaps with an interfering payload. We conclude that missed detections are also mostly due to interference with a

payload.

The above results suggest that most of the packet errors are due to an interfering payload. This also makes sense from the perspective that a burst in the payload contains four times more energy than a pulse of the preamble. Furthermore, the payload is much longer than the preamble, making a collision with a payload more likely.

8.3 Discussion and Conclusion

We have evaluated the effect of MUI on an IEEE 802.15.4a physical layer that uses an energy detection receiver. The architecture of the energy detection receiver that we use is extremely simple. In particular, it does not use the information on the power-delay profile of the channel as best as it could, contrary to [37]. But the work in [37] does not consider the fact that bursts of pulses are sent. This is one of the issue that we address in the following chapter. Furthermore, to the best of our knowledge, none of the previous work in Section 3.2 in the area of energy detection receivers considers MUI, and hardly any the performance evaluation of a complete system, with both timing acquisition and data reception.

Our results in this chapter have shown that an energy detection receiver is a good and well-balanced solution if no MUI is present. However, already in low traffic cases, the performance is severely degraded in the presence of MUI. One of the most appealing benefits of UWB, specifically its robustness to MUI and thus the possibility of allowing for parallel transmissions is completely annihilated by the energy detection receiver. Both timing acquisition and data decoding are affected. For future work, it might be interesting to take into account the clear channel assessment (CCA) mode 5 and 6 of the IEEE 802.15.4a amendment [64]. We might also compare our results with those obtained when using a realistic coherent receiver.

But, what looks more promising, is to explore the possibilities of mitigating the effect of MUI, even with a low-complexity receiver based on energy detection. Along with fully taking into account the specifics of the modulation format of the IEEE 802.15.4a physical layer, the design of an interference mitigation scheme for an energy detection based receiver our main motive for the next chapter.

8.4 Acknowledgments

We would like to thank Armin Wellig and Julien Zory, from STMicroelectronics, for the initial motive behind the content of this chapter, and also to provide us with the model of the energy

detection receiver and for all the discussions and comments on this paper.

Chapter 9

An Energy Detection Receiver Robust to Multi-User interference for IEEE 802.15.4a Networks

For IEEE 802.15.4a low data-rate networks, where energy consumption is of primary importance and devices should be inexpensive, energy detection receivers are appealing. With a relatively low hardware complexity, these receivers can exploit the ranging capabilities and multipath resistance of IR-UWB.

Unfortunately, the performance of energy detection receivers is greatly affected by multi-user interference (MUI). In the previous chapter, we analyzed the performance of an IEEE 802.15.4a compliant, energy detection receiver in the presence of several transmitters using an Aloha medium access control (MAC) layer (which is the mandatory MAC in IEEE 802.15.4a). The packet error rate (PER) was severely increased by MUI, even at low data-rates.

One solution to the performance loss may be to prevent MUI by using a more sophisticated MAC to coordinate access to the physical layer. But, this cannot prevent MUI due to uncontrolled activities in neighboring networks (e.g., several IEEE 802.15.4a piconets running in parallel). Interference must be taken into account already in the design of the physical layer. Furthermore, we also know (from Chapters 4 and 5) that with an interference mitigation scheme at the physical layer it is optimal to not prevent interference in IR-UWB networks: instead, the MAC must manage interference with rate adaptation, and an interference mitigation scheme used at the physical layer.

Hence, there is a need to develop interference mitigation schemes for IR-UWB energy

detection receivers. The low complexity of energy detection receivers makes them perfect candidates for IEEE 802.15.4a networks. But, because of uncontrolled interference, and from the point of view of the optimal design, they need to be more robust against MUI.

We already discussed in Sections 2.2.4 and 3.3.1 that the MUI in low data-rate IR-UWB networks is non-Gaussian, and its probability density function exhibits an impulsive shape. With non-Gaussian interference, [126, 127] suggest applying a non-linear function on the received signal prior to demodulation, for instance, a simple thresholding operation [128]. Recently, [46] showed the benefits of a thresholding structure on the achievable rate in IR-UWB networks. And we further confirmed in this thesis, in Sections 4.1.2 and 5.1.3, the performance gains that can be obtained with a simple interference mitigation scheme based on thresholding. We also presented more sophisticated interference mitigation schemes in the related work in Section 3.3.3.

The energy detection receiver used in the previous chapter also has two design shortcomings. First, according to [37], a binary channel mask is not optimal; second, the receiver we used is not adapted to the specifics of the IEEE 802.15.4a modulation format. In particular, it does not take into account the transmission of bursts of pulses in the data part.

Our contribution in this chapter is a non-coherent receiver architecture robust to MUI and compliant with IEEE 802.15.4a. It is built around an energy detection receiver, and uses an adaptive non-linearity, based on thresholding, to mitigate MUI. In order to correctly set the threshold, the power delay profile of the received signal needs to be properly estimated. This is done during the preamble that precedes the payload of an IEEE 802.15.4a packet. However, there is one specific difficulty: The structure of the signal in IEEE 802.15.4a differs between the preamble and the payload (see Section 2.2.6). Consequently, the power delay profile of the payload signal is time-varying due to the scrambling operation and it is impossible to estimate it with a classic energy detection receiver. Our receiver overcomes this issue. It does so in a way that is robust to MUI and only with a moderate increase in complexity.

In this chapter, we concentrate on the robust estimation of the power delay profile and on robust data decoding. We do not consider robust timing acquisition. But we point out the work in [63, 144] that already suggests potential solutions for robust timing acquisition. The remainder of this chapter is organized as follows: We describe the architecture of our receiver in Section 9.1, evaluate its performance in Section 9.2, and conclude the chapter in Section 9.3.

9.1 Architecture of the Robust Receiver

Before we begin with the description of the architecture of the receiver, we recall two useful equations for the remainder of this chapter: first, the received signal for the preamble, equation (2.18) in Section 2.2.6

$$r^{pre}(t) = \sum_i c_i^{pre} \cdot h(t - iL_{up}T_c) + n(t). \tag{9.1}$$

where c_i^{pre} is the preamble code, $h(t)$ is the unknown channel response (including the transmitted waveform, the response of the multipath channel and the bandpass filter), and $n(t)$ accounts for thermal noise and MUI. Second, the received signal during the payload, equation (2.16) in Section 2.2.6

$$r(t) = \sum_{i=0}^{L_p-1} \sum_{j=0}^{L_b-1} b_{i,j} \cdot h(t - iT_f - c_i L_b T_c - d_i T_f/2 - jT_c) + n(t). \tag{9.2}$$

where $b_{i,j} \in \pm 1$ is the pseudo-random polarity of the j-th pulse of the i-th symbol specified by the scrambling sequence, and $\left[c_o, c_1, \ldots, c_{L_p-1}\right]$ is the time-hopping sequence. Without loss of generality, we can consider only the first symbol for the received signal of the payload (i.e., we set $i = 0$ and drop the index i) and assume $c_0 = 0$, yielding

$$r(t) = \sum_{j=0}^{L_b-1} b_j \cdot h(t - dT_f/2 - jT_c) + n(t). \tag{9.3}$$

Additional details for the notation can be found in Section 2.2.6.

The received signal is first processed by a squaring operation followed by an integrator sampled at a rate $\frac{1}{T}$ and yielding the discrete time signals

$$y_{m,i}^{pre} = \int_{mT+iL_{up}T_c}^{(m+1)T+iL_{up}T_c} [r^{pre}(t)]^2 dt \tag{9.4}$$

for the preamble, and

$$y_m = \int_{mT}^{(m+1)T} r(t)^2 dt \tag{9.5}$$

for the payload, where $m = 0, \ldots, N-1$, with $N = L_{up}T_c/T$.

9.1.1 Optimal and Approximated Decision Rules for Burst Transmissions

Assuming that $n(t)$ is purely AWGN with power spectral density $N_0/2$ bandlimited to B, the samples y_m are independently and identically distributed according to a non-central chi-square distribution with $2BT$ degrees of freedom and non-centrality parameter $\lambda_{m,d} = \frac{1}{N_0/2} p_{m,d}$ [217], i.e.

$$y_m \sim NC\chi^2_{2BT,\lambda_m} \tag{9.6}$$

where

$$p_{m,d} = \int_{mT}^{(m+1)T} \left[\sum_{j=0}^{L_b-1} b_j \cdot h(t - dT_f/2 - jT_c) \right]^2 dt \tag{9.7}$$

for $d = 0, 1$. Let $N_f = T_f/T$ and observe that $p_{m,1} = p_{m-N_f/2,0}$. Thus, we can simplify the notation by introducing $p_m \doteq p_{m,0}$. Under the above assumptions, the optimal decision rule according to the maximum likelihood criterion is found as

$$\sum_{m=0}^{N-1} \ln \left(\frac{I_\alpha \left(\frac{\sqrt{y_m p_m}}{N_0/2} \right)}{\sqrt{y_m^\alpha}} \right) \underset{\hat{d}=1}{\overset{\hat{d}=0}{\gtrless}} \sum_{m=0}^{N-1} \ln \left(\frac{I_\alpha \left(\frac{\sqrt{y_{m+N_f/2} p_m}}{N_0/2} \right)}{\sqrt{y_{m+N_f/2}^\alpha}} \right) \tag{9.8}$$

where $\alpha = BT - 1$ and $I_\alpha(y)$ denotes the α-th order modified Bessel function of the first kind. Equation (9.8) can be linearly approximated [37] resulting in a more practical decision rule

$$\sum_{m=0}^{N-1} y_m \cdot p_m \underset{\hat{d}=1}{\overset{\hat{d}=0}{\gtrless}} \sum_{m=0}^{N-1} y_{m+N_f/2} \cdot p_m \tag{9.9}$$

Hence, the optimal detector applies a weighting function with coefficients p_m prior to comparing the energies in the first and second half of a data frame. With $L_b > 1$, equations (9.7) to (9.9) give us a generalization of the result found in [37]. With $L_b = 1$ the weighting function reduces to the one found in [37]. How to estimate the weights p_m is shown in Section 9.1.3.

9.1.2 A Thresholding Mechanism to Reduce the Impact of MUI

We know from the related work in Section 3.3.1 that, in the presence of MUI, the assumption of $n(t)$ being AWGN does not generally hold. Therefore, we additionally use a thresholding mechanism to mitigate MUI. As stated before, $y_m \sim NC\chi^2_{2BT,\lambda_m}$ if the interference is only AWGN. If MUI occurs, the distribution of y_m will deviate from (9.6). A deviation can be detected by comparing the received signal samples with a threshold ν_m. This threshold can be

calculated by the receiver as follows

$$\nu_m = \frac{N_0}{2} F^{-1}_{NC\chi^2_{2BT,\lambda_m}}(1 - P_{FA}) \tag{9.10}$$

where $F_{NC\chi^2_{2BT,\lambda_m}}(x)$ is the cumulative distribution function of the non-central chi-square distribution and P_{FA} is a small false-alarm probability that allows us to set the sensitivity of the threshold. The threshold ν_m can be made adaptive by adjusting P_{FA}, for instance according to feedback from the physical layer.

Hence, prior to the decision process, the receiver applies a non-linear threshold operation governed by ν_m to the received samples in order to mitigate or even reject high interference terms. Different non-linear operations are possible. The one we found to work best is to set samples larger than the threshold to the value of the corresponding weight p_m

$$y_m = \begin{cases} y_m & \forall m : y_m \leq \nu_m \\ p_m & \forall m : y_m > \nu_m \end{cases} \tag{9.11}$$

As can be seen from (9.10), the threshold ν_m depends on the weights p_m as well as on the thermal noise level. How to estimate these quantities is explained in Section 9.1.3.

9.1.3 Estimation of the Weighting Coefficients p_m

To show how the weighting coefficients p_m can be estimated from the preamble, we rewrite equation (9.7)

$$\begin{aligned} p_m &= \sum_{j=0}^{L_b-1} b_j^2 \int_{mT}^{(m+1)T} h^2(t - jT_c)dt \\ &\quad + 2\sum_{j=0}^{L_b-1}\sum_{k=j+1}^{L_b-1} b_j b_k \int_{mT}^{(m+1)T} h(t - jT_c)h(t - kT_c)dt. \end{aligned} \tag{9.12}$$

By applying the change of variables $s \doteq t - jT_c$ and introducing $K \doteq T_c/T$, we obtain

$$p_m = \sum_{j=0}^{L_b-1} \int_{(m-jK)T}^{(m-jK+1)T} h^2(s)ds + 2\sum_{j=0}^{L_b-1}\sum_{k=j+1}^{L_b-1} b_j b_k \int_{(m-jK)T}^{(m-jK+1)T} h(s)h(s-(k-j)T_c)ds \tag{9.13}$$

$$= \sum_{j=0}^{L_b-1} w_{m-jK}^{(0)} + 2\cdot\sum_{j=0}^{L_b-1}\sum_{k=i+1}^{L_b-1} b_j b_k \cdot w_{m-jK}^{(k-j)} \tag{9.14}$$

where $w_m^{(l)}, l = 1, \ldots, L_b - 1$ is given by

$$w_m^{(l)} = \int_{mT}^{(m+1)T} h(t)h(t - l\cdot T_c)dt \tag{9.15}$$

To estimate p_m, we have to estimate the parameters $w_m^{(l)}$. Note that $w_m^{(0)}$ (with $l = 0$) represents the energy-delay profile of the channel and corresponds to the weight applied in [37]. Plugging (9.1) into (9.4) and taking expectations yields

$$\mathbb{E}[y_{m,i}^{pre}] = (c_i^{pre})^2 \underbrace{\int_{mT}^{(m+1)T} h^2(t)dt}_{w_m^{(0)}} + \underbrace{\mathbb{E}\left[\int_0^T n^2(t)dt\right]}_{\bar{n}} = (c_i^{pre})^2 w_m^{(0)} + \bar{n}. \tag{9.16}$$

This suggests that we can get an estimate $\hat{\bar{n}}$ of $\bar{n}$ from the sample mean of the samples $y_{m,i}^{pre}$ for which $c_i^{pre} = 0$. We can further get an estimate $\hat{w}_m^{(0)}$ of $w_m^{(0)}$ by first averaging over the samples $y_{m,i}^{pre}$ for which $c_i^{pre} \neq 0$ and then subtracting $\hat{\bar{n}}$. Note that using the sample mean as a practical estimator for (9.16) is not robust if $n(t)$ is non-Gaussian. We address this issue in Section 9.1.4.

Also note that there is no way for $w_m^{(l)}$, $l \neq 0$, to be estimated by an existing energy detection receiver architecture. Consequently, equations (9.14) and (9.15) not only define a new weighting function but also show the necessity for a new receiver structure that allows for the estimation of the parameters $w_m^{(l)}$. To this end, we propose a receiver employing $L_b - 1$ additional branches with respect to a classic energy detection receiver as shown in Figure 9.1. However, the additional branches are only needed during the preamble, while estimating the parameters $w_m^{(l)}$. During the other phases of packet reception, synchronization and decoding, the additional circuitry is *not* used. The added complexity and power consumption should thus

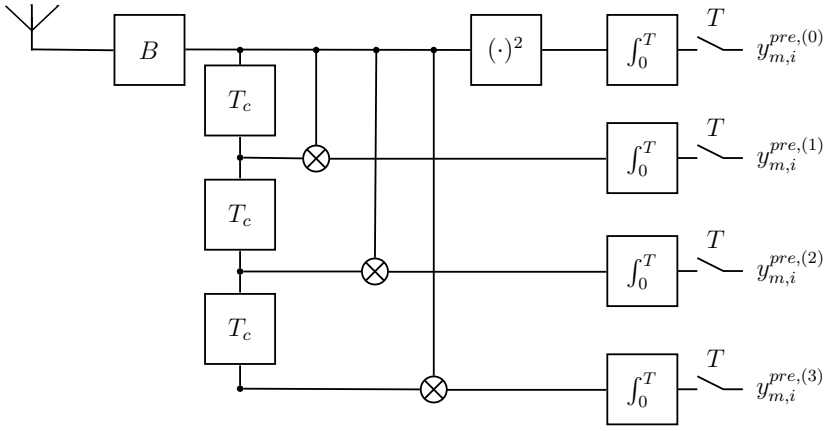

Figure 9.1: Proposed receiver structure in the case of payload signaling with bursts of four pulses ($L_b = 4$). The additional branches are needed *only* during estimation of the parameters $w_m^{(l)}$ given in (9.15). They are not needed for data decoding where only the upper branch is required. Hence, their impact on power consumption is minimal.

be moderate. This also limits the additional memory requirements of this more sophisticated receiver. The l-th additional branch delays the received signal by lT_c and multiplies the received signal with this delayed version. The resulting signal is then integrated and sampled to yield the samples $y_{m,i}^{pre,(l)}$.

The quantity $\hat{w}_m^{(0)}$ can be obtained from the undelayed branch $y_{m,i}^{pre,(0)}$ (see Figure 9.1) as before according to equation (9.16). $\hat{w}_m^{(l)}, l \in \{1, \ldots, L_b - 1\}$ can be obtained in a similar way from the l-th branch, thanks to the observation that

$$\mathbb{E}[y_{m,i}^{pre,(l)}] = (c_i^{pre})^2 \underbrace{\int_{mT}^{(m+1)T} h(t)h(t - l \cdot T_c)dt}_{w_m^{(l)}} = w_m^{(l)} \tag{9.17}$$

From the parameters $\hat{w}_m^{(l)}, l \in \{0, \ldots, L_b - 1\}$ an estimate of the weights $\hat{p}_m$ can be directly calculated using (9.14) under the condition that $K = T_c/T$ is an integer greater than or equal to one or in other words $T \leq T_c$.

If $K < 1$, p_m can still be calculated but the integrators in Figure 9.1 have to be replaced by a bank of time-delayed parallel integrators to obtain the shifted parameters $w_{m-jK}^{(l)}$. We do not go into the details of this alternative design in this chapter. Nevertheless, a trade-off between a lower possible sampling frequency and additional required circuitry is possible.

In addition to the weights p_m, we also have to estimate the power spectral density $N_0/2$ of the noise; it is used to calculate the threshold ν_m. An estimate can be obtained from $\hat{\bar{n}}$ given in

(9.16) as

$$\frac{\hat{N}_0}{2} = \frac{\hat{\bar{n}}}{2BT}. \tag{9.18}$$

9.1.4 Robust Parameter Estimation Using Order Statistics

If done according to equations (9.16), (9.17), and (9.18) the estimation of $\hat{w}_m^{(l)}$ and $\hat{\bar{n}}$ is not robust to MUI if the number of samples used to calculate the sample mean is small and/or if the interference level is very high.

A more robust option in these cases is to use order statistics to calculate these estimates by replacing the sample mean by the sample median which is more robust to outliers. If $\hat{\bar{n}}$ has been calculated in this way, the estimation of the power spectral density of the noise is replaced by

$$\frac{\hat{N}_0}{2} = \frac{\hat{\bar{n}}}{2BT - 2/3}.$$

9.2 Performance Evaluation

In this section, we evaluate the performance of an IEEE 802.15.4a physical layer that uses our robust receiver in the presence of MUI. The main performance metric is the packet error rate (PER).

9.2.1 Performance Metrics and Simulation Parameters

The performance metric is the packet error rate (PER). As in the previous chapter, we perform a packet-based simulation. There is one receiver and N_u transmitters. We simulate the estimation of the power delay profile of the channel followed by data decoding (with the $(63, 55)$ Reed-Solomon code). Contrary to the previous chapter, we assume that synchronization always succeeds.

We also recall from the previous chapter the model that we use to generate MUI: each transmitter has a queue with packet arrival rate λ_i, $i = 0, 1, \ldots, N_u - 1$. For each packet reaching the front of the queue, we draw a backoff time according to the IEEE 802.15.4a procedure with the backoff exponent set to its maximum value. When the backoff expires, the packet is transmitted on the channel. A utilization of 100% corresponds to roughly $\lambda = 226.4$ packets. We send 1014 bits per packet.

The parameters of the physical layer are identical to the previous chapter (see Table 8.2).

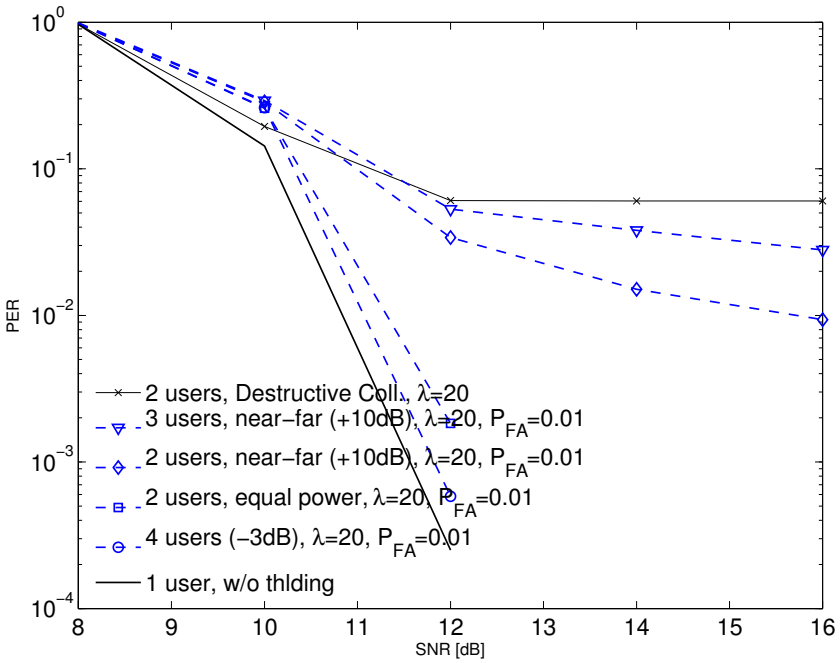

Figure 9.2: PER with MUI in a low traffic case ($\lambda = 20$ packet/s). With equal or lower power interferers, performance is close to single user. Even in a harsh near-far scenario the receiver shows some capture effect when compared to the worst-case "Destructive Collisions" model.

However, the receiver operates at a higher sampling frequency of 500 MHz, i.e. $T = T_c = 2$ ns. The mandatory frequency band 3 is used, where the two possible preamble codes are code 5 and 6 [64]. The transmitter of interest uses code 5 and the others use code 6. We use the IEEE 802.15.4a channel model 1 [22]. We simulate the physical layer with an accuracy of 100 ps (a *simulation* sampling frequency of 10 GHz). In our simulations, the signal to noise ratio (SNR) is $\mathrm{SNR} = \frac{E_p}{N_0}$ where E_p is the received energy *per pulse*, after the convolution of the pulse with the impulse response of the channel.

For comparison purpose, we again use a "Destructive Collisions" model: With this model, a packet is lost whenever there is more than one active transmission at the same time and single user performance is assumed when there is only the transmitter of interest. However, because we do not simulate packet detection and timing acquisition, we do not have a "Perfect Capture" case. Without packet detection and timing acquisition, it is not meaningful any more.

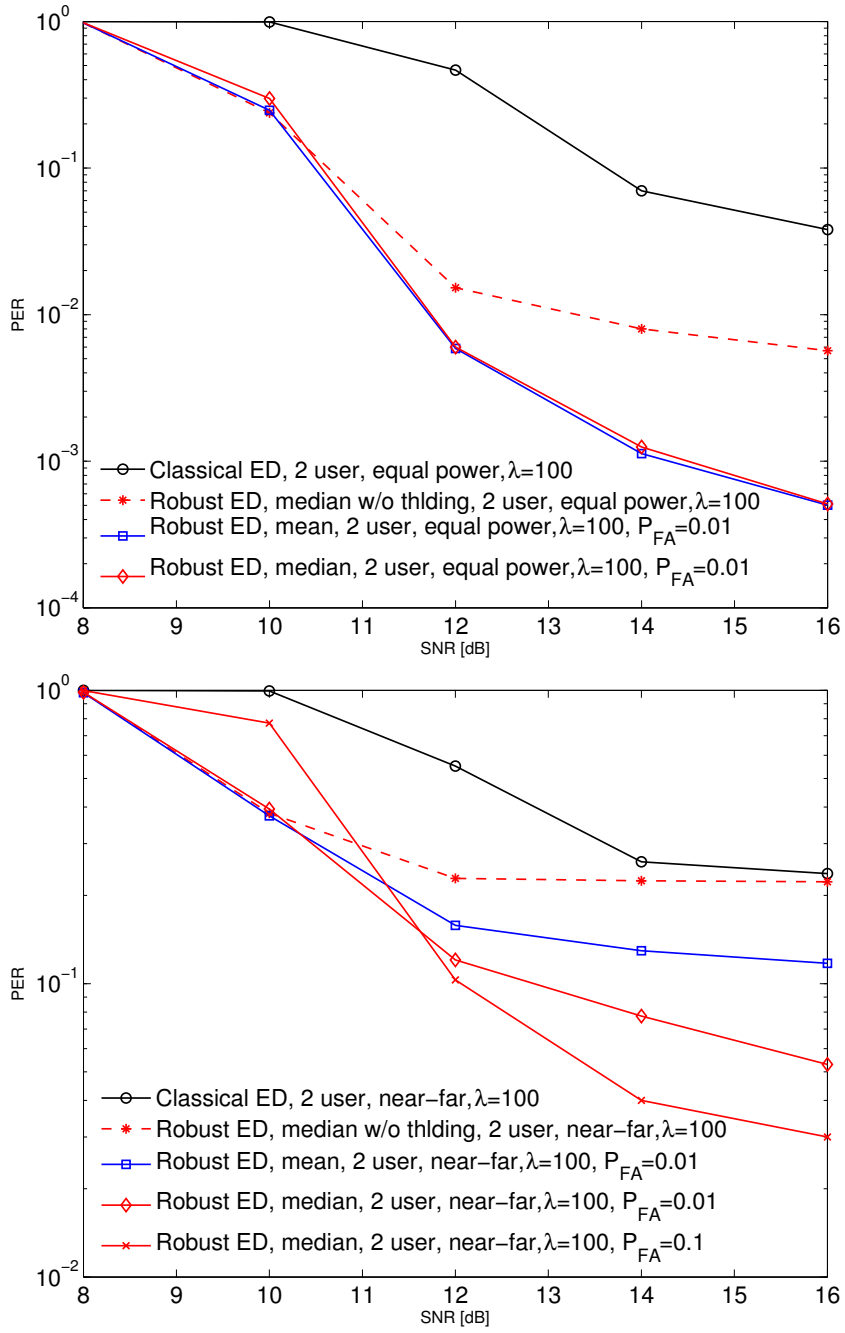

Figure 9.3: Comparison of a classic receiver (performing weighting but no burst adaptation and no thresholding) to our receiver ($\lambda = 100$ packets). On the top we show simulations with one equal power interferer. The performance improvement is roughly two orders of magnitude in PER. On the bottom we show a near-far scenario. In this case the sample mean is not robust to MUI. Also, by using a more aggressive threshold ($P_{FA} = 0.1$), we can push the performance improvement to one order of magnitude in PER. Both figures underline that burst adaptation and thresholding are required.

9.2.2 Performance Evaluation Results

In Figure 9.2, we show the PER obtained with our receiver, using the sample median for power delay profile estimation and the threshold set according to $P_{FA} = 0.01$. We have $\lambda = 20$ packet/s for scenarios with N_u from one to four and various received powers. For both cases with two equal power users and with three additional weaker-power users (at -3 dB), the PER is close to the one of the single user scenario.

In near-far cases, the additional transmitters have a 10 dB higher power: there is still a significant performance increase compared to the worst case "Destructive Collisions" curve. Note that with a conventional receiver where no thresholding is done, the near-far cases correspond to the "Destructive Collisions" curve already at a lower rate of $\lambda = 10$ packets (see Chapter 8).

In Figure 9.3, we consider an equal power (top) and a near-far (bottom) scenario. In both cases, we have first the performance of a classic energy detection receiver without thresholding [37], where the weighting function does not take the bursts into account; second, an energy detection receiver with the weighting function taking the bursts into account but without thresholding; third, our receiver with thresholding, using the sample mean or the sample median. For both scenarios, $\lambda = 100$ packet/s.

Clearly, the sample mean is not robust to interference in near-far cases. Also, both a thresholding mechanism and taking into account the bursts are necessary. Our receiver achieves a performance improvement of up to roughly two orders of magnitude in PER in the equal power case and of one order of magnitude in the near-far case. We observed that this result does not seem to depend on λ; we found it to be the same for $\lambda = 20, 100, 200$ packets.

9.3 Discussion and Conclusion

We have presented a robust energy detection receiver, yielding an excellent performance, even in near-far scenarios. The complexity increase with respect to a classic energy detection receiver is minimal; it is necessary only during the estimation of the power delay profile of the channel. Thanks to the interference mitigation scheme presented in this chapter, we obtain a receiver that allows for taking advantage of all the features of IR-UWB, but at a low complexity: ranging, robustness against multipath propagation, and robustness to MUI that leads to the possibility to allow for parallel transmissions.

Compared to the receiver in the previous chapter, the sampling frequency is higher. This appears to be the price to pay for a proper estimation of the power-delay profile of the channel

when bursts of pulses are sent. There is however a trade-off between the sampling frequency and the hardware complexity as we pointed out in Section 9.1.3. The effect on the performance of the receiver of this trade-off needs to be explored. We also, do not take advantage of the erasures correction capability of the RS code.

But, the more important future work is a robust packet detection and timing acquisition scheme. The work in [63, 144] already suggest potential solutions for robust timing acquisition. We also plan to have the parameter P_{FA} adaptive to the level of interference.

Part III

Simulation of IR-UWB Networks

Chapter 10

An Architecture for the Simulation of IR-UWB Networks in ns-2

The network simulator ns-2 [181] is a popular and widely used discrete-event based simulator for wireless and wired networks[1]. It allows researchers to simulate a wide range of network configurations, supports various protocols at the application layer, and mainly TCP and UDP at the transport layer. Regarding the implementation of wireless physical layers, ns-2 offers an implementation for the IEEE 802.11 protocol. There is also an implementation of the IEEE 802.15.4 protocol, but its support and user base is by far not as large as 802.11.

Developments and research in the fields of wireless communication and networking prompt tools to evaluate and understand the performance of new protocols and new wireless physical layers. Simulation tools such as ns-2 are obviously very important in this aspect. Indeed, when evaluating the performance of wireless protocols on a complex topology (for instance, 802.11 in a multi-hop scenario), simulation is an invaluable and necessary tool.

Unfortunately, with the current implementation of ns-2, it is far from easy to implement new wireless physical layers or to modify the existing 802.11 implementation. There are several reasons, and we discuss them in Section 10.1. But the most important one is probably a large dependence of the codebase of the wireless physical layer of ns-2 on the IEEE 802.11 physical layer.

Our objective for the work presented in this chapter is to be able to simulate the DCC-MAC protocol (presented in Chapter 5) with an IR-UWB physical layer. In addition, with the

[1]The latest release at this time of writing is ns-2.33, see `http://nsnam.isi.edu/nsnam/index.php/Main_Page`. Furthermore, the ns-3 simulator is under active development.

development of the IEEE 802.15.4a amendment, there is clearly a need for the support and availability of an IR-UWB physical layer in a simulator such as ns-2.

Our contributions in this chapter are the following:

- A modified architecture of the wireless physical layer in ns-2: It brings support for multiple sub-channels (see Section 10.1.1); for the computation of bit error rate (BER) and packet error rate (PER); for different modulations (through the addition of a modulation object); a model for cumulative interference, and a model for packet detection and timing acquisition. Our modified architecture of the wireless physical layer allows for an easier integration of other physical layer models in ns-2.

- A particular implementation of an IR-UWB physical layer (see Section 10.1.3) that uses our modified architecture. The physical layer modeled by this implementation assumes a binary phase-shift keying (BPSK) modulation with a variable rate convolutional code. For each received packet, a signal to interference and noise ratio (SINR) is calculated. The BER corresponding to this SINR is then obtained by lookup tables computed offline. These lookup tables need only be computed once for a given combination of modulation, coding, multi-user statistic, and receiver implementation. For simplicity reasons, a Gaussian approximation is currently used for the multi-user interference and for computing the SINR. From the computed BER, the PER is obtained by standard approximation. The PER is used as the parameter of a binary random variable used to decide whether the packet is properly received or not. We also implement a propagation model for UWB channels [21]. All our code is freely and publicly available [207].

As already discussed in Section 3.3.1, it is well known that the Gaussian approximation is not sufficiently accurate. But it is still a viable solution in the short term. It allows for focusing the development and implementation on architectural issues and for debugging. In the long term, a more accurate model for the computation of the BER and PER is necessary. We are currently investigating these issues. For instance, the next chapter presents a possible solution that incorporates a multipath propagation channel, makes no assumption about the power levels at the receiver and accurately takes into account the multi-user interference.

The remainder of this chapter is organized as follows. In Section 10.1.1, we present the design issues of the current wireless physical layer implementation in ns-2. In Section 10.1.2, we present the difference of our implementation with respect to the one in ns-2 and in Section 10.1.3, we focus on the details specific to our IR-UWB implementation. In Section 10.2,

we illustrate the path of a packet trough our physical layer implementation, and we present simulation results in Section 10.3. We conclude this chapter in Section 10.4.

10.1 Adapting ns-2 for the Simulation of IR-UWB Physical Layers

10.1.1 Implementation Issues in the Wireless Physical Layer of ns-2

We describe and discuss what we believe are the current design issues and features missing in the current implementation of the ns-2 wireless physical layer.

Dependence on the 802.11 PHY and MAC

Today, there is a strong interdependence between the wireless physical layer implementation and the MAC layer implementation of 802.11 in ns-2. It is very hard to actually extend the current wireless physical layer implementation without changing parts of the 802.11 implementation: for instance, when a packet starts to be received, it is directly delivered to the MAC layer. Packet reception actually occurs in the MAC layer rather than in the physical layer.

Furthermore, there are also various dependencies on the rest of the codebase in ns-2. Consequently, adding a new wireless physical layer requires many non-trivial changes in several sections of the code.

Lack of Multiple Sub-Channels

All modern physical layers offer the possibility of sharing their available spectrum into several sub-channels. Sub-channels can appear in different ways, for instance:

- By having multiple transmission frequencies. A typical example is 802.11b where there are fourteen available transmission frequencies.
- With spread-spectrum physical layers, sub-channels appear naturally. Using either *direct-sequence* modulation as in direct-sequence CDMA (DS-CDMA), *frequency hopping* as in frequency-hopping CDMA (FH-CDMA) or *time-hopping* as with IR-UWB physical layers with time-hopping. A hybrid combination of these techniques is also possible. The reader is referred to [62] for an excellent explanation and details about direct-sequence and frequency hopping.

Unfortunately, there is no support currently in ns-2 for such a feature: it is not possible to simulate a scenario of 802.11b stations in the infrastructure mode with several access points using different frequencies or an IR-UWB network.

Simplistic Model of Packet Detection and Timing Acquisition

Packet detection models the detection of a packet on the wireless channel. With ns-2, this is performed using a simple threshold for the received signal strength. For example, with IR-UWB physical layers, this operation necessitates active decoding of the received signal. It is typically much more error-prone than packet detection in narrow-band radios.

Packet detection schemes are traditionally characterized by parameters such as probability of missed detection (the probability that a receiver misses a packet) and probability of false alarm (the probability that a receiver believes it has detected a packet when there is actually no transmission).

After having detected that there is a packet on the channel, timing acquisition consists in detecting exactly when the payload of the packet begins. This is important for a proper demodulation and decoding of the payload. Any mistiming will lead to a degraded performance of the demodulation and decoding of the payload.

Absence of Error Model

The current model for packet reception in ns-2 assumes that a packet is properly received if the received power is higher than a given threshold and no single interferer is strong enough to cause a collision. No bit errors can occur during the packet transmission. Furthermore, the model does not take into account variations of the received signal power or of the multi-user interference power.

No Model of Cumulative Interference

The current model for packet reception does also not take into account the effect of interference from concurrent transmissions in the network. It only considers the received power from the source of the packet. The only exception is the implementation of a capture effect for 802.11. Obviously, if there are many ongoing transmissions from other stations in the network, the probability that the packet is correctly received should be lower than if there is no interference.

10.1.2 Key Features of our Modified Wireless Physical Layer Architecture

In this section, we describe the key features of our modified physical layer architecture for ns-2. We make a few important assumptions: (1) the physical layer cannot transmit and receive a packet at the same time; (2) it can receive only one packet at a time (no multi-user reception); (3) it can listen on more than one sub-channel.

Complete Packet Reception at the Physical Layer

Before being passed to the MAC layer, the packet is first completely received at the physical layer. At the end of the reception of the packet, the PER is calculated. Only then is the packet delivered to the upper layer.

Multiple Transmission Sub-Channels

It is possible to specify a particular transmission sub-channel for each packet to be transmitted. Conversely, the physical layer can listen on more than one sub-channel. Typically, the physical layer would listen to a broadcast sub-channel and a receive sub-channel.

In our case, we have implemented support for multiple sub-channels by adding a specific header to each packet. This header contains the index of the sub-channel used for transmitting the packet. The field of the header corresponding to the particular transmission sub-channel is set at the physical layer before the packet is passed to the wireless channel in order to be distributed to the stations in the network. When the reception of a packet begins, the physical layer can read the field corresponding to the sub-channel to check whether it corresponds to the one the physical layer is currently listening to.

The number of sub-channels and their relative orthogonality (i.e. whether there is interference between transmissions on different sub-channels) depends on the particular implementation.

Packet Detection and Timing Acquisition

In order to add support for packet detection and timing acquisition, we implemented an additional SYNC state to the physical layer. Hence the states of the physical layer are

- IDLE: the physical layer listens to the medium.
- SYNC: the physical layer believes it has detected a packet on the wireless medium and attempts to synchronize with the beginning of this packet.

- RECV: the physical layer receives the packet. It assumes that the physical layer has correctly detected that there is packet and is synchronized with its beginning.
- SEND: the physical layer transmits a packet.

Furthermore, there is a detection and acquisition preamble assumed for each transmitted packet. The length of this preamble is t_{pr} seconds. When the physical layer begins to receive a packet and it is in the IDLE state, it enters the SYNC state. The physical layer then sets the `end_of_timing_acquisition` timer to expire t_{pr} seconds later and adds the packet to the *synchronization list*: this list keeps track of all the candidate packets for detection and acquisition while the physical layer is in the SYNC state. If the packet is not transmitted on a sub-channel that the receiver is currently listening to, the packet can still be added to the synchronization list, but with a very small probability.

If the physical layer is not in the IDLE state but already in the SYNC state, it does not prevent a packet from being potentially received. Instead, it directly adds this packet to the synchronization list.

Finally, when the `end_of_timing_acquisition` timer expires, one particular packet is selected from the synchronization list. How this packet is selected depends on the particular implementation. The remaining packets are not received but considered as interference: they are added to the *interference list* (see Section 10.1.2).

Cumulative Interference

Cumulative interference is considered for the whole duration of the transmission of the packet (minus the duration of the acquisition preamble). The cumulative interference is the sum of the interferences created by the simultaneous transmissions of packets from other stations in the network. Note that these interfering transmissions might occur on the same channel as the one used for the reception of the packet, or on another channel.

In order to implement this feature, we use an interference list at the physical layer in order to keep track of interfering transmissions. The following information about interfering packets is put in the interference list:

- The time corresponding to the beginning of the transmission of the interfering packet.
- The time corresponding to the end of the transmission of the interfering packet.
- The power at which the interfering packet is received.

- The sub-channel on which the interfering packet is transmitted.

Then, whenever a packet is completely received by the physical layer, the cumulative interference during the transmission of this packet is calculated for use in the error model using the information in the interference list (see Section 10.1.2).

Implementation of an Error Model

At the end of the reception of packet, the following three steps are performed:

1 The cumulative interference during the transmission of the packet is calculated.

2 The cumulative interference is used to compute the average SINR during the transmission of the packet.

3 The average SINR is used to compute the PER of the packet. The PER is then used as the parameter of a binary random variable used to decide whether the packet is properly received or not.

How the PER is calculated depends on the particular physical layer implemented.

Flexibility when Computing the Channel and Packet Statistics

Our architecture is designed in a way that easily allows for the replacement of a particular physical layer implementation. The general architecture can be kept, but the following items must be modified: packet detection and timing acquisition, the calculation of the cumulative interference, the modelling of interference from other sub-channels, and the calculation of the PER.

10.1.3 An IR-UWB Physical Layer for ns-2

In this section, we detail the implementation-specific aspects of the previous section in the case of an IR-UWB physical layer.

Physical Layer Characteristics, Modulation and Channel Coding

Our physical layer implementation currently models an IR-UWB radio with time-hopping (see Section 2.2.1) and a variable rate channel code (see Section 2.2.7). With IR-UWB, a sub-channel corresponds to the time-hopping sequence used by a transmitter.

The modulation is binary phase-shift keying (BPSK). The channel codes are the RCPC codes presented in Section 2.2.7.

Packet Detection and Timing Acquisition Model for IR-UWB

As explained in the introduction, packet detection and timing acquisition in IR-UWB networks is more challenging than in narrow-band networks. However, it has interesting properties; if several packets are sent from different sources to the same destination at roughly the same time, all the packets sent with a time-hopping sequence that the receiver is listening to will trigger packet detection and timing acquisition at the receiver concurrently. In this case, with a very high probability, one packet will be acquired [63].

We assume that the packet detection and timing acquisition mechanism is the one described in [63]. In the following, we explain how a particular packet is selected from the synchronization list and how packets are inserted in the synchronization list depending on the sub-channel (i.e. time-hopping sequence for IR-UWB) the packet was transmitted on.

At the end of the timing acquisition phase, a packet needs to be selected from the synchronization list. In our case, the packet in the list is chosen randomly with a uniform distribution. This packet is further received by the physical layer with a probability $1 - P_{\text{MD}}$, where P_{MD} is the probability of missed detection. The value of P_{MD} depends on the current level of interference, i.e. on the number of packets sent with a time-hopping sequence other than the ones the receiver is listening to.

How packets are inserted into the list depends on the sub-channels the potential receiver is currently listening to. We add to the synchronization list all the packets that are sent on the same sub-channels that the receiver is currently listening to. For packets sent on the sub-channels that the receiver is not listening to, we add them to the list with a probability Θ that depends on the particular algorithm used for packet detection and timing acquisition (see Chapter 6).

Cumulative Interference and SINR

For a given packet being received from station i and concurrent transmissions of packets from stations $k \neq i$, the following factors are taken into account when computing the cumulative interference:

- The received power $P_{rx}^{(k)}$ from the kth station.
- The time $T_{overlap}^{(k)}$ during which the transmission of the packet from station i overlaps with the transmission of the packet from station k.

- A parameter Γ that takes into account the average orthogonality with respect to the transmissions using different time-hopping sequences and a parameter γ that takes into account the orthogonality between transmissions using the same time-hopping sequence. The parameters Γ and γ are computed following the expressions in [113, Equ. 12].

Hence, the cumulative interference I_c is

$$I_c = \Gamma \sum_{k \neq i} T_{overlap}^{(k)} P_{rx}^{(k)} + \gamma \sum_{l \neq i} T_{overlap}^{(l)} P_{rx}^{(l)} \tag{10.1}$$

Then, the SINR is

$$\frac{P_{rx}^{(i)}}{I_c + N_{th}} \tag{10.2}$$

where $P_{rx}^{(i)}$ is the received power from the station i, and N_{th} is the thermal noise.

Packet Error Rate Calculation

In its current implementation, the PER is calculated as follows: For a given SINR and a given channel code rate, a BER value is obtained using a lookup table and linear interpolation. The PER is then calculated as $PER = 1 - (1 - BER)^L$ where L is the length of the payload. The lookup tables were computed offline with extensive Matlab simulations. There is one lookup table for each possible rate of the RCPC codes. Note that these lookup tables need only be computed once for a given combination of modulation, coding, multi-user statistic and receiver implementation.

10.2 End-to-End Path of a Packet Through the MAC and the Physical Layer

This section describes the path of a packet through our physical layer implementation. We begin this journey of a packet at the MAC layer:

- The MAC layer has a packet ready to be sent to the physical layer. The MAC layer checks whether the physical layer is idle or not. If it is idle, the MAC layer sends the packet to the physical layer.

- The physical layer receives the packet from the MAC layer. First, if the physical layer is not idle, the packet is dropped. Else, the state of the PHY layer is set to SEND. A

timer set to expire at the end of the packet transmission sets the PHY layer state back to IDLE. Then, the physical layer sets the transmission rate (i.e. the proper modulation and coding), computes the transmission time and sets the particular time-hopping sequence. It adds the preamble for packet detection and timing acquisition. We could also set the transmission power if necessary. But in the particular case of the DCC-MAC protocol, we always send at maximum power and hence it is not implemented.

- The physical layer places the packet on the channel. The channel delivers the packet to the physical layer of other nodes.

As many nodes might receive the packet, the following steps might be executed by several of them.

- First, the power of the packet received from the channel is computed. The computation is based on the propagation model in [21]. Then, a set of tests are applied on the packet to check the following conditions:
  - If the physical layer is not busy transmitting (SEND state) or receiving a packet (RECV state).
  - If the receiver is listening to with the same time-hopping sequence as the time-hopping sequence used for transmitting this packet.

  If any of these tests fail, then the packet is an interfering packet and is put in the interference list. If, on the contrary, the packet satisfies these tests, then the packet detection and timing acquisition phase can start. Remember that if the physical layer is in the SYNC state, this does not prevent the packet from being received. The packet is added to the synchronization list.

- The physical layer of the receiving node performs packet detection. In its current form, the implementation consists in testing whether the received power of the packet is sufficiently high to trigger the packet detection and timing acquisition part. If so, then the packet detection is considered successful. The state of the physical layer is set to SYNC.

- The physical layer performs timing acquisition. This consists in adding the packet to the synchronization list. The first packet that triggers the SYNC state also starts the timer scheduled to expire after t_{pr} seconds. When the timer expires, there will be at most one packet from the synchronization list for which the timing acquisition is successful. The

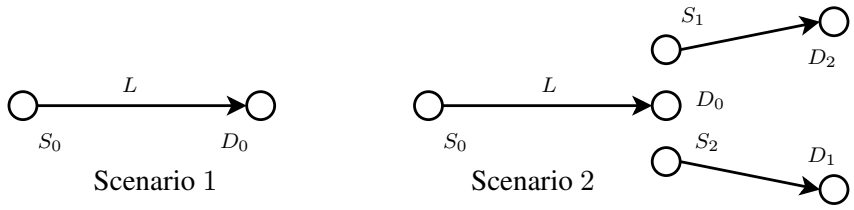

Figure 10.1: Scenarios used for the simulations. Scenario 1: a single source destination pair S_0 to D_0. Scenario 2: the same source-destination pair S_0 to D_0 but with two interfering sources S_1 and S_2 located at one meter from D_0. S_1 and S_2 transmit to D_1 and D_2 respectively which are ten meters away. Scenario 2 is a near-far scenario.

receiver will have "locked" itself on this particular received packet and can proceed with the decoding of this packet. All the other packets from the synchronization list are added to the interference list and the synchronization list is emptied. The state of the PHY layer is set to RECV.

- The physical layer decodes the header and payload of the packet.
- When the packet reception is over, the PER is computed as explained in Section 10.1.3. Finally, the PER is used to decide whether the packet is properly received or not and whether the physical layer delivers the packet to the MAC layer.

In the next section, we present several simulation results that show some of the features of our implementation.

10.3 Simulations Examples

10.3.1 Performance Metric and Simulation Parameters

Our performance metric is the saturation throughput; this throughput is computed with sources having always a packet available to transmit and queuing at the sources ignored. Each simulation was run ten times for a duration of 300 seconds. We calculated the 95% confidence intervals for the median for each set of runs.

The parameters of our physical layer implementation correspond to a typical 802.15.4a physical layer with a bitrate of 1 Mbit/s. For the channel code, we use three different rates; code rate $\frac{8}{11}$, $\frac{1}{2}$ and $\frac{1}{3}$ corresponding to code index 2, 7 and 15 in Section 2.2.7. For packet detection and timing acquisition, values for P_{MD} and Θ (see Section 10.1.3) are derived from [63] according to Chapter 6. The MAC layer protocol used is DCC-MAC. The transport protocol is

UDP and the UDP agent in ns-2 is used with a maximum segment size of 1000 bytes. A constant bit rate (CBR) traffic generator with a packet size of 1000 bytes and random inter-packet departure is attached to the UDP agent. The propagation model used is [21] in the line-of-sight case without the random component. Hence, path loss is a deterministic function of the distance. Because IR-UWB networks have a very low transmission power, the transmission range is of the order of a few tens of meters.

We use two scenarios (see Figure 10.1). The first is a single source-destination pair where we vary the link distance L. The second scenario is again a source-destination pair with a variable link distance L, but with two sources located one meter away from the receiver and transmitting to their respective destination ten meters away. This is a typical near-far scenario. Note that in both cases, we only look at the performance of the link S_0 to D_0. With the DCC-MAC protocol, sources transmitting to a given destination use the time-hopping sequence specific to the destination (see Section 5.2.2). Hence with the second scenario, S_0 and S_1 do not use the same time-hopping sequence. There are concurrent transmissions occurring on different sub-channels.

10.3.2 Simulation Results

In Figure 10.2, we use the first scenario to illustrate the effect of the error model. We look at the saturation throughput as a function of the link distance for three different channel code rates. As the link distance increases, the received power and SINR at the destination decrease. This gradually increases the average PER, which leads to the smooth degradation of throughput.

In Figures 10.3(a) and 10.3(b), we use the second scenario to illustrate the effect of cumulative interference. We look again at the saturation throughput of the original source-destination link S_0 to D_0 of the first scenario, but this time, there is interference created by the two other sources. As can be clearly seen, the cumulative interference induces a net throughput reduction. Indeed, for a given link distance, the cumulative interference reduces the SINR and consequently the PER is higher as seen in Figure 10.3(b).

Finally, in Figure 10.4, we again use the second scenario, but this time to observe the impact of the packet detection and timing acquisition model. We compare the throughput of the link S_0 to D_0 versus the link distance for two cases. One where sources use the time-hopping sequence of the destination (private time-hopping sequences) and one where all sources are forced to use the same unique time-hopping sequence. In other words, one where there are sub-channels and one where all nodes share the same sub-channel. In the case of the single time-hopping

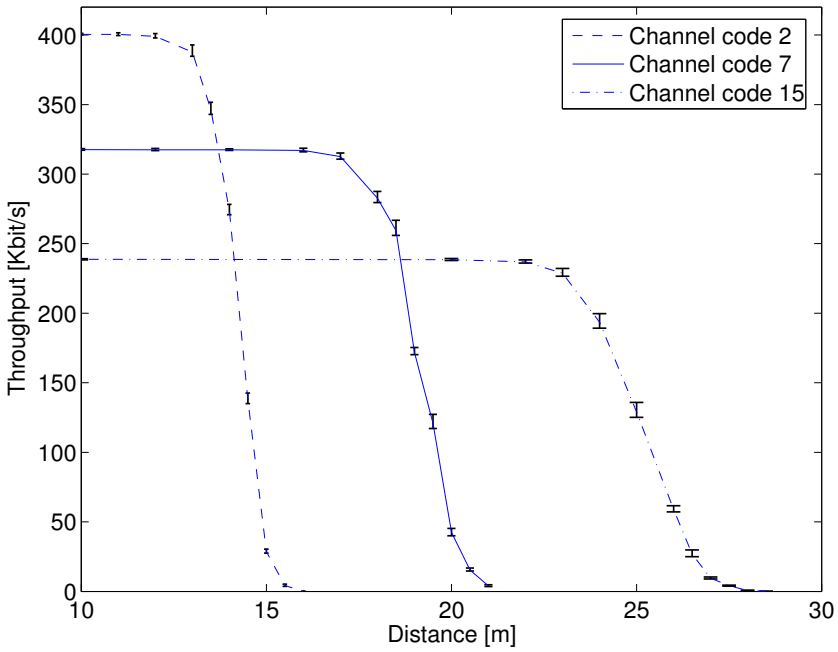

Figure 10.2: Saturation throughput of the link S_0 to D_0 versus the link distance L for three different channel code rates. The topology is scenario 1. Due to the error model, the throughput smoothly decreases with the distance.

sequence, the destination of the link of interest acquires many packets from the interferers, which greatly reduces the throughput. The slightly better throughput obtained for link distance 13.5 to 14.5 is explained from the fact that with a single time-hopping sequence, the interfering sources also receive packets from the source and are prevented from sending. As such, there are a few packets that are transmitted with less interference than in the case where sources use the time-hopping sequence of the destination. By using a code with a slightly lower rate but a better protection against interference, this difference disappears.

More complicated scenarios, such as a line of nodes with UDP or TCP, or random topologies, can be found in Chapters 5 and 6.

10.4 Discussion and Conclusion

We have presented an architecture for wireless simulation in a packet based network simulator. We have used this architecture to implement an IR-UWB physical layer in ns-2. Our architecture attempts to allow for the proper modeling of the characteristics of modern physical layers: cumulative interference and the calculation of a packet error rate, packet detection and timing acquisition, and the possibility of having multiple sub-channels.

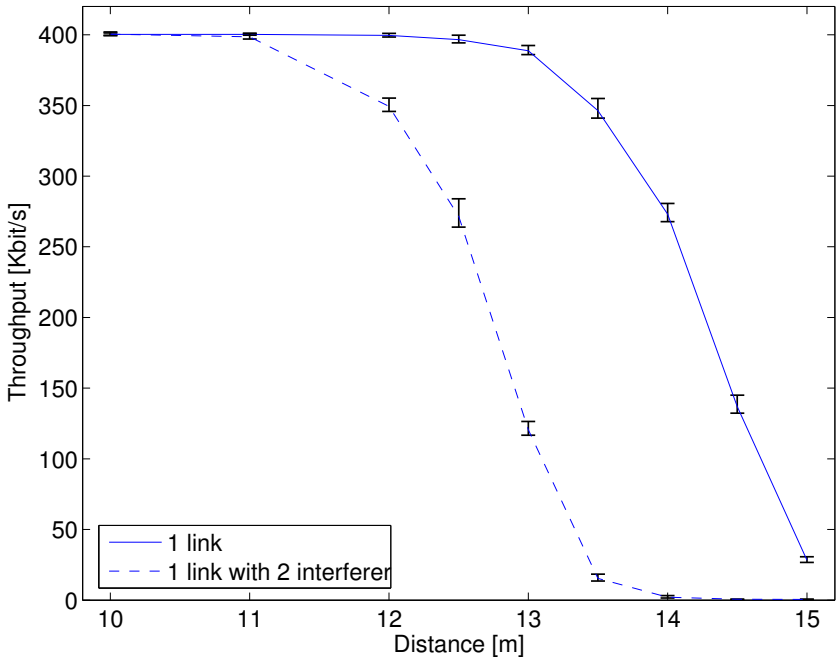

(a) Saturation throughput versus link distance with channel code rate $\frac{8}{11}$.

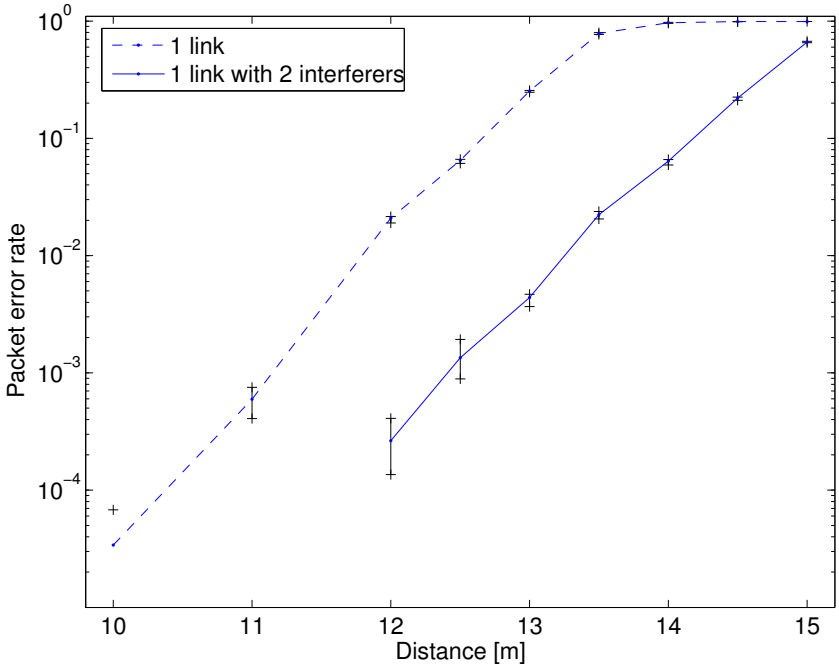

(b) Packet error rate versus link distance with channel code rate $\frac{8}{11}$.

Figure 10.3: Saturation throughput and packet error rate of the link S_0 to D_0 versus the link distance L with channel code rate $\frac{8}{11}$. We compare scenario 1 (plain curve) with scenario 2 (dashed curve). Cumulative interference clearly degrades the throughput and increases the PER.

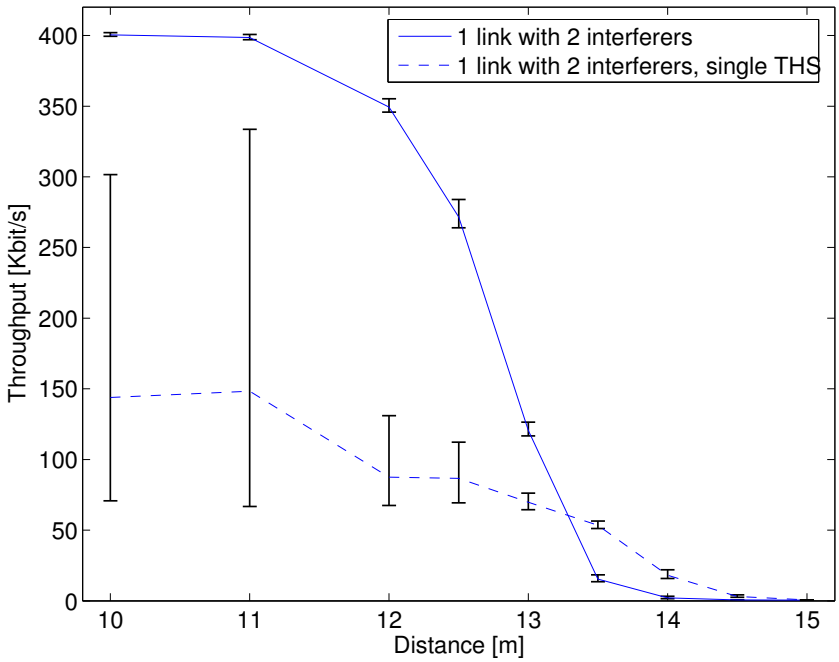

Figure 10.4: Saturation throughput of the link S_0 to D_0 versus the link distance L with channel code rate $\frac{8}{11}$. The topology is scenario 2. Using a single time-hopping sequence (dashed curve) in the network decreases the throughput compared to private time-hopping sequences (plain curve). Indeed, in this case, the nodes can acquire packets not sent to them.

Future work should integrate a better BER and PER calculation model for IR-UWB. An important effort is also necessary to validate physical layer models with actual hardware. With the emergence of the IEEE 802.15.4a standard, we can adapt our model to this standard, and further refine and validate our implementation.

The calculation of the PER, the effect of cumulative interference, and the packet detection and timing acquisition phase are elements that need further enhancement and validation. The work on the testbed in Chapter 7 goes in this direction.

Chapter 11

Bit Error Rate of an IR-UWB Channel with Multi-User Interference for a Network Simulator

The development of new MAC or routing protocols for IR-UWB networks requires extensive and large-scale simulations with packet-level simulators such as ns-2 or Qualnet. As explained in the previous chapter, it is necessary to compute a packet error rate (PER) to declare if a packet is properly received. This PER depends on several factors: the current level of interference and background noise; the propagation channel between the transmitters and the receiver; and physical layer parameters such as the coding and modulation schemes that are used. Of course, obtaining proper simulation results is not only dependent on an accurate computation of the PER, but it is one of the essential components.

In this chapter, we assume that the computation of the PER is based on the computation of the bit error rate (BER). The PER can then be derived from it, either exactly or, by using upper and lower bounds [219].

For each packet, the BER can be obtained by a pulse-level simulation, directly in the physical layer of the network simulator. But, physical layer events take place on a sub-nanosecond timescale, and higher layer events such as packet reception and forwarding occur on a timescale of milliseconds. This creates an extremely large number of events, and the complexity of directly deriving the BER from a pulse-level simulation of the IR-UWB physical layer becomes prohibitive. Hence, instead of a direct physical layer simulation, the BER can be computed: our problem is now to find a fast and accurate algorithm for computing the BER of an IR-UWB

link in the presence of noise and MUI.

It is tempting to make the Gaussian assumption, which consists in approximating the interference stemming from concurrent transmitters as a Gaussian random variable. With this assumption, a closed-form analytical expression for the BER of an IR-UWB network can be obtained [113]. However, we discussed in Section 3.3.1 that the Gaussian assumption is not valid in many scenarios, especially when the data-rate is low or in the absence of power control.

We discussed existing work on the computation of the BER assuming a non-Gaussian model for the interference in Section 3.3.2. In particular, methods based on using a characteristic function approach are promising, for instance [51]. But, in our case, there is a major difference in the underlying model of the physical layer that we consider. The existing work computes the *average* BER over many channels and transmitter-receiver delay realizations. In the case of packet-level network simulations, we are interested in computing a *conditional* BER, given some realizations of the channels from sources/interferers to a destination and of delay differences. The reason is that, for each packet, there is a different set of channels and of interferers and consequently a different BER. In fact, most network simulators assume a block fading channel model: During the transmission of a block of bits, all channels and delays between concurrent transmitters and the receiver are fixed. Indeed, the coherence time of a UWB channel can be as large as 200 milliseconds. Also, most of the related work presented in Section 3.3.2 assumes AWGN channels and, except [51], makes the assumption of perfect power control.

Our contribution in this chapter is an algorithm to compute the conditional BER of an IR-UWB link given some realizations of the channels from sources/interferers to destination and of delay differences. Our solution is based on a novel combination of large deviation [220, 221] and importance sampling [222]. It is explained in Section 11.1. Our results can be used with any method for drawing the different channel realizations; in Section 11.2, we evaluate our method on numerical cases where we draw the different channels from source and interferers to a specific destination independently and according to an IEEE 802.15.4a multipath channel model. We assume that the power levels can be completely heterogeneous. Our algorithm is appropriate to be included in a packet-level simulator. We conclude this chapter in Section 11.3.

11.1 A Fast and Efficient Method to Compute the BER

In this section, we develop a fast method to sample the BER of an IR-UWB link in the presence of concurrent transmitters in a multipath channel environment.

11.1.1 Modeling Assumptions

We assume that the receiver is a Rake performing MRC with BPSK modulation. As shown in Section 2.2.3, in equation (2.12), the received signal at the output of the Rake receiver can be written as

$$Y[i] = Y_0[i] + \sum_{u=1}^{U-1} Y_u[i] + N[i] \tag{11.1}$$

where $Y_0[i]$ is given by equation (2.13) and $Y_u[i]$ by equation (2.14) and $N[i] \sim \mathcal{N}(0, \sigma_N^2)$ is the filtered white noise with $\sigma_N^2 = \frac{N_0}{2}$.

In addition, we assume that N_g is sufficiently large to avoid any inter-symbol interference (ISI). This assumption is not strictly necessary, but will simply ease the calculation in the following. We also assume that the receiver is perfectly synchronized with the user of interest i.e. $\hat{\nu}^{(0)} = 0$.

11.1.2 Expression for the BER

We assume that decoding is bit by bit. Given that the source transmitted 1 (respectively -1), a decoding error occurs when $\gamma + \sum_{u=1}^{U-1} Y_u[i] + N[i] < 0$ (respectively $-\gamma + \sum_{u=1}^{U-1} Y_u[i] + N[i] > 0$) where $\gamma = Y_0[i]$. By symmetry, both have the same probability, thus we can write

$$\mathcal{P}_{e|\vec{\nu},\vec{g}} = \mathbb{P}\left(N[i] + Y_1[i] + \ldots + Y_{U-1}[i] > \gamma | \vec{\nu}, \vec{g}\right) \tag{11.2}$$

We want to compute the conditional bit error probability $\mathcal{P}_{e|\vec{\nu},\vec{g}}$, given that the vector of channel impulse responses is $\vec{g} = \left[g^{(0)}, g^{(1)}, \ldots, g^{(U-1)}\right]$ and that the vector of delays is $\vec{\nu} = \left[\nu^{(0)}, \nu^{(1)}, \ldots, \nu^{(U-1)}\right]$. As we condition on channel realizations and delays, the only remaining randomness is in the sequence of the transmitted bits and the time-hopping sequences of every user. Note that $\mathcal{P}_{e|\vec{\nu},\vec{h}}$ is different from the usual bit error probability, which can be expressed as $\mathbb{E}\left[\mathcal{P}_{e|\vec{\Upsilon},\vec{\mathcal{G}}}\right]$ where $\vec{\Upsilon}$ and $\vec{\mathcal{G}}$ are random.

As mentioned earlier, we cannot simply assume that the sum of interference $\sum_{u=1}^{U-1} Y_u[i]$ is Gaussian; also, we have to assume that interferers have different channels. Furthermore, the inspection of equation (2.14) in Section 2.2.3 reveals that all $Y_u[i]$, $u = 1, \ldots, U-1$ depend on $c_i^{(o)}$. Therefore, the $Y_u[i]$ for $u = 1, \ldots, U-1$ do not have the same distribution and are not independent.

11.1.3 Distribution of the Interference Y_u

We already consider the conditional distribution of Y_u given $\vec{\nu}$ and $\vec{g}$. By further conditioning on the value of the time-hopping sequence of the user of interest $c_i^{(0)}$, it turns out that the $Y_u[i]$ in $\sum_{u=1}^{U-1} Y_u[i]$ become independent. It is then a bit messy, but relatively easy to compute the conditional distribution of $Y_u[i]$ given $c_i^{(0)}$. If $c_i^{(0)}$ is fixed, then $Y_u[i]$ depends only on $c_i^{(u)}$ *and* $c_{i-1}^{(u)}$. The probability that a particular chip is chosen in a frame is $q = \frac{1}{N_c - N_g}$. Because the time-hopping sequences are independently and identically distributed, a sample $\left(c_i^{(u)}, c_{i-1}^{(u)}\right)$ has probability

$$q^2 = \left(\frac{1}{N_c - N_g}\right)^2.$$

Consequently, each interference sample has probability q^2. But, thanks to time-hopping, many samples have a zero value. In addition, the assumption that there is no ISI has the following implication: a non-zero value of $Y_u[i]$ stems from an overlap between the signal of user 0 and the signal of user 1 in the ith frame *or* the $(i-1)$th frame, but not both. For instance, let us say that $Y_u[i]$ has a non-zero value for a given $c_{i-1}^{(u)}$. This value will be the same for all occurrences of $c_i^{(u)}$ and simply has probability $\left(\frac{1}{N_c - N_g}\right)^2 \cdot (N_c - N_g) = q$.

Hence, the conditional distribution of $Y_u[i]$ given $\vec{\nu}$, $\vec{g}$, and $c_i^{(0)}$ has a discrete support. It can be represented by a set of $2n+1$ values: 0 and $2n$ non-zero values that essentially depend on the delays spread of the channel impulse responses of user 0 and user u. The factor two occurs from the BPSK modulation: an interference sample has a positive or negative value. For the probabilities, we have

$$\begin{aligned}
\mathbb{P}\left(Y_u[i] = 0 \mid c_i^{(0)}\right) &= 1 - nq \\
\mathbb{P}\left(Y_u[i] = +x_{u,k|c_i^{(0)}} \mid c_i^{(0)}\right) &= \frac{q}{2}, \qquad \text{if } d_i^{(u)} = 1 \text{ or } d_{i-1}^{(u)} = 1 \\
\mathbb{P}\left(Y_u[i] = -x_{u,k|c_i^{(0)}} \mid c_i^{(0)}\right) &= \frac{q}{2}, \qquad \text{if } d_i^{(u)} = -1 \text{ or } d_{i-1}^{(u)} = -1
\end{aligned}$$

for $k = 0, 1, \ldots, n-1$ where we abuse the $\mid$ notation in $x_{u,k|c_i^{(0)}}$ to stress that the values depend on a particular $c_i^{(0)}$. These values are obtained by computing the non-zero values of

$$d_{i-1}^{(u)} \sum_{l=0}^{L^{(0)}-1} \hat{\alpha}_l^{(0)} \sum_{l=0}^{L^{(u)}-1} \alpha_l^{(u)} \, \Theta\left(T_f + \left(c_i^{(0)} - c_{i-1}^{(u)}\right) T_c + \hat{\tau}_l^{(0)} - \tau_l^{(u)} - \nu^{(u)}\right)$$

if $c_i^{(0)} < \nu^{(u)}$ or

$$d_i^{(u)} \sum_{l=0}^{L^{(0)}-1} \hat{\alpha}_l^{(0)} \sum_{l=0}^{L^{(u)}-1} \alpha_l^{(u)} \, \Theta\left(\left(c_i^{(0)} - c_i^{(u)}\right) T_c + \hat{\tau}_l^{(0)} - \tau_l^{(u)} - \nu^{(u)}\right)$$

otherwise, for a given $c_i^{(0)}$, $\vec{\nu}$, and $\vec{g}$ in equation (2.14). For the remainder of this chapter, we will drop the index i. Hence, equation (11.3) becomes

$$\mathcal{P}_{e|\vec{\nu},\vec{g}} = \mathbb{P}\left(N + Y_1 + \ldots + Y_{U-1} > \gamma \mid \vec{\nu}, \vec{g}\right) \tag{11.3}$$

where $\gamma = Y_0$.

Because the distribution of Y_u has a discrete support, we can use a brute force (enumeration) approach in order to evaluate (11.3). This would work as follows. Let $\varphi_j(x)$ be the right-hand side of (11.3), as a function of x and $j = U$. We have $\varphi_j(x) = \mathbb{E}(\varphi_{j-1}(x - Y_j))$ and $\varphi_1(x) = \frac{1}{2}\mathrm{erfc}(\frac{x}{\sqrt{2}\sigma_N})$, which can be used recursively to compute $\mathcal{P}_{e|\vec{\nu},\vec{g}} = \varphi_U(x)$. The number of evaluations of $\varphi_U(x)$ is n^U, which for even small values of U is very large (for example with $n = 50$ and $U = 5$ we have $3 \cdot 10^8$ evaluations). An alternative could be to use the fast Fourier transform, but the supports of all Y_u are all different, so one would first need to find a regular grid that approximates well the union of all the supports of the Y_u. We use another approach, that is easier to implement in an automatic way (as is required by our desire to implement our computations in a packet level simulator).

Our method is a combination of large deviation and importance sampling. We first present each of these two ingredients separately, and then describe our combination.

11.1.4 Computing the BER Using Large Deviation

We expect this to work well when interference is significant due to a large number of small interferers (remember that even in this case the Gaussian approximation is not valid).

We begin with a few necessary definitions. The cumulant generating function (CGF) of a random variable $\mathcal{X}$ is defined by

$$\Lambda(a) = \ln \mathbb{E}\left(e^{a\mathcal{X}}\right).$$

The *rate function* is

$$\Lambda^*(x) = \sup_{a \in \mathbb{R}^+} \left(ax - \Lambda(x)\right),$$

which can be computed by

$$\Lambda^*(x) = a^* x - \Lambda(a^*), \tag{11.4}$$

where a^* is the unique a that satisfies $\frac{d}{da}\left(ax - \Lambda(a)\right) = 0$ [221].

Definition 4 (Twisted distribution and twisted expectation)**.** *For a fixed random variable $\mathcal{X}$, we define a new family of probabilities indexed by a by*

$$\mathbb{P}_a\left(\mathcal{A}\right) = K\mathbb{P}\left(e^{a\mathcal{X}} 1_{\mathcal{A}}\right) \tag{11.5}$$

for all event $\mathcal{A}$. Similarly,

$$\mathbb{E}_a\left(\mathcal{Y}\right) = K\mathbb{E}\left(e^{a\mathcal{X}}\mathcal{Y}\right) \tag{11.6}$$

for any random variable $\mathcal{Y}$. The normalizing constant K is equal to $e^{-\Lambda(a)} = \frac{1}{\mathbb{E}(e^{a\mathcal{X}})}$.

Note that (11.5) and (11.6) are valid for any a.

Lemma 2. *For a random variable $\mathcal{X}$*

$$\mathbb{P}\left(\mathcal{X} > x\right) = e^{\Lambda(a^*)}\mathbb{E}_{a^*}\left(1_{\{\mathcal{X}>x\}} e^{-a^*\mathcal{X}}\right) \tag{11.7}$$

or equivalently

$$\mathbb{P}\left(\mathcal{X} > x\right) = e^{-\Lambda^*(x)}\mathbb{E}_{a^*}\left(1_{\{\mathcal{X}>x\}} e^{-a^*(\mathcal{X}-x)}\right) \tag{11.8}$$

Proof. See [221] □

The previous Lemma can be used to compute $\mathcal{P}_{e|\vec{\phi},\vec{h}}$. Let us define the random variable

$$\mathcal{I} = \sum_{u=1}^{U-1} Y_u + N \tag{11.9}$$

Then, applying (11.8) to $\mathcal{I}$ and (11.3) yields

$$\mathbb{P}\left(\mathcal{I} > \gamma\right) = e^{-\Lambda_{\mathcal{I}}^*(x)}\mathbb{E}_{a^*}\left(1_{\{\mathcal{I}\geq\gamma\}} e^{-a^*(\mathcal{I}-\gamma)}\right) \tag{11.10}$$

where $\Lambda_{\mathcal{I}}^*(x)$ is the rate function of $\mathcal{I}$, $1_{\{\cdot\}}$ is the indicator function, and $\mathbb{E}_{a^*}\left(1_{\{\mathcal{I}\geq\gamma\}} e^{-a^*(\mathcal{I}-\gamma)}\right)$ is the expectation of $1_{\{\mathcal{I}\geq\gamma\}} e^{-a^*(\mathcal{I}-\gamma)}$ under the twisted distribution of $\mathcal{I}$.

Hence, to compute $\mathbb{P}\left(\mathcal{I} > \gamma\right)$ requires three steps. First to solve (11.4) for a^*. Second, to compute a twisted expectation $\mathbb{E}_{a^*}\left(\cdot\right)$, and third to normalize the result with the appropriate constant.

A Modified Bahadur-Rao Approximation of $\mathcal{P}_{e|\vec{\nu},\vec{g}}$

Our approach is similar to [220] but differs in that we use the exact expression instead of an upper bound for the Gaussian Q-function. In the large deviation setting, a good approximation of $\mathcal{P}_{e|\vec{\nu},\vec{g}} = \mathbb{P}\left(\mathcal{I} > \gamma\right)$ is found if we replace the *twisted* distribution of $\mathcal{I}$ in $\mathbb{E}_{a^*}\left(1_{\{\mathcal{I}>\gamma\}} e^{-a^*(\mathcal{I}-\gamma)}\right)$ by its normal approximation, i.e.

$$\mathbb{E}_{a^*}\left(1_{\{\mathcal{I}>\gamma\}} e^{-a^*(\mathcal{I}-\gamma)}\right) \approx \int_{\gamma}^{\infty} e^{-a^*(u-\gamma)} d\mu(u), \tag{11.11}$$

where

$$\mu = \mathcal{N}\left(\mathbb{E}_{a^*}\left(\mathcal{I}\right), {\sigma^*}^2\right) = \mathcal{N}\left(\gamma, \Lambda''\left(a^*\right)\right).$$

Note that this does not at all have the same effect as using a normal approximation of the interference under the original, non-twisted distribution.

Hence

$$\mathbb{E}_{a^*}\left(1_{\{\mathcal{I}>\gamma\}} e^{-a^*(\mathcal{I}-\gamma)}\right) \approx \frac{1}{\sqrt{\pi}} e^{\frac{(a^*\sigma^*)^2}{2}} \int_{\frac{a^*\sigma^*}{\sqrt{2}}}^{\infty} e^{-u^2} du \tag{11.12}$$

and we obtain

$$\mathcal{P}_{e|\vec{\nu},\vec{g}} \approx \frac{1}{2} e^{{a^*}^2 \frac{\Lambda''_{\mathcal{I}}(a^*)}{2}} \operatorname{erfc}\left(a^* \sqrt{\frac{\Lambda''_{\mathcal{I}}\left(a^*\right)}{2}}\right) e^{-\Lambda^*_{\mathcal{I}}(x)} \tag{11.13}$$

where $\operatorname{erfc}\left(x\right) = \frac{2}{\sqrt{\pi}} \int_x^{\infty} e^{-t^2} dt$. In order to apply (11.13), we need to compute $\Lambda''_{\mathcal{I}}$ and a^*, which is explained next.

Computing the CGF of $\mathcal{I}$ and its First and Second Derivative

We begin with the CGF of $\mathcal{I}$, which is given by

$$\begin{aligned}
\Lambda_{\mathcal{I}}(a) &= \ln \mathbb{E}\left[e^{a\left(\sum_{u=1}^{U-1} Y_u + N\right)}\right] = \ln \mathbb{E}\left[e^{a\left(\sum_{u=1}^{U-1} Y_u\right)}\right] + \ln \mathbb{E}\left[e^{aN}\right] \\
&= \ln \sum_{\mathcal{C}} \mathbb{E}\left[e^{a\left(\sum_{u=1}^{U-1} Y_u\right)} \mid C^{(0)}\right] \mathbb{P}\left(C^{(0)}\right) + \ln \mathbb{E}\left[e^{aN}\right] \\
&= \ln \sum_{\mathcal{C}} \left(\prod_{u=1}^{U-1} \mathbb{E}\left[e^{aY_u} \mid C^{(0)}\right]\right) \mathbb{P}\left(C^{(0)}\right) + \ln \mathbb{E}\left[e^{aN}\right]
\end{aligned} \tag{11.14}$$

where $C^{(0)}$ is the random variable corresponding to the time-hopping sequence of user 0 and $\mathcal{C} = \{0, 1, \ldots, N_C - N_g\}$ is the set of possible values for $C^{(0)}$. Let us define

$$\tilde{\Lambda}_{\mathcal{X}}(a) = e^{\Lambda_{\mathcal{X}}(a)} = \mathbb{E}\left[e^{a\mathcal{X}}\right], \qquad \tilde{\Lambda}_{\mathcal{X}|\mathcal{Y}}(a) = \mathbb{E}\left[e^{a\mathcal{X}} \mid \mathcal{Y}\right]$$

where $\mathcal{X}$ and $\mathcal{Y}$ are random variables. Then, for the CGF of $\mathcal{I}$, the equation (11.14) can be slightly rewritten:

$$\begin{aligned} \Lambda_{\mathcal{I}}(a) &= \Lambda_{\sum_{u=1}^{U-1} Y_u}(a) + \Lambda_N(a) \\ &= \ln \sum_{\mathcal{C}} \left(\prod_{u=1}^{U-1} \tilde{\Lambda}_{Y_u|C^{(0)}}(a) \right) \mathbb{P}\left(C^{(0)}\right) + \Lambda_N(a) \end{aligned} \tag{11.15}$$

where $\tilde{\Lambda}_{Y_u|C^{(0)}}(a)$ is simply

$$\tilde{\Lambda}_{Y_u|C^{(0)}}(a) = 1 - nq + \frac{q}{2} \sum_{k=0}^{n-1} \left[e^{a x_{u,k|c^{(0)}}} + e^{-a x_{u,k|c^{(0)}}} \right], \tag{11.16}$$

and $\Lambda_N(a) = \frac{a^2 \sigma_N^2}{2}$.

For the first and second derivatives of the CGF of $\mathcal{I}$, we have

$$\Lambda'_{\mathcal{I}}(a) = \Lambda'_{\sum_{u=1}^{U-1} Y_u}(a) + \Lambda'_N(a), \qquad \Lambda''_{\mathcal{I}}(a) = \Lambda''_{\sum_{u=1}^{U-1} Y_u}(a) + \Lambda''_N(a) \tag{11.17}$$

where $\Lambda'_N(a) = a\sigma_N^2$ and $\Lambda''_N(a) = \sigma_N^2$. It remains to compute $\Lambda'_{\sum_{u=1}^{U-1} Y_u}(a)$ and $\Lambda''_{\sum_{u=1}^{U-1} Y_u}(a)$. For a random variable $\mathcal{X}$, it turns out that

$$\Lambda'_{\mathcal{X}}(a) = \frac{d}{da} \ln \mathbb{E}\left[a^{a\mathcal{X}}\right] = \frac{\frac{d}{da}\mathbb{E}\left[a^{a\mathcal{X}}\right]}{\mathbb{E}\left[a^{a\mathcal{X}}\right]} = \frac{\tilde{\Lambda}'_{\mathcal{X}}(a)}{\tilde{\Lambda}_{\mathcal{X}}(a)},$$

and

$$\Lambda''_{\mathcal{X}}(a) = \frac{\tilde{\Lambda}''_{\mathcal{X}}(a)}{\tilde{\Lambda}_{\mathcal{X}}(a)} - \left[\frac{\tilde{\Lambda}'_{\mathcal{X}}(a)}{\tilde{\Lambda}_{\mathcal{X}}(a)} \right]^2.$$

Hence, we need to compute $\tilde{\Lambda}_{\sum_{u=1}^{U-1} Y_u}(a)$, $\tilde{\Lambda}'_{\sum_{u=1}^{U-1} Y_u}(a)$, and $\tilde{\Lambda}''_{\sum_{u=1}^{U-1} Y_u}(a)$. First

$$\tilde{\Lambda}_{\sum_{u=1}^{U-1} Y_u}(a) = \sum_{\mathcal{C}} \left(\prod_{u=1}^{U-1} \tilde{\Lambda}_{Y_u|C^{(0)}}(a) \right) \mathbb{P}\left(C^{(0)}\right).$$

Then, for the first derivative of $\tilde{\Lambda}_{\sum_{u=1}^{U-1} Y_u}(a)$

$$\tilde{\Lambda}'_{\sum_{u=1}^{U-1} Y_u}(a) = \frac{d}{da}\tilde{\Lambda}_{\sum_{u=1}^{U-1} Y_u}(a) = \sum_{\mathcal{C}} \left(\frac{d}{da} \prod_{u=1}^{U-1} \tilde{\Lambda}_{Y_u|C^{(0)}}(a) \right) \mathbb{P}\left(C^{(0)}\right)$$

where

$$\frac{d}{da} \prod_{u=1}^{U-1} \tilde{\Lambda}_{Y_u|C^{(0)}}(a) = \sum_{u=1}^{U-1} \left(\prod_{v=1, v\neq u}^{U-1} \tilde{\Lambda}_{Y_v|C^{(0)}}(a) \right) \tilde{\Lambda}'_{Y_u|C^{(0)}}(a).$$

And for the second derivative of $\tilde{\Lambda}_{\sum_{u=1}^{U-1} Y_u}(a)$

$$\tilde{\Lambda}''_{\sum_{u=1}^{U-1} Y_u}(a) = \sum_{\mathcal{C}} \left(\frac{d^2}{da^2} \prod_{u=1}^{U-1} \tilde{\Lambda}_{Y_u|C^{(0)}}(a) \right) \mathbb{P}\left(C^{(0)}\right)$$

where

$$\begin{aligned} \frac{d^2}{da^2} \prod_{u=1}^{U-1} \tilde{\Lambda}_{Y_u|C^{(0)}}(a) \;=\; & \sum_{u=1}^{U-1} \Bigg\{ \left(\sum_{v=1, v\neq u}^{U-1} \left[\prod_{w=1, w\neq v, w\neq u}^{U-1} \tilde{\Lambda}_{Y_w|C^{(0)}}(a) \right] \tilde{\Lambda}'_{Y_v|C^{(0)}}(a) \right) \tilde{\Lambda}'_{Y_u|C^{(0)}}(a) \\ & + \left(\prod_{v=1, v\neq u}^{U-1} \tilde{\Lambda}_{Y_v|C^{(0)}}(a) \right) \tilde{\Lambda}''_{Y_u|C^{(0)}}(a) \Bigg\}. \end{aligned} \tag{11.18}$$

Finally, we need

$$\tilde{\Lambda}'_{Y_u|C^{(0)}}(a) = \frac{q}{2} \sum_{k=0}^{n-1} x_{u,k|c^{(0)}} \left[e^{a x_{u,k|c^{(0)}}} - e^{-a x_{u,k|c^{(0)}}} \right], \tag{11.19}$$

and

$$\tilde{\Lambda}''_{Y_u|C^{(0)}}(a) = \frac{q}{2} \sum_{k=0}^{n-1} x^2_{u,k|c^{(0)}} \left[e^{a x_{u,k|c^{(0)}}} + e^{-a x_{u,k|c^{(0)}}} \right]. \tag{11.20}$$

Note that, for a random variable $\mathcal{X}$, $\Lambda_{\mathcal{X}}(a)$ must satisfy the conditions $\Lambda_{\mathcal{X}}(0) = 0$, $\Lambda'_{\mathcal{X}}(0) = \mu_{\mathcal{X}}$, and $\Lambda''_{\mathcal{X}}(0) = \sigma^2_{\mathcal{X}}$ [221]. Indeed, we have

$$\Lambda_{\mathcal{I}}(0) = \ln \sum_{\mathcal{C}} \mathbb{P}\left(C^{(0)}\right) + \Lambda_N(0) = \ln 1 + 0 = 0$$

because $\Lambda_{Y_u|C^{(0)}}(0) = 1, \forall u$. Then,

$$\Lambda'_{\mathcal{I}}(0) = \frac{\tilde{\Lambda}'_{\sum_{u=1}^{U-1} Y_u}(0)}{\tilde{\Lambda}_{\sum_{u=1}^{U-1} Y_u}(0)} + \Lambda'_N(0) = \frac{0}{1} + 0 = 0$$

because $\Lambda'_{Y_u|C^{(0)}}(0) = 0 \, \forall u$. Lastly

$$\begin{aligned} \Lambda''_{\mathcal{I}}(0) &= \frac{\tilde{\Lambda}''_{\mathcal{I}}(0)}{\tilde{\Lambda}_{\mathcal{I}}(0)} + \Lambda''_N 0 = \sum_{\mathcal{C}} \left(\sum_{u=1}^{U-1} \tilde{\Lambda}''_{Y_u|C^{(0)}}(0) \right) \mathbb{P}\left(C^{(0)}\right) + \sigma_N^2 \\ &= q \sum_{\mathcal{C}} \sum_{u=1}^{U-1} \sum_{k=0}^{n-1} x_{u,k|c}^2 \mathbb{P}\left(C^{(0)} = c\right) + \sigma_N^2, \end{aligned}$$

which is correct since

$$\begin{aligned} \mathbb{E}\left[\left(\sum_{u=1}^{U-1} Y_u \right)^2 \right] &= \sum_{\mathcal{C}} \mathbb{E}\left[\left(\sum_{u=1}^{U-1} Y_u \right)^2 \middle| C^{(0)} \right] \mathbb{P}\left(C^{(0)}\right) = \sum_{\mathcal{C}} \sum_{u=1}^{U-1} \mathbb{E}\left[Y_u^2 | C^{(0)} \right] \mathbb{P}\left(C^{(0)}\right) \\ &= q \sum_{\mathcal{C}} \sum_{u=1}^{U-1} \sum_{k=0}^{n-1} x_{u,k|c}^2 \mathbb{P}\left(C^{(0)} = c\right). \end{aligned}$$

Computing a^* and the Rate Function of $\mathcal{I}$

As mentioned above, a^* is found by solving the equation

$$\frac{d}{da}\big(ax - \Lambda_{\mathcal{I}}(a)\big) = x - \Lambda'_{\mathcal{I}}(a) = 0|_{a=a^*}. \tag{11.21}$$

Although (11.21) cannot be solved analytically, it is straightforward to solve numerically (for example by dichotomic search).

11.1.5 BER Computation Using Importance Sampling

Our second ingredient is importance sampling. It does not make the assumption that interferers are small, and its complexity is linear in the number of interferers. The idea is to evaluate the probability in (11.3) by Monte Carlo simulation. However, a straight application of Monte Carlo is grossly inefficient: a large number of samples is required since the BER is expected to be very small. This can be fixed by using importance sampling, which consists in using a twisted distribution for sampling the random variable $\mathcal{I}$.

Importance Sampling Estimate

We use the same twisted distribution as in (11.5), with $a = a^*$ as in (11.21). However, instead of using equation (11.8), we apply (11.7) to $\mathcal{I}$ and (11.3) to obtain

$$\mathbb{P}(\mathcal{I} > \gamma) = \mathbb{E}(1_{\{\mathcal{I}>\gamma\}}) = e^{\Lambda_{\mathcal{I}}(a^*)}\mathbb{E}_{a^*}\left(1_{\{\mathcal{I}>\gamma\}}e^{-a^*\mathcal{I}}\right). \tag{11.22}$$

We evaluate (11.22) by Monte-Carlo under the twisted distribution, as follows. We compute a^* by (11.21). We draw R replicate samples $\mathcal{I}^1, \ldots, \mathcal{I}^R$ of $\mathcal{I}$ under the twisted distribution of $\mathcal{I}$ (see below) and estimate $\mathbb{P}(\mathcal{I} > \gamma)$ by

$$\bar{P}_R = e^{\Lambda_{\mathcal{I}}(a^*)}\frac{1}{R}\sum_{r=1}^{R} 1_{\{\mathcal{I}^r>\gamma\}}e^{-a^*\mathcal{I}^r} \tag{11.23}$$

We compute R such that the 95% confidence interval gives a relative accuracy of 10% (see later at the end of this section). Note that it can be shown that, under the twisted distribution with parameter a^*, the expectation of $\mathcal{I}$ is γ, and thus $\mathcal{I} > \gamma$ has a probability close to 0.5 (in contrast, under the original distribution, $\mathcal{I} > \gamma$ is a rare event). This explains why a small value of R is needed to obtain a good confidence interval.

Sampling Under the Twisted Distribution

In this section, we explain how to sample from the twisted distribution of $\mathcal{I}$. To simplify the notation, we define $Y = \sum_{i=1}^{U-1} Y_u$ and we have $\mathcal{I} = Y + N$. Our first step is to show that, under the twisted distribution, Y and N are independent and can be sampled separately. In fact,

$$\mathbb{E}_a[YN] = \frac{\mathbb{E}\left[YNe^{a\mathcal{I}}\right]}{\mathbb{E}\left[e^{a\mathcal{I}}\right]} = \frac{\mathbb{E}\left[YNe^{a(Y+N)}\right]}{\mathbb{E}\left[e^{a(Y+N)}\right]}. \tag{11.24}$$

Under the normal distribution, Y and N are independent. Equation (11.24) becomes

$$\mathbb{E}_a[YN] = \frac{\mathbb{E}\left[Ye^{aY}Ne^{aN}\right]}{\mathbb{E}\left[e^{aY}e^{aN}\right]} = \frac{\mathbb{E}\left[Ye^{aY}\right]\mathbb{E}\left[Ne^{aN}\right]}{\mathbb{E}\left[e^{aY}\right]\mathbb{E}\left[e^{aN}\right]} = \mathbb{E}_a[Y]\,\mathbb{E}_a[N]. \tag{11.25}$$

Hence, under the twisted distribution, Y and N are independent. Furthermore, it also implies that we can compute the twisted distribution of Y under the random variable Y only. We do not need to consider $Y + N$. Similarly, we can compute the twisted distribution of N under the random variable N only. To get to the twisted distribution of Y, we first compute the twisted

distribution of Y_u given $C^{(0)}$. To do so, we begin with

$$\begin{aligned}\mathbb{E}_a\left[f(Y_u)|\, C^{(0)}=c\right] &= \frac{\mathbb{E}_a\left[f(Y_u)1_{\{C^{(0)}=c\}}\right]}{\mathbb{P}_a\left(C^{(0)}=c\right)} = \frac{\mathbb{E}\left[f(Y_u)e^{aY}1_{\{C^{(0)}=c\}}\right]}{\mathbb{E}\left[e^{aY}\right]\mathbb{P}_a\left(C^{(0)}=c\right)} \\ &= \frac{\mathbb{E}\left[f(Y_u)e^{aY}|\, C^{(0)}=c\right]\mathbb{P}\left(C^{(0)}=c\right)}{\mathbb{E}\left[e^{aY}\right]\mathbb{P}_a\left(C^{(0)}=c\right)} \end{aligned} \tag{11.26}$$

where $\mathbb{P}_a\left(C^{(0)}=c\right)$ is the twisted distribution of $C^{(0)}$. Now

$$\begin{aligned}\mathbb{P}_a\left(C^{(0)}=c\right) &= \mathbb{E}_a\left[1_{\{C^{(0)}=c\}}\right] = \frac{1}{\mathbb{E}\left[e^{aY}\right]}\mathbb{E}\left[1_{\{C^{(0)}=c\}}e^{aY}\right] \\ &= \frac{1}{\mathbb{E}\left[e^{aY}\right]}\mathbb{E}\left[e^{aY}|\, C^{(0)}=c\right]\mathbb{P}\left(C^{(0)}=c\right). \end{aligned} \tag{11.27}$$

If we replace $\mathbb{P}_a\left(C^{(0)}=c\right)$ by (11.27) in (11.26), we obtain

$$\begin{aligned}\mathbb{E}_a\left[f(Y_u)|\, C^{(0)}=c\right] &= \frac{\mathbb{E}\left[f(Y_u)e^{aY}|\, C^{(0)}=c\right]}{\mathbb{E}\left[e^{aY}|\, C^{(0)}=c\right]} \\ &= \frac{\prod_{l=1,l\neq u}^{U-1}\mathbb{E}\left[e^{aY_l}|\, C^{(0)}=c\right]}{\prod_{l=1}^{U-1}\mathbb{E}\left[e^{aY_l}|\, C^{(0)}=c\right]}\mathbb{E}\left[f(Y_u)e^{aY_u}|\, C^{(0)}=c\right] \\ &= \frac{\mathbb{E}\left[f(Y_u)e^{aY_u}|\, C^{(0)}=c\right]}{\mathbb{E}\left[e^{aY_u}|\, C^{(0)}=c\right]}, \end{aligned} \tag{11.28}$$

which yields the conditional twisted distribution $\mathbb{P}_a\left(Y_u|\, C^{(0)}=c\right)$ of Y_u given $C^{(0)}$ if we replace $f(Y_u)$ by $1_{\{Y_u=y\}}$. Indeed,

$$\mathbb{P}_a\left(Y_u=y|\, C^{(0)}\right) = e^{-\Lambda_{Y_u|C^{(0)}}(a)}\mathbb{P}\left(Y_u=y|\, C^{(0)}\right)e^{ay} \tag{11.29}$$

because $\ln\mathbb{E}\left[e^{aY_u}|\, C^{(0)}\right] = \Lambda_{Y_u|C^{(0)}}(a)$. Note how, under the twisted distributions, large values of Y_u are more likely to occur.

We know how to sample from the (conditional) twisted distribution of Y_u, but we still do not know how to sample from the twisted distribution of $Y = \sum_{u=1}^{U-1} Y_u$. Hence, we know compute $\mathbb{E}_a\left[f(Y)\right] = \frac{1}{\mathbb{E}[e^{aY}]}\mathbb{E}\left[f(Y)e^{aY}\right]$. Conditioning on $C^{(0)}$,

$$\begin{aligned}\mathbb{E}\left[f(Y)e^{aY}\right] &= \sum_{\mathcal{C}}\mathbb{E}\left[f(Y)e^{aY}|\, C^{(0)}=c\right]\mathbb{P}\left(C^{(0)}=c\right) \\ &= \sum_{\mathcal{C}}\mathbb{E}\left[f(Y)e^{a\sum Y_k}|\, C^{(0)}=c\right]\mathbb{P}\left(C^{(0)}=c\right). \end{aligned} \tag{11.30}$$

Under the normal, non-twisted distribution, the Y_u given $C^{(0)}$ are independent, hence $f(Y) = \prod_{u=1}^{U-1} f(Y_u)$. Consequently

$$\begin{aligned}
\mathbb{E}\left[f(Y)e^{aY}\right] &= \sum_{\mathcal{C}} \mathbb{E}\left[\prod_{u=1}^{U-1} f(Y_u)e^{a\sum Y_u} \middle| C^{(0)} = c\right] \mathbb{P}\left(C^{(0)} = c\right) \\
&= \sum_{\mathcal{C}} \prod_{u=1}^{U-1} \mathbb{E}\left[f(Y_u)e^{a\sum Y_u} \middle| C^{(0)} = c\right] \mathbb{P}\left(C^{(0)} = c\right) \\
&= \sum_{\mathcal{C}} \prod_{u=1}^{U-1} \mathbb{E}\left[f(Y_u)e^{a\sum Y_u} \middle| C^{(0)} = c\right] \frac{\mathbb{E}\left[e^{aY} \middle| C^{(0)} = c\right]}{\mathbb{E}\left[e^{aY} \middle| C^{(0)} = c\right]} \mathbb{P}\left(C = c_i\right).
\end{aligned} \tag{11.31}$$

Since $\mathbb{E}\left[e^{aY} \middle| C^{(0)} = c\right] = \prod_{u=1}^{U-1} \mathbb{E}\left[e^{aY_u} \middle| C^{(0)} = c\right]$, we obtain

$$\mathbb{E}\left[f(Y)e^{aY}\right] = \sum_{\mathcal{C}} \left(\prod_{u=1}^{U-1} \frac{\mathbb{E}\left[f(Y_u)e^{a\sum Y_u} \middle| C^{(0)} = c\right]}{\mathbb{E}\left[e^{aY_u} \middle| C^{(0)} = c\right]}\right) \mathbb{E}\left[e^{aY} \middle| C^{(0)} = c\right] \mathbb{P}\left(C^{(0)} = c\right). \tag{11.32}$$

Hence,

$$\mathbb{E}_a\left[f(Y)\right] = \sum_{\mathcal{C}} \left(\prod_{u=1}^{U-1} \frac{\mathbb{E}\left[f(Y_u)e^{a\sum Y_u} \middle| C^{(0)} = c\right]}{\mathbb{E}\left[e^{aY_u} \middle| C^{(0)} = c\right]}\right) \frac{\mathbb{E}\left[e^{aY} \middle| C^{(0)} = c\right]}{\mathbb{E}\left[e^{aY}\right]} \mathbb{P}\left(C^{(0)} = c\right). \tag{11.33}$$

Replacing $f(Y_u)$ by $1_{\{Y_u = y\}}$, we recognize $\frac{\mathbb{E}\left[f(Y_u)e^{a\sum Y_u} \middle| C^{(0)} = c\right]}{\mathbb{E}\left[e^{aY_u} \middle| C^{(0)} = c\right]}$, which is the twisted distribution of Y_u given $C^{(0)}$ from equation (11.28), and

$$\frac{\mathbb{E}\left[e^{aY} \middle| C^{(0)} = c\right]}{\mathbb{E}\left[e^{aY}\right]} \mathbb{P}\left(C^{(0)} = c\right) = \mathbb{P}_a\left(C^{(0)} = c\right) \tag{11.34}$$

is the twisted distribution of $C^{(0)}$ from equation (11.27). Hence, to sample from the twisted distribution of $\sum_{u=1}^{U-1} Y_u$, we first draw a sample c^r from the twisted distribution of $C^{(0)}$. Then, using this sample, we draw $U-1$ samples $Y^r_{1|c^r}, \ldots, Y^r_{U-1|c^r}$ from the conditional twisted distributions of Y_u, $u = 1, \ldots, U-1$ given c^r. The sample from the twisted distribution of $\sum_{u=1}^{U-1} Y_u$ is obtained by summing the samples $Y^r_{1|c^r}, \ldots, Y^r_{U-1|c^r}$.

We use the inversion method to sample from a particular distribution, such as (11.28) or (11.27), as follows. For a given discrete random variable $\mathcal{X}$, let $\{\tilde{x}_0, \tilde{x}_1, \ldots, \tilde{x}_{n-1}\}$ be the ordered set of all possible values of interferer $\mathcal{X}$. Then let $F_{\mathcal{X}}(j) = \sum_{i=0}^{j} \mathbb{P}\left(\mathcal{X} = \tilde{x}_i\right)$ for $j = 0, 1, \ldots, n-1$. A sample value X^r is obtained by drawing a random number $\mathcal{U}$ uniform

in $[0,1]$, finding the index j such that $F_{\mathcal{X}}(j) \leq \mathcal{U} < F_{\mathcal{X}}(j+1)$, and letting $X^r = \tilde{x}_j$.

Similarly, one finds that the twisted distribution of the noise N is $\mathcal{N}(a^*\sigma_N^2, \sigma_N^2)$ and sampling is done using a standard method for sampling from the normal distribution. Hence, if N^r is sampled from the twisted distribution of the noise, a sample of the twisted distribution of the interference is obtained as

$$\mathcal{I}^r = \sum_{u=1}^{U-1} Y^r_{1|c^r}, \ldots, Y^r_{U-1|c^r} + N^r$$

A Stopping Criterion for the Number R of Replicate Samples

We use standard confidence interval theory. Let us define $X_r = e^{\Lambda_{\mathcal{I}}(a^*)} 1_{\{\mathcal{I}^r > \gamma\}} e^{-a^*\mathcal{I}^r}$. Then, a 95% confidence interval for $\bar{P}_R$ is $\bar{P}_R \pm 1.96\frac{s_R}{\sqrt{R}}$ where $s_R^2 = \frac{1}{R}\sum_{r=1}^{R}\left(X_r - \bar{P}_R\right)^2$. To obtain a 10% relative accuracy, we choose R such that

$$1.96\frac{s_R}{\sqrt{R}} \leq \varepsilon \bar{P}_R \tag{11.35}$$

with $\varepsilon = 0.1$.

11.1.6 Our Proposed Method: a Combination of Large Deviation and Importance Sampling

Large deviation is faster than importance sampling, but works well only when all interferers are small. In contrast, importance sampling always works, but its complexity grows linearly with the number of interferers. We combine the two methods as follows. We fix a threshold θ. Then, an interferer $u = 1, ..., U-1$ such that

$$\max_{\mathcal{C}}\left(\max_{k}\left(x_{u,k|c_i^{(0)}}\right)\right) > \theta \cdot \gamma \tag{11.36}$$

is declared large (or near-far), whereas other interferers are declared small (or weak). Whether a given interferer u is declared large depends on its power and distance to the destination, but also on its channel realization and delay.

Therefore, we can write $\mathcal{I} = \mathcal{I}_L + \mathcal{I}_S$ where $\mathcal{I}_L = \sum_{i=1}^{i_0} I_i$ denotes the large interferers and $\mathcal{I}_S = \sum_{i=i_0+1}^{U-1} I_i + N$ denotes the small interferers plus noise. We apply the same distribution twist as before, by computing a^* as in (11.21), where $\Lambda_{\mathcal{I}}$ is the CGF for the total interference (large and small) and noise, as before. Under the conditional twisted distribution given $C^{(0)}$,

we approximate $\mathcal{I}_S$, the sum of all small interferers plus noise by a Gaussian distribution, with mean $\mathbb{E}_{a^*}\left(\mathcal{I}_S \mid C^{(0)}\right)$ and variance $\mathbb{E}_{a^*}\left({\mathcal{I}_S}^2 - \mathbb{E}_{a^*}\left(\mathcal{I}_S \mid C^{(0)}\right)^2 \mid C^{(0)}\right)$. If we replicate most of the steps involved in equations (11.26), (11.27) and (11.28), we can write

$$\mathbb{E}_{a^*}\left(\mathcal{I}_S \mid C^{(0)}\right) = \frac{\mathbb{E}\left[e^{a^*\mathcal{I}}\mathcal{I}_S \mid C^{(0)}\right]}{\mathbb{E}\left[e^{a^*\mathcal{I}} \mid C^{(0)}\right]} = e^{-\Lambda_{\mathcal{I}|C^{(0)}}(a^*)}\mathbb{E}\left[e^{a^*\mathcal{I}}\mathcal{I}_S \mid C^{(0)}\right]. \tag{11.37}$$

Now,

$$\begin{aligned}
\mathbb{E}_{a^*}\left(\mathcal{I}_S \mid C^{(0)}\right) &= e^{-\Lambda_{\mathcal{I}|C^{(0)}}(a^*)}\mathbb{E}\left[e^{a^*\mathcal{I}}\mathcal{I}_S \mid C^{(0)}\right] \\
&= e^{-\Lambda_{\mathcal{I}|C^{(0)}}(a^*)}\mathbb{E}\left[e^{a^*\mathcal{I}_L}e^{a^*\mathcal{I}_S}\mathcal{I}_S \mid C^{(0)}\right] \\
&= e^{-\Lambda_{\mathcal{I}|C^{(0)}}(a^*)}\mathbb{E}\left[e^{a^*\mathcal{I}_L} \mid C^{(0)}\right]\mathbb{E}\left[e^{a^*\mathcal{I}_S}\mathcal{I}_S \mid C^{(0)}\right] \\
&= e^{-\Lambda_{\mathcal{I}|C^{(0)}}(a^*)}\mathbb{E}\left[e^{a^*\mathcal{I}_L} \mid C^{(0)}\right]\frac{e^{\Lambda_{\mathcal{I}_S|C^{(0)}}(a^*)}}{e^{\Lambda_{\mathcal{I}_S|C^{(0)}}(a^*)}}\mathbb{E}\left[\frac{d}{da^*}e^{a^*\mathcal{I}_S} \mid C^{(0)}\right] \\
&= e^{-\Lambda_{\mathcal{I}|C^{(0)}}(a^*)}\mathbb{E}\left[e^{a^*\mathcal{I}_L} \mid C^{(0)}\right]e^{\Lambda_{\mathcal{I}_S|C^{(0)}}(a^*)}\Lambda'_{\mathcal{I}_S|C^{(0)}}(a^*) \\
&= \Lambda'_{\mathcal{I}_S|C^{(0)}}(a^*)
\end{aligned} \tag{11.38}$$

since $\mathbb{E}\left[e^{a^*\mathcal{I}_L} \mid C^{(0)}\right] = e^{\Lambda_{\mathcal{I}_L|C^{(0)}}(a^*)}$. By similar arguments, we can show that

$$\mathbb{E}_{a^*}\left({\mathcal{I}_S}^2 - \mathbb{E}_{a^*}\left(\mathcal{I}_S \mid C^{(0)}\right)^2 \mid C^{(0)}\right) = \Lambda''_{\mathcal{I}_S|C^{(0)}}(a^*) \tag{11.39}$$

Hence, under the conditional twisted distribution given $C^{(0)}$, we approximate $\mathcal{I}_S$ with

$$\mathcal{I}_S \sim \mathcal{N}\left(\Lambda'_{\mathcal{I}_S|C^{(0)}}(a^*), \Lambda''_{\mathcal{I}_S|C^{(0)}}(a^*)\right). \tag{11.40}$$

This is the main step performed by the large deviation method.

However, for the large interferers, we use importance sampling, as in Section 11.1.5. We sample $i_0 - 1$ interferers from their twisted distributions, plus one value from a normal distribution $\mathcal{N}\left(\Lambda'_{\mathcal{I}_S|C^{(0)}}(a^*), \Lambda''_{\mathcal{I}_S|C^{(0)}}(a^*)\right)$. The combined method is described in detail in algorithm 1.

Algorithm 1: Fast BER computation.

Input: U, N_c, N_g, $\vec{g}$, $\vec{\nu}$, σ_N^2 and q, K
Output: $\bar{P}_R$
begin
  for *interferer* $u = 1$ *to* $U - 1$ **do**
    for $c \in \mathcal{C}$ **do**
      Compute $x_{u,k|c}$, $k = 0, 1, \ldots, n-1$;
    end
  end
  Solve (11.21) to obtain a^* ;
  Classify the interferers between small and large using equation (11.36);
  for $c \in \mathcal{C}$ **do**
    Compute $\mu_{S|c} \leftarrow \Lambda'_{\mathcal{I}_S|c}(a^*)$ and $\sigma^2_{S|c} \leftarrow \Lambda''_{\mathcal{I}_S|c}(a^*)$;
  end
  Create an array Π to store the samples;
  while *confidence interval on* $\bar{P}_R > \varepsilon \bar{P}_R$ **do**
    $R \leftarrow R + K$;
    Draw K samples $c^1, c^2, \ldots, c^K$ from the twisted distribution of $C^{(0)}$ (equation (11.27));
    for $k = 1, \ldots, K$ **do**
      Draw $I_S^k \sim \mathcal{N}(\mu_{S|c^k}, \sigma^2_{S|c^k})$;
      for *each large interferer* $i = 2$ *to* i_0 **do**
        Draw I_i^k from the twisted distribution Y_i given c (equation (11.34));
      end
      Add $I_S^k + \sum_{i=2}^{i_0} I_i^k$ to the array Π;
    end
    Use a^* and Π to obtain $\bar{P}_R$ from (11.23);
  end
end

11.2 Performance Evaluation

11.2.1 Performance Metric and Simulation Parameters

The performance metric is the bit error rate (BER). The parameters of the physical layer correspond to an IEEE 802.15.4a physical layer. We have $T_c = 8$ ns, $N_c = 128$, $N_g = 64$, and $n = 13$. The rate is 1 Mbit/s. The auto-correlation function of the information bearing pulse is

$$\Theta(\tau) = \left[1 - 4\pi\left(\frac{\tau}{\tau_p}\right)^2 + \frac{4\pi^2}{3}\left(\frac{\tau}{\tau_p}\right)^4\right] \exp\left[-\pi\left(\frac{\tau}{\tau_p}\right)^2\right]$$

where $\tau_p = 0.2877$ is a time normalization factor.

The channel model is the modified Saleh-Valuenza (SV) model used by the IEEE 802.15.4a working group. We use the first LOS channel model (model 1) from [22]. For a given topology, the channels $\vec{g}$ between each transmitter and the receiver are drawn independently and the delays $\vec{\nu}$ chosen independently and uniformly in $[0, N_c T_c[$. For the channel impulse response of user u, we denote by $A^{(u)} = \sum_{l=0}^{L-1} \left(\alpha_l^{(u)}\right)^2$ the total energy of the channel. We have $A^{(u)} = 1$. The SNR is defined as $\frac{A^{(0)}}{N_0}$.

For completeness, we compute a purely normal approximation of the interference. We will compare it with the other methods. Let us denote by $\mathcal{I}^N$ the normal approximation of $\sum_{u=1}^{U-1} Y_u \; + \; N$. Then

$$\mathcal{I}^N \sim \mathcal{N}\left(0, \sigma_N^2 + q \sum_{\mathcal{C}} \sum_{u=1}^{U-1} \sum_{k=1}^{n} x_{u,k|c}^2 \mathbb{P}\left(C^{(0)} = c\right)\right)$$

and the BER under this approximation is given by

$$\mathcal{P}_{e|\vec{\phi},\vec{h}}^N = \frac{1}{2}\mathrm{erfc}\left(\frac{x}{\sqrt{2}\sqrt{\sigma_N^2 + q\sum_{\mathcal{C}}\sum_{u=1}^{U-1}\sum_{k=1}^{n} x_{u,k|c}^2 \mathbb{P}\left(C^{(0)} = c\right)}}\right). \tag{11.41}$$

All our simulations have been performed using Matlab.

11.2.2 Performance Evaluation Results

In Figure 11.1, we validate our approach by comparing the importance sampling method with direct simulation (regular Monte Carlo) results for $U = \{64, 8, 3\}$ with one set of channels and delays for each U. For $U = 65$, $[A^{(1)}, \ldots, A^{(59)}]$ were uniformly drawn in $[0, 2]$ and $[A^{(60)}, \ldots, A^{(63)}] = [2, 10, 20, 200]$. For $U = 8$, $[A^{(1)}, \ldots, A^{(7)}] = [1, 1, 1, 4, 7, 20, 100]$ and for $U = 3$, $[A^{(1)}, A^{(2)}] = [2, 10]$. In addition, we show the Gaussian approximation computed with (11.41) which completely underestimates the BER. Table 11.1 contains the average computation time for a single BER sample for $U = 65$ at an SNR of 12 dB. The computation time of the importance sampling method is one order of magnitude faster than direct simulation. The combined method, although not shown in Figure 11.1 for clarity reasons, reduces the computation time even more by an additional order of magnitude.

In Figure 11.2, we show the accuracy of the combined method with respect to pure importance sampling. We also add the simpler large deviation method. The topology is the same

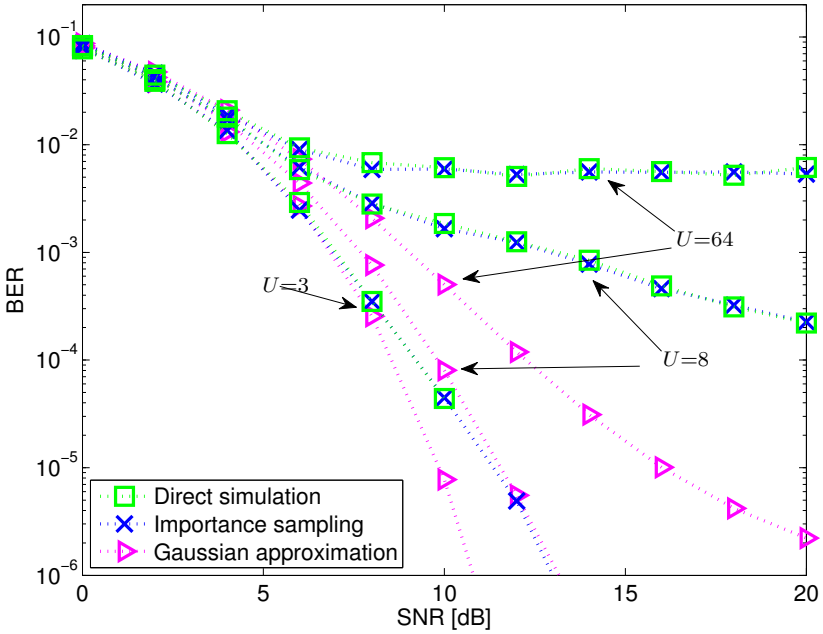

Figure 11.1: We validate our approach by comparing the importance sampling method with direct simulation results. There are three different topologies where $U = \{64, 8, 3\}$. In each case, there is a mixture of near-far and weak interferers. The results obtained with a direct Monte-Carlo simulation and the importance sampling method agree. Note how the Gaussian approximation underestimates the BER. The channel is a UWB 802.15.4a LOS.

for all sets of BER curves: we have $U = 21$, $[A^{(1)} \dots A^{(18)}]$ uniformly selected in $[0, 2]$ and $[A^{(21)}\ A^{(22)}] = [20\ 100]$). However, we draw four sets $[g_i, \nu_i], i = 1, 2, 3, 4$ of channel and delay samples. The results show a perfect agreement between our combined method and the importance sampling method. But the combined method provides an additional computation time saving since sampling is required only for the interferers that have a strong impact on the BER. Furthermore, we observe in Figure 11.2(b) that the Bahadur-Rao approximation alone used in the large deviation method becomes inaccurate when near-far interference is present. Also, large $A^{(i)}$ do not always imply a strong near-far case as can be observed in Figure 11.2(a)

Table 11.1: Average computation time for a single BER sample with $U = 65$, an SNR of 12 dB, and 95% confidence interval (using Matlab).

Direct Simulation	Importance Sampling	Combined
30.4 s	2.0 s	0.5 s

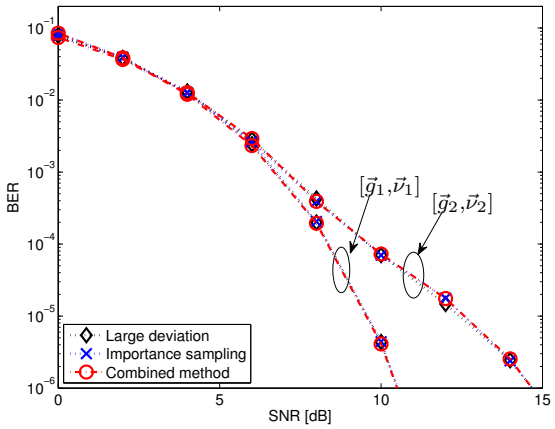

(a) Low BER case: the large deviation approximation and the combined method are accurate.

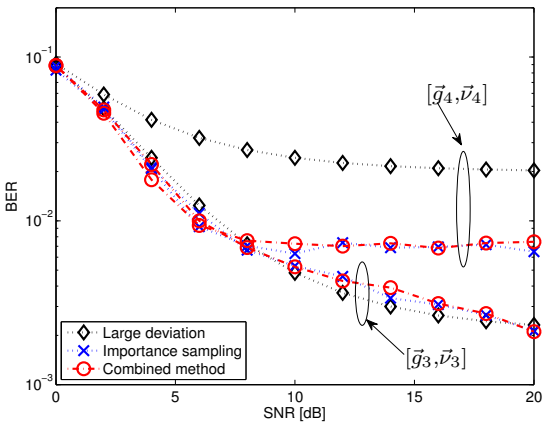

(b) High BER case: the large deviation approximation is inaccurate but the combined method is still accurate.

Figure 11.2: The large deviation method (Bahadur-Rao) and the combined method are compared with importance sampling. The parameters U and $A^{(i)}, i = 1, \ldots, U-1$ are constant (fixed topology and received powers), but there are three sets $[\vec{g}_1, \vec{\nu}_1]$, $[\vec{g}_2, \vec{\nu}_2]$, $[\vec{h}_3, \vec{\nu}_3]$, and $[\vec{h}_4, \vec{\nu}_4]$ of channel and delay samples. There are two cases: a low BER (left) and a high BER (right). Note how the BER can be vastly different depending on the particular instances of delays and channels (even though the topology and received powers remain the same). The combined method matches perfectly with the importance sampling result. The large deviation approximation is not accurate when the BER is high. The channels are chosen according to a UWB 802.15.4a LOS.

with $[\vec{g}_1, \vec{\nu}_1]$ and $[\vec{g}_2, \vec{\nu}_2]$. Indeed, even if a collision occurs, due to the multipath delays and the additional asynchronism between the source and the interferer, the received pulses might not completely overlap. In this case, the Bahadur-Rao approximation is accurate.

11.3 Discussion and Conclusion

To efficiently and accurately compute the conditional BER for a multi-user IR-UWB physical layer in multipath channel environment, we have proposed a novel combination of large deviation and importance sampling theory . Our method provides a high reduction in computation time. Although we used BPSK modulation and a perfect Rake receiver, our method is usable with minor modifications with sub-optimal Rake receivers, other modulation formats and non-coherent receivers. Of particular interest is the IEEE 802.15.4a modulation format and energy detection receivers.

With our modeling of the physical layer, the BER can also be computed with a characteristic

function approach. However, our approach is more flexible. Furthermore, with the appropriate modification of the computation of the distribution of the interference $\sum_{u=1}^{U-1} Y_u$, our approach can also be used to compute the average BER, instead of the conditional BER given channel states. Interesting future work might consist in extending our approach to a physical layer with channel coding and implement our model in a network simulator such as ns-2 or Qualnet.

Chapter 12

Conclusion

We began the work for this thesis by asking two questions (1) *What* are the optimal design principles and architectures for IR-UWB networks? and (2) *How* do we implement them with practical schemes and protocols? We decided to focus on the link layer and the physical layer with a low data-rate, self-organized, and multi-hop setting.

Chapters 4 and 6 answer the first question on the optimal design of low-data rate IR-UWB networks. The main findings from Chapter 4 are that interference should not be prevented, but it should managed. In fact, no exclusion mechanism is necessary. Interference must be managed with rate adaptation and no power control, and an interference mitigation scheme used at the physical layer. These findings are optimal from a rate efficiency point of view and are close to optimal from an energy efficiency point of view. These results are clearly in favor of an uncoordinated and decentralized protocol. Chapter 6 shows the benefits of using private acquisition preambles for IR-UWB networks, instead of a common acquisition preamble for the entire network. With private acquisition preambles, all communications for a given destination use an acquisition preamble and a time-hopping sequence that are private to this destination. Such a design inherently creates one contention domain per destination. In Chapter 6, we demonstrate the huge throughput gain obtained with private acquisition preambles and exhibit several performance anomalies that occur only if a common preamble is used.

Therefore, the optimal design for IR-UWB networks should use an interference mitigation scheme at the physical layer, manage interference with rate adaptation at the link layer, use private acquisition preambles and time-hopping sequences, and let sources send whenever they have a packet ready.

Most of the other chapters in this thesis aim at answering the second question: How do

we implement the optimal design in practice? In particular Chapter 5 describes DCC-MAC, which is a protocol for low data-rate, multi-hop IR-UWB networks that is built on the findings of Chapter 4: We implement a rate adaptation algorithm that does not require interference estimation; we address contention at destinations with the private MAC; and we overcome the absence of carrier-sensing with an elaborate signaling protocol. With DCC-MAC we obtain a stable throughput over multi-hop topologies.

Chapter 9 presents a low-complexity IR-UWB receiver for IEEE 802.15.4a networks based on energy detection with an integrated interference mitigation scheme. It yields excellent performance, even in near-far scenarios. The complexity increase with respect to a classic energy detection receiver is minimal; it is necessary only during the estimation of the power delay profile of the channel. The sampling frequency might be higher though. This appears to be the price to pay for a proper estimation of the power-delay profile of the channel when bursts of pulses are sent. This robust receiver allows for taking advantage of all the features of IR-UWB, but at a low complexity: ranging, robustness against multipath propagation, and robustness to MUI that leads to the possibility of allowing for parallel transmissions. In Chapter 7, we obtain the evidence that concurrent transmissions are really feasible in IR-UWB networks. Indeed, we successfully implement and verify the functioning of a timing acquisition scheme that is robust to MUI on an IR-UWB testbed.

The previous paragraphs describe the core results of this thesis on the optimal design and architecture of IR-UWB networks. We have additional contributions and observations that we list in the following:

- In Chapter 4, we describe the functions of PHY-aware MAC protocols and the various ways they can be implemented. This is directly useful for protocol designers to understand and exploit the large range of possibilities they have for designing PHY-aware MAC protocols for UWB or *other* physical layers.

- In Chapter 4, we propose an original energy consumption model for impulse-radio systems. It is based on the energy consumed per chip.

- It is interesting to observe that DCC-MAC is actually quite close to the mandatory MAC protocol in the IEEE 802.15.4a amendment [64] with the following notable exceptions: In IEEE 802.15.4a a common acquisition preamble is used, there is no rate adaptation, no idle/busy flag in the acknowledgement packet, and no idle packet.

- In Chapter 6, in order to analyze how using a private or common acquisition preamble af-

fects the performance of IR-UWB networks, we develop an analytical model to compute the saturation throughput of an IR-UWB network. One novelty of this model is to explicitly take into account packet detection and timing acquisition. We obtain the equivalent of Bianchi's formula for our case. This model can be easily used with different MAC layers or different acquisition algorithms.

- One of the most appealing benefits of UWB, specifically its robustness to MUI and thus the possibility of allowing for parallel transmissions, is completely annihilated if a simple energy detection receiver is used. Furthermore, in addition to MUI, an energy detection receiver for an IEEE 802.15.4a network must also take into account the burst structure of the modulation format.

- In Chapter 10, we present an architecture for packet-based simulations of wireless networks. We use this architecture to implement an IR-UWB physical layer in ns-2. This architecture allows for the proper modeling of the characteristics of modern physical layers: cumulative interference and the calculation of a packet error rate, packet detection and timing synchronization, and the possibility of having multiple sub-channels.

- Finally, in Chapter 11, we propose a novel combination of large deviation and importance sampling theory to efficiently and accurately compute the BER for an IR-UWB physical layer in a network setting, with MUI and multipath channels.

12.1 Future Work and Possible Extensions

For the optimal design and architecture of IR-UWB networks in Chapter 4, a complete design targeting energy efficiency should also consider energy efficient routing. A first step in this direction is [158]. The guidelines in Chapter 4 and the protocol we develop in Chapter 5 are guided by the idea of arranging the physical layer and the MAC protocol such that collisions may be replaced by rate reduction. This idea is optimal for our setting, but it could prove interesting in other settings as well. The optimal MAC protocol in narrow-band systems is likely to be a combination of rate adaptation and mutual exclusion. Mutual exclusion has severe performance problems, as witnessed by the intense research on improving the 802.11 MAC protocol for use in ad-hoc and mobile networks. In contrast, rate adaptation does not appear to have these problems, because it is a private affair between a source and a destination. Therefore, it would be interesting to add this component to existing MAC layers. For the

modeling in Chapter 6, there are several extensions that are of interest: to take interference on the payload into account; to consider multi-hop network; and to add an additional sleeping state to the nodes.

The robust energy detection receiver of Chapter 9 needs to be completed by a robust packet detection and timing acquisition scheme. The work in [63, 144] already suggests potential solutions for robust timing acquisition. Adapting the parameter P_{FA} to the level of interference during packet reception might also prove worthwhile. It will make the receiver fully robust to cases where interference occurs after the acquisition preamble. We also do not take advantage of the erasures correction capability of the Reed-Solomon code. That could add a further performance increase.

For the simulation of IR-UWB networks in Chapter 10, it is important to integrate a better BER and PER calculation model for IR-UWB. The work of Chapter 11 goes in this direction. With the emergence of IEEE 802.15.4a, there is also an interest in adapting the BER computation method of Chapter 11 to the 802.15.4a modulation format and to energy detection receivers. In addition, an important effort is necessary to validate physical layer models with actual hardware.

What This Thesis is Not About

We can also suggest possible extensions to our work by looking at several topics that are not addressed in this thesis. In particular:

- We did not address quality of service (QoS) issues in the design of the DCC-MAC protocol. Some applications running on sensor networks might require guarantee on the throughput or delay in the network.

- We did not discussed routing. It is certainly interesting to study how a routing protocol can take advantage of the features of IR-UWB networks. In fact, the optimal design of the MAC protocol uses private time-hopping sequences per destination. In other words, it favors the use of a private channel for each destination and avoids the use of a common, broadcast channel. On the contrary, existing routing protocols extensively use the broadcast channel.

- Finally, a lot of the interest for UWB comes from the high precision ranging capabilities. There is definitely work to be done on joint ranging and communication protocols, as well

as how to use the ranging information to efficiently complement and enhance existing protocols.

12.2 What Can we Learn From IR-UWB Networks?

From our work, we draw two conclusions for the design of IR-UWB network: (1) Interference matters, always. It must be considered early in the design phase of any component of IR-UWB networks; (2) interference in IR-UWB networks must be managed. For the design of wireless networks, this work shows that it is important to explicitly take into account the underlying physical layer. This is the key to the excellent performance of DCC-MAC, and to the performance of our robust energy detection receiver.

Finally, if we abstract the IR-UWB physical layer with interference mitigation, we obtain the following model: We have a wireless network with quasi-orthogonal multiple-access channels that have very little co-channel interference; furthermore, we use one channel per destination. This model yields a stable multi-hop performance. Hopefully, this result can be applied elsewhere, possibly in the context of narrow-band wireless networks.

Bibliography

[1] C. Thompson, "Everything is alive," *IEEE Internet Comput.*, vol. 8, no. 1, pp. 83–86, 2004.

[2] ——, "Smart devices and soft controllers," *IEEE Internet Comput.*, vol. 9, no. 1, pp. 82–85, 2005.

[3] L. Kleinrock and F. A. Tobagi, "Packet switching in radio channels: Part I–carrier sense multiple-access modes and their throughput-delay characteristics," *IEEE Trans. Commun.*, vol. 23, no. 12, pp. 1400–1416, December 1975.

[4] Federal Communications Commission, United States, "FCC 02–48, First Report and Order, available at http://hraunfoss.fcc.gov/edocs_public/attachmatch/FCC-02-48A1.pdf," February 14th 2002.

[5] European Radiocommunications Office (ERO), Electronic Communications Committee, "Document ECC/DEC/(06)04, available at http://www.ero.dk/documentation/docs/doc98/official/pdf/ECCDEC0604.pdf," July 2007.

[6] Federal Office of Communication (OFCOM), Switzerland, "National frequency allocation plan, applications UWB / WB SRD, available at http://www.bakom.admin.ch/themen/frequenzen/00652/00653/02091/index.html?lang=en," January 2008.

[7] R. Scholtz, "Multiple access with time-hopping impulse modulation," in *IEEE Military Communications Conference (MILCOM)*, vol. 2, 1993, pp. 447–450 vol.2.

[8] M. Z. Win and R. A. Scholtz, "Impulse radio: how it works," *IEEE Commun. Lett.*, vol. 2, no. 2, pp. 36–38, 1998.

[9] ——, "Ultra-wide bandwidth time-hopping spread-spectrum impulse radio for wireless multiple-access communications," *IEEE Trans. Commun.*, vol. 48, no. 4, pp. 679–691, April 2000.

[10] M. Z. Win, "A unified spectral analysis of generalized time-hopping spread-spectrum signals in the presence of timing jitter," *IEEE J. Sel. Areas Commun.*, vol. 20, no. 9, pp. 1664–1676, 2002.

[11] A. Ridolfi and M. Z. Win, "Ultrawide bandwidth signals as shot noise: a unifying approach," *IEEE J. Sel. Areas Commun.*, vol. 24, no. 4, pp. 899–905, 2006.

[12] J. G. Proakis, *Digital Communications*, 4th ed. New York, NY: McGraw–Hill, 2001.

[13] F. Ramirez-Mireles, "On the performance of ultra-wide-band signals in gaussian noise and dense multipath," *IEEE Trans. Veh. Technol.*, vol. 50, no. 1, pp. 244–249, 2001.

[14] H. Hashemi, "The indoor radio propagation channel," *Proc. IEEE*, vol. 81, no. 7, pp. 943–968, 1993.

[15] M. Z. Win and R. A. Scholtz, "On the robustness of ultra-wide bandwidth signals in dense multipath environments," *IEEE Commun. Lett.*, vol. 2, no. 2, pp. 51–53, 1998.

[16] J. M. Cramer, R. A. Scholtz, and M. Z. Win, "Spatio-temporal diversity in ultra-wideband radio," in *IEEE Wireless Communications and Networking Conference*, 1999, pp. 888–892 vol.2.

[17] R. J. M. Cramer, R. A. Scholtz, and M. Z. Win, "Evaluation of an ultra-wide-band propagation channel," *IEEE Trans. Antennas Propag.*, vol. 50, no. 5, pp. 561–570, 2002.

[18] A. Saleh and R. Valenzuela, "A statistical model for indoor multipath propagation," vol. 5, no. 2, pp. 128–137, 1987.

[19] D. Cassioli, M. Win, and A. Molisch, "The ultra-wide bandwidth indoor channel: from statistical model to simulations," *IEEE J. Sel. Areas Commun.*, vol. 20, no. 6, pp. 1247–1257, August 2002.

[20] A. F. Molisch, J. R. Foerster, and M. Pendergrass, "Channel models for ultrawideband personal area networks," vol. 10, no. 6, pp. 14–21, 2003.

[21] S. Ghassemzadeh, R. Jana, C. Rice, W. Turin, and V. Tarokh, "Measurement and modeling of an ultra-wide bandwidth indoor channel," *IEEE Trans. Commun.*, vol. 52, no. 10, pp. 1786–1796, October 2004.

[22] A.-F. Molisch, K. Balakrishnan, C.-C. Chong, S. Emami, A. Fort, J. Karedal, J. Kunisch, H. Schantz, U. Schuster, and K. Siwiak, "IEEE 802.15.4a channel model - final report, document 04/662r1," http://www.ieee802.org/15/pub/TG4a.html, November 2004.

[23] A. F. Molisch, "Ultrawideband propagation channels-theory, measurement, and modeling," *IEEE Trans. Veh. Technol.*, vol. 54, no. 5, pp. 1528–1545, 2005.

[24] A. F. Molisch, D. Cassioli, C. C. Chong, S. Emami, A. Fort, B. Kannan, J. Karedal, J. Kunisch, H. G. Schantz, H. G. Schantz, K. Siwiak, and M. Z. Win, "A comprehensive standardized model for ultrawideband propagation channels," *IEEE Trans. Antennas Propag.*, vol. 54, no. 11, pp. 3151–3166, 2006.

[25] J. Tsao, D. Porrat, and D. Tse, "Prediction and modeling for the time-evolving ultrawideband channel," *IEEE J. Sel. Areas Commun.*, vol. 1, no. 3, pp. 340–356, 2007.

[26] U. G. Schuster and H. Bolcskei, "Ultrawideband channel modeling on the basis of information-theoretic criteria," *IEEE Trans. Wireless Commun.*, vol. 6, no. 7, pp. 2464–2475, 2007.

[27] L. J. Greenstein, S. S. Ghassemzadeh, S.-C. Hong, and V. Tarokh, "Comparison study of UWB indoor channel models," *IEEE Trans. Wireless Commun.*, vol. 6, no. 1, pp. 128–135, 2007.

[28] R. Price and P. E. Green, "A communication technique for multipath channels," *Proc. IRE*, vol. 46, pp. 555–570, March 1958.

[29] D. Tse and P. Viswanath, *Fundamentals of Wireless Communication*. Cambridge University Press, June 2005.

[30] J. D. Choi and W. E. Stark, "Performance of ultra-wideband communications with suboptimal receivers in multipath channels," *IEEE J. Sel. Areas Commun.*, vol. 20, no. 9, pp. 1754–1766, 2002.

[31] D. Cassioli, M. Z. Win, F. Vatalaro, and A. F. Molisch, "Low complexity rake receivers in ultra-wideband channels," *IEEE Trans. Wireless Commun.*, vol. 6, no. 4, pp. 1265–1275, 2007.

[32] L. Yang and G. Giannakis, "Ultra-wideband communications: an idea whose time has come," *IEEE Signal Process. Mag.*, vol. 21, no. 6, pp. 26–54, November 2004.

[33] V. Lottici, A. D'Andrea, and U. Mengali, "Channel estimation for ultra-wideband communications," *IEEE J. Sel. Areas Commun.*, vol. 20, no. 9, pp. 1638–1645, 2002.

[34] W. M. Lovelace and J. K. Townsend, "The effects of timing jitter and tracking on the performance of impulse radio," *IEEE J. Sel. Areas Commun.*, vol. 20, no. 9, pp. 1646–1651, 2002.

[35] Z. Tian and G. B. Giannakis, "Ber sensitivity to mistiming in ultra-wideband impulse radios-part i: nonrandom channels," *IEEE Trans. Signal Process.*, vol. 53, no. 4, pp. 1550–1560, 2005.

[36] Y. Souilmi and R. Knopp, "On the achievable rates of ultra-wideband PPM with non-coherent detection in multipath environments," in *IEEE International Conference on Communications (ICC)*, vol. 5, 2003, pp. 3530–3534 vol.5.

[37] A. A. D'Amico, U. Mengali, and E. Arias-De-Reyna, "Energy-detection UWB receivers with multiple energy measurements," *IEEE Trans. Wireless Commun.*, vol. 6, no. 7, pp. 2652–2659, 2007.

[38] M. Weisenhorn and W. Hirt, "Robust noncoherent receiver exploiting UWB channel properties," in *IEEE joint Conference on Ultra Wideband Systems and Technologies & International Workshop on Ultra Wideband Systems*, May 2004, pp. 156–160.

[39] S. Dubouloz, A. Rabbachin, S. de Rivaz, B. Denis, and L. Ouvry, "Performance analysis of low complexity solutions for UWB low data rate impulse radio," in *IEEE ISCAS 06*, May 2006.

[40] T. Zasowski, F. Troesch, and A. Wittneben, "Partial channel state information and intersymbol interference in low complexity UWB PPM detection," in *IEEE ICUWB 06*, September 2006, pp. 369 – 374.

[41] M. Ho, V. S. Somayazulu, J. Foerster, and S. Roy, "A differential detector for an ultra-wideband communications system," in *IEEE 55th Vehicular Technology Conference (VTC Spring)*, vol. 4, 2002, pp. 1896–1900 vol.4.

[42] R. Hoctor and H. Tomlinson, "Delay-hopped transmitted-reference rf communications," in *IEEE Conference on Ultra Wideband Systems and Technologies*, 2002, pp. 265–269.

[43] T. Q. S. Quek and M. Z. Win, "Analysis of UWB transmitted-reference communication systems in dense multipath channels," *IEEE J. Sel. Areas Commun.*, vol. 23, no. 9, pp. 1863–1874, 2005.

[44] Y.-L. Chao and R. A. Scholtz, "Ultra-wideband transmitted reference systems," *IEEE Trans. Veh. Technol.*, vol. 54, no. 5, pp. 1556–1569, 2005.

[45] F. Tufvesson, S. Gezici, and A. F. Molisch, "Ultra-wideband communications using hybrid matched filter correlation receivers," *IEEE Trans. Wireless Commun.*, vol. 5, no. 11, pp. 3119–3129, 2006.

[46] R. Knopp and Y. Souilmi, "Achievable rates for UWB peer-to-peer networks," in *International Zurich Seminar on Communications*, 2004, pp. 82–85.

[47] M. Flury and J.-Y. Le Boudec, "Interference mitigation by statistical interference modeling in an impulse radio UWB receiver," in *Ultra-Wideband, The 2006 IEEE 2006 International Conference on*, September 2006, pp. 393–398.

[48] J. Mitra and L. Lampe, "Robust detectors for TH IR-UWB systems with multiuser interference," in *Ultra-Wideband, 2007. ICUWB 2007. IEEE International Conference on*, September 2007, pp. 745–750.

[49] S. Gezici, H. Kobayashi, H. V. Poor, and A. F. Molisch, "Performance evaluation of impulse radio UWB systems with pulse-based polarity randomization," *IEEE Trans. Signal Process.*, vol. 53, no. 7, pp. 2537–2549, 2005.

[50] A. Forouzan, M. Nasiri-Kenari, and J. Salehi, "Performance analysis of time-hopping spread-spectrum multiple-access systems: uncoded and coded schemes," *IEEE Trans. Wireless Commun.*, vol. 1, no. 4, pp. 671–681, October 2002.

[51] B. Hu and N. Beaulieu, "Accurate evaluation of multiple-access performance in TH-PPM and TH-BPSK UWB systems," *IEEE Trans. Commun.*, vol. 52, no. 10, pp. 1758–1766, October 2004.

[52] G. Giancola, L. De Nardis, and M.-G. Di Benedetto, "Multi user interference in power-unbalanced ultra wide band systems: analysis and verification," in *2002 IEEE Conference on Ultra Wideband Systems and Technologies*, 2003, pp. 325–329.

[53] Y. Dhibi and T. Kaiser, "On the impulsiveness of multiuser interferences in TH-PPM-UWB systems," *IEEE Trans. Signal Process.*, vol. 54, no. 7, pp. 2853–2857, 2006.

[54] J. Fiorina and W. Hachem, "On the asymptotic distribution of the correlation receiver output for time-hopped UWB signals," *IEEE Trans. Signal Process.*, vol. 54, no. 7, pp. 2529–2545, 2006.

[55] R. C. Qiu, H. Liu, and X. Shen, "Ultra-wideband for multiple access communications," *IEEE Commun. Mag.*, vol. 43, no. 2, pp. 80–87, 2005.

[56] I. Bergel, E. Fishler, and H. Messer, "Narrowband interference mitigation in impulse radio," *IEEE Trans. Commun.*, vol. 53, no. 8, pp. 1278–1282, 2005.

[57] C. R. C. M. da Silva and L. B. Milstein, "The effects of narrowband interference on UWB communication systems with imperfect channel estimation," *IEEE J. Sel. Areas Commun.*, vol. 24, no. 4, pp. 717–723, 2006.

[58] J. Ibrahim and R. M. Buehrer, "NBI mitigation for UWB systems using multiple antenna selection diversity," *IEEE Trans. Veh. Technol.*, vol. 56, no. 4, pp. 2363–2374, 2007.

[59] S. M. Mishra, R. W. Brodersen, S. T. Brink, and R. Mahadevappa, "Detect and avoid: an ultra-wideband/WiMAX coexistence mechanism [topics in radio communications]," *IEEE Commun. Mag.*, vol. 45, no. 6, pp. 68–75, 2007.

[60] R. Scholtz, "Frame synchronization techniques," *IEEE Trans. Commun.*, vol. 28, no. 8, pp. 1204–1213, 1980.

[61] L. Franks, "Carrier and bit synchronization in data communication–a tutorial review," *IEEE Trans. Commun.*, vol. 28, no. 8, pp. 1107–1121, 1980.

[62] R. Pickholtz, D. Schilling, and L. Milstein, "Theory of spread-spectrum communications–a tutorial," *IEEE Trans. Commun.*, vol. 30, no. 5, pp. 855–884, May 1982.

[63] A. El Fawal and J.-Y. Le Boudec, "A robust signal detection method for ultra wide band (UWB) networks with uncontrolled interference," *IEEE Trans. Microw. Theory Tech.*, vol. 54, no. 4, pp. 1769–1781, June 2006.

[64] IEEE Computer Society, LAN/MAC Standard Committee, "IEEE P802.15.4a/D7 (amendment of IEEE std 802.15.4), part 15.4: Wireless medium access control (MAC) and physical layer (PHY) specifications for low-rate wireless personal area networks," Jan. 2007.

[65] ——, "IEEE standard for information technology- telecommunications and information exchange between systems- local and metropolitan area networks- specific requirements part 15.4: Wireless medium access control (MAC) and physical layer (PHY) specifications for low-rate wireless personal area networks (WPANs)," IEEE Std 802.15.4-2006 (Revision of IEEE Std 802.15.4-2003), 2006.

[66] E. Callaway, P. Gorday, L. Hester, J. Gutierrez, M. Naeve, B. Heile, and V. Bahl, "Home networking with IEEE 802.15.4: a developing standard for low-rate wireless personal area networks," *IEEE Commun. Mag.*, vol. 40, no. 8, pp. 70–77, August 2002.

[67] J. Hagenauer, "Rate-compatible punctured convolutional codes (RCPC codes) and their applications," *IEEE Trans. Commun.*, vol. 36, no. 4, pp. 389–400, April 1988.

[68] P. Frenger, P. Orten, T. Ottosson, and A. Svensson, "Rate-compatible convolutional codes for multirate DS-CDMA systems," *IEEE Trans. Commun.*, vol. 47, no. 6, pp. 828–836, June 1999.

[69] W. Hirt, "Ultra-wideband radio technology: overview and future research," *Computer Communications*, vol. 26, no. 1, pp. 46–52, January 2003.

[70] D. Porcino and W. Hirt, "Ultra-wideband radio technology: Potential and challenges ahead," *IEEE Commun. Mag.*, pp. 66–74, July 2003.

[71] D. D. Wentzloff, R. Blazquez, F. S. Lee, B. P. Ginsburg, J. Powell, and A. P. Chandrakasan, "System design considerations for ultra-wideband communication," *IEEE Commun. Mag.*, vol. 43, no. 8, pp. 114–121, 2005.

[72] L. Chalard, D. Helal, L. Verbaere, A. Wellig, and J. Zory, "Wireless sensor networks devices: Overview, issues, state-of the art and promising technologies," *ST Journal of Research, Wireless Sensor Networks*, vol. 4, no. 1, pp. 4–18, April 2007.

[73] S. Gezici, Z. Tian, G. Giannakis, H. Kobayashi, A. Molisch, H. V. Poor, and Z. Sahinoglu, "Localization via ultra-wideband radios: a look at positioning aspects for future sensor networks," *IEEE Signal Process. Mag.*, vol. 22, no. 4, pp. 70–84, July 2005.

[74] R. Scholtz, "The origins of spread-spectrum communications," *IEEE Trans. Commun.*, vol. 30, no. 5, pp. 822–854, 1982.

[75] J. Wittman, "Categorization of multiple-access/random-access modulation techniques," *IEEE Trans. Commun.*, vol. 15, no. 5, pp. 724–725, 1967.

[76] F. Ramirez-Mireles, "Performance of ultrawideband ssma using time hopping and m-ary ppm," *IEEE J. Sel. Areas Commun.*, vol. 19, no. 6, pp. 1186–1196, 2001.

[77] N. V. Kokkalis, P. T. Mathiopoulos, G. K. Karagiannidis, and C. S. Koukourlis, "Performance analysis of M-ary PPM TH-UWB systems in the presence of MUI and timing jitter," *IEEE J. Sel. Areas Commun.*, vol. 24, no. 4, pp. 822–828, 2006.

[78] E. Telatar and D. Tse, "Capacity and mutual information of wideband multipath fading channels," *IEEE Trans. Inf. Theory*, vol. 46, no. 4, pp. 1384–1400, 2000.

[79] R. C. Qiu, "A study of the ultra-wideband wireless propagation channel and optimum UWB receiver design," *IEEE J. Sel. Areas Commun.*, vol. 20, no. 9, pp. 1628–1637, 2002.

[80] M. Win and R. Scholtz, "Energy capture vs. correlator resources in ultra-wide bandwidth indoor wireless communications channels," vol. 3, November 1997, pp. 1277–1281.

[81] B. D. Woerner, J. H. Reed, and T. S. Rappaport, "Simulation issues for future wireless modems," *IEEE Commun. Mag.*, vol. 32, no. 7, pp. 42–53, 1994.

[82] J.-Y. Lee and R. A. Scholtz, "Ranging in a dense multipath environment using an UWB radio link," *IEEE J. Sel. Areas Commun.*, vol. 20, no. 9, pp. 1677–1683, 2002.

[83] C. L. Bennett and G. F. Ross, "Time-domain electromagnetics and its applications," *Proc. IEEE*, vol. 66, no. 3, pp. 299–318, 1978.

[84] R. J. Fontana and S. J. Gunderson, "Ultra-wideband precision asset location system," in *IEEE Conference on Ultra Wideband Systems and Technologies*, 2002, pp. 147–150.

[85] N. S. Correal, S. Kyperountas, Q. Shi, and M. Welborn, "An UWB relative location system," in *Ultra Wideband Systems and Technologies, 2003 IEEE Conference on*, 2003, pp. 394–397.

[86] I. Oppermann, L. Stoica, A. Rabbachin, Z. Shelby, and J. Haapola, "UWB wireless sensor networks: UWEN - a practical example," *IEEE Commun. Mag.*, vol. 42, no. 12, pp. S27–S32, 2004.

[87] B. Denis, J. B. Pierrot, and C. Abou-Rjeily, "Joint distributed synchronization and positioning in UWB ad hoc networks using toa," *IEEE Trans. Microw. Theory Tech.*, vol. 54, no. 4, pp. 1896–1911, 2006.

[88] A. H. Sayed, A. Tarighat, and N. Khajehnouri, "Network-based wireless location," *IEEE Signal Process. Mag.*, vol. 22, no. 4, pp. 24–40, 2005.

[89] F. Gustafsson and F. Gunnarsson, "Mobile positioning using wireless networks: possibilities and fundamental limitations based on available wireless network measurements," *IEEE Signal Process. Mag.*, vol. 22, no. 4, pp. 41–53, 2005.

[90] N. Patwari, J. N. Ash, S. Kyperountas, A. O. Hero, R. L. Moses, and N. S. Correal, "Locating the nodes: cooperative localization in wireless sensor networks," *IEEE Signal Process. Mag.*, vol. 22, no. 4, pp. 54–69, 2005.

[91] G. R. Aiello and G. D. Rogerson, "Ultra-wideband wireless systems," *IEEE Microw. Mag.*, vol. 4, no. 2, pp. 36–47, 2003.

[92] IEEE Computer Society, LAN/MAC Standard Committee, "IEEE 802.15.3 MAC standard, available at http://www.ieee.org."

[93] D. Hélal and P. Rouzet, "ST Microelectronics Proposal for IEEE 802.15.3a Alternate PHY," IEEE 802.15.3a / document 139r5, July 2003.

[94] W. Q. Malik, C. J. Stevens, and D. J. Edwards, "Multipath effects in ultrawideband rake reception," vol. 56, no. 2, pp. 507–514, 2008.

[95] G. Durisi and G. Romano, "Simulation analysis and performance evaluation of an UWB system in indoor multipath channel," in *IEEE Conference on Ultra Wideband Systems and Technologies*, 2002, pp. 255–258.

[96] F. Ramirez-Mireles, "Signal design for ultra-wide-band communications in dense multipath," *IEEE Trans. Veh. Technol.*, vol. 51, no. 6, pp. 1517–1521, 2002.

[97] A. Rabbachin and I. Oppermann, "Synchronization analysis for UWB systems with a low-complexity energy collection receiver," in *IEEE joint Conference on Ultra Wideband Systems and Technologies & International Workshop on Ultra Wideband Systems*, 2004, pp. 288–292.

[98] M. Weisenhorn and W. Hirt, "ML receiver for pulsed UWB signals and partial channel state information," in *IEEE International Conference on Ultra-Wideband*, 2005, pp. 6 pp.+.

[99] F. S. Lee and A. P. Chandrakasan, "A 2.5nj/b 0.65v 3-to-5ghz subbanded UWB receiver in 90nm CMOS," in *ISSCC 07*, February 2007.

[100] R. Tesi, M. Hamalainen, J. Iinatti, J. Oppermann, and V. Hovinen, "On the multi-user interference study for ultra wideband communication systems in AWGN and modified saleh-valenzuela channel," in *IEEE joint Conference on Ultra Wideband Systems and Technologies & International Workshop on Ultra Wideband Systems*, 2004, pp. 91–95.

[101] A. A. D'Amico, U. Mengali, and L. Taponecco, "Impact of mai and channel estimation errors on the performance of rake receivers in UWB communications," *IEEE Trans. Wireless Commun.*, vol. 4, no. 5, pp. 2435–2440, 2005.

[102] G. Durisi, A. Tarable, J. Romme, and Benedetto, "A general method for error probability computation of UWB systems for indoor multiuser communications," *Journal of Communications and Networks*, vol. 5, no. 4, pp. 354–364, December 2003.

[103] C. Carbonelli and U. Mengali, "M-ppm noncoherent receivers for UWB applications," *IEEE Trans. Wireless Commun.*, vol. 5, no. 8, pp. 2285–2294, 2006.

[104] M. E. Sahin, I. Guvenc, and H. Arslan, "Optimization of energy detector receivers for UWB systems," in *IEEE Spring VTC 05*, vol. 2, 2005.

[105] S. Paquelet and L. M. Aubert, "An energy adaptive demodulation for high data rates with impulse radio," 2004, pp. 323–326.

[106] S. Paquelet, L. M. Aubert, and B. Uguen, "An impulse radio asynchronous transceiver for high data rates," 2004, pp. 1–5.

[107] M. Nemati, U. Mitra, and R. Scholtz, "Optimum integration time for UWB transmitted reference and energy detector receivers," in *IEEE MILCOM 06*, October 2006, pp. 1–7.

[108] X. Peng, F. Chin, S. H. Wong, K. Y. Sam, and L. Zhongding, "A rake combining scheme for an energy detection based noncoherent OOK receiver in UWB impulse radio systems," in *IEEE ICUWB 06*, September 2006, pp. 73–78.

[109] Z. Tian and B. Sadler, "Weighted energy detection of ultra-wideband signals," in *IEEE SPAWC*, June 2005, pp. 10 168–1072.

[110] E. Arias-De-Reyna, A. A. D'Amico, and U. Mengali, "UWB energy detection receivers with partial channel knowledge," in *IEEE ICC 06*, vol. 10, 2006, pp. 4688–4693.

[111] M. Villanti, M. Sabattini, G. Maggio, and L. Milstein, "Non-coherent code acquisition for UWB systems in dense multipath fading channels," in *IEEE Spring VTC 05*, vol. 3, June 2005, pp. 2018 – 2022.

[112] P. S. Z. M. A. F. Duan, Chunjie Orlik, "A non-coherent 802.15.4a UWB impulse radio," in *Ultra-Wideband, 2007. ICUWB 2007. IEEE International Conference on*, September 2007, pp. 146–151.

[113] G. Durisi and G. Romano, "On the validity of gaussian approximation to characterize the multiuser capacity of UWB TH PPM," in *IEEE Conference on Ultra Wideband Systems and Technologies*, 2002, pp. 157–161.

[114] B. Hu and N. C. Beaulieu, "On characterizing multiple access interference in TH-UWB systems with impulsive noise models," in *IEEE Radio and Wireless Symposium*, 2008, pp. 879–882.

[115] N. C. Beaulieu and B. Hu, "Soft-limiting receiver structures for time-hopping UWB in multiple-access interference," *IEEE Trans. Veh. Technol.*, vol. 57, no. 2, pp. 810–818, 2008.

[116] S. de Rivaz, B. Denis, M. Pezzin, and L. Ouvry, "Performance of IEEE 802.15.4a UWB systems under multi-user interference," in *IEEE 18th International Symposium on Personal, Indoor and Mobile Radio Communications (PIMRC)*, 2007, pp. 1–7.

[117] D. Middleton, "Statistical-physical models of electromagnetic interference," *IEEE Trans. Electromagn. Compat.*, vol. EMC-19, no. 3, pp. 106–127, 1977.

[118] ——, "Canonical and quasi-canonical probability models of class a interference," *IEEE Trans. Electromagn. Compat.*, vol. EMC-25, no. 2, pp. 76–106, 1983.

[119] B. Radunovic and J. Y. Le Boudec, "Optimal power control, scheduling and routing in UWB networks," *IEEE J. Sel. Areas Commun.*, vol. 22, no. 7, pp. 1252–1270, September 2004.

[120] K. Hamdi and X. Gu, "On the validity of the gaussian approximation for performance analysis of TH-CDMA/OOK impulse radio networks," in *The 57th IEEE Semiannual Vehicular Technology Conference*, vol. 4. VTC 2003-Spring, 2003, pp. 2211–2215.

[121] M. Sabattini, E. Masry, and L. Milstein, "A non-gaussian approach to the performance analysis of UWB TH-BPPM systems," in *IEEE Conference on Ultra Wideband Systems and Technologies*, November 2003, pp. 52–55.

[122] S. Niranjayan, A. Nalianathan, and B. Kannan, "A new analytical method for exact bit error rate computation of TH-PPM UWB multiple access systems," in *IEEE PIMRC*, 2004, pp. 2968–2972.

[123] C. Bi and J. Hui, "Multiple access capacity for ultra-wide band radio with multi-antenna receivers," in *IEEE Conference on Ultra Wideband Systems and Technologies*, 2002, pp. 151–155.

[124] J. Fiorina and D. Domenicali, "Revisiting TH-IR-UWB performance limits dependency on essential system parameters using the generalized gaussian approximation," in *Ultra-Wideband, 2007. ICUWB 2007. IEEE International Conference on*, 2007, pp. 751–754.

[125] G. Giancola and M.-G. Di Benedetto, "A novel approach for estimating multi-user interference in impulse radio UWB networks: the pulse collision model," *Signal Process.*, vol. 86, no. 9, pp. 2185–2197, September 2006.

[126] A. Spaulding and D. Middleton, "Optimum reception in an impulsive interference environment–part I: Coherent detection," *IEEE Trans. Commun.*, vol. 25, no. 9, pp. 910–923, 1977.

[127] ——, "Optimum reception in an impulsive interference environment–part II: Incoherent reception," *IEEE Trans. Commun.*, vol. 25, no. 9, pp. 924–934, 1977.

[128] K. Vastola, "Threshold detection in narrow-band non-gaussian noise," *IEEE Trans. Commun.*, vol. 32, no. 2, pp. 134–139, 1984.

[129] A. El-Sawy and V. Vandelinde, "Robust detection of known signals," *IEEE Trans. Inf. Theory*, vol. 23, no. 6, pp. 722–727, 1977.

[130] S. A. Kassam and H. V. Poor, "Robust signal processing for communication systems," *IEEE Commun. Mag.*, vol. 21, no. 1, pp. 20–28, 1983.

[131] ——, "Robust techniques for signal processing: A survey," *Proc. IEEE*, vol. 73, no. 3, pp. 433–481, 1985.

[132] S. A. Kassam, *Signal Detection in Non-Gaussian Noise*. Springer Verlag, 1988.

[133] B. Aazhang and H. V. Poor, "Performance of ds/ssma communications in impulsive channels. ii. hard-limiting correlation receivers," *IEEE Trans. Commun.*, vol. 36, no. 1, pp. 88–97, 1988.

[134] G. D. Weeks, J. K. Townsend, and J. A. Freebersyser, "Performance of hard decision detection for impulse radio," in *IEEE Military Communications Conference Proceedings (MILCOM)*, vol. 2, 1999, pp. 1201–1206 vol.2.

[135] W. Lovelace and J. Townsend, "Chip discrimination for large near far power ratios in UWB networks," in *IEEE MILCOM*, vol. 2, October 2003, pp. 13–16.

[136] W. M. Lovelace and J. K. Townsend, "Threshold discrimination and blanking for large near-far power ratios in UWB networks," *IEEE Trans. Commun.*, vol. 53, no. 9, pp. 1447–1450, 2005.

[137] E. Fishler and H. V. Poor, "Low-complexity multiuser detectors for time-hopping impulse-radio systems," *IEEE Trans. Signal Process.*, vol. 52, no. 9, pp. 2561–2571, September 2004.

[138] N. Guney, H. Delic, and M. Koca, "Robust detection of ultra-wideband signals in non-gaussian noise," *IEEE Trans. Microw. Theory Tech.*, vol. 54, no. 4, pp. 1724–1730, 2006.

[139] B. S. Kim, J. Bae, I. Song, S. Y. Kim, and H. Kwon, "A comparative analysis of optimum and suboptimum rake receivers in impulsive UWB environment," *IEEE Trans. Veh. Technol.*, vol. 55, no. 6, pp. 1797–1804, 2006.

[140] N. C. Beaulieu and B. Hu, "An adaptive threshold soft-limiting UWB receiver with improved performance in multiuser interference," in *Ultra-Wideband, The 2006 IEEE 2006 International Conference on*, 2006, pp. 405–410.

[141] J. Fiorina, "On the benefit of a one-bit sampling receiver and hard decoding in impulse radio ultra wide band communications with multi-user interferences," in *Personal, Indoor and Mobile Radio Communications, 2006 IEEE 17th International Symposium on*, 2006, pp. 1–4.

[142] G. A. Tsihrintzis and C. L. Nikias, "Incoherent receivers in alpha-stable impulsive noise," *IEEE Trans. Signal Process.*, vol. 43, no. 9, pp. 2225–2229, 1995.

[143] S. Yoon, I. Song, and S. Y. Kim, "Code acquisition for ds/ss communications in non-gaussian impulsive channels," *IEEE Trans. Commun.*, vol. 52, no. 2, pp. 187–190, 2004.

[144] Z. Sahinoglu and I. Guvenc, "Multiuser interference mitigation in noncoherent UWB ranging via nonlinear filtering," *EURASIP Journal on Wireless Communications and Networking*, pp. 1–10, 2006.

[145] D. Dardari, A. Giorgetti, and M. Z. Win, "Time-of-arrival estimation of UWB signals in the presence of narrowband and wideband interference," in *Ultra-Wideband, 2007. ICUWB 2007. IEEE International Conference on*, 2007, pp. 71–76.

[146] V. Cellini and G. Dona, "A novel joint channel and multi-user interference statistics estimator for UWB-IR based on Gaussian mixture model," in *IEEE International Conference on Ultra-Wideband (ICU)*, 2005, pp. 655–660.

[147] J. Fiorina, "A simple IR-UWB receiver adapted to multi-user interferences," in *IEEE Global Telecommunications Conference (GLOBECOM)*, 2006, pp. 1–4.

[148] T. Erseghe, V. Cellini, and G. Dona, "UWB impulse radio receivers derived from a Gaussian mixture interference model," in *IEEE International Conference on Communications (ICC)*, 2007, pp. 5757–5762.

[149] I. Guvenc and H. Arslan, "A review on multiple access interference cancellation and avoidance for IR-UWB," *Signal Processing*, vol. 87, no. 4, pp. 623–653, April 2007.

[150] B. Radunovic, J.-Y. Le Boudec, and R. Knopp, "Optimal PHY and MAC Protocols for Wide-Band Ad-Hoc Networks," in *Forty-Fifth Annual Allerton Conference*, 2007.

[151] S. Toumpis and A. Goldsmith, "Capacity regions for wireless ad hoc networks," *IEEE Trans. Wireless Commun.*, vol. 24, no. 5, pp. 736–748, May 2003.

[152] C. Zou and Z. Haas, "Optimal resource allocation for UWB wireless ad hoc networks," in *IEEE International Symposium on Personal, Indoor and Mobile Radio Communications (PIMRC)*, vol. 1, 2005, pp. 452–456.

[153] A. Rajeswaran, G. Kim, and R. Negi, "Joint power adaptation, scheduling, and routing for ultra wide band networks," *IEEE Trans. Wireless Commun.*, vol. 6, no. 5, pp. 1964–1972, 2007.

[154] F. Cuomo, C. Martello, A. Baiocchi, and C. Fabrizio, "Radio resource sharing for ad hoc networking with UWB," *IEEE J. Sel. Areas Commun.*, vol. 20, no. 9, pp. 1722–1732, December 2002.

[155] P. Baldi, L. De Nardis, and M. G. Di Benedetto, "Modeling and optimization of UWB communication networks through a flexible cost function," *IEEE J. Sel. Areas Commun.*, vol. 20, no. 9, pp. 1733–1744, 2002.

[156] Q. Wu, Y. Xiong, Q. Zhang, Z. Guo, X.-G. Xia, and Z. Li, "Joint routing and topology formation in multihop UWB networks," *IEEE J. Sel. Areas Commun.*, vol. 24, no. 4, pp. 843–849, 2006.

[157] Y. Shi, Y. T. Hou, H. D. Sherali, and S. F. Midkiff, "Optimal routing for UWB-based sensor networks," *IEEE J. Sel. Areas Commun.*, vol. 24, no. 4, pp. 857–863, 2006.

[158] M. Neely, E. Modiano, and C. Rohrs, "Dynamic power allocation and routing for time-varying wireless networks," *IEEE J. Sel. Areas Commun.*, vol. 23, no. 1, pp. 89–103, January 2005.

[159] S. Raj, E. Telatar, and D. Tse, "Job scheduling and multiple access," DIMACS Series in Discrete Mathematics and Theoretical Computer Sciences, 2003.

[160] S. Kolenchery, J. Townsend, and J. Freebersyser, "A novel impulse radio network for tactical military wireless communications," in *IEEE MILCOM*, vol. 1, October 1998, pp. 59–65.

[161] A. Hicham, Y. Souilmi, and C. Bonnet, "Self-balanced receiver-oriented MAC for ultra-wide band mobile ad hoc networks," in *IEEE International Workshop on Ultra Wideband Systems*, 2003, p. June.

[162] N. August, H.-J. Lee, and D. Ha, "Pulse sense: A method to detect a busy medium in pulse-based ultra wideband (UWB) networks," in *IEEE Conference on Ultra Wideband Systems and Technologies*, May 2004, pp. 366–370.

[163] N. August and D. Ha, "An efficient UWB radio architecture for busy signal MAC protocols," in *IEEE SECON*, October 2004, pp. 325–334.

[164] M.-G. Di Benedetto, L. Nardis, M. Junk, and G. Giancola, "$(UWB)^2$: Uncoordinated, wireless, baseborn, medium access control for UWB communication networks," *Mobile Networks and Applications*, vol. 10, no. 5, October 2005.

[165] X. Shen, W. Zhuang, H. Jiang, and J. Cai, "Medium access control in ultra-wideband wireless networks," *IEEE Trans. Veh. Technol.*, vol. 54, no. 5, pp. 1663–1677, 2005.

[166] R. Jurdak, P. Baldi, and C. V. Lopes, "U-MAC: a proactive and adaptive UWB medium access control protocol," *Wireless Commun. and Mobile Comput. J., Special Issue on Ultrawideband (UWB) Communications*, vol. 5, no. 5, pp. 551–566, August 2005.

[167] N. J. August, H. J. Lee, and D. S. Ha, "Enabling distributed medium access control for impulse-based ultrawideband radios," *IEEE Trans. Veh. Technol.*, vol. 56, no. 3, pp. 1064–1075, 2007.

[168] N. Shi, L. Xia, and I. Niemegeers, "A novel approach for the link layer in impulse-based UWB ad hoc networks," *Wireless Personal Communications*, vol. 42, no. 2, pp. 143–159, July 2007.

[169] I. Broustis, M. Molle, S. Krishnamurthy, M. Faloutsos, and J. Foerster, "A new binary conflict resolution-based mac protocol for impulse-based UWB ad hoc networks," *Wireless Commun. and Mobile Comput. J.*, vol. 6, no. 7, pp. 933–949, 2006.

[170] I. Broustis, S. V. Krishnamurthy, M. Faloutsos, M. Molle, and J. R. Foerster, "Multiband media access control in impulse-based UWB ad hoc networks," *IEEE Trans. Mobile Comput.*, vol. 6, no. 4, pp. 351–366, 2007.

[171] F. Tobagi and L. Kleinrock, "Packet switching in radio channels: Part II–the hidden terminal problem in carrier sense multiple-access and the busy-tone solution," *IEEE Trans. Commun.*, vol. 23, no. 12, pp. 1417–1433, 1975.

[172] W. Horie and Y. Sanada, "Novel CSMA scheme for DS-UWB ad-hoc network with variable spreading factor," in *IEEE joint Conference on Ultra Wideband Systems and Technologies & International Workshop on Ultra Wideband Systems*, May 2004, pp. 361–365.

[173] G. Holland, N. Vaidya, and P. Bahl, "A rate-adaptive MAC protocol for multi-hop wireless networks," in *MobiCom '01*, 2001, pp. 236–251.

[174] B. Sadeghi, V. Kanodia, A. Sabharwal, and E. Knightly, "Opportunistic media access for multirate ad hoc networks," in *8th Annual Int. Conf. on Mobile Computing and Networking*, 2002.

[175] A. Muqattash and K. Marwan, "CDMA–based MAC protocol for wireless ad hoc networks," in *Proceedings of the International Symposium on Mobile Ad Hoc Networking and Computing (MOBIHOC'03)*, June 2003, pp. 153–164.

[176] J. Mo, S. Wilson, and J. Walrand, "Comparison of multichannel MAC protocols," *IEEE Trans. Mobile Comput.*, vol. 7, no. 1, pp. 50–65, 2008.

[177] G. Bianchi, "Performance analysis of the IEEE 802.11 distributed coordination function," *IEEE J. Sel. Areas Commun.*, vol. 18, no. 3, pp. 535–547, March 2000.

[178] G. Bianchi and I. Tinnirello, "Remarks on IEEE 802.11 DCF performance analysis," *IEEE Commun. Lett.*, vol. 9, no. 8, pp. 765–767, August 2005.

[179] C. Bordenave, D. Mc Donald, and A. Proutière, "Random multi-access algorithms, a mean field analysis," in *Forty-third annual Allerton conference on Communication, Control, and Computing*, 2005.

[180] A. Kumar, E. Altman, D. Miorandi, and M. Goyal, "New insights from a fixed-point analysis of single cell IEEE 802.11 wlans," *IEEE/ACM Trans. Netw.*, vol. 15, no. 3, pp. 588–601, 2007.

[181] "The network simulator ns-2, http://nsnam.isi.edu/nsnam/," January 2008.

[182] M. Lacage and T. R. Henderson, "Yet another network simulator," in *WNS2, The workshop on ns-2: the IP network simulator*, 2006.

[183] G. F. Riley, "The georgia tech network simulator," in *MoMeTools '03: Proceedings of the ACM SIGCOMM workshop on Models, methods and tools for reproducible network research*, 2003, pp. 5–12.

[184] J. M. Dricot and P. De Doncker, "High-accuracy physical layer model for wireless network simulations in ns-2," in *Wireless Ad-Hoc Networks, 2004 International Workshop on*, 2004, pp. 249–253.

[185] "New 802.11 support for ns-2," http://spoutnik.inria.fr/ns-2-80211/, 2006.

[186] Q. Chen, D. Jiang, V. Taliwal, and L. Delgrossi, "IEEE 802.11 based vehicular communication simulation design for ns-2," in *VANET '06: Proceedings of the 3rd international workshop on Vehicular ad hoc networks*, 2006, pp. 50–56.

[187] A. Mishra, V. Shrivastava, S. Banerjee, and W. Arbaugh, "Partially overlapped channels not considered harmful," in *SIGMETRICS '06/Performance '06: Proceedings of the joint international conference on Measurement and modeling of computer systems*, 2006.

[188] M. Takai, J. Martin, and R. Bagrodia, "Effects of wireless physical layer modeling in mobile ad hoc networks," in *MobiHoc '01*, 2001, pp. 87–94.

[189] D. Kotz, C. Newport, R. S. Gray, J. Liu, Y. Yuan, and C. Elliott, "Experimental evaluation of wireless simulation assumptions," in *MSWiM '04: Proceedings of the 7th ACM international symposium on Modeling, analysis and simulation of wireless and mobile systems*, 2004, pp. 78–82.

[190] J. Heidemann, K. Mills, and S. Kumar, "Expanding confidence in network simulations," *IEEE Netw.*, vol. 15, no. 5, pp. 58–63, 2001.

[191] A. Doufexi, S. Armour, M. Butler, A. Nix, D. Bull, J. McGeehan, and P. Karlsson, "A comparison of the HIPERLAN/2 and IEEE 802.11a wireless LAN standards," *IEEE Commun. Mag.*, vol. 40, no. 5, pp. 172–180, May 2002.

[192] L. Tong, V. Naware, and P. Venkitasubramaniam, "Signal processing in random access," *IEEE Signal Process. Mag.*, vol. 21, no. 5, pp. 29–39, September 2004.

[193] N. Abramson, "The aloha system—another alternative for computer communications," in *AFIPS Conf. Proc. Fall Joint Computer Conference*, vol. 37, 1970, pp. 281–285.

[194] ——, "Development of the alohanet," *IEEE Trans. Inf. Theory*, vol. 31, no. 2, pp. 119–123, 1985.

[195] P. Karn, "Maca - a new channel access method for packet radio," in *ARRL/CRRL Amateur Radio 9th Computer Networking Conference*, 1990, pp. 134–140.

[196] C. L. Fullmer and J. J. Garcia-Luna-Aceves, "Floor acquisition multiple access (fama) for packet-radio networks," in *SIGCOMM*, 1995, pp. 262–273.

[197] Z. Fu, P. Zerfos, H. Luo, S. Lu, L. Zhang, and M. Gerla, "The impact of multihop wireless channel on TCP throughput and loss," in *IEEE INFOCOM*, vol. 3, March-April 2003, pp. 1744–1753.

[198] L. Kleinrock and S. Lam, "Packet switching in a multiaccess broadcast channel: Performance evaluation," *IEEE Trans. Commun.*, vol. 23, no. 4, pp. 410–423, 1975.

[199] M. Ferguson, "On the control, stability, and waiting time in a slotted aloha random-access system," *IEEE Trans. Commun.*, vol. 23, no. 11, pp. 1306–1311, 1975.

[200] W. Ye, J. Heidemann, and D. Estrin, "Medium access control with coordinated adaptive sleeping for wireless sensor networks," *IEEE/ACM Trans. Netw.*, vol. 12, no. 3, pp. 493–506, June 2004.

[201] J. Polastre, J. Hill, and D. Culler, "Versatile low power media access for wireless sensor networks," in *Proceedings of the 2nd international conference on Embedded networked sensor systems (SenSys)*, 2004, pp. 95–107.

[202] E. Ferro and F. Potorti, "Bluetooth and Wi-Fi wireless protocols: a survey and a comparison," *IEEE Wireless Commun. Mag.*, vol. 12, no. 1, pp. 12–26, February 2005.

[203] J. So and N. H. Vaidya, "Multi-channel mac for ad hoc networks: handling multi-channel hidden terminals using a single transceiver," in *MobiHoc '04: Proceedings of the 5th ACM international symposium on Mobile ad hoc networking and computing*, 2004, pp. 222–233.

[204] International Standards Organization, Geneva, "High rate ultra wideband phy and mac standard," International Standard ISO/IEC 26907 Information technology Telecommunications and information exchange between systems, March 2007.

[205] V. M. Vishnevsky, A. I. Lyakhov, A. A. Safonov, S. S. Mo, and A. D. Gelman, "Study of beaconing in multihop wireless PAN with distributed control," *IEEE Trans. Mobile Comput.*, vol. 7, no. 1, pp. 113–126, 2008.

[206] B. Radunovic and J.-Y. Le Boudec, "Rate performance objectives of multi-hop wireless networks," *IEEE Trans. Mobile Comput.*, vol. 03, no. 4, pp. 334–349, October-December 2004.

[207] "UWB research at EPFL-IC," http://icawww1.epfl.ch/uwb/, 2008.

[208] B. Radunovic, "A cross-layer design of wireless ad-hoc networks," Ph.D. dissertation, EPFL, Ph.D thesis 3301, June 2005.

[209] B. Chen, K. Jamieson, H. Balakrishnan, and R. Morris, "Span: an energy-efficient coordination algorithm for topology maintenance in ad hoc wireless networks," *ACM Wireless Networks Journal*, vol. 8, no. 5, September 2002.

[210] M. Grossglauser and D. Tse, "Mobility increases the capacity of ad hoc wireless networks," *IEEE/ACM Trans. Netw.*, vol. 10, no. 4, pp. 477–486, August 2002.

[211] H.-Y. Hsieh and R. Sivakumar, "IEEE 802.11 over multi-hop wireless networks: Problems and new perspectives," in *IEEE VTC-Fall*, vol. 2, September 2002, pp. 748–752.

[212] F. Baccelli and P. Brémaud, *Palm Probabilities and Stationary Queues*. Springer Verlag Lecture Notes in Statistics, March 1987.

[213] J.-Y. Le Boudec, "Performance evaluation lecture notes (methods, practice and theory for the performance evaluation of computer and communication systems)," Lecture notes, available at http://icawww1.epfl.ch/perfeval, 2007.

[214] K. Xu, M. Gerla, L. Qi, and Y. Shu, "Enhancing TCP fairness in ad hoc wireless networks using neighborhood RED," in *MobiCom '03*, 2003, pp. 16–28.

[215] G. Quintero Diaz de Leon and A. Skrivervik, "Analysis of UWB antennas for carrier-based UWP impulse radio," in *European Conference on Antennas and Propagation, 2007. EuCAP 2007.*, November 2007, pp. 1–4.

[216] H. Zhan, J. Ayadi, J. Farserotu, and J.-Y. Le Boudec, "High-resolution impulse radio ultra wideband ranging," in *IEEE International Conference on Ultra-Wideband, 2007. ICUWB 2007.*, September 2007, pp. 568–573.

[217] H. Urkowitz, "Energy detection of unknown deterministic signals," *Proc. IEEE*, vol. 55, no. 4, pp. 523–531, 1967.

[218] N. C. Beaulieu and C. C. Tan, "An FFT method for generating bandlimited Gaussian noise variates," in *IEEE GLOBECOM 97*, vol. 2, 1997, pp. 684–688.

[219] R. Mukhtar, S. Hanly, M. Zukherman, and F. Cameron, "A model for the performance evaluation of packet transmissions using type-II hybrid ARQ over a correlated error channel," *Wireless Networks*, vol. 10, no. 1, pp. 7–16, 2004.

[220] R. R. Bahadur and R. Rao, "On deviations of the sample mean," *Ann. Math. Statis*, vol. 31, pp. 1015–1027, 1960.

[221] A. Dembo and O. Zeitouni, *Large Deviations Techniques and Applications*. London: Jones and Bartlett, 1993.

[222] P. Heidelberger, "Fast simulation of rare events in queueing and reliability models," *ACM Transactions on Modeling and Computer Simulation*, vol. 5, no. 1, pp. 43–85, January 1995.

Chapter A

Appendices for Part I

A.1 Simulations for rate-maximization and lifetime-maximization problems in Section 4.2.3

The simulations for the rate maximization and lifetime maximization problems Section 4.2.3 are done in three steps.

In the first step we create a random network topology. We then vary the size of the exclusion region, and for each size of the exclusion region we calculate all possible slots: they are the sets of links that do not share a common source node or a destination node, and that can be active at the same time by satisfying exclusion region rules. Each slot then define a number of nodes that are transmitting and a number of nodes that are receiving. All active transmitters are assumed to transmit with the maximum power since it is shown in [208] that this policy is optimal for both rate maximization and power minimization.

In the second step we take each slot, and for each link we calculate its achievable rate, assuming the presence of interferers as defined with the slot. We simulate an IR-UWB physical layer to calculate the maximum rate a source-destination pair can achieve, given the locations of active interferers. At the output of the second step, for each link in each slot we obtain its maximum achievable rate.

In the third step, we construct schedules. A schedule is a set of slots with corresponding durations. A schedule also defines average rates and power consumption for links. The average rate of a link is the sum of rates of a link achieved in every slot, multiplied by the duration of a slot. The average power consumption is similarly defined as the sum of power consumptions in each slot multiplied by the duration of a slot.

The remaining optimization problem is to optimize slot durations with respect to a given performance metric. As described in Section 4.2.2, we consider two performance metrics: the sum of the log of the rates, and the sum of the log of the lifetimes. Both corresponding optimization problems are convex, so we can easily solve them, for each exclusion region range separately. Some of the slots will have zero duration, which will mean that they should not be used in the optimal MAC. Finally, we plot the values of the metrics for the optimal schedules, for different size of the exclusion regions, and visually obtain the optimal value of the size of the exclusion region.

A.2 List of components used for the IR-UWB software radio testbed

FPGA	Virtex II Pro XC2VP70, Xilinx
Acquisition board	AC-240 with 512 MB of SDRAM, Acqiris
Duroid substrate	RO4003B, Rogers Corporation
Mixer	HMC128, Hittite Corporation
SiGe NPN transistor	NESG2030M04, NEC
Power Amplifier	HMC-C026, Hittite Corporation
LNA MMIC	MGA-85563, Agilent
IF Amplifier	ZX60-3018G, Mini-Circuits

Publications

Journal Papers

- R. Merz and J.-Y. Le Boudec, "Performance Evaluation of Impulse Radio UWB Networks using Common or Private Acquisition Preambles", *IEEE Transactions on Mobile Computing*, submitted
- A. El Fawal, J.-Y. Le Boudec, R. Merz, B. Radunovic, J. Widmer, G. M. Maggio, "Trade-off Analysis of PHY-aware MAC in Low-Rate, Low-Power UWB networks", *IEEE Communications Magazine*, Volume 43, Issue 12, December 2005
- R. Merz, J. Widmer, J.-Y. Le Boudec, B. Radunovic, "A Joint PHY/MAC Architecture for Low-Radiated Power TH-UWB Wireless Ad-Hoc Networks", *Wireless Communications and Mobile Computing Journal, Special Issue on Ultrawideband (UWB) Communications*, Volume 5, Issue 5, August 2005

Conference Papers

- M. Flury, R. Merz, J.-Y. Le Boudec, "An Energy Detection Receiver Robust to Multi-User Interference for IEEE 802.15.4a Networks", *IEEE International Conference on Ultra-Wideband (ICUWB 2008)*, Hannover, Germany, 10-12 September 2008
- M. Flury, R. Merz, J.-Y. Le Boudec and J. Zory, "Performance Evaluation of an IEEE 802.15.4a Physical Layer with Energy Detection and Multi-User Interference", *IEEE International Conference on Ultra-Wideband (ICUWB 2007)*, Singapore, 24-26 September 2007
- R. Merz, J.-Y. Le Boudec and J. Widmer, "An Architecture for Wireless Simulation in NS-2 Applied to Impulse-Radio Ultra-Wide Band Networks", *10th Communications and*

Networking Simulation Symposium (CNS'07), Norfolk, VA, USA, 25-29 March 2007

- R. Merz, J.-Y. Le Boudec, S. Vijayakumaran, "Effect on Network Performance of Common versus Private Acquisition Sequences for Impulse Radio UWB Networks", *IEEE International Conference on Ultra-Wideband (ICUWB 2006)*, Waltham, MA, USA, 24-27 September 2006

- R. Merz, J.-Y. Le Boudec, "Conditional Bit Error Rate for an Impulse Radio UWB Channel with Interfering Users", *IEEE International Conference on Ultra-Wideband (ICU 2005)*, Zürich, Switzerland, 5-8 September 2005

- J.-Y. Le Boudec, R. Merz, B. Radunovic, J. Widmer, "DCC-MAC: A Decentralized MAC Protocol for 802.15.4a-like UWB Mobile Ad-Hoc Networks Based on Dynamic Channel Coding", *BroadNets 2004*, San Jose, CA, USA, 25-29 October 2004

- R. Merz, J.-Y. Le Boudec, J. Widmer, B. Radunovic, "A Rate-Adaptive MAC Protocol for Low-Power Ultra-Wide Band Ad-hoc Networks", *Third International Conference on Ad hoc Networks and Wireless (ADHOC-NOW 2004)*, Vancouver, British Columbia, Canada, 22-24 July 2004

Patent

- M. Flury, R. Merz, J.-Y. Le Boudec, "Method for retrieving data from ultra wideband radio transmission signals", *US Patent Application 61/006,972*, February 2008

Invited Papers

- M. Flury, R. Merz and J.-Y. Le Boudec, "Managing Impulsive Interference in Impulse Radio UWB Networks", *ST Journal of Research*, vol. 4, no 1, May 2007

- R. Merz, A. El Fawal, J.-Y. Le Boudec, B. Radunovic, J. Widmer, "The Optimal MAC Layer for Low-Power UWB is Non-Coordinated", *IEEE International Symposium on Circuits and Systems (ISCAS 2006)*, Island of Kos, Greece, 21-24 May 2006

- R. Merz, J.-Y. Le Boudec, "Effect of Interfering Users on the Modulation Order and Code Rate for UWB Impulse-Radio Bit-Interleaved Coded M-ary PPM", *IEEE UWBNETS 2005*, Boston, MA, USA, 7 October 2005

Curriculum Vitæ

Ruben Merz was born in Lausanne, Switzerland. In March 2003, he graduated from EPFL, School of Computer and Communication Sciences, where he earned a Master of Science (MSc) in Communication Systems. In the Summer of 2000, he interned at the Swisscom research center in Bern, Switzerland. Between April and October 2001, he was a software engineer intern for Fast Forward Networks in San Francisco, California. From August 2002 to March 2003, he worked at the Department of Electrical Engineering, Indian Institute of Technology, Delhi (IITD) in India. During that time, he carried out his master thesis on "Differential Schemes for Multiple-Antenna Systems".

In June 2003, he joined the Laboratory for Computer Communication and Applications (LCA) at EPFL, School of Computer and Communication Sciences , and started his PhD thesis under the supervision of Professor Jean-Yves Le Boudec. There, he participated to the National Center of Competence in Research on Mobile Information and Communication Systems (NCCR-MICS). He was a teaching assistant for the Performance Evaluation and TCP/IP Networking courses. He was awarded a best student paper award at the 2005 IEEE International Conference on Ultra-Wideband (ICU 2005) and a best demo award at the 2006 MICS Scientific Conference for the demo "An Impulse-Radio Ultra-Wide Band Testbed with Interference". His current research interests focus on the design and performance evaluation of wireless networks.